INFORMATION TO USERS

This manuscript has been reproduced from the microfilm master. UMI films the text directly from the original or copy submitted. Thus, some thesis and dissertation copies are in typewriter face, while others may be from any type of computer printer.

The quality of this reproduction is dependent upon the quality of the copy submitted. Broken or indistinct print, colored or poor quality illustrations and photographs, print bleedthrough, substandard margins, and improper alignment can adversely affect reproduction.

In the unlikely event that the author did not send UMI a complete manuscript and there are missing pages, these will be noted. Also, if unauthorized copyright material had to be removed, a note will indicate the deletion.

Oversize materials (e.g., maps, drawings, charts) are reproduced by sectioning the original, beginning at the upper left-hand corner and continuing from left to right in equal sections with small overlaps.

Photographs included in the original manuscript have been reproduced xerographically in this copy. Higher quality 6" x 9" black and white photographic prints are available for any photographs or illustrations appearing in this copy for an additional charge. Contact UMI directly to order.

UMI®

NORTHWESTERN UNIVERSITY

The Local Variation of the Critical Current Along
$YBa2Cu3O7-x$ Grainboundary and Ramp-Edge
Josephson Junctions

A DISSERTATION

SUBMITTED TO THE GRADUATE SCHOOL
IN PARTIAL FULFILLMENT OF THE REQUIREMENTS

for the degree

DOCTOR OF PHILOSOPHY

Field of Materials Science and Engineering

By

Michael William Carmody

EVANSTON, ILLINOIS

December 2000

UMI®

ABSTRACT

The Local Variation of the Critical Current Along
YBa2Cu3O7-x Grainboundary and Ramp-Edge
Josephson Junctions

Michael W. Carmody

High temperature (high-T_c) superconductors have been extensively studied for basic research purposes and for their potential technological applications. One of the most promising applications is the potential for superconducting quantum interference devices (SQUIDs) operating at temperature above the boiling point of liquid nitrogen (77 K). Grain boundaries in high-T_c systems where found to exhibit the Josephson effect that can be used to fabricate microelectronic devices. Tilt grain boundaries with tilt angles of 24° and 45° are studied for a basic understanding of the transport properties across single grain boundaries in [001] oriented thin film $YBa_2Cu_3O_{7-x}$ (YBCO).

A novel technique involving phase retrieval is developed for determining the local current distribution J(x) from measurements of the critical current across a Josephson junction as a function of an applied magnetic field $I_c(H)$. The $I_c(H)$ data is related to the local current density J(x) along the length of the junction as the modulus of the Fourier

ii

transform of J(x). The Fourier relation is used to extract for the first time local current information along the length of the boundary. The highly non-uniform current distributions are discussed in terms of local boundary microstructure, boundary stoichiometry and the d-wave symmetry of the order parameter.

The phase retrieval technique is also applied to superconductor-normal layer-superconductor multilayer structures (ramp-edge Josephson junctions). The highly uniform current distributions J(x) are compared to the non-uniform current distributions in grain boundary junctions and compared to the uniform microstructure of ramp-edge junctions and discussed in terms of the symmetry of the order parameter across the boundary plane.

Thesis Advisors:

_____

Dr. Laurence D. Marks
Northwestern University

_____
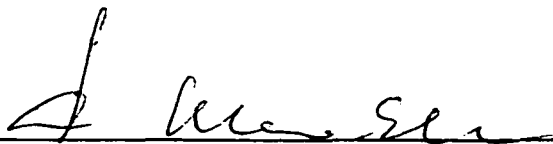
Dr. Karl L. Merkle
Argonne National Laboratory

Dedication

To those who loved me first, Mom and Dad.

iv

Acknowledgments

Few graduate students make the journey to their thesis alone, and I am no exception. Along the way I have been challenged and encouraged by many people whom I owe a great deal to. I would like to thank foremost my two thesis advisors: Dr. Laurie Marks and Dr. Karl Merkle for challenging me and encouraging me to focus and be creative. I owe many thanks to Loren Thompson of Argonne National Laboratory for the hours of work and patience he has shown to me teaching me countless hands-on laboratory lessons. I would also like to thank Dr. Paul Markworth and Dr. Mike Chudzik of Northwestern University and Dr. Brian Moeckly or Conductus for growing the thin films that were used for this thesis. Also I would like to thank Dr. Dean Miller for allowing me to freely use the photolithography equipment at Argonne National Laboratory.

There are many people at both Argonne National Laboratory and Northwestern University who have given of their time, energy and their equipment to help in my research. Specifically I would like to thank the members of Professor Marks research group both past and present and members of the Interface group at Argonne National Laboratory.

v

Finally, I would like to thank my family for being patient and understanding the effort that is required for the completion of a thesis and always being there to help me relax when I had a free moment. Also I would like to thank Dr. Peter Carmody and Francine Cannarozzi for proof reading the text. Most of all, I would like to thank my wife Nadine for being there when I needed her to be.

Abbreviations

$YBa_2Cu_3O_7$	YBCO	
Magnetic Flux	(B)	Gauss
Magnetic Field	(H)	Tesla
Flux Quanta	$\dfrac{h}{2e} = \Phi_o$	Tesla·meters^2
Temperature	K	Kelvin
Angstrom	Å	10^{-12} meters
Permeability of vacuum	μ_o	$4\pi \times 10^{-7}$ N/A^2
Electron charge	e	1.6022×10^{-19} C
Plank's constant	h	6.6261×10^{-34} J·s
Boltzmann's constant	k_b	1.38×10^{-23} J/K

Table of Contents

ix

List of Figures

x

xi

Chapter I. Introduction

This thesis studies the variation of the local current along thin film high-T_c $YBa_2C_3uO_{7-x}$ (YBCO) Josephson junctions. Thin film [001] oriented YBCO grain boundaries and ramp-edge interface engineered junctions were studied using a novel technique that was developed specifically for this thesis. The local transport properties of thin film $24°$ [001] symmetric tilt grain boundaries grown on $SrTiO_3$ substrates and $45°$ [001] asymmetric tilt grain boundaries grown on MgO were studied to understand the local variations of the critical current along the boundary length. The large variations in the local current and the corresponding microstructure have for the first time given direct evidence of parallel conduction channels that have been proposed for grain boundary current transport. The local current distributions and corresponding microstructure of ramp-edge interface engineered Josephson junctions were studied using phase retrieval techniques. The variation of both the current distributions and the underlying microstructure highlights the role that the microstructure plays in controlling the uniformity of junction transport properties.

The unique properties of high-T_c Josephson junctions have been an extremely useful research tool for exploring the fundamental relationships in superconducting systems. Josephson junctions also have the potential for significant device applications if the basic physical properties can be understood and controlled. The realization of

1

practical cost efficient devices has been difficult due to the complex nature of the oxide materials in high-T_c systems.

Originally it was hoped that the new high-T_c materials could simply be substituted for low-T_c materials in existing devices. The major difference and obstacle to direct substitution was the length scale of the superconducting coherence length that is significantly shorter in high-T_c materials. For $YBa_2Cu_3O_{7-x}$ (YBCO) the coherence length in the a-b direction is approximately 1.5 nm (ξ_{a-b} = 1-1.5 nm)(Welp *et al.* 1989), therefore any distortions, structural or chemical, on this length scale will diminish the superconducting properties locally. In high-T_c materials, most high angle grain boundaries create significant distortions on the length scale of the coherence length and thus act as "weak links" (areas of suppressed critical current) to current transport (Dimos *et al.* 1988; Dimos *et al.* 1990). For bulk applications where high current transport is required, weak links are detrimental to possible industrial applications. However, these high angle grain boundary weak links exhibit the Josephson effect that can be used for microelectronic applications. This thesis uses the Josephson properties of high angle grain boundaries to study the local current transport along Josephson junctions.

The Josephson effect is the macroscopic interaction of the superconducting wave function from one side of a junction interfering with the wave function from the other side of a junction. The interference of the two wave functions is extremely sensitive to magnetic fields. The current response to an applied magnetic field can be used as a

magnetic field detector and has been used to fabricate a device known as a SQUID (superconducting quantum interference device). SQUIDs can detect magnetic field variations four orders of magnitude better than any existing technology for magnetic field sensing, and are currently used for biomagnetic applications in the medical field for magnetoencephylograms (MEG) and magnetocardiograms (MCG). These practical applications, along with possible new applications for SQUIDS in the wireless communications industry as high-Q filters, have prompted significant research into the fundamental understanding of Josephson junctions.

One of the most striking features of Josephson junctions is the large variation of their transport properties as reported in the literature. Junctions fabricated with identical processing parameters, and at times within the same batch, have shown two-three orders of magnitude variations in the maximum critical current capacity of the junction. For tilt grain boundary junctions, there are several orders of magnitude variation when the tilt angle is increased form 0° to 45° with these large variations yet to be completely understood. The bulk averaged transport data such at the critical current (I_c) and the normal state resistance (R_n) of grain boundary junctions have been exhaustively studied. The large variations in properties from sample to sample are often indirectly attributed to microstructure variations, local chemistry variations and recently to the symmetry of the order parameter. Unfortunately, there has never been a technique for determining how the current varies locally along the length of the junction. Therefore, most models

assume a current distribution and then indirectly make a correlation between current transport and microstructure and chemistry variations.

This thesis attempts, for the first time, to directly measure the local current transport along the length of a Josephson junction. A novel technique was developed using the Josephson relationship between current variation and an applied magnetic field. The relationship is a Fourier transform relationship where the Fourier modulus is measured experimentally. The technique for calculating the local current distribution involves restoring the phase with a phase retrieval algorithm. This is the standard phase retrieval problem familiar to many areas of physics. The large variations found for the local current distributions are explained in terms of microstructure variations and the underlying symmetry of the order parameter that is locked into the crystal structure of high-T_c superconductors.

This thesis first develops the relevant background information on superconductivity, high-T_c thin films, grain boundary junctions and ramp-edge Josephson junctions. The experimental procedures used to measure the transport data and study the microstructure are outlined and the phase retrieval technique is developed in detail. The experimental data on [001] oriented symmetric thin film 24° tilt grain boundaries, [001] asymmetric 45° tilt grain boundaries and ramp-edge Josephson junctions is detailed and explained in terms of microstructural models and the symmetry of the order parameter.

Chapter II. Background

II.1 Introduction

This chapter reviews the fundamental background information relevant to understand high T_c superconductor and Josephson junctions. The basic electromagnetic theory necessary for understanding the transport properties of high T_c superconductors is presented in terms of basic transport equations. The equations necessary for later discussions and data analysis are presented in detail.

II.2 Background

In 1908 Kamerlingh Onnes liquefied helium (4.2 K) (de Bruyn Outboter 1987). In 1911 he observed that upon cooling mercury to 4.2 K it appeared to loose all of its electrical resistance. This discovery initiated the study of a new class of materials called superconductors that lose their electrical resistance below some transition temperature, T_c. Since the discovery of superconductivity in 1911 many materials, both pure metals and alloys, have been found to be superconductors at low temperature. In 1957 a theory put forth by Bardeen, Cooper and Schieffer, commonly referred to as BCS theory, was able to consistently explain most of the known properties of superconductivity (Bardeen *et al.* 1957). In 1986 Bednorz and Müller discovered a La-Ba-Cu-O material with a perovskite structure and a superconducting transition temperature (T_c) of 30 K (Bednorz

5

et al. 1986). This discovery paved the way for a flood of research activity into high-T_c complex oxide superconductors.

Lanthanum (La) was eventually replaced by yttrium (Y) to create the new compound $YBa_2Cu_3O_{7-x}$ (YBCO) with a T_c of 92 K (Wu *et al.* 1987). The discovery of YBCO was significant because its transition temperature was above the boiling temperature of liquid nitrogen (77 K) making practical superconducting applications economically feasible.

Since the discovery of YBCO, many new oxide superconductors have been discovered with higher T_c values, but none have been as extensively studied as YBCO. The primary reason for the research effort behind YBCO is that high quality epitaxial films with critical current densities in excess of 10^5 A/cm^2 at 77 K necessary for potential microelectronic device applications can be fabricated.

II.3 Superconductor Electrical Transport Properties

The loss of all electrical resistance below a transition temperature (T_c) denotes the onset of superconductivity. In 1956, L.N. Cooper determined that electrons in superconducting systems at a temperature below T_c tend to form pairs (called Cooper pairs) to reduce the total energy of the system (Cooper 1956). The pair consists of two

electrons with opposite spin. They have a mass of 2m (m is the mass of an electron) and a total charge of 2e (e is the charge of an electron). All electrons in a single crystal superconductor exist in a single quantum state described by a complex order parameter ψ containing a phase factor θ and a modulus $|\psi_o|$ where;

$$\psi = |\psi_o| \exp(i\theta).$$
(2.1)

The density of superconducting electrons (n_s) is equal to the square of the order parameter,

$$n_s = |\psi|^2.$$
(2.2)

The parameter ψ is zero above T_c and increases continuously as the temperature falls below T_c. At temperatures below T_c, the paired electrons are said to be "correlated" over a mean distance called the coherence length because they maintain phase coherence with each other. Strictly defined, the coherence length (ξ) can be written as:

$$\xi = \frac{hv_f}{2\Delta\pi^2}$$
(2.3)

where 2Δ is the energy gap and v_f is the Fermi velocity and h is Plank's constant. The coherence length is the distance over which the order parameter can vary appreciably and

is considered a fundamental length in superconductors. The coherence length for most

low-T_c materials is on the order of 10-100 nm. The coherence length for YBCO is 15 Å

in the a-b plane and 3 Å in the c- plane (Oh *et al.* 1988; Welp *et al.* 1989). In general, the

coherence length for high-T_c superconductors is significantly shorter (usually an order of

magnitude) than in low-T_c superconductors.

II.4 Magnetic Properties

A perfect superconductor is a material that exhibits two characteristic properties,

the loss of all resistance below a transition temperature and perfect diamagnetism.

Perfect diamagnetism means that a superconductor does not permit an externally applied

magnetic field to penetrate into its interior. Superconductors that totally exclude an

applied magnetic field are known as Type I superconductors. Type II superconductors

exclude an applied magnetic field when the field strength is low, but only partially

exclude the field at higher strengths. In the region of partial expulsion of the magnetic

field the superconductor is not in a perfect diamagnetic state but rather a complex mixed

state. In general, the superconducting elements are Type I superconductors and alloys

and compounds are Type II superconductors (Poole *et al.* 1995).

II.4.1 Type I. Superconductors

A Type I superconductor is one that exhibits perfect diamagnetism which means that the susceptibility $\chi = -1$. Thus from Maxwell's equations;

$$B = \mu_o H(1 + \chi) = 0 \tag{2.4}$$

$$= \mu_o(H + M)$$

$$M = -H$$

where M is the magnetization and H is the magnetic field. From equation (2.4), the magnetization M is oriented in the opposite direction of the applied field (H) and thus cancels the internal field resulting in a zero field condition inside the superconductor. The requirement that the magnetic field be zero inside a Type I superconductor results in two important consequences of perfect diamagnetism: Flux exclusion and flux expulsion.

Flux exclusion is when a Type I superconductor in the normal state is cooled below T_c in a zero magnetic field environment. When a magnetic field is applied the superconductor excludes the magnetic field from penetrating the material thus maintaining the zero internal field requirement.

Flux expulsion is when a Type I superconductor is placed in a magnetic field at a temperature above T_c where the material is in a normal state. Above T_c, the magnetic field will completely penetrate the sample and have almost the same value inside the material as outside. If the sample is cooled below T_c in the presence of the applied

magnetic field, the field will be expelled from the material to maintain the zero internal field requirement. This phenomenon is known as the Meissner effect.

II.4.2 Type II Superconductors

Type II superconductors behave the same as Type I superconductors for field strengths below a critical field strength H_{c1} (H_{c1} for YBCO $\approx$ 200 Gauss)(Poole *et al.* 1995). Thus for field strengths below H_{c1}, Type II superconductors act as perfect diamagnets and completely exclude applied magnetic fields. For a Type II superconductor above H_{c1} it becomes energetically more favorable for the superconductor to allow magnetic flux penetration into the sample and to form domain walls between superconducting and normal regions containing trapped flux (Poole *et al.* 1995). Therefore, above H_{c1}, magnetic flux is able to penetrate the superconductor in quantized units by forming cylindrically symmetric domains called vortices. The magnetic field inside a Type II superconductor is strong in the normal cores of the vortices and decreases exponentially with distance from the cores. As the magnetic field is increased above H_{c1} the number of vortices, and thus the volume of normal regions, increases. Eventually a magnetic field strength is reached (H_{c2}) above which the vortices have overlapped and formed a continuous normal region with magnetic flux completely penetrating the material. Therefore, above H_{c2}, a Type II superconductor is in the normal state and is no longer superconducting.

Below H_{c1}, the internal magnetic field in a perfect diamagnetic superconductor

is defined to be zero, however in the neighborhood of a boundary, edge effects can result

in non-ideal diamagnetism for a small region of the superconductor near the interface.

Specifically, at the interface between a superconductor and a normal material, the

magnetic field decreases exponentially with increasing distance from the interface into

the superconductor. The variation of the magnetic field with position (H(x)) from the

interface can be written as;

$$H(x) = H_o \exp\left(\frac{-x}{\lambda_L}\right)$$ (2.5)

where H_0 is the externally applied magnetic field value and H(x) is the value of the

magnetic field a distance (x) from the interface and λ_L is defined as the London

penetration depth and is considered a fundamental length scale and material property for

superconductors. Figure 2.1 shows a schematic of the magnetic field intensity variation

near the boundary between a superconducting and normal region. The penetration depth

can be thought of as the distance from the surface that the magnetic field penetrates

inside a perfect diamagnetic superconductor. The penetration depth varies as a function

of temperature and can be written as;

$$\lambda_L(T) = \lambda_o \left[1 - \left(\frac{T}{T_c}\right)^4\right]^{-\frac{1}{2}}$$ (2.6)
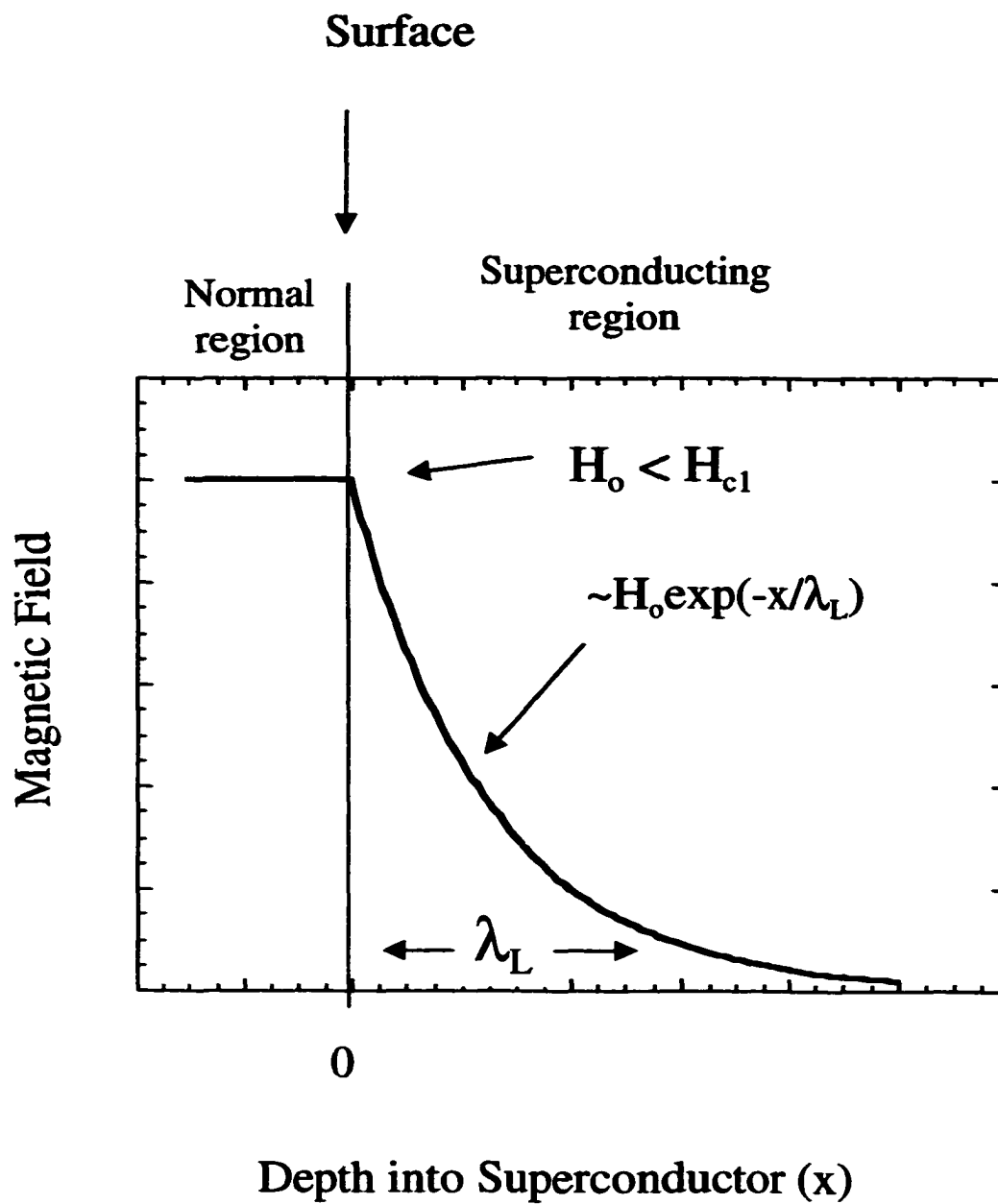
Surface

Figure 2.1 Schematic of the decay of a magnetic field penetration into a superconductor from the surface.

where λ_0 is the penetration depth at 0 K and is an intrinsic property of the material.

Figure 2.2 shows the variation of the penetration depth with temperature. Note that as

$T \rightarrow T_c$ the length of the penetration depth approaches infinity and thus at T_c the magnetic

field completely penetrates the sample and the material is no longer superconducting.

II.4.3 Temperature Variation of Critical Fields

The critical field values H_{c1} and H_{c2} for a Type II superconductor vary as a

function of temperature.   The functional form of $H_c(T)$ is approximated as a power law

written as;

$$H_c \approx H_c(0)\left[1-\left(\frac{T}{T_c}\right)^n\right] \tag{2.7}$$

where n = 2 and is plotted in figure 2.3. For a Type II superconductor, the magnetic field

behavior as a function of temperature can be plotted as a phase diagram with a two phase

"mixed" region separating two single phase regions with the triple point at T_c (see figure

2.4).
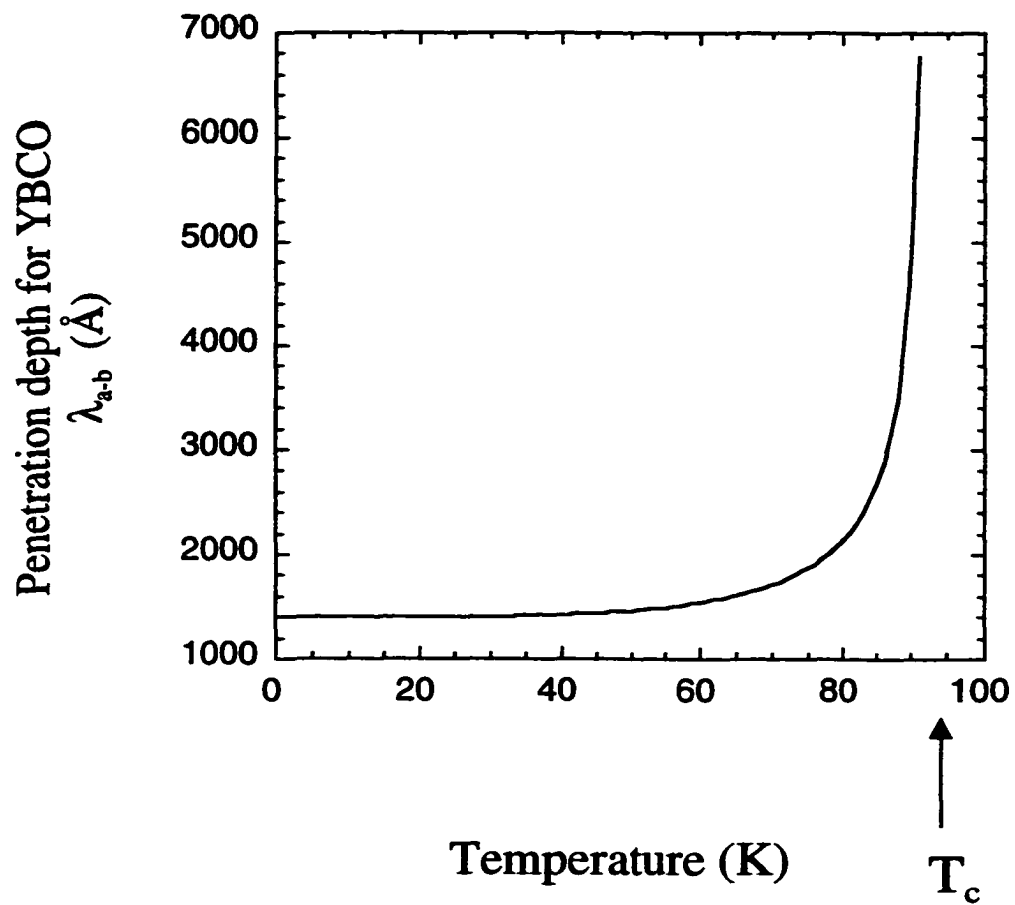
Figure 2.2 Variation of the penetration depth with temperature of YBCO.

$$H_c(T) \approx H_c(0)\left[1 - \left(\frac{T}{T_c}\right)^2\right]$$
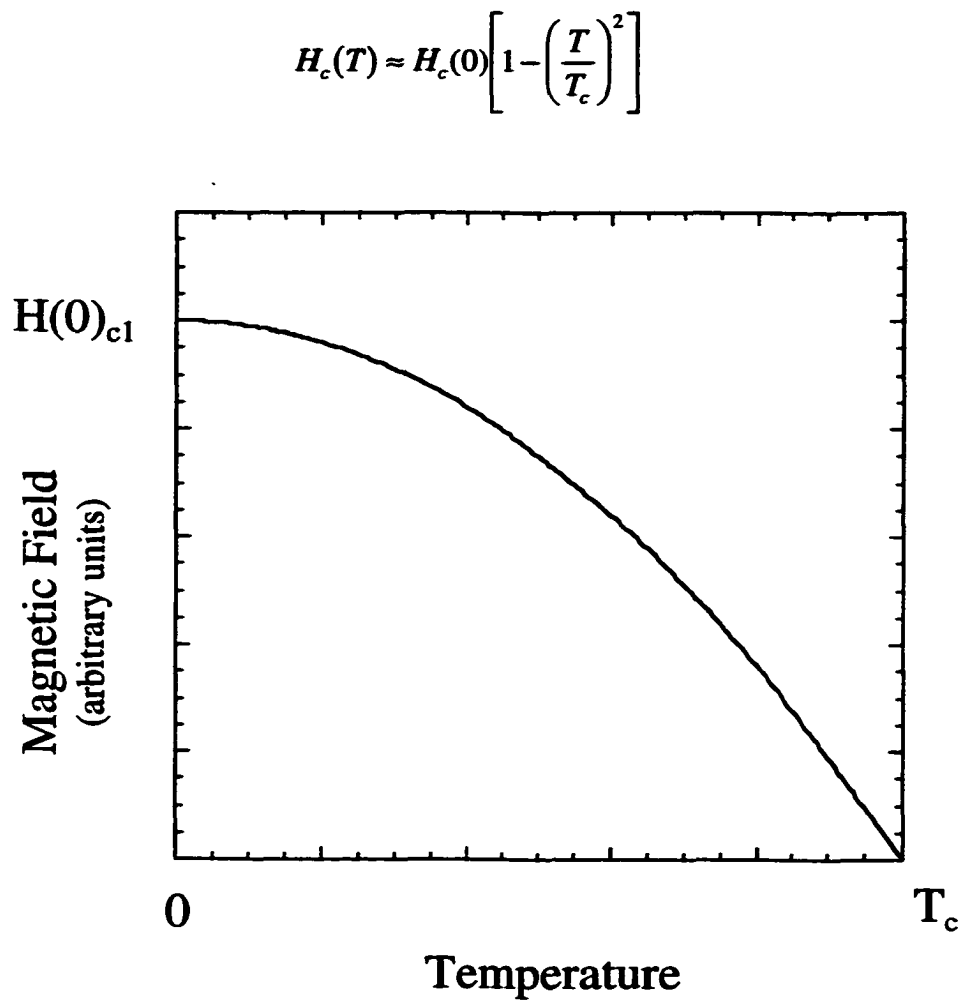
Figure 2.3 Schematic of the temperature variation of the critical field H_{c1} for a superconductor. The first critical field value for for YBCO $\approx$ 200 Gauss.
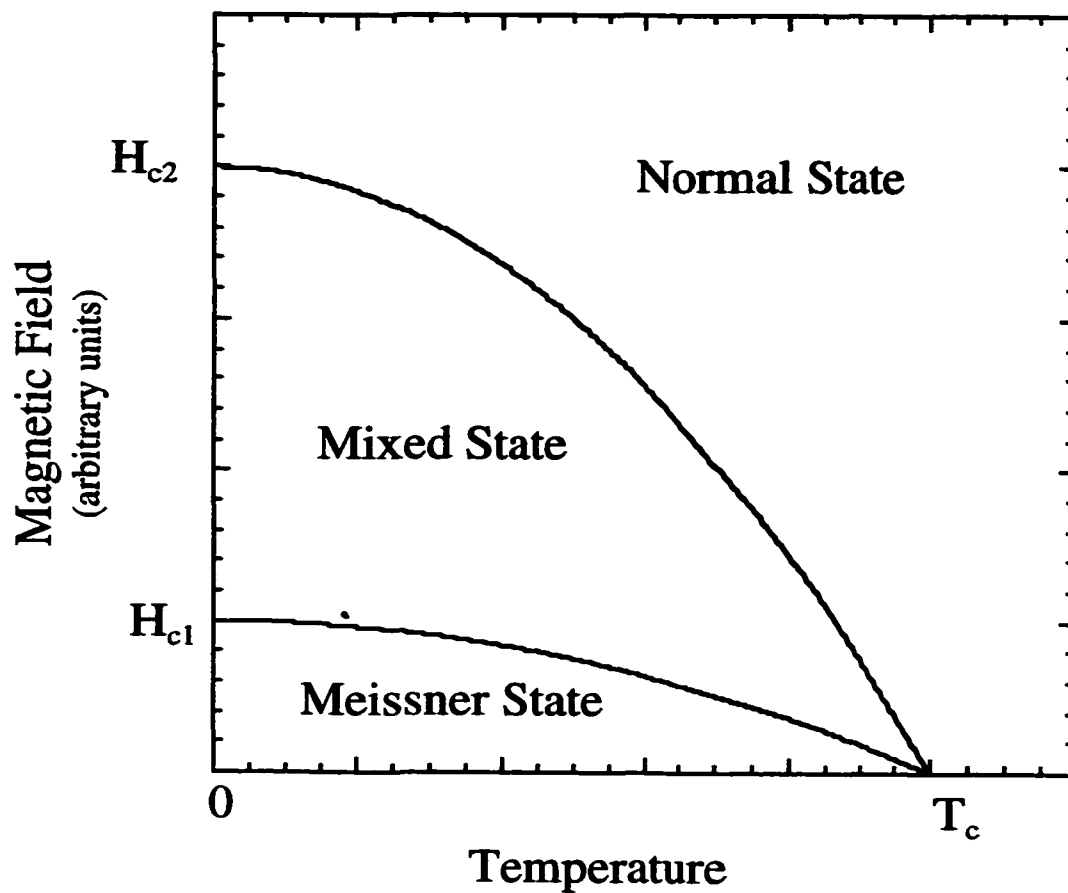
Figure 2.4 Schematic of the Meissner, Mixed and Normal state regions in high-T_c superconductor.

Chapter II.5 Josephson Junctions

In 1962 Brian Josephson predicted that Cooper pairs in a superconductor could

tunnel across a thin insulating layer without a bias across the barrier (Josephson 1962).

Anderson and Rowell verified the prediction in 1963 (Anderson *et al.* 1963). The

superconductor-barrier-superconductor structure that exhibits the Josephson effect is

known as a Josephson junction.

All electrons in a superconductor at a temperature below the transition

temperature share a common phase and can be described by a single wave equation

(Barrone *et al.* 1982)

$$\Psi = n_s^{1/2} \exp(i\phi) \tag{2.8}$$

where ϕ is the phase common to all electrons in the superconductor and n_s is the electron

density ($|\psi|^2$). Considering the two superconductors of figure 2.5, when the

superconductors are far apart the phase of each superconductor can change

independently. If the barrier is too thin it is possible for coherence to be maintained

across the barrier and thus the system behaves as one superconductor. As the

superconductors are brought closer together they reach a distance at which Cooper pairs

can flow from one superconductor to the other. The long-range order of the

superconductor is transmitted across the boundary and the phase of each is said to be

barrier

Length (x)

current

Superconductor | Superconductor

Film thickness
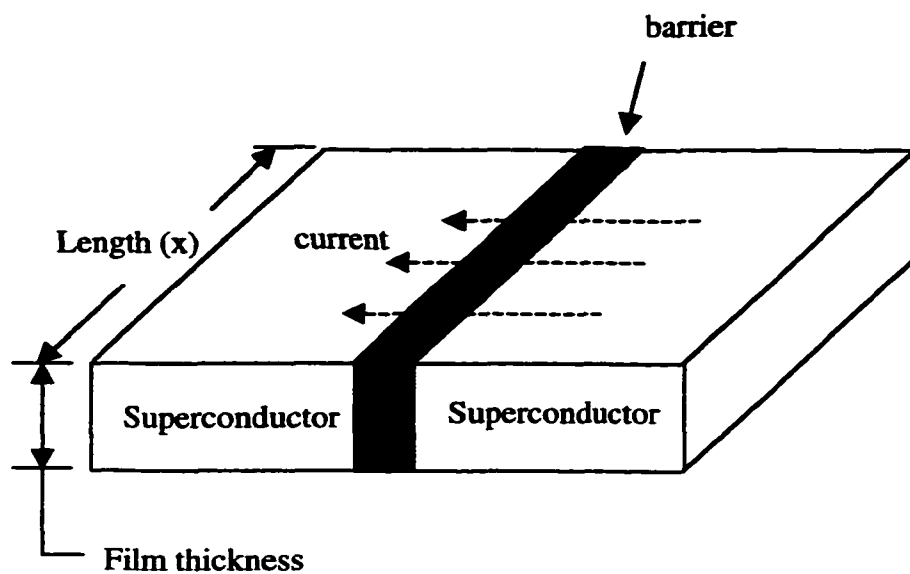
$$J = J_0 \sin(\theta)$$

$$\theta = \theta_{right} - \theta_{left}$$

Figure 2.5 Schematic of Josephson junction geometry showing two superconducting electrodes separated by a thin barrier layer. The junction length in the (x) direction is shown.

"correlated" across the boundary. The resulting current of Cooper pairs (J) tunneling across the barrier is related to the phase difference of the two superconductors by:

$$J = J_c \sin(\phi) \tag{2.9}$$

$$\phi = \phi_l - \phi_r \tag{2.10}$$

Where $\phi_l - \phi_r$ is the difference between the phase on the left and right hand side of the junction (see figure 2.5).

Josephson derived five differential equations that relate the difference in the superconducting macroscopic wave-function phase across the Josephson barrier layer. In conjunction with equation (2.9) the four remaining equations of motion can be written as;

$$\frac{\partial \phi}{\partial x} = 2\pi d \frac{By}{\Phi_o} \tag{2.11}$$

$$\frac{\partial \phi}{\partial y} = 2\pi d \frac{Bx}{\Phi_o} \tag{2.12}$$

$$\frac{\partial \phi}{\partial t} = \frac{4\pi e V}{h} \tag{2.13}$$

$$\frac{\partial H_y}{\partial x} - \frac{\partial H_x}{\partial y} = J_z + C\frac{\partial V}{\partial t}$$

(2.14)

where C is the capacitance per unit area of the junction, V is the junction voltage, H and B are the magnetic field components ($B = \mu_o H$), d is the junction width and Φ_0 is defined as one flux quanta $\left(\frac{h}{2e}\right)$.

II.6 Magnetic Field Behavior of Josephson junctions

This thesis will consider experimentally the direct current (d.c.) steady state transport measurements of Josephson junctions. The mathematical details of the steady state will be considered in this section.

The five equations of motion that describe the transport process in a Josephson junction suggest that the phase difference across a junctions (ϕ), and thus the current crossing the junction, can be modified by an applied magnetic field (H). If a steady state is assumed $\left(\frac{\partial}{\partial t}\right) = 0$, then equation (2.12 and 2.13) are equal to zero. If the thickness of the junction is negligible, as is the case for a thin film junction, the phase difference in the y direction $\left(\frac{\partial \phi}{\partial y}\right)$ can be assumed to be zero. Therefore equation (2.11) can be integrated and written as;

$$\phi(x) = 2\pi d \frac{B_y}{\Phi_o} x + \phi_o$$

(2.15)

where d is the thickness of the barrier, x is the position along the boundary perpendicular to the magnetic field and ϕ_o is an integration constant. From equation 2.15, for a constant magnetic field, the phase varies linearly with position along the length of the junction. Substituting equation (2.15) into equation (2.9), the current density along the boundary becomes:

$$J(x) = J_o(x) \sin\left(2\pi d \frac{B_y}{\Phi_o} x + \phi_o \right)$$

(2.16)

From equation (2.16), the current crossing the boundary layer is modulated in a sinusoidal fashion by both the magnetic field and the position along the boundary in the x direction (see figure 2.5 for the definition of the x direction). If the local current density $J_o(x)$ from equation (2.16) is assumed to be constant along the length of the junction ($J_o(x)$ = constant), then integrating the current along the length of the boundary (L), the total current as a function of an applied magnetic field becomes:

$$I_c(H) = I_{c,o} \left| \frac{\sin(\Phi / \Phi_o)}{(\Phi / \Phi_o)} \right|$$

(2.17)

where the total current $I_c = J_c/A$ and A is the cross-sectional area of the junction,

$\Phi_o = \left(\dfrac{h}{2e}\right)$ and Φ is equal to $H\mu_{oy}Ld$. Equation (2.17) is the Fraunhofer diffraction

equation familiar to many areas of physics and is plotted in figure (2.6). It highlights the

important similarities between the magnetic field behavior of Josephson junctions and the

diffraction process.

The geometry of the junction plotted in figure 2.6 was assumed to be rectangular

and the local current J(x) along the length of the junction was assumed to be constant thus

simplifying to the Fraunhofer pattern. For a general boundary where J(x) ≠ constant, the

critical current as a function of an applied magnetic field is defined by the Fourier

transform of the current density along the junction length:

$$I_c(u) = \left| \int_{-\infty}^{\infty} J(x)\exp(iux)dx \right| \tag{2.18}$$

$$u = (2\lambda_L + d)\dfrac{2\pi H}{\Phi_o} \tag{2.19}$$

where x is the distance along the junction, λ_L is the London penetration depth

($\lambda_L \approx 140$ nm for YBCO) and d is the thickness of the junction barrier (Josephson 1962).
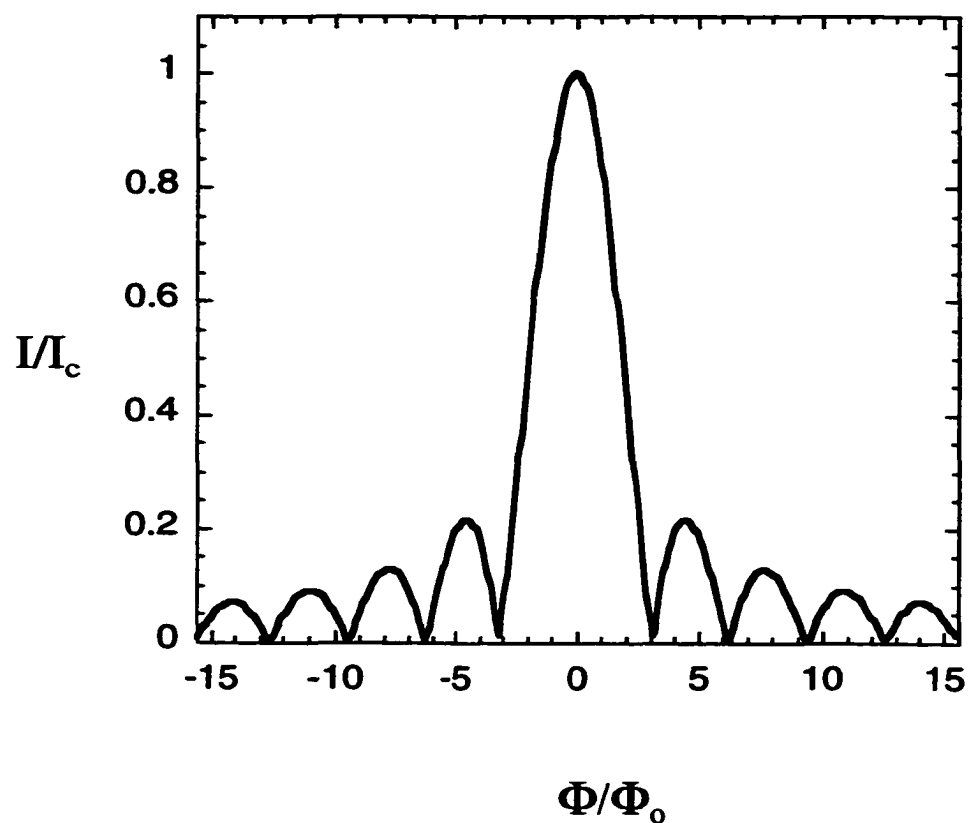
Figure 2.6 Critical current oscillations as a function of an applied magnetic field for an ideal Josephson junction with J(x) = constant along the length of the boundary.

Equation (2.18) suggest that it may be possible to obtain information about the local

current J(x) by measuring $I_c(u)$. This relationship will be exploited in later chapters.

II.7 Current Voltage Characteristics

Stewart and McCumber modeled the d.c. driven current-voltage characteristics of

Josephson junctions using a resistively shunted junction model (RSJ model) where a

Josephson element, capacitive element and a resistive element are placed in parallel (see

figure 2.7)(Stewart 1968; McCumber 1968).

The total current flowing through the circuit as a function of time is:

$$I(t) = I_c \sin(\phi(t)) + GV(t) + C\frac{dV(t)}{dt} \qquad (2.20)$$

Rearranging the terms, it is possible to write;

$$\beta_c = \left(\frac{4\pi e}{h}\right)\left(\frac{I_c C}{G^2}\right) \qquad (2.21)$$

$$\theta = \frac{2eI_c t}{hG} \qquad (2.22)$$

$$G = 1/R$$
$$C = \text{Capacitance}$$
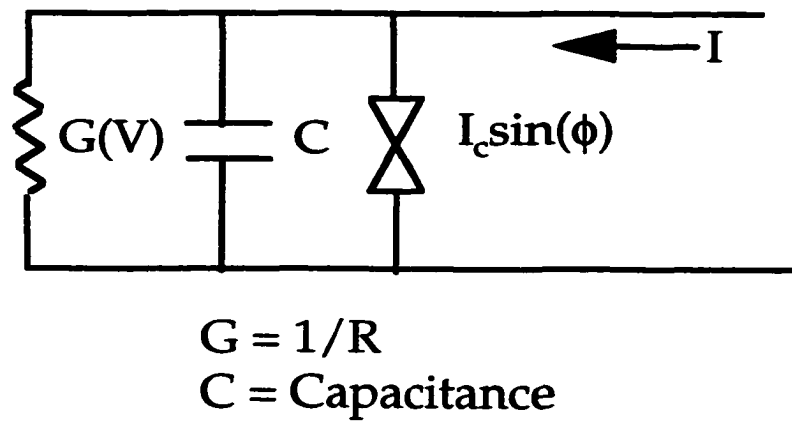
Figure 2.7 Schematic of R.S.J. circuit diagram with a resistive element, capacitive element and a Josephson element all in parallel.

Then equation (2.20) can be written as;

$$\frac{I}{I_c} = \beta_c\left(\frac{d^2\phi}{d\theta^2}\right) + \left(\frac{d^2\phi}{d\theta^2}\right) + \sin(\phi)$$ (2.23)

where β_C is known as the Stewart-McCumber parameter and is the ratio of the capacitance to conductance in the junction (Stewart 1968; McCumber 1968). High-T_c Josephson junctions can be modeled by a zero capacitance ($C = 0$, $\beta_c = 0$) R.S.J. model where the voltage drop across the boundary reduces to:

$$V = I_c R_n\left(\left(\frac{I}{I_c}\right)^2 - 1\right)^{\frac{1}{2}}$$ (2.24)

where I_C is the critical current and R_n is the normal state resistance. Figure 2.8 shows a plot of equation 2.24 and highlights the general shape of a typical current-voltage response of a high T_c Josephson junction. The crucial information obtained from I-V data is the critical current (I_c) and the normal state resistance (R_n) which is the slope of the I-V curve in the linear region at high voltages.
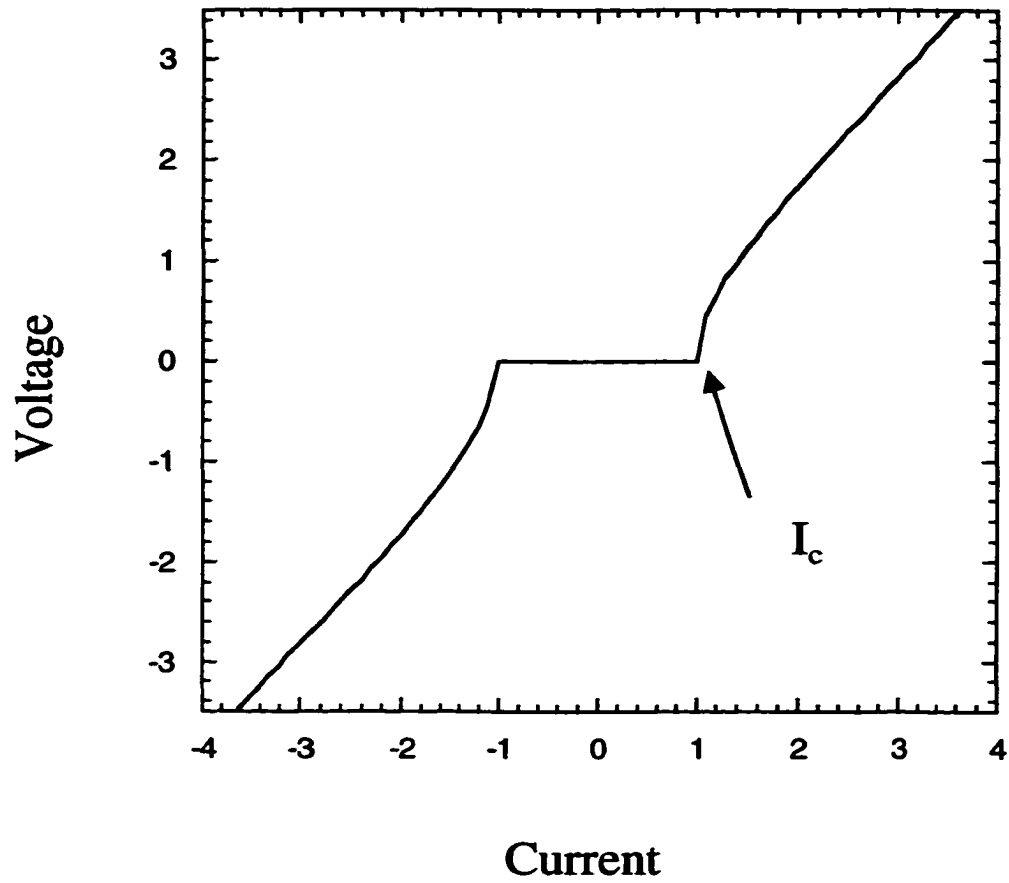
Figure 2.8 R.S.J. model IV curve showing I_c and the linear normal region.

II.8 Josephson Penetration Depth

Junctions that have large tunneling currents traversing them may have self-induced magnetic fields that modify the current density distribution along the length of the boundary. The Josephson penetration depth (λ_J) is defined as the distance from the edge of the junction that carries most of the tunneling current.

$$\lambda_J = \left(\frac{h}{4\pi e J_c (2\lambda_L + d)} \right)^{\frac{1}{2}}$$

(2.25)

Equation (2.25) is used as the criterion for determining if self-field effects are important. Junctions are usually classified as long or short junctions, and are considered long if the width of the junction (W) is larger than $4\lambda_J$. Junctions wider than $4\lambda_J$ have most of the current contained at the edges of the junction. A large edge current can induce a magnetic field at the center of the junction and decrease the phase difference (ϕ) across the barrier. Junctions that have widths of less than $4\lambda_J$ are considered short junctions. Self-induced magnetic fields are assumed to be negligible in the short junction limit and thus the magnetic field along the length of the junction is believed to be uniform and constant. For YBCO, if the junction width is less than ≈ 5 μm the junction is within the short junction limit and self-field effects can be ignored.

Chapter III. YBa$_2$Cu$_3$O$_{7-x}$

The highly directional properties and fabrication difficulties encountered while working with high-T$_c$ superconductor are directly attributable to their complex crystal structures. It is important to understand the crystal structure of YBCO and the resulting stoichiometric relationships to be able to understand the transport properties of YBCO grain boundaries and how the transport properties across gain boundaries can be related to microstructural and chemical variations.

III.1 YBa$_2$Cu$_3$O$_{7-x}$ Structure

In 1987 Wu and co-workers discovered a compound YBa$_2$Cu$_3$O$_{7-x}$ (YBCO) with a T$_c$ of 92 K (Wu *et al.* 1987). The discovery of YBCO was significant because its transition temperature was above the boiling temperature of liquid nitrogen (77 K). YBCO has been extensively studied because of its high transition temperature and the ease with which high quality epitaxial films can be grown.

YBa$_2$Cu$_3$O$_{7-x}$ (YBCO) has an oxygen deficient perovskite structure (see figure 3.1). The crystal structure of the superconducting phase is orthorhombic (Pmmm symmetry, a$\neq$b) with lattice parameters for x=0.07: a=3.82 Å, b=3.89 Å and c=11.68 Å. YBa$_2$Cu$_3$O$_{7-x}$ is a non-stoichiometric oxide where the properties are

29
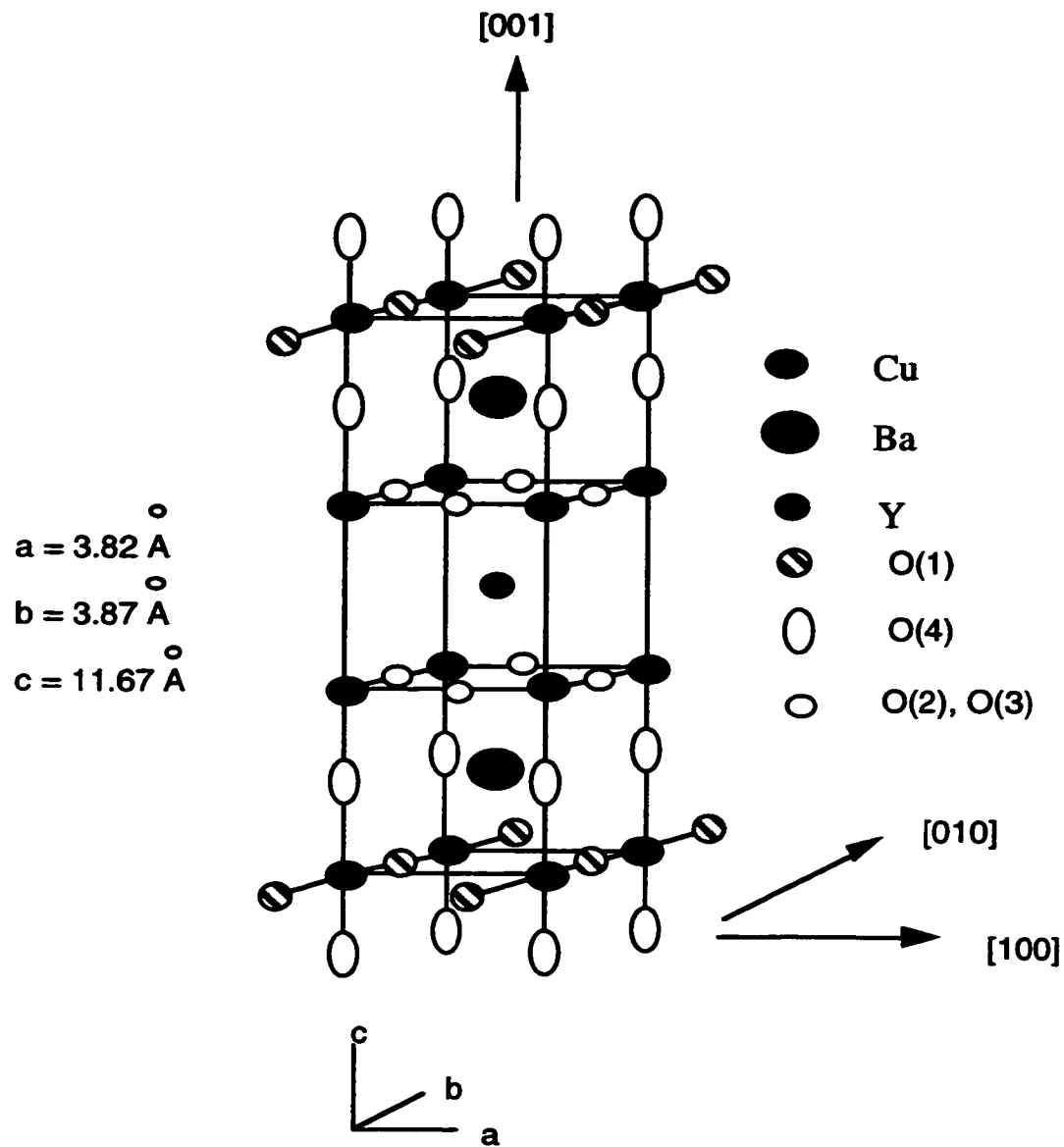
Figure 3.1 YBa$_2$Cu$_3$O$_{7-x}$ oxygen deficient orthorhombic crystal structure.

dependent on the oxygen content. The oxygen varies for x=0 to x=1 with a orthorhombic to tetragonal (P4/mmm) phase transition at x=0.6. As the oxygen content changes from x=0 to x=1 the O(1) site oxygens (see figure 3.1) are removed while the O(2), O(3) and O(4) sites remain fully occupied (Jorgensen *et al.* 1987; Jorgensen*et al.* 1990; Marezio 1991; Cava *et al.* 1990).

YBCO is a Type II superconductor with highly anisotropic transport properties because of its complex crystal structure. The CuO planes, which are responsible for current transport, are highly coupled in the a- and b- directions and weakly coupled in the c- direction. Thus there are large variations in transport properties between the c- direction and the a- and b- directions. Due to the very small variation between the a- and b- axis lattice parameter (a= 3.82 Å, b = 3.89 Å), the a- and b- axis directions are usually not distinguished from one another when referring to material properties. However, the properties are often cited separately for the a-b direction and the c- direction.

The superconducting transition temperature (T_c) is dependent on the oxygen stoichiometry. The orthorhombic to tetragonal phase transition is related to the dependence of T_c on oxygen content. The orthorhombic phase is the superconducting phase while the tetragonal phase is semiconducting. Figure 3.2 shows the dependence of T_c on oxygen content for YBCO. Cava *et al.* (Cava *et al.* 1990) proposed that the CuO planes are responsible for carrying the supercurrent. Each unit
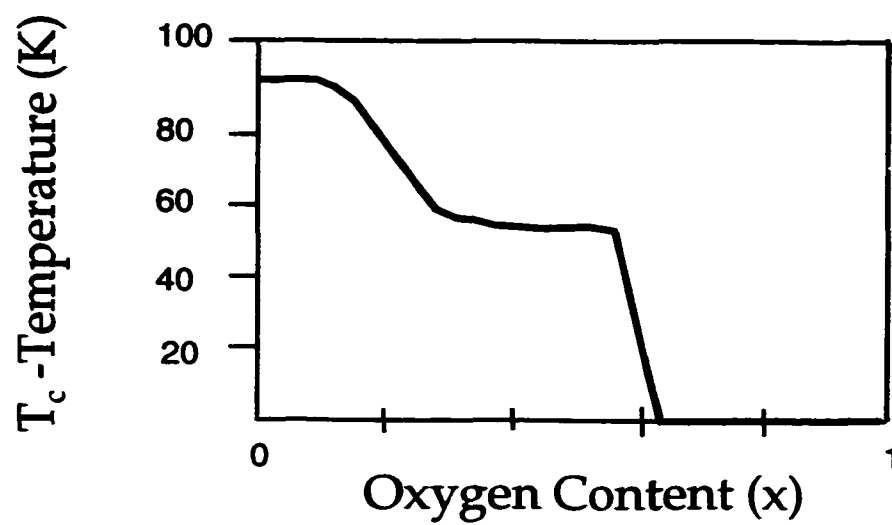
Figure 3.2 T_c vs. oxygen content for YBCO. (from Marezio *et al.* 1991)

cell has two CuO_2 planes that carry the supercurrent with the O(2) and O(3) oxygen and two CuO planes that act as charge reservoirs that supply the conduction planes with carriers. As the oxygen content is decreased, oxygen from the CuO chains are removed until there are no O(1) sites occupied. The two plateau behavior of YBCO shown in figure 3.2 has been attributed to a change in valence of the Cu(2) atoms which lie in the CuO_2 planes. Understanding the variation of T_c with oxygen stoichiometry can be important since local deviations of the oxygen content due to defects and grain boundaries can cause local areas of suppressed T_c (Marezio *et al.* 1991).

III.2 YBa2Cu3O7-x Thin Films

The growth of thin YBCO films has been extensively studied by numerous research groups (Buchholz *et al.* 1994; Duray *et al.* 1991; Huang *et al.* 1998; Scholm 1992a; Schlom *et al.* 1992b). Thin epitaxial films have been grown in various orientations on many different substrates and using a variety of different growth techniques including chemical vapor deposition, co-evaporation, pulsed laser ablation and e-beam evaporation (Chaudhari *et al.* 1987; Giess *et al.* 1990; Hollmann *et al.* 1994; Schieber 1991a; Schieber 1991b). Studies using atomic force microscopy (AFM) and transmission electron microscopy (TEM) have examined the growth mechanism for YBCO thin films (Streiffer *et al.* 1990; Mannhart *et al.* 1993). The growth of YBCO in the a-b plane is significantly faster than in the c- axis direction.

During the early sages of film growth small nuclei are formed that are 2-3 unit cells high which propagate and grow in the a-b direction. These steps act as favorable ad-sites for the depositing film.

YBCO film growth has been shown to be highly sensitive to substrate defects sites such as steps or dislocations that act as nucleation sites. Atomic force microscopy work by Mannhart *et al.* showed screw dislocations emanating from the substrate's surface defects (Mannhart *et al.* 1993). This type of growth is believed to be the result of disruptions at the substrate surface caused by the substrate defects, followed by incoherent growth of the film around the nuclei. The screw dislocations propagate through the film by ledge growth which spiral upward as the film grows laterally. Mannhart *et al.* resolved the ledge height to be 11 Å (which is approximately one unit cell height in the c- direction) with scanning tunneling microscopy (STM)(Mannhart *et al.* 1993). This growth mechanism has been termed step flow growth since it is neither layer-by-layer growth, Stranski-Krastanov (S-K) growth or island growth. The step flow growth mode has been observed with YBCO films grown on numerous substrates, therefore seems to be independent of the substrate. The spiral ledge growth (step-flow) is important to grain boundaries since the lateral growth of the spirals cause an overgrowth of the boundary plane and result in a meandering grain boundary that will be discussed later.

III.3 YBa₂Cu₃O₇₋ₓ Grain Boundary Properties

This section will detail the current understanding of YBCO Josephson

junctions and grain boundary transport.   YBCO is a Type II superconductor with

highly anisotropic properties due to the crystal structure and the conduction along the

CuO planes. The basic understanding of high-T_c superconductors comes from work

on low-T_c materials. Most of the high-T_c transport concepts were adapted from low-

T_c theories and have been subsequently modified to fit existing experimental data.

The current carrying capacity of a superconductor is a fundamental concern

for potential industrial applications of high-T_c superconductors. It was found by Ekin

et al. that grain boundaries act as weak links in polycrystalline high-T_c films (Ekin *et*

al. 1987). Strictly defined, a weak link is a region of suppressed superconductivity.

Any structural defect of the same length scale as the coherence length is capable of

locally destroying superconductivity.   The coherence length of YBCO is defined in

equation (1.3) is ξ_oa-b = 1.25 nm in the a-b plane and in the c- direction (ξ_oc = 0.3

nm). High angle grain boundaries provide sufficient structural distortion locally to

reduce the order parameter at the boundary and create a weak link. The weak link

nature of grain boundaries is highly detrimental to high current carrying applications

such as power transmission lines where a maximum current must be driven along the

wire. High-T_c research in high current carrying superconductors has led to the study

of low angle grain boundaries and single crystals with relatively high current carrying

capacities.

The transport properties of high-T_c grain boundaries were found to depend

sensitively on the misorientation angle of the boundary. The critical current crossing

a grain boundary as a function of boundary orientation ($J_c(\theta)$) has been studied for

thin film [001] tilt grain boundaries. Figure 3.3 shows the basic bicrystal tilt grain

boundary geometry. For a given boundary symmetry, the supercurrent (J_c) crossing

the boundary was found to decrease approximately exponentially with increasing

misorientation (θ) from $0°$ to $45°$ (see figure 3.4). Ivanov and coworkers found that

besides the angular dependence of the current on the grain boundary plane, the

relative orientation of the grain boundary with respect to the bicrystal substrate has a

significant influence on J_c (Ivanov *et al.* 1991a; Ivanov *et al.* 1991b). Dimos and

coworkers studied [100] twist and [100] tilt boundaries and found that the angular

dependence of the current $J_c(\theta)$ was the same as that found for [001] tilt boundaries

(Dimos *et al.* 1991; Gross 1992; Ivanov *et al.* 1991a; Ivanov *et al.* 1991b; Mannhart

et al. 1998).

III.4 Magnetic Properties

Grain boundaries with misorientation angles between ~ $15°$ and $45°$ were

found to exhibit the Josephson effect which may be potentially useful in
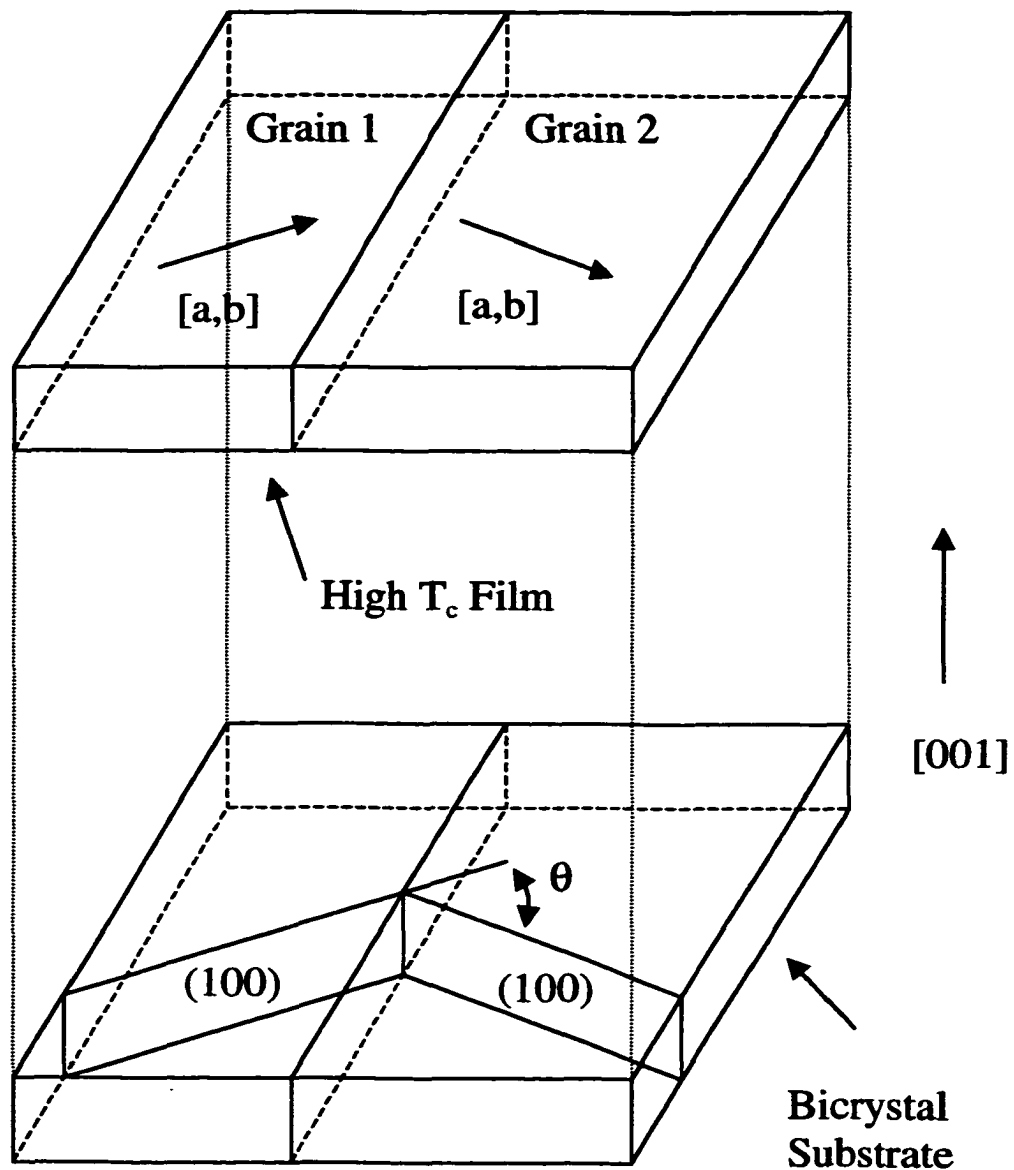
Figure 3.3 Schematic of the bicrystal geometry where a substrate with a tilt grain boundary with a misorientation of θ is used as a template for thin film growth.
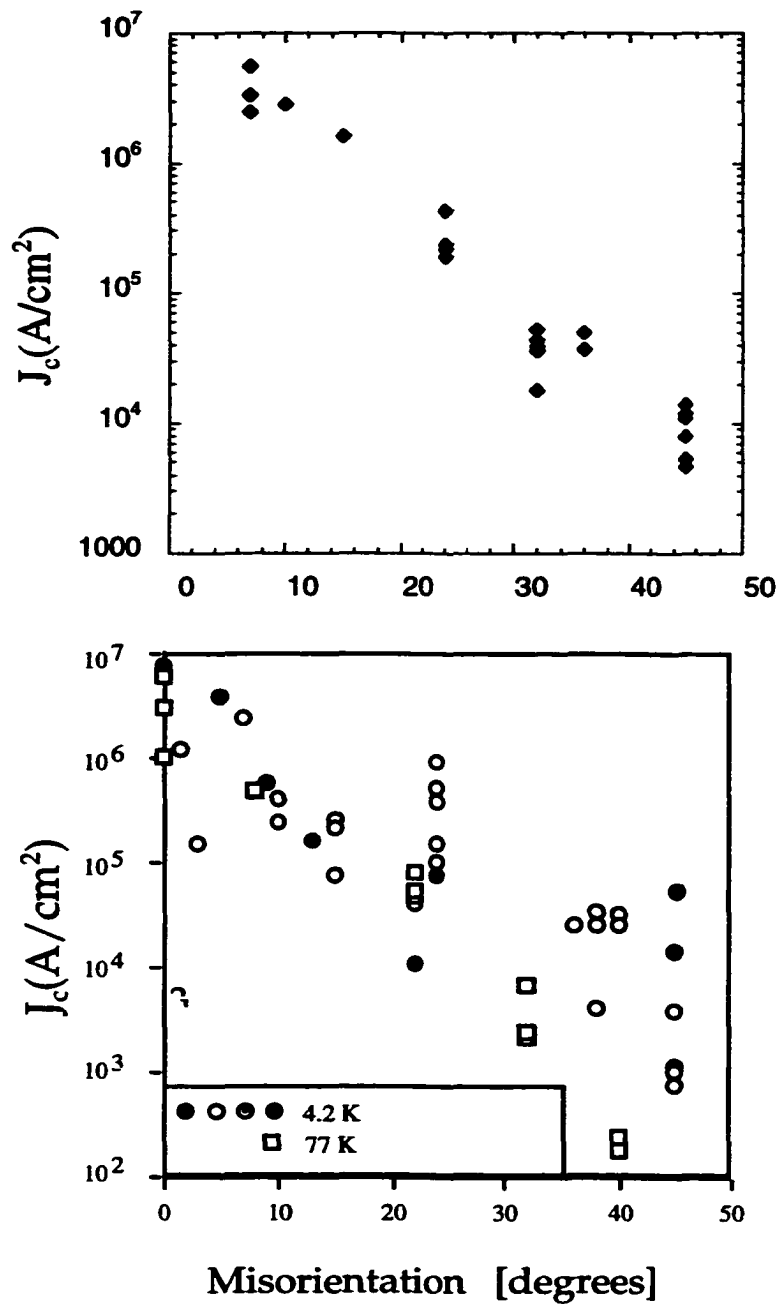
Figure 3.4 Critical current as a function of misorientation angle (J(θ)).
(from Mannhart *et al.* 1998 top and Dimos *et al.* 1991)

microelectronic applications. The critical currents in high-T_c grain boundaries show large variations with an applied magnetic field which is angular dependent. Low angle grain boundaries (less than ~ 15°) are insensitive to an applied magnetic field. For misorientation angles above 15° Josephson oscillations of the current are observed. The magnetic field dependence of the critical current across thin film grain boundary junctions has been studied by numerous groups (Beck *et al.* 1996; Carmody *et al.* 1999; Carmody *et al.* 2000; Daumling *et al.* 1992; Froehlich *et al.* 1995; Humphreys *et al.* 1993a; Humphreys *et al.* 1993a; Lathrop *et al.* 1991; Mannhart *et al.* 1996; Mayer *et al.* 1993; Nesher *et al.* 1997; Rosenthal *et al.* 1991; Sarnelli *et al.* 1993b; Sarnelli *et al.* 1993c; Schuster *et al.* 1993; Xiu *et al.* 1999). For tilt angles near 15° the magnetic field oscillates in a Fraunhofer type behavior (Humphreys *et al.* 1993; Nesher *et al.* 1997). As the tilt angle is increased, variations in the magnetic field patterns are observed to increase until at 45° the patterns observed are often non-Fraunhofer in shape with large maximum currents located at H ≠ 0 (Copetti *et al.* 1995; Hilgenkamp *et al.* 1996; Mannhart *et al.* 1996a; Mannhart *et al.* 1996b). Mannhart and coworkers have extensively studied the magnetic field behavior of 45° tilt grain boundaries. They have reported a distinct difference in the magnetic field patterns between symmetric and asymmetric grain boundary configurations. They report that 45° [001] asymmetric tilt grain boundaries in YBCO show large variations from the ideal Fraunhofer pattern with J_c ~ 0 at zero applied magnetic field (H = 0), and that symmetric 45° boundaries have magnetic field patterns with the maximum J_c (J_c,max) at H = 0 similar to the ideal Fraunhofer pattern. Copetti and coworkers have

reported similar results with some of their asymmetric 45° grain boundaries showing

$J_c$max at magnetic fields other than zero while some of their data suggest that $J_c$max

for asymmetric 45° boundaries is at H = 0 (Copetti *et al.* 1995). Recent work by

Mannhart *et al.* showed the dominant role that the symmetry of the order parameter

has in controlling the current response in 45° tilt boundaries (Mannhart *et al.* 1996;

Mannhart *et al.* 1998; Mannhart *et al.* 1999). Chapter IV will outline the important

concepts of d-wave symmetry and highlight the aspects relevant to transport along

high-T_c grain boundaries.

Studies of the current response for YBCO grain boundary junctions at high

magnetic fields (1-5 T) show oscillations of the current at high magnetic fields

(Daumling *et al.* 1992; Froehlich *et al.* 1995; Sarnelli *et al.* 1993a; Sarnelli *et al.*

1993b; Sarnelli *et al.* 1993c). These oscillations have been explained in terms of

small length scale inhomogeneities along the length of the grain boundary. These

measurements suggest that the current can vary locally at near angstrom (Å) length

scales for grain boundary junctions. Calculations of the correlation function from

magnetic field data also suggests current variations on the sub-nanometer length scale

(Alff *et al.* 1994; Beck *et al.* 1996; Froehlich *et al.* 1995a; Froehlich *et al.* 1995b;

Schuster *et al.* 1993; Xiu *et al.* 1997; Zappe 1975).

III.5 Resistive Transition

The temperature dependence of J_c across a grain boundary changes almost linearly over a wide temperature range. At temperature near T_c, the thermal energy exceeds the Josephson coupling energy, causing thermally activated phase slippage (TAPS) of the phase angle by 2π which manifests as boundary resistance below T_c. The boundary resistance can be identified as a foot structure in a RT curve of the grain boundary (Gross 1992). The resistance transition can be used to understand the critical temperature as well as some of the normal state properties of the grain boundary. The RT curve of a grain boundary usually has two distinctive transitions. As the temperature of the junction is increased from low temperatures, the grain boundary will transform from a superconducting state to a resistive state (if the boundary is a weak link). As the temperature is increased further, the two adjacent grains will transform from a superconducting state to a resistive state.

Theoretically the phase transition from the superconducting state to the non-superconducting state is an abrupt transition, however experimentally it has been shown that the onset of superconductivity is often gradual. Bednorz and Muller reported a gradual decrease in resistivity near T_c in their first article on the new superconductors (Bednorz et al. 1986). Recent work on single crystal YBCO has shown a sharp transition of approximately 0.3 K at T_c. Factors such as alloying elements, crystal strain and microstructure play a key role in determining the

abruptness of the superconducting transition. The foot-structure resistance across a

single grain boundary has been modeled by Liu and co-workers as a series of

thermally activated conduction channels (Liu *et al.* 1995).

III.6 Current-Voltage Characteristics

Most high angle grain boundary junctions with misorientation angles between

15° and 45° can be modeled as a strongly coupled SNS (superconductor-normal-

superconductor) junction (Mannhart *et al.* 1988). The basic transport behavior is that

of a zero capacitance $(C = 0, \beta_c = 0)$ resistively shunted junction (RSJ) model

described in Chapter II. The shape of the I-V curve follows a standard RSJ type

model as plotted in figure 2.8. The basic I-V measurement gives the critical current

(I_c) of a particular cross-section of boundary. The measurement is performed with the

current being ramped up across the boundary until a specific offset voltage is

measured (typically 1 μV). Voltages above the offset voltage define the normal state

of the material. The weak-link nature of grain boundaries was first identified by I-V

measurements. The normal state resistance (R_n) can be determined from the slope of

the I-V curve at high voltages. The I_cR_n product is considered a characteristic value

of a junction and is used as a key design parameter. The normal state resistance is

usually considered independent of temperature and thus most of the variation of the

I_cR_n product is due to the variation of I_c with temperature.

The shape of the I-V curve can be indicative of the type of junction behavior.
Most high angle grain boundaries can be described as RSJ junctions. When the zero
capacitance assumption is enforced, the voltage onset is sharp. At higher
temperatures, near T_c, the voltage onset can become more rounded indicating a flux-
flow type behavior as opposed to the RSJ-type behavior.

The maximum supercurrent that can be driven across a grain boundary I_c
varies as a function of temperature between 0 Kelvin and T_c. The temperature
variation of the critical current $I_c(T)$ can be used to analyze the junction type.
Ambegaokar *et al.* demonstrated that the scaling behavior of a junction can identify
the difference between low-T_c S-N-S and S-I-S junctions (Ambegaokar *et al.* 1963).
The temperature dependence of the critical current for a grain boundary junction can
be written as

$$I_c(T) = I_{c,0}\left(1 - \frac{T}{T_c}\right)^n.$$

(3.1)

According to Ambegaokar and Baratoff, the temperature dependence of the critical
current for a superconductor-normal metal-superconductor (S-N-S) junction can be
modeled with n = 2. For a superconductor-insulator-superconductor (S-I-S) junction,
the $I_c(T)$ behavior can be modeled with n = 1. The critical current as a function of
temperature for most high-T_c grain boundary junctions can be modeled with n = 2

indicating a thin normal region at the grain boundary. However, the boundary

structure is often complex with no clear normal layer identifiable.

III.7 Grain Boundary Structure

A general grain boundary has five macroscopic degrees of freedom (DOF)

which can be represented by (a) a magnitude of the relative rotation θ that would

bring the grains into perfect registry, (b) the axis of relative rotation, and (c) the

orientation of the boundary (Merkle $et\ al.$ 1990; Merkle $et\ al.$ 1991; Wolf $et\ al.$ 1989).

When the axis of rotation is perpendicular to the boundary, a pure "twist boundary" is

formed which consists of a grid of pure screw dislocations. When the axis of rotation

is parallel to the boundary plane, a pure tilt boundary is formed which consists of an

array of pure edge dislocations.

The transport properties of a grain boundary can vary due to the structural

features along the boundary. Variations of the structure on the same length scale as

the coherence length can cause disruption of the phase coherence across the boundary

and thus vary the current transport along the boundary. On the macroscopic scale,

precipitates and boundary phases can cause interruptions of the current flow along the

boundary.

On the microscopic scale, variations near the length scale of the coherence

length can cause interruptions of current flow. Microstructural investigations of

YBCO grain boundaries using TEM techniques have found significant variations

along the length of the grain boundary. The boundary structure of high-T_c low angle

tilt boundaries ($\theta < 15°$) follow standard dislocation theory (Chisholm *et al.* 1989;

Gao *et al.* 1991). To accommodate the lattice mismatch at the boundary, an array of

discrete edge dislocations is formed. The dislocations are separated by well lattice

matched regions. For symmetric pure tilt boundaries (see figure 3.5) the spacing of

the edge dislocations can be written as;

$$D = \frac{b}{2\sin(\theta/2)} \tag{3.2}$$

where θ is the tilt angle, b the Burgers vector and D the dislocation spacing.
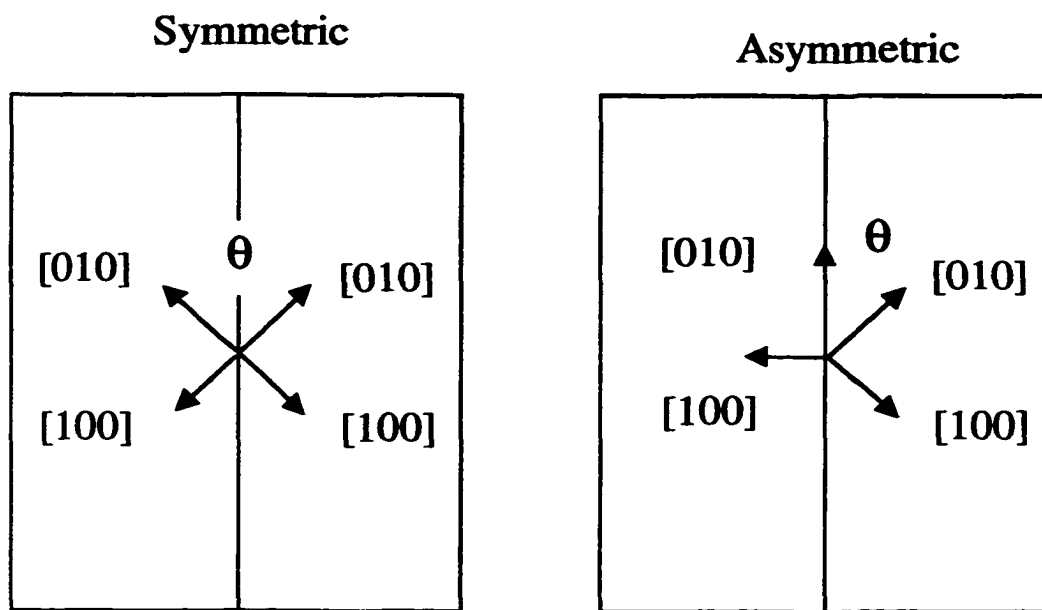
Figure 3.5 Symmetric and asymmetric tilt geometry with tilt angle θ.

Models have been put forth that correlate the decrease in critical current across a

grain boundary with increasing grain boundary tilt and the spacing of the

accompanying dislocations where the current density crossing the grain boundary

plane J_{GB} can be written as;

$$J_{GB} = J_{grain} \frac{(D - 2r_m)}{D}$$ (3.5)

where D is the spacing between dislocations and r_m is the radius of the grain boundary

core (Dimos *et al.* 1990; Chisholm *et al.* 1991).

For high angle boundaries ($\theta > 15°$) the dislocations merge and form a

continuous layer which in many cases is highly inhomogeneous. The general

microstructure along high angle grain boundaries has three distinct structural

characteristics; precipitates, faceting and meandering (Alarco *et al.* 1993; Babcock *et

al.* 1988; Babcock *et al.* 1989; Batson 1993; Browning *et al.* 1998; Chang *et al.* 1990;

Chan 1994; Chisholm *et al.* 1989; Chisholm *et al.* 1991; Dimos *et al.* 1988; Dravid *et

al.* 1993; Gao *et al.* 1991; Jia *et al.* 1992; Kabius *et al.* 1994; Kroeger *et al.* 1998;

Laval *et al.* 1991; Miller *et al.* 1995; Nakahara *et al.* 1987; Nucker *et al.* 1989;

Nucker *et al.* 1990; Ravi *et al.* 1990; Rosner *et al.* 1992; Seo *et al.* 1995; Traeholt *et

al.* 1994; Tsu *et al.* 1998; Vuchic *et al.* 1996; Wen *et al.* 1999; Yu *et al.* 1997;

Zandbergen *et al.* 1988).

Various oxide precipitates (usually a copper oxide or yttrium oxide depending on the growth method of the film) have been reported to decorate the length of the grain boundary for YBCO films. The precipitates can disrupt the current flow along the length of the boundary. However, most microstructural work has reported precipitates along only a small faction of the boundary length.

Thin film grain boundaries generally do not follow the template of the bicrystal substrate, rather they meander typically on a length scale similar to that of the film thickness. The meandering is due to the overgrowth and interpenetrating islands of YBCO across the grain boundary plane (Miller *et al.* 1995). Figure 3.6 shows a schematic of the boundary meandering. To accommodate for the boundary meandering, thin film YBCO grain boundaries form facets. The orientation and length of the facets is dependent on the extent of boundary meandering, the orientation of the adjacent grains, the substrate, defects and film growth conditions. The faceting takes place in three dimensions and has been observed in most YBCO grain boundaries. YBCO grain boundaries usually consist of facets with orientations corresponding to the bicrystal misorientation and the low-index planes of one of the grains such as (100) or (110) type facets. The length of the individual facets is typically < 100 nm. Recent work has been shown that the rate of the film growth can

YBCO

[001]

bicrystal substrate
grain boundary
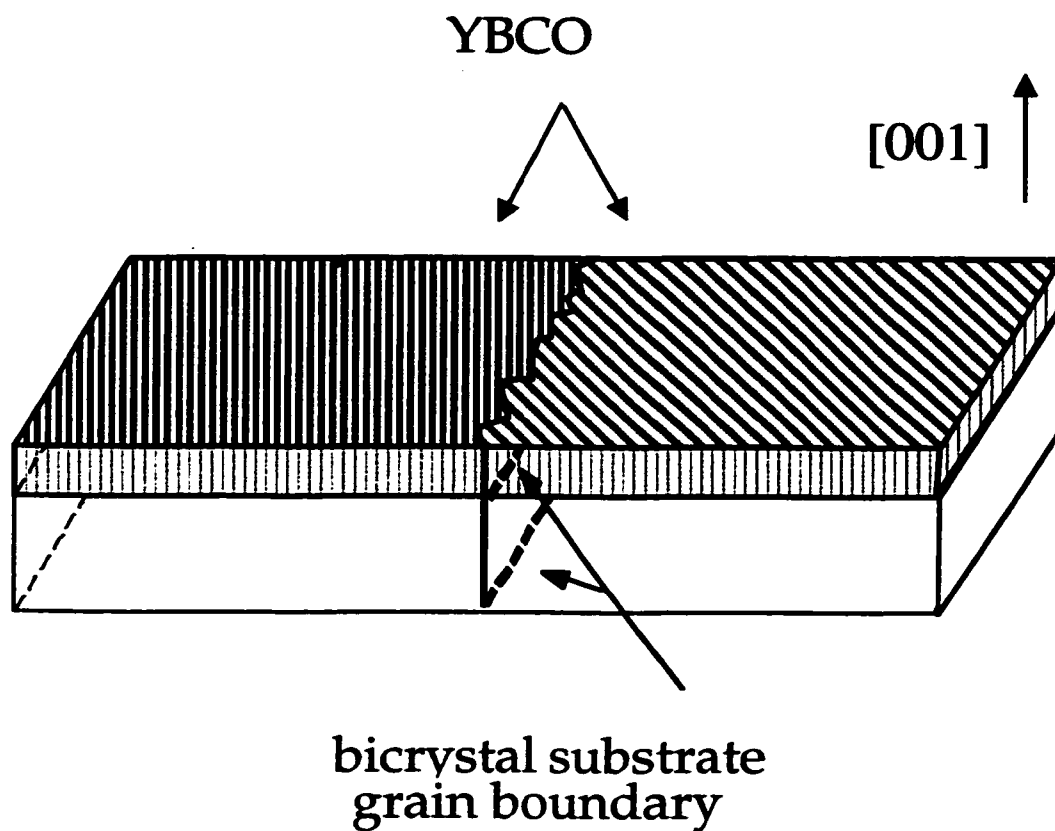
Figure 3.6 Schematic of grain boundary meandering along straight bicrystal
substrate.

be used to control the length of the facets with slower growth rates producing longer
facet lengths (Zhang *et al.* 1996).

III.8 Twin Boundaries

YBCO forms (110) type twins where the a- and b- axes reverse in order to
relieve strain upon cooling through the tetragonal to orthorhombic phase transition.
Thin films in YBCO can be highly twinned because of the structural constraint of the
substrate. Twin boundaries in YBCO were studied extensively and were shown not
to exhibit any weak link behavior such as a reduced critical currents relative to the
bulk (Fleshe *et al.* 1993; Gyorgy *et al.* 1990; Kwok *et al.* 1990; Welp *et al.* 1994).
Therefore, twin boundaries should not effect the Josephson junction current
measurements of this study. However, twin boundaries can act as pinning sites for
magnetic flux and thus can increase the critical current density for samples in low
magnetic fields.

III.9 Grain Boundary Chemistry

The transition temperature of YBCO and therefore the critical current has
been shown to be strongly dependent on the oxygen content (Marezio *et al.* 1991). In
general, the chemical content of the grain boundary is very significant in controlling
the transport properties along the boundary. Variations in the boundary stoichiometry

can result in secondary phases or precipitates forming along the boundary plane

which can act to disrupt supercurrent flow. Several studies confirm stoichiometric

variations at the grain boundary. Auger electron spectroscopy revealed that the grain

boundary plane tended to be rich in Cu and deficient in O relative to the adjacent

grains (Babcock *et al.* 1989; Chiang *et al.* 1988; Kroeger *et al.* 1988). Babcock *et al.*

and Shin *et al.* used energy dispersive spectroscopy (EDS) to study the local

boundary composition with a 5-8 nm spatial resolution revealing the grain boundary

was Cu rich and O deficient at various locations along the boundary (Babcock *et al.*

1988; Babcock *et al.* 1989; Shin *et al.* 1989).

Nücker correlated the oxygen content and the oxygen pre-edge structure using

electron energy loss spectroscopy (EELS)(Nucker *et al.* 1989; Nucher *et al.* 1990).

The hole carriers were determined to be at the oxygen O(4) sites. The local hole

carrier concentration along the boundary plane was determined using parallel electron

energy loss spectroscopy (PEELS) by various groups (Babcock *et al.* 1994; Batson

1993; Browning *et al.* 1992; Dravid *et al.* 1993; Zhu *et al.* 1993b). PEELS work by

Browning *et al.* on symmetric and asymmetric tilt boundaries found significant

difference between the two. Asymmetric boundaries were found to be oxygen

depleted while no oxygen depletion was found for symmetric boundaries. This work

suggested that there could potentially be significant differences in transport data

between symmetric and asymmetric grain boundaries, however, no transport

measurements of the samples used for the study were performed. Dravid *et al.*

studied the hole carrier concentration along the length of the grain boundary plane
(Dravid *et al.* 1993). Both symmetric and asymmetric boundaries with various
misorientation angles have been studied.

The variation of the oxygen content between the two adjacent grains and the
grain boundary plane as well as the variation of the oxygen content along the length
of the boundary indicate the strong role that the local stoichiometry plays in
determining the transport properties of the grain boundary. Unfortunately, little direct
correlation work between transport properties and local chemistry has been
performed. Also, little work has been reported that elucidates the difference between
local microstructure effects and local chemistry effects on boundary transport.

III.10 Grain Boundary Transport Models

Attempts have been made to model the transport data of high temperature
grain boundaries using microstructural information. Many models are capable of
describing some of the reported transport data, however, none are completely
successful at describing all of the known data. Most models are based on empirical
data and thus lack the power of direct correlation. The first model was proposed by
Dimos *et al.* who argued that the critical current density was proportional to the
spacing of the dislocations along the grain boundary because the dislocation cores
produced significant structural disorder on the length scale of the coherence length

and thus destroyed the superconductivity locally (Dimos *et al.* 1988). Consequently, as the tilt angle of a boundary is increased, the density of dislocations also is increased. Therefore the spacing between dislocations decreases resulting in a reduction of I_c with increasing tilt angle. TEM work confirmed the network of edge dislocations for low angle grain boundaries, however, at higher angles the cores overlap and thus the model breaks down (Gao *et al.* 1991a).

Sarnelli *et al.* modeled the boundary considering high magnetic field data of grain boundary junctions (Sarnelli *et al.* 1993a; Sarnelli *et al.* 1993c). The model is known as the Dayem bridge model and consists of a series of Dayem bridges lying in parallel along the boundary (Dayem *et al.* 1967). A Dayem bridge defines a constriction in a superconductor down to the size of the coherence length and was developed from low-T_c superconductors. Close to T_c the Dayem bridge model predicts a dependence of equation (3.1) with $n = 2$. Although this model is highly suggestive and useful, it is difficult to directly confirm the model.

Others expanded upon the Dayem bridge model incorporating information about the local carrier concentration at the boundary. Specifically, the varying oxygen content along the length of a boundary was included in the Dayem bridge model. Thus regions with different carrier concentration would have different transport properties. The modified model by Dravid *et al.* also argued that the average distance between the various regions would be greater than the Dayem bridge

model would predict (Dravid *et al.* 1993). The Dayem bridge model predicted variation at the same length scale as the coherence length, while the modified models suggested that the variation would occur at the 20-50 nm length scale.

Moeckly *et al.* worked out another grain boundary model by studying the electromigration of oxygen (Moeckly *et al.* 1993). The boundary was modeled as consisting of parallel superconducting filaments across a normal resistive junction. The superconducting filaments are assumed to be randomly distributed along the length of the boundary. The average width of the filaments was estimated to be between the coherence length (1.5 nm) and a correlation length determined from magnetic field data but usually on the μm scale. Figure 3.7 shows a schematic of the boundary model proposed by Moeckly. The non-superconducting regions are assumed to exist due to oxygen disorder caused by structural consideration of the grain boundary geometry and electromigration of the oxygen due to applied current biases. Early also suggested a model similar to the one proposed by Moeckly (Early *et al.* 1994).

All of the models are successful at describing some of the measured transport data, however, none can completely describe all the existing data. All of the models are based on the total current measured crossing the boundary, not direct information about the local current variation, therefore no direct correlation between transport data and microstructure has been possible. Mannhart described another model based

on the symmetry of the order parameter and will be discussed in detail in chapter

IV(Mannhart *et al.* 1996). The Mannhart model has been successful at understanding

the behavior of 45° tilt boundaries that show anomalous magnetic field responses.

Grain boundary plane

☐ - superconducting regions

■ - highly disordered, highly resistive "normal" regions

▨ -disordered superconducting regions
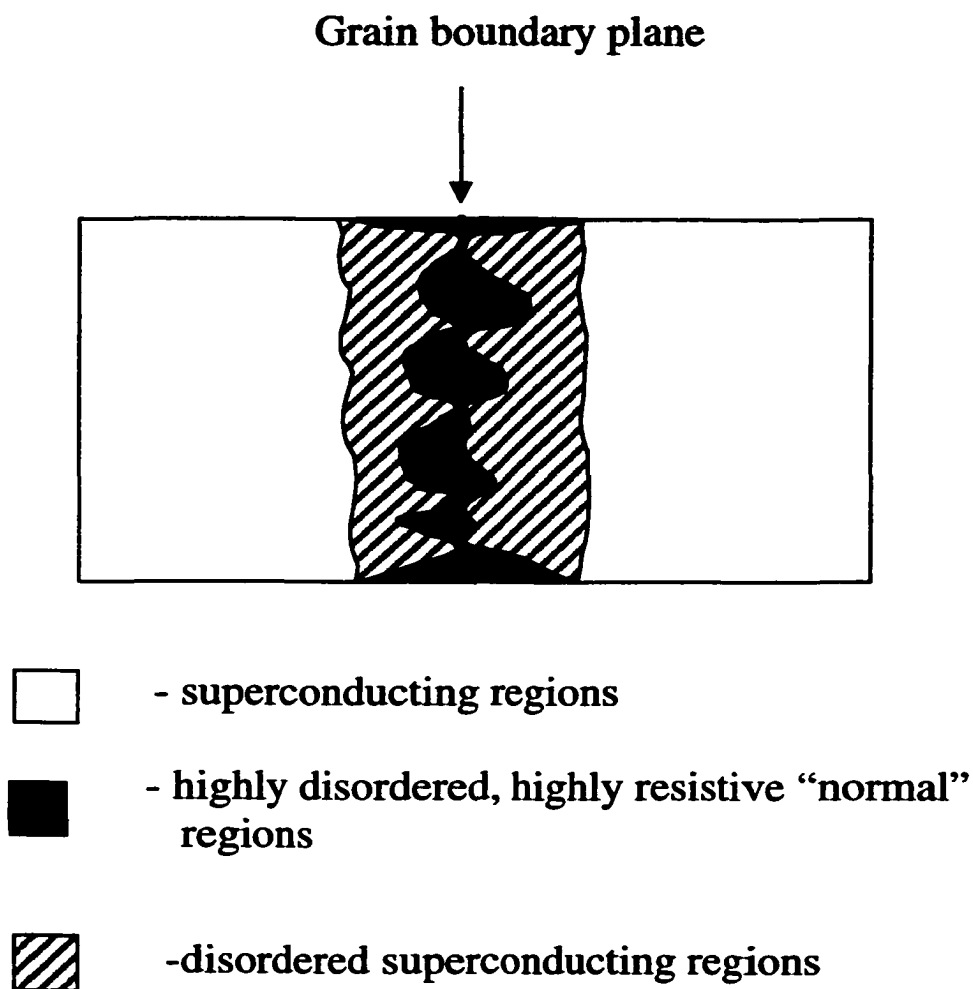
Figure 3.7 Schematic of grain boundary model from Moeckly *et al.* showing the grain boundary as being composed of large areas that carry little or no supercurrent separated by well connected regions that carry the majority of the total current (Moeckly *et al.* 1993).

Chapter IV. Symmetry of the Order Parameter

IV.1 Introduction

Most high-T_c superconductors are characterized by a predominant $d_{x^2-y^2}$ symmetry of the order parameter describing the superconducting condensate. The highly directional wave function plays a dominant role in determining the transport properties of high angle grain boundary Josephson junctions and can be used to explain the anomalous magnetic field data for 45° tilt grain boundaries. This chapter highlights the key concepts of d-wave symmetry and details the role of the order parameter symmetry in grain boundary transport.

IV.2 Order Parameter Symmetry

The order parameter ψ in a superconducting system is defined in chapter II as;

$$\psi = |\psi_o| \exp(i\theta). \tag{4.1}$$

The electromagnetic transport equations for low -T_c superconductors were developed assuming s - wave (spherical) symmetry of the order parameter and have been successful in explaining most of the low-T_c experimental data. The spherical symmetry of the order parameter suggests non-directional transport properties. Thus the relative orientation of

57

the two adjacent grains across a grain boundary in a s-wave superconductor should have minimal effect on the boundary transport.

Phase sensitive tricrystal experiments on high T_c superconductors suggest that the symmetry of the order parameter for YBCO is $d_{x^2-y^2}$ (Tsuei *et al.* 1994; Miller *et al.* 1995; Iguchi *et al.* 1994; Wollman *et al.* 1993). Figure 4.1 shows a schematic of the basic s - and $d_{x^2-y^2}$ wave geometry. It has been argued that the symmetry of the order parameter is locked into the underlying crystal lattice of YBCO and thus controls the highly directional properties measured in grain boundary junctions. Still other experiments have shown that there is also a substantial s-wave component to YBCO. Thus it appears that the order parameter symmetry of YBCO is of a mixed character being partly s-wave and partly $d_{x^2-y^2}$. From chapter III, the crystal symmetry of the superconducting phase of YBCO is orthorhombic. The distinct Cu-O bond length in the a- and b- directions with the CuO_2 planes allows for an arbitrary mixing of the d- and s-wave components.

The highly directional geometry of the $d_{x^2-y^2}$ wave function allows for angular dependent transport properties. Figure 4.2 is a schematic of the tilt grain boundary geometry. When the tilt angle $\theta = 0°$ the interaction of the two wave functions from each side of the grain boundary is similar to that for an s-wave superconductor. As the
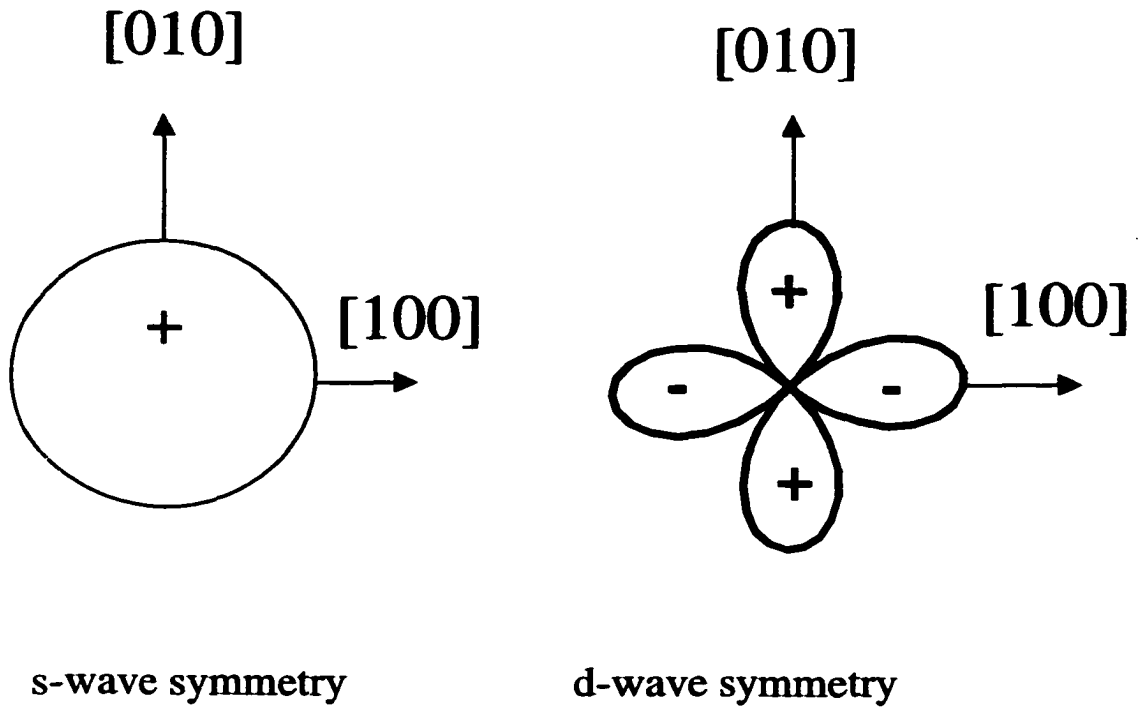
Figure 4.1 Schematic of s-wave and $d_{x^2-y^2}$ geometry. The geometry of the wave function is locked into the crystal structure of the superconductor.
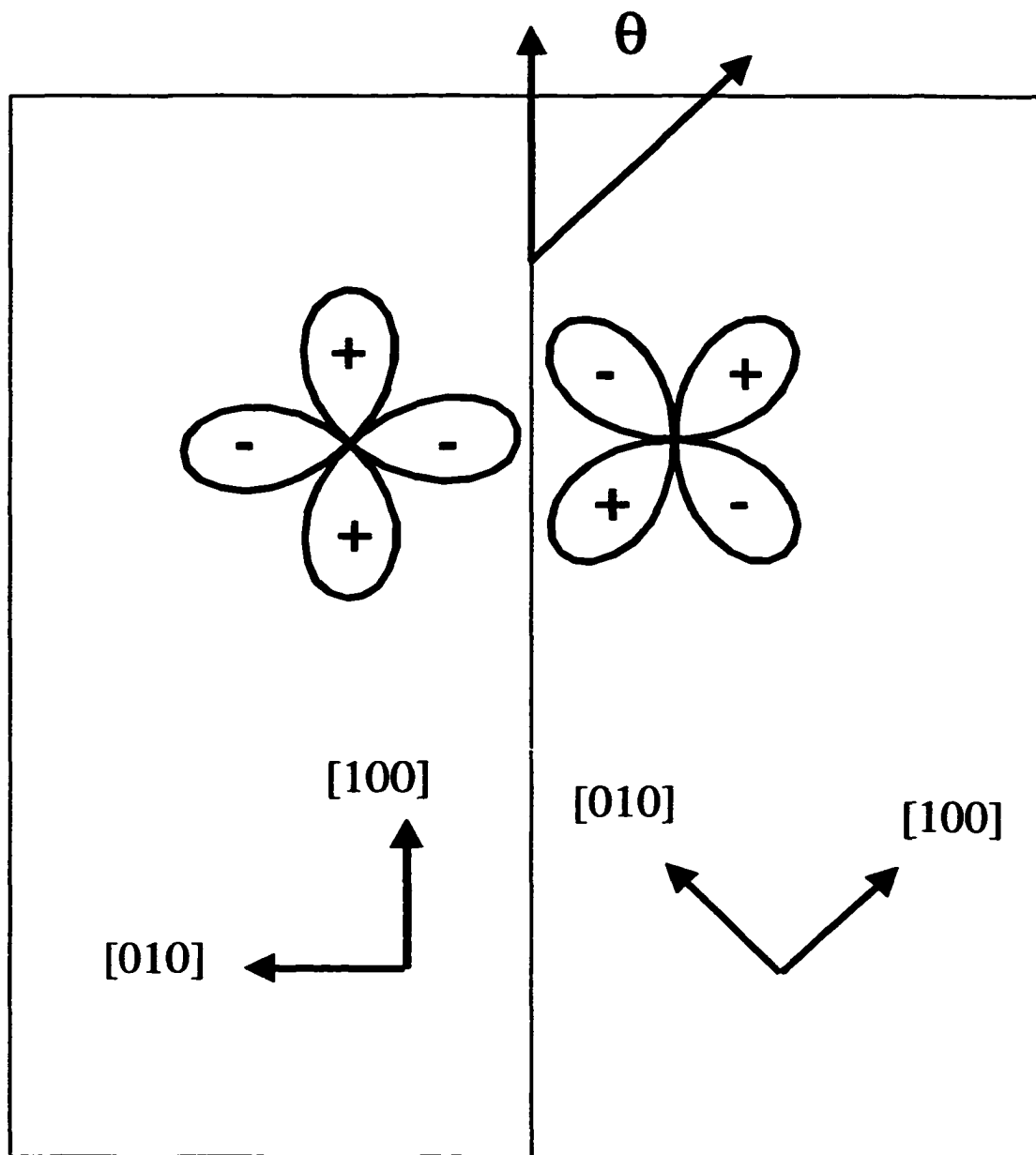
Figure 4.2 Asymmetric tilt boundary configuration. As the tilt angle is increased from 0° to 45° the symmetry of the order parameter plays in increasing significant role. At 45° there exists a node-lobe alignment across the boundary plane.

tilt angle is increased, the d-wave symmetry of the order parameter starts to play an increasingly dominant role in controlling the current transport. When the tilt angle is increased to 45° a unique condition exists where the node of one wave function can be aligned across the grain boundary to a lobe of another wave function. Thus there theoretically should exist no current transport across 45° tilt boundaries. Critical current vs. applied magnetic field measurements for 45° boundaries have shown near zero critical currents at zero applied magnetic field (see figure 4.3).

Critical current vs. applied magnetic field measurements for most high angle grain boundary junctions have Fraunhofer like $I_c(H)$ patterns with large current peaks centered about H = 0 and smaller oscillations of the current at higher field values (see figure 4.4). When the tilt angle is less than 45° the critical current vs. applied magnetic field data can be described by existing standard s-wave models. There have been a series of experiments in which the correlation function (defined by equation 4.2);

$$C(x) = \left| \int_{-\infty}^{\infty} |I_c(H)|^2 \exp[i\phi(x)]dx \right| \tag{4.2}$$

was calculated for 24° grain boundary junctions to obtain spatial information about the local current variation J(x). Critical current vs. applied magnetic field measurements $I_c(H)$ were performed for 24° grain boundary junctions and the correlation function was calculated for each of these samples (Froehlich *et al.* 1995; Beck *et al.* 1996; Schuster *et al.* 1993; Nesher *et al.* 1997; Xiu *et al.* 1997). High magnetic field results show
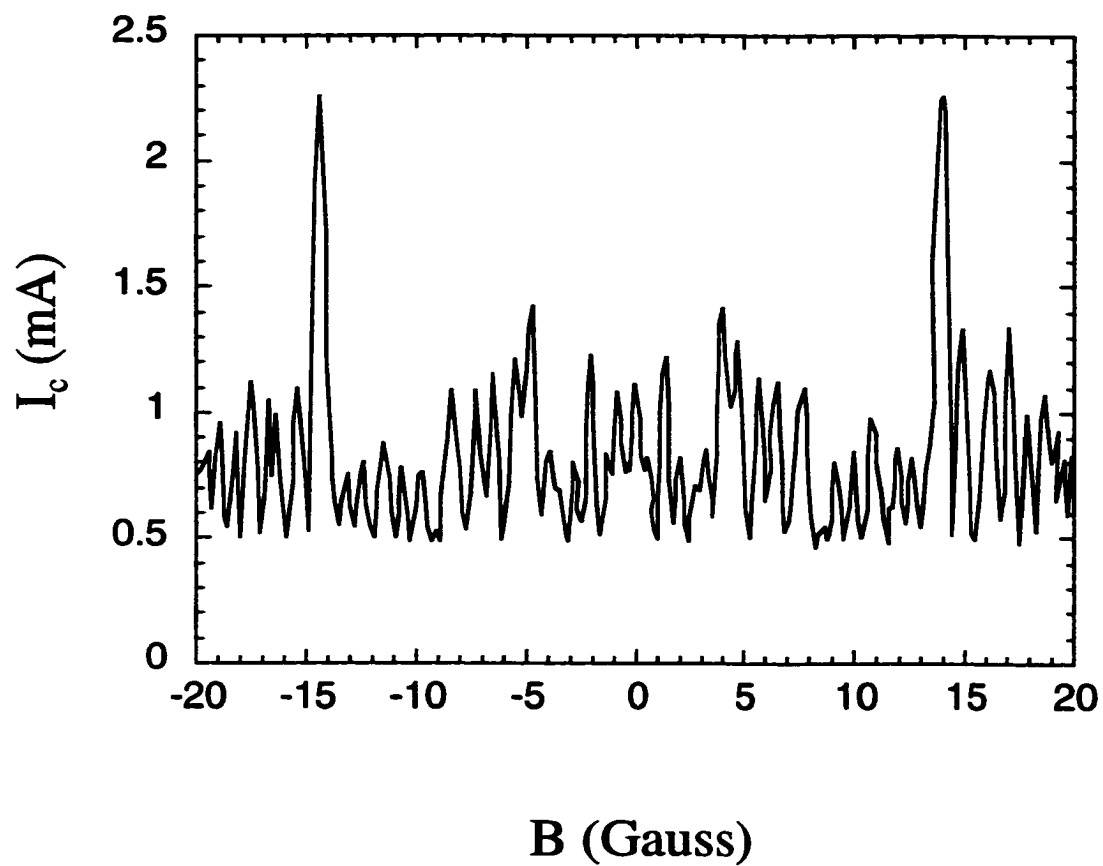
Figure 4.3 Critical current vs. applied magnetic field measurements for [001] asymmetric 45° grain boundary. Note the maximum current is not at H = 0. (from Mannhart *et al.* 1996)
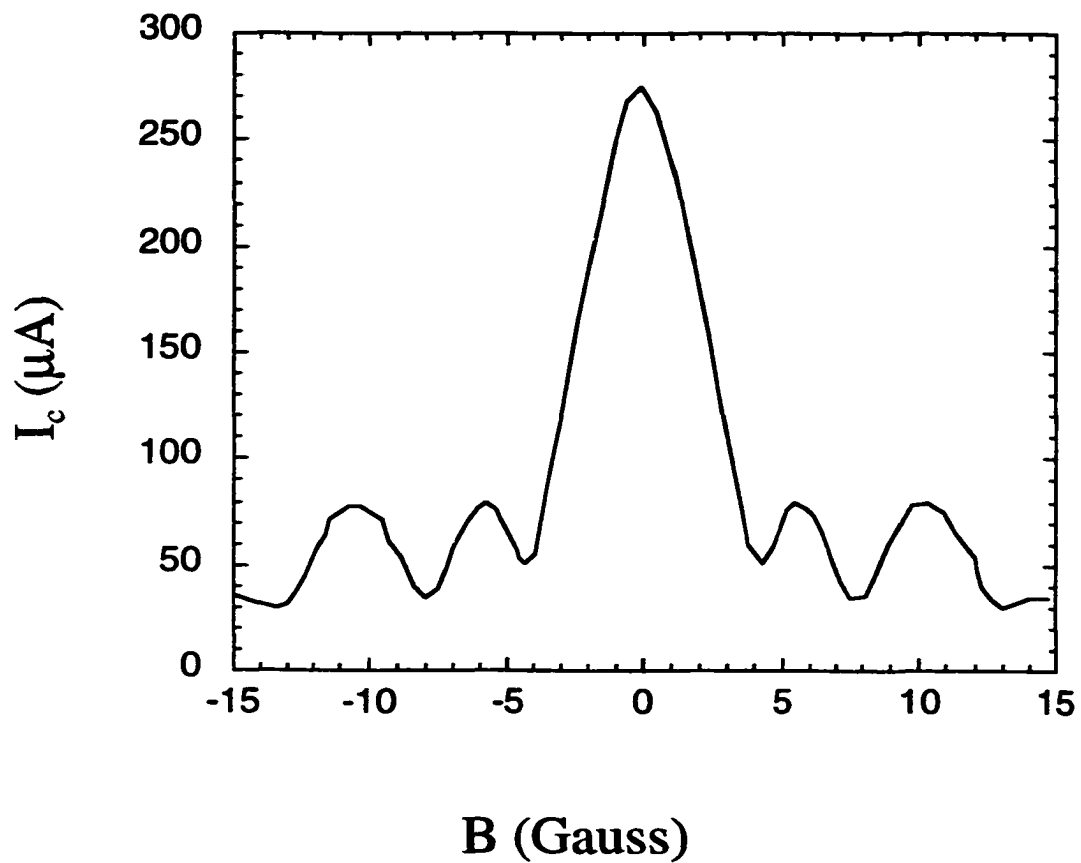
Figure 4.4 Critical current vs. applied magnetic field measurements for [001]
symmetric 24° grain boundary. Note the near Fraunhofer diffraction pattern.
(from Mannhart et al. 1999)

variations of the current at length scales consistent with existing microfilamentary

models that ignore d-wave contributions (Sarnelli *et al.* 1993a; Sarnelli *et al.* 1993b).

The most compelling example is from Alf *et al.* where a series of 11 parallel bridges

were patterned across a single grain boundary (Alf *et al.* 1994). Critical current vs.

applied magnetic field measurements were performed on the boundary and the

correlation function was calculated. Within the resolution of the measurements, the

resulting calculated spacings correspond extremely well with the expected spacings

assuming a series of 11 identical parallel junctions, thus, it appears that the d-wave

contribution for a 24° tilt boundary is small.

When the tilt angle is increased to 45° a number of studies have shown that the

magnetic field behavior of these junctions is quite different (Copetti *et al.* 1995;

Hilgenkamp *et al.* 1996; Mannhart *et al.* 1996a; Mannhart *et al.* 1996b; Nicoletti *et al.*

1997). Very few of the critical current vs. applied magnetic field measurements are close

to the ideal Fraunhofer pattern and many do not have a large central peak located at zero

magnetic field but rather have a maximum critical current at field values other than at H =

0. Models involving the symmetry of the order parameter and the unique microstructure

of 45° boundaries have been proposed to explain these induced magnetic fields.

Microstructure analysis on 45° tilt boundaries has shown that the length of the

boundary is dominated by a staircase structure of (100)(110) type facets (Copetti *et al.*

1995; Vuchic *et al.* 1996). Figure 4.5 shows a schematic of a (100)(110) type facet that
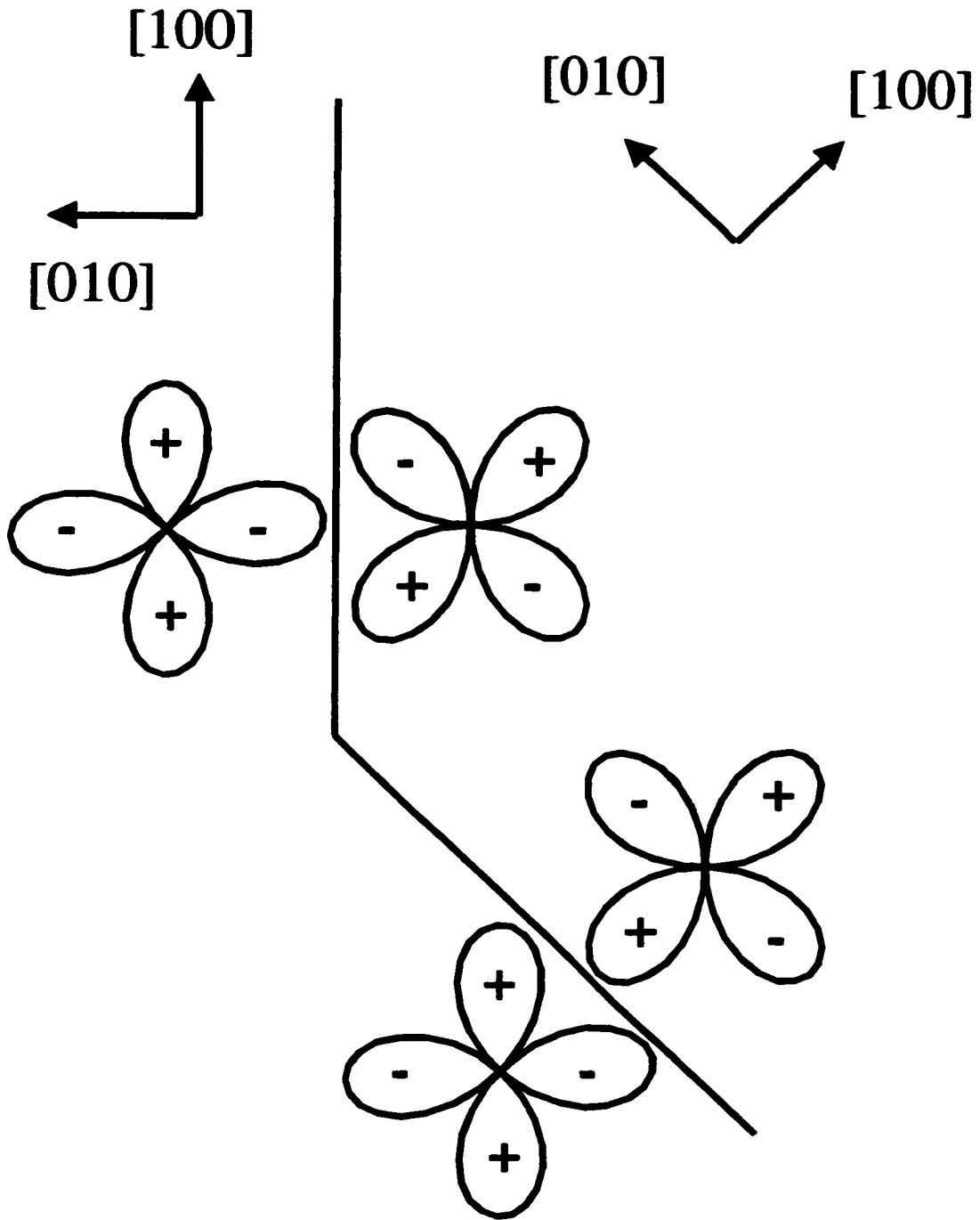
Figure 4.5 Schematic of d_{x2-y2} π junction where the phase angle can change by π due to the reversal of symmetry of the interaction of the wave function across the boundary.

dominates the length of [001] oriented 45° tilt grain boundaries in YBCO. The basic d-wave grain boundary model proposed by Sigrist *et al.*, Mannhart *et al.* and Copetti *et al.* suggest that the boundary can be modeled as a series of "0" and "π" junctions where each facet of the boundary experiences a phase shift of π relative to the adjacent facet (Sigrist *et al.* 1995; Mannhart *et al.* 1996a; Mannhart *et al.* 1996b; Copetti *et al.* 1995; Hilgenkamp *et al.* 1996). Remembering that the current transport equation across a Josephson junction can be written as;

$$J(x) = J_o(x)\sin\left(2\pi d\frac{\mu H}{\Phi_o}x + \phi_o\right)$$

(4.3)

where the current is oscillated by an applied magnetic field H. When H = 0, equation 4.3 can be written as;

$$J(x) = J_o(x)\sin(\phi_o)$$

(4.4)

where ϕ_o is a constant. Allowing each facet to change phase by a factor of "π" results in equation 4.4 being written as;

$$J(x) = J_o(x)\sin(\phi_o + \pi).$$

(4.5)

Since equation 4.4 and 4.5 are sinusoidal equations, each π phase shifts results in a

sign change of $J(x)$. Thus the startling conclusion is that along 45° tilt boundaries in

YBCO, there can exists regions along the boundary that have critical currents flowing in

the opposite direction as the applied d.c. current even in zero magnetic field (H = 0).

Adjacent areas along the boundary with positive and negative local currents can also be

thought of as circulating currents. These locally circular currents result in spontaneously

generated flux along the boundary at zero applied magnetic field (Mannhart et al. 1996).

These non-quantized self induced magnetic fields are the fields that have been measured

with scanning SQUID magnometers in a zero field environment (see figure 4.6). The

presence of flux cores along the grain boundary plane in 45° tilt boundaries has been

presented as evidence of current reversals along the boundary length.

A model proposed by Mints and Kogan suggest that the standard Fourier relation

of equation (4.3) is valid for a d-wave superconductor Josephson junction (Mints et al.

1997). The main difference that they point out is that the local critical current $J_c(x)$ can

be either positive or negative with respect to the applied current bias due to the "0" and

"π" facets along the boundary. Allowing locally negative currents results in $I_c(H)$

patterns with maximum peaks at locations other than H = 0. Their model is consistent

with existing 45° grain boundary junction $I_c(H)$ data where the $I_c(H)$ maximum is not at H

= 0 and is also consistent with $I_c(H)$ data from 45° junctions measured by Nicoletti and

Villegier in which the diffraction pattern is near Fraunhofer despite its 45° misorientation

angle (see figure 4.7)(Nicoletti et al. 1997).
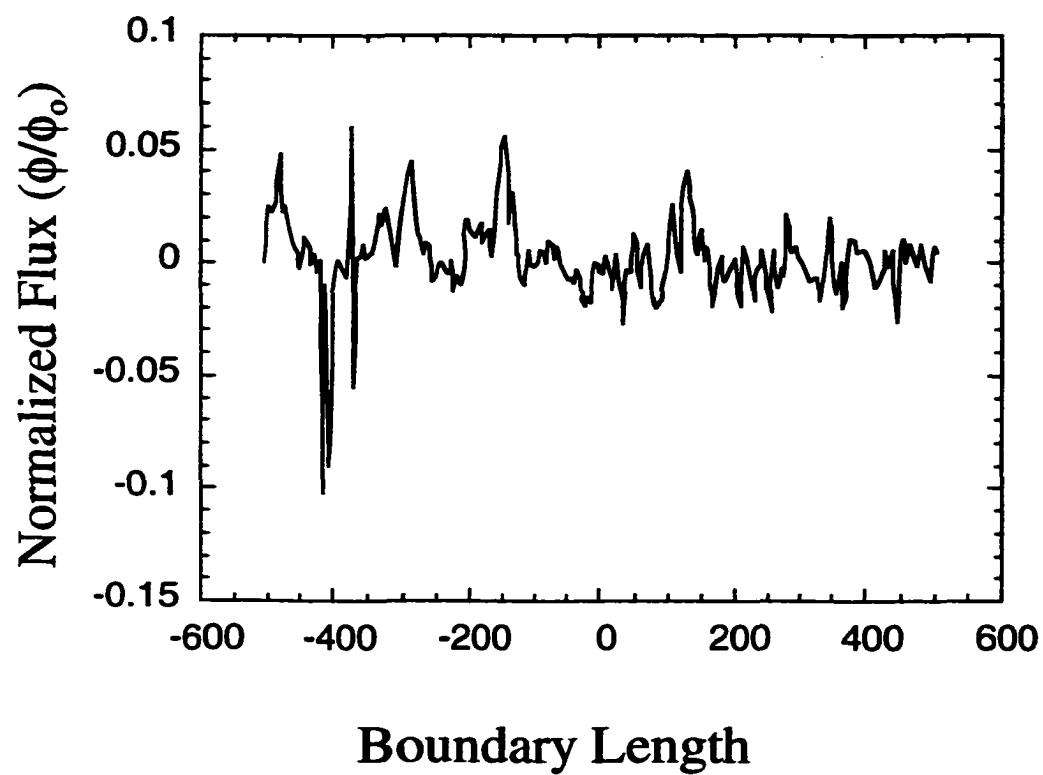
Figure 4.6 Scanning SQUID microscope scan of [001] 45° asymmetric tilt
YBCO grain boundary cooled in a zero field environment. Note the
presence of spontaneously generated flux along the boundary.
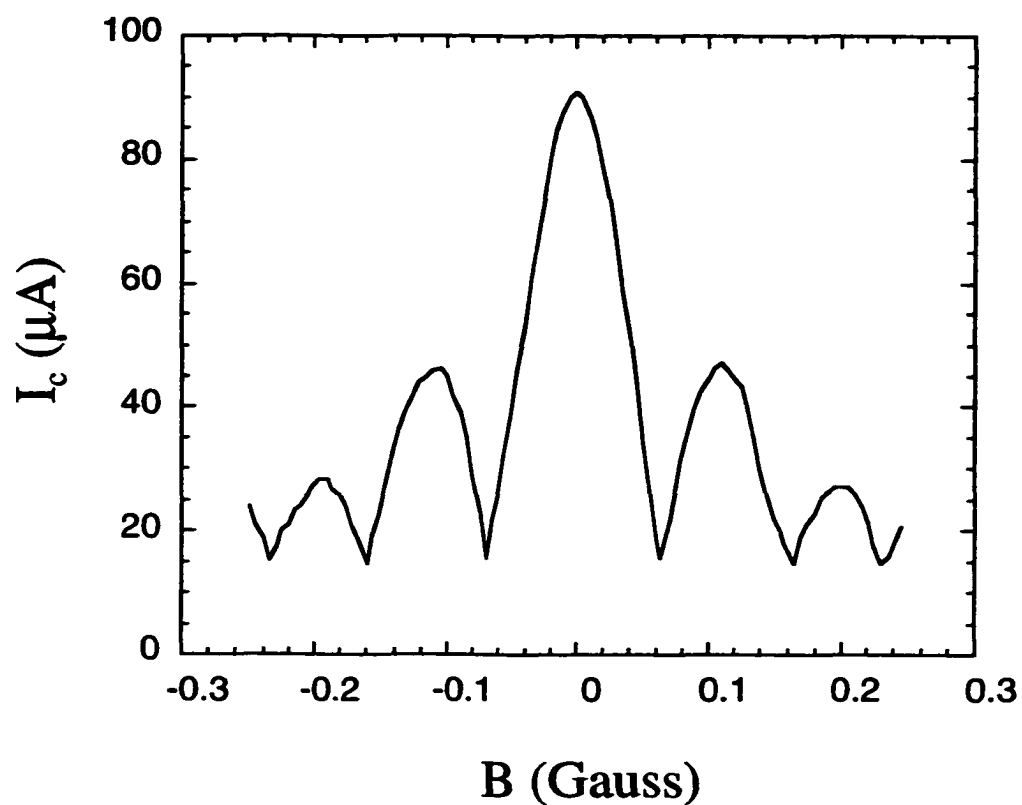
Figure 4.7 Critical current vs. applied magnetic field measurements for [001] asymmetric 45° grain boundary. Note the maximum current is at H = 0 and the shape is near Fraunhofer. Compare with diffraction pattern from figure 4.3. Note the significant differences from similar junctions.
(from Nicoletti et al.)

The key points regarding d-wave symmetry can be summarized as: The symmetry of the order parameter in YBCO is predominately d-wave in character. At low tilt angles, the d-wave nature of YBCO does not play a significant role and standard s-wave models can be used to describe current transport along the boundary plane. When the tilt angle is increased to 45° the reversal of the symmetry of the order parameter along adjacent (100)(110) type facets results in locally negative currents along the grain boundary. These locally negative (circular) currents induce magnetic fields with cores at the current reversal centers. These locally negative currents also result in anomalous $I_c(H)$ behavior for 45° tilt boundaries.

Chapter V. Phase Retrieval

The key to understanding the basic transport mechanisms across a single grain boundary is to understand the local variation of the current along the length of the boundary. By understanding how the current crossing the boundary varies from point to point, it may be possible to directly correlate local microstructural features to local current behavior. Ultimately, a direct microstructural model of the current transport across a single grain boundary in YBCO would be possible. At the start of this project a method for determining the local current did not exist. A novel phase retrieval technique for determining the local current variation was developed specifically for this thesis and will be presented in detail. Test models were used to explore the robustness of the algorithm and problems pertaining to the uniqueness of the solutions will be discussed. The application of this numerical technique to Josephson junctions will be explored and the possibility of using this technique to obtain for the first time a sub-micron map of the local current distribution along the length of a Josephson junction will be discussed.

V.1 Introduction

One of the hallmark traits of high-T_C Josephson junctions has been the large scatter in the reported transport properties. Several orders of magnitude variation in J_c from junction to junction are common. The large variation in transport properties has often been attributed to the large variation in the microstructure of Josephson junctions. The basic premise being that variations in the microstructure cause variations in the local current and thus results in large variations in the total current $J_{c,max}$ from junction to junction. Unfortunately, until now there did not exist a technique for measuring or calculating the

7 1

local current distribution along the length of a Josephson junction. Low temperature scanning electron microscopy and scanning laser microscopy have demonstrated potential for mapping large - scale variations in the local current, however, these techniques have a resolution limit on the order of 1 µm and thus are limited in their potential (Bosch *et al.* 1987; Gerdemann *et al.* 1994; Gross *et al.* 1989; Fisher *et al.* 1994; Mannhart *et al.* 1990; Divin *et al.* 1991; Divin *et al.* 1994; Divin *et al.* 1996; Shadrin *et al.* 1998). The local microstructure varies on the sub-micron length scale, therefore these scanning techniques are not adequate for obtaining a direct correlation between the transport properties and the microstructure.

V.2 Phase Retrieval

Figure 5.1 shows a schematic of the Josephson junction geometry that will be used for discussion. The basic equation relating the modulation of the critical current as a function of an applied magnetic field across a Josephson junction (discussed in detail in Chapter III.) can be written as a Fourier transform such that

$$I_c(u) = \left| \int_{-\infty}^{\infty} J_c(x) \exp(iux) dx \right|, \tag{5.1}$$

where $J_c(x)$ is the current density flowing in the z-direction along the length of the boundary (see Fig 5.1.), $u = \left(\dfrac{2\pi D \mu_o H_y}{\Phi_o} \right)$ and is the normalized magnetic field where H_y is the magnetic field threading the junction(including both the applied magnetic field and the field generated by the currents flowing in the junction), and μ_o is the permeability of free

space (Josephson 1962; Dynes *et al.* 1971). Φ_0 is defined as one flux quantum

$$\left(\left(\frac{h}{2e}\right) = 2.07 \times 10^{-7} G \cdot cm^2\right) \text{and } D = \lambda_1 + \lambda_2 + d \text{ where d is the thickness of the barrier}$$

and λ the London penetration depth of the superconductors on each side of the barrier. For a grain boundary junction, it is usually assumed that the London penetration depth (λ) is the same on both sides of the junction ($\lambda_1 = \lambda_2$) and that the width of the grain boundary (d) is negligibly small compared to 2λ such that $D \approx 2\lambda$. From equation 5.1 it is evident that the magnetic field response of the critical current $I_c(u)$ is related to the variation of the local current, therefore, it may be possible to obtain spatial information about the local current by measuring the magnetic field response of a Josephson junction.

Experimentally $I_C(B)$, where $B = \mu_0 H$, is measured to analyze the junction current response for an applied magnetic field. If the current distribution is uniform, equation (1) simplifies to the familiar Fraunhofer diffraction pattern from chapter III:

$$I_c(u) = I_{max} \left| \frac{\sin(ua/2)}{(ua/2)} \right| \tag{5.2}$$

where (a) is the junction width as illustrated in Fig. 5.1. However, for most real junctions, it is believed that the current distribution $J(x)$ along the boundary is not uniform.
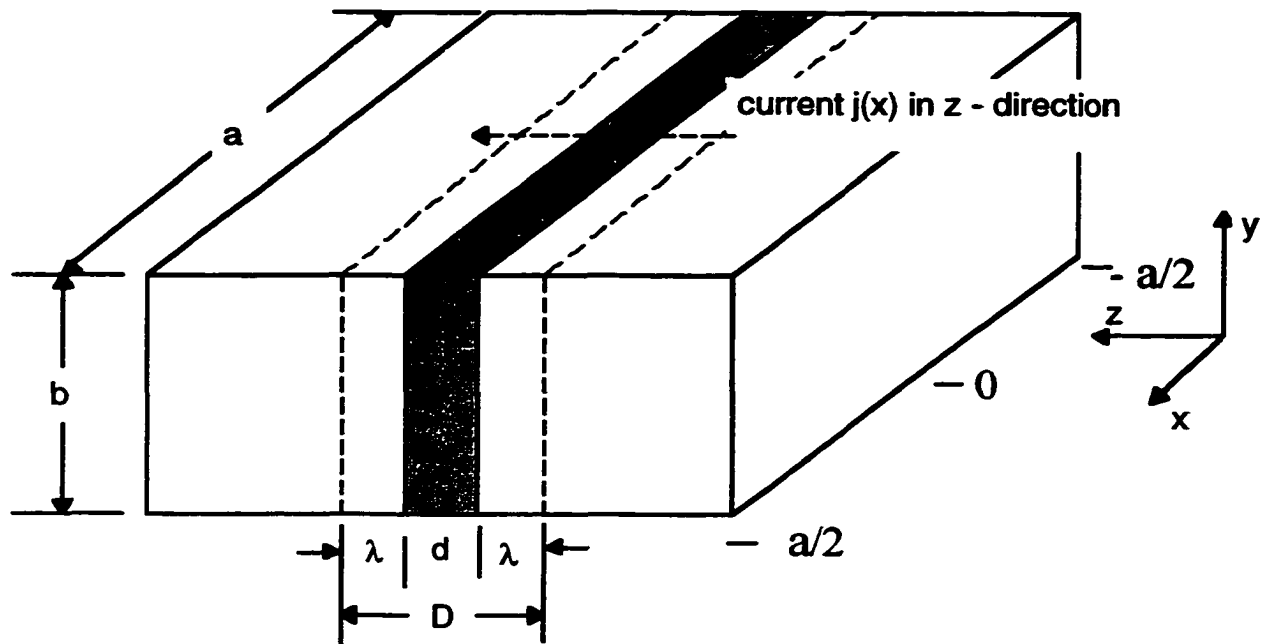
Figure 5.1 Schematic of Josephson junction used for illustration of junction terms.

The experimentally measured $I_C(u)$ from equation (5.1) is defined as the modulus of the Fourier transform of $J_c(x)$. The Fourier transform of $J_c(x)$ (written as F(u)) is a complex quantity that can be described by a modulus factor and a phase factor;

$$F(u) = I_c(u)\exp(i\phi(u))$$

(5.3)

where $I_c(u)$ is the modulus factor defined by equation 5.1 and is measured experimentally. To calculate $J_c(x)$ requires knowledge of F(u) which requires knowledge of both the modulus $I_c(u)$ and the phase $\exp(i\phi(u))$. Since the modulus is measured experimentally, the problem becomes one of restoring the phase $\phi(u)$. This is the classic "phase problem" that is familiar to many areas of physics.

Dynes and Fulton attempted to solve for the local current distribution $J_c(x)$ in low-T_c Josephson junctions by assuming a minimum-phase-type function (Dynes *et al.* 1971). By making this assumption it was possible to use the formalisms of Hilbert transforms to calculate $J_c(x)$ directly (Papoulis 1962). Zappe showed that the minimum-phase assumption used by Dynes and Fulton is not in general a valid assumption for a Josephson junction (Zappe 1975). Zappe argued that without making further assumptions about J(x), it was impossible to reconstruct $J_c(x)$ from $I_C(u)$ uniquely because there can be multiple one dimensional (1-D) real space objects $J_c(x)$ that when Fourier transformed produce the same modulus $I_C(u)$. This is the basic uniqueness issue for 1-D phase retrieval problems and it will be discussed in detail in a later chapter.

The problem of phase retrieval is not a new subject (Gerchberg *et al.* 1972; Gerchberg 1974; Walther 1962; Fienup 1972). In general, without further information

about the phase or the real space object it is not possible to uniquely determine the phase from moduli measurements. However, in most cases, other information or "constraints" exist that can be used to solve the phase problem. Many iterative algorithms for phase recovery have been developed. One of the first was developed by Gerchberg and Saxton which utilizes a series of iterative Fourier transforms to find the missing phases, otherwise known as the Gerchberg-Saxton error-reduction algorithm (Gerchberg *et al.* 1972; Gerchberg 1974). This method was further improved with the use of a feedback approach and evolved into what is known as the input-output algorithm (Fienup 1978; Fienup 1982). The phase restoration algorithm described hereafter is a modified version of the input-output algorithm developed by Gerchberg and Saxton.

The general approach involves iterative Fourier transformation back and forth between the object domain and the Fourier domain. Figure 5.2 is a schematic of the generalized Gerchberg-Saxton algorithm.

This generalized algorithm for phase retrieval using iterative Fourier transforms is best explained in terms of set-theoretic methods involving successive projection onto sets, an iterative method that finds feasible solutions consistent with a set of constraints which are defined by *a priori* information about the real space object (Sezan 1992). A feasible solution is defined as any solution that satisfies the constraints (Sezan 1992). A feasible solution is found by successively projecting an initial estimate of the object onto the constraint sets. This method, involving mathematical projection operators, can be generalized to involve non-convex constraint sets and is known as the method of generalized projections (MGP).
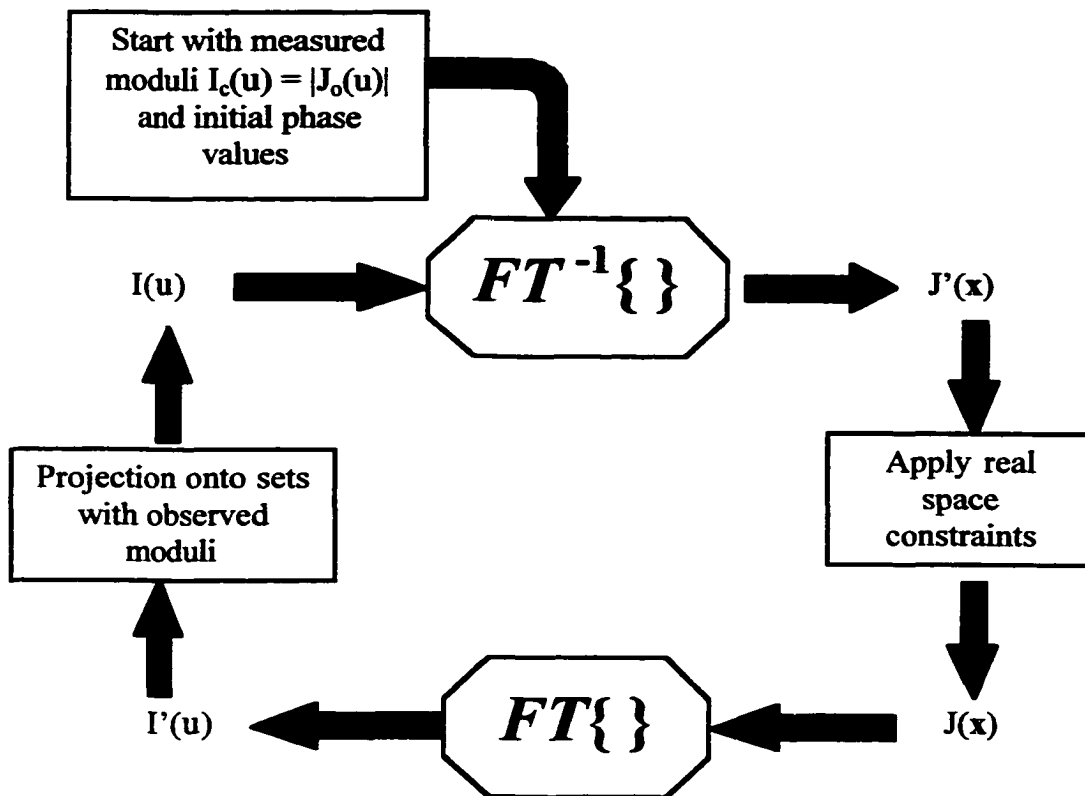
Figure 5.2 Flow chart of Gerchberg-Saxton type phase retrieval algorithm used for solving current density profiles $J(x)$.

The algorithm used to solve the phase restoration problem for Josephson junctions involves projecting an initial estimate onto two constraint sets. The first constraint set (S_1) correspond to the set of all solutions whose value is confined by the known object constraints. The second set (S_2) is the set of all solutions whose moduli are equal to those of the experimentally measured moduli and may be written as;

$$S_1 = \{J(x): J(x) = 0, |x| > a/2: J_c \geq J(x) \geq 0: J(x) = \text{real}\} \quad (5.4)$$

$$S_2 = \{J(x): |FT\{J(x)\}| = I_c(u)\}. \quad (5.5)$$

It can be shown that the constraint set S_1 is a closed convex set and the set S_2 is a non-convex set (Sezan 1992; Levi et al. 1987).

The phase retrieval algorithm can be written in terms of mathematical projections as;

$$J_{n+1} = T_2 T_1 J_n = T J_n, \quad (5.6)$$

where J_{n+1} is the current best estimate of J, J_n is the previous estimate of J and T_1 and T_2 are projection operators (defined by equations (5.4) and (5.5)), represented by T, such that when T operates on J_n it produces J_{n+1}. T_1 corresponds to the correction of the function, J_n, with the experimentally observed moduli, $I_0(u)$, and T_2 is the correction for the real space constraints:

$$T_1 = 1 + \delta_1(P_1 - 1) \quad (5.7)$$

$$T_2 = 1 + \delta_2(P_2 - 1) \qquad (5.8)$$

where

$$P_1 I(u) = I_o(u) \qquad (5.9)$$

and I(u) is obtained from the mapping of J(x) into I(u) via a Fourier transformation. P_2 is defined such that

$$P_2 J(x) = \begin{cases} J(x): & 0 \le J(x) \le J_c(x) \\ (1-\delta_2)J(x): & J(x) < 0 \\ J_c - (\delta_2 - 1): & J(x) > J_c \\ (1-\delta_2)J(x): & |x| > a/2 \end{cases} \qquad (5.10)$$

where δ_1 and δ_2 are scalar constants between 1 and 2 and J_c is the bulk critical current density across the junction. When $\delta_1 = \delta_2 = 1$, the phase retrieval algorithm is identical to the Gerchberg-Saxton algorithm (Levi *et al.* 1987).

If one or more of the constraint sets is non-convex then it is possible that the convergence may take place locally. Specifically, there can exist various local minima all consistent with the object constraints (Combettes 1996). Since multiple solutions are possible when projecting onto non-convex sets it is important to rigorously search solution space to find all possible solutions.

V.3 Phase Retrieval Algorithm

The measured moduli $I_C(u)$ are initially seeded with phases. The initial phases and measured moduli are then inverse Fourier transformed into real space where the real space domain constraints are applied by a projection onto sets operation (Fienup 1982). The solution is then Fourier transformed back to reciprocal space where the new moduli are corrected using a projection onto sets operation of the form of equation (5.9)(Levi *et al.* 1987).

For the 1-D phase restoration problem a genetic algorithm has been applied to search for the best starting set of phases (typically the strongest 10%) such that after a fixed number of iterations the solution converges to the best possible fit of the applied constraints. Many different search algorithms can be used to search phase space for different starting sets of phases. A genetic algorithm was used most of the time, but random searchers were also used. Several nice reviews of Genetic Algorithms exist and therefore they will not be discussed in detail in this thesis. The reader is advised to search out Goldberg and Holland for reviews of genetic algorithms if they are interested (Holland 1975; Goldberg 1989). The initial phase guesses need only be approximate values, therefore quadrant searching ($\pi/4$, $3\pi/4$, $5\pi/4$, $7\pi/4$) or binary searching (0 or π) is sufficient.

After each iteration of the algorithm, a figure of merit (FOM) is calculated to monitor the convergence of each solution and was later used by the genetic algorithm to rank the solutions. Each population of the genetic algorithm is run for a relatively small number of iterations to avoid over-convergence of the solutions. After a final solution set is

obtained, the solutions are re-run for a larger number of iterations to push the solutions to a lower FOM.

It is important at this point to make a distinction between two possible situations. The missing phase information contains all information pertaining to the actual structure. Therefore, in order to make no assumptions about the solution, one must consider solutions that are centrosymmetric as well as non-centrosymmetric. This is particularly important when deciding how to define the possible initial phases, either binary or quadrant searches. If one only considers the quadrant searches, one reduces the possibility of finding solutions that may be centrosymmetric in nature in favor of a non-centrosymmetric solution. It is possible for a solution to be nearly centrosymmetric or "pseudo-centrosymmetric". By enforcing a centrosymmetric search algorithm (phases are only allowed to be 0 or π), one finds a solution that is close to the correct solution. Using these starting phases and then allowing the solution to refine for a larger number of iterations and allowing the phases to vary between 0 and 2π, from these pseudo-centrosymmetric starting values, the non-centrosymmetric solution is found.

Therefore, for each set of measured moduli, it is necessary to run under two different conditions, a true non-centrosymmetric (quadrant search) and a pseudo-centrosymmetric algorithm (whose search strategy begins by searching for the best solution whose phases are confined to be either 0 or π). The best set of solutions for both cases are then used as starting phases for a non-centrosymmetric solution refinement (allowing phases to be anything between 0 and 2π).

V.4. Figure of Merit

The phase retrieval algorithm is only useful if it produces solutions consistent with the known boundary constraints. After each iteration of the algorithm a Figure of Merit (FOM) or goodness of fit parameter was calculated to determine the quality of each solution. The FOM used was of the form

$$FOM = \sum_{u=0}^{N} |I_{k-1}(u) - I_k(u)|^2 \tag{5.11}$$

where $I_{k-1}(u)$ are the moduli and phase of the k-1th iteration in the error-reduction algorithm and $I_k(u)$ are the moduli and phase for the kth iteration. Equation (10) is similar to the FOM used by Fienup (Fienup 1982).

V.5 Calibration of the FOM

Accuracy of the FOM was determined using a second "correctness" factor (CFOM) which monitors the accuracy of the phases determined by the algorithm to the true phases for a given model. This CFOM is defined as

$$CFOM = \frac{1}{N} \sum_{u} |1 - \cos(\phi_c(u) - \phi_t(u))| \tag{5.12}$$

where $\phi_c(u)$ is the calculated phase, $\phi_t(u)$ the true phase, and N the number of phases used for the restoration. Figure 5.3 is an example of the calculated FOM and corresponding CFOM for four different total number of iteration within the phase restoration algorithm. The CFOM versus FOM plots were calculated for the asymmetric model described by Zappe (Zappe 1975).

It is important to note that any starting set of phases will converge towards a small FOM, however, correct solution sets seem to converge more quickly (more locally convergent). Thus, possible correct solutions can be distinguished from poor solutions based on the relative speed of convergence. Figure 5.3 shows that for a fixed number of iterations the correct solution converges faster to a low FOM. Increasing the number of iterations improves the overall convergence (reduces the FOM) of each solution, however, the relative difference between solutions remains (see Fig 5.3(a-d)). Thus there is no added benefit to running each possible set of phases for a large number of iterations. After a final solution set is obtained, each solution may then be run for a larger number of iterations thus reducing the overall calculation time and improving the speed of the algorithm.

a.
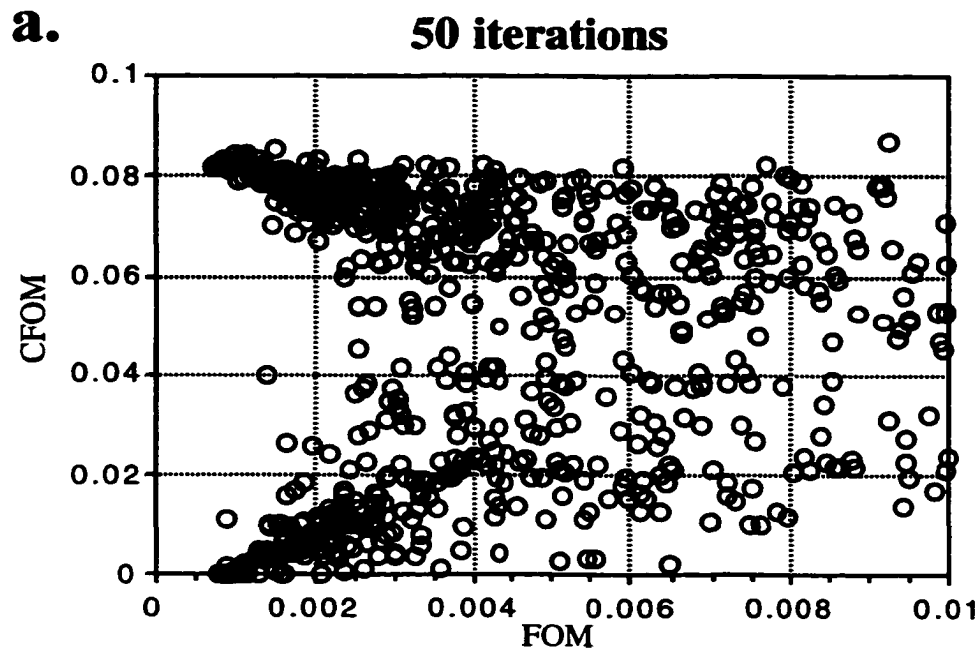
50 iterations

Figure 5.3 (a) Correctness factor (CFOM) vs. Figure of Merit (FOM) for (a) 50, (b) 100, (c) 250, and (d) 1000 iterations of the phase retrieval algorithm For the Zappe model. Two distinct solutions are evident.
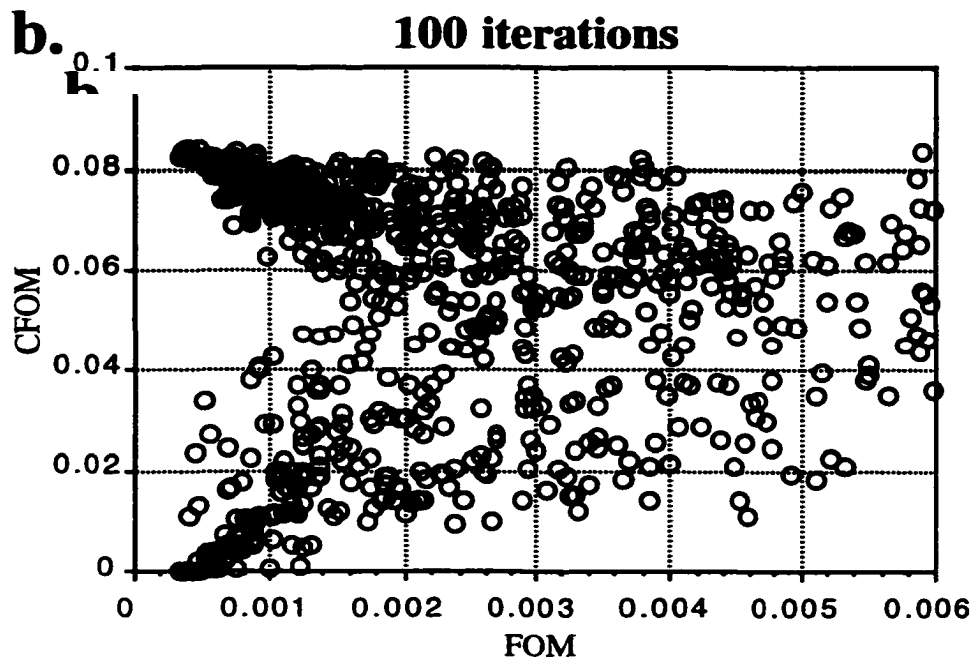
b. 100 iterations

Figure 5.3 (b). CFOMvs. FOM for 100 iterations.

c
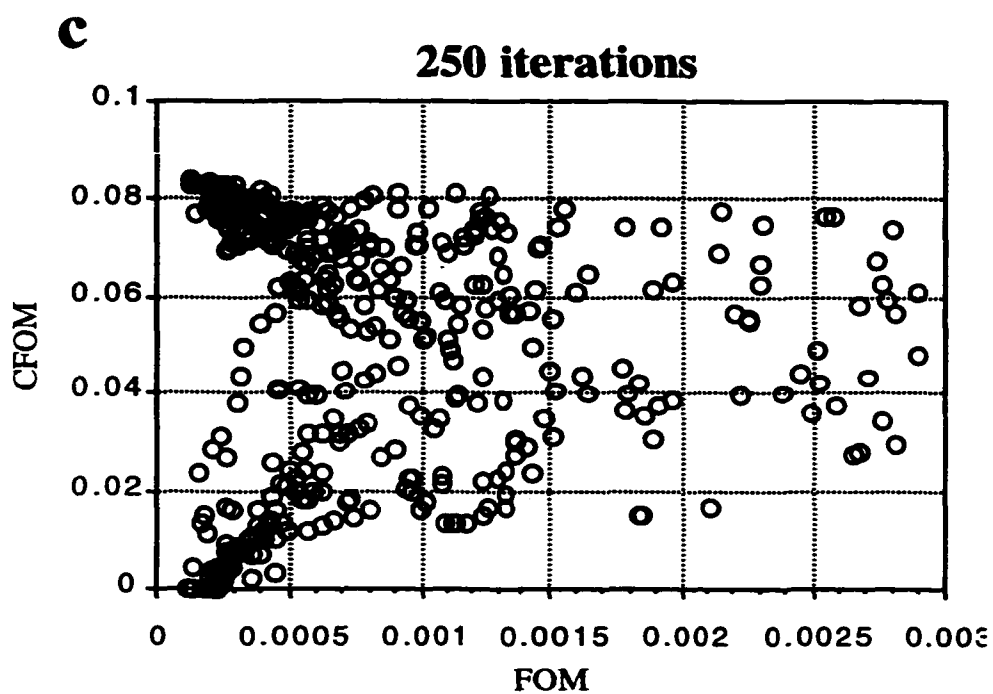
250 iterations

Figure 5.3 (c) CFOM vs. FOM for 250 iterations of the phase retrieval algorithm.

d.
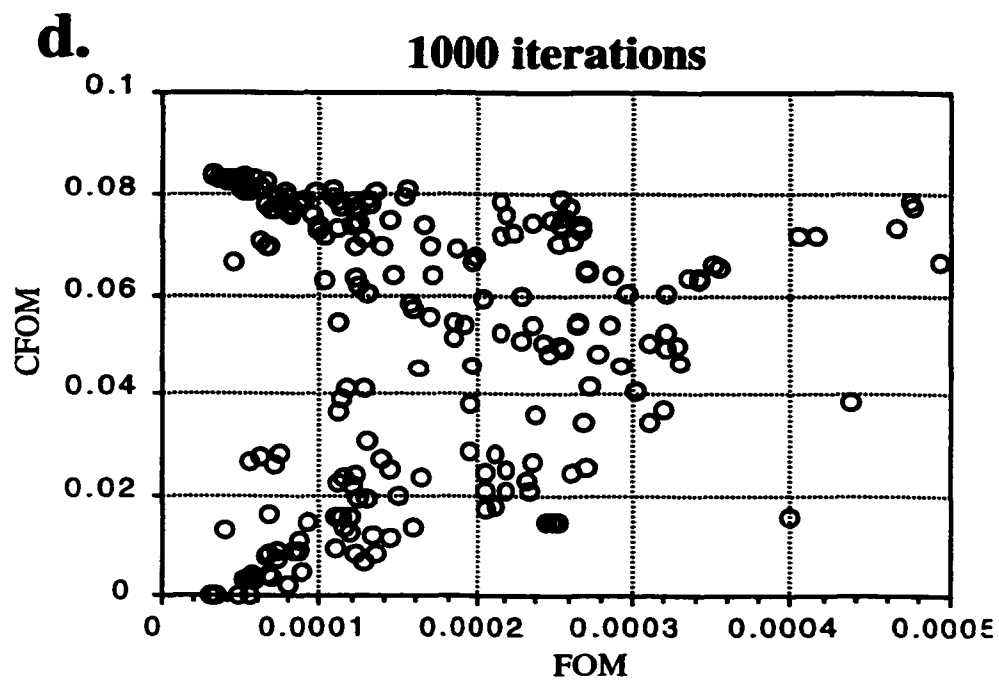
1000 iterations

Figure 5.3 (d) CFOM vs. FOM for 1000 iterations. Note two distinct solutions with a zero FOM have been found.

V.6 Test Models

The phase retrieval algorithm described above in conjunction with the genetic algorithm was used to solve the phase problem for a number of test models, 256 pixels in width.

Figures 5.4 -5.7 are square and sinusoidal models from Barone used for testing the algorithm (Barone 1982). In all of the above models from Barone, only one solution for each model was found and it corresponded to the known correct solution. Inspection of the graphs shows small oscillations about the true solution.

Figures 5.8 and 5.9 are two different real space models from Zappe that are known to have identical Fourier moduli IF(u)I but different phases $\phi(u)$ (see figure 5.10)(Zappe 1975). By using the same Fourier moduli, the phase retrieval algorithm was able to find both solutions (sets of phases).

Figures 5.11 - 5.13 show a model with solutions designed to represent a complicated boundary structure (it is in fact a profile of Chicago). A pseudo-centrosymmetric search approach described above was found to give the best fit to the model. Although the solution did not correspond to an exact fit, the algorithm was able to find solutions that had the correct "feel" which will be discussed more below.
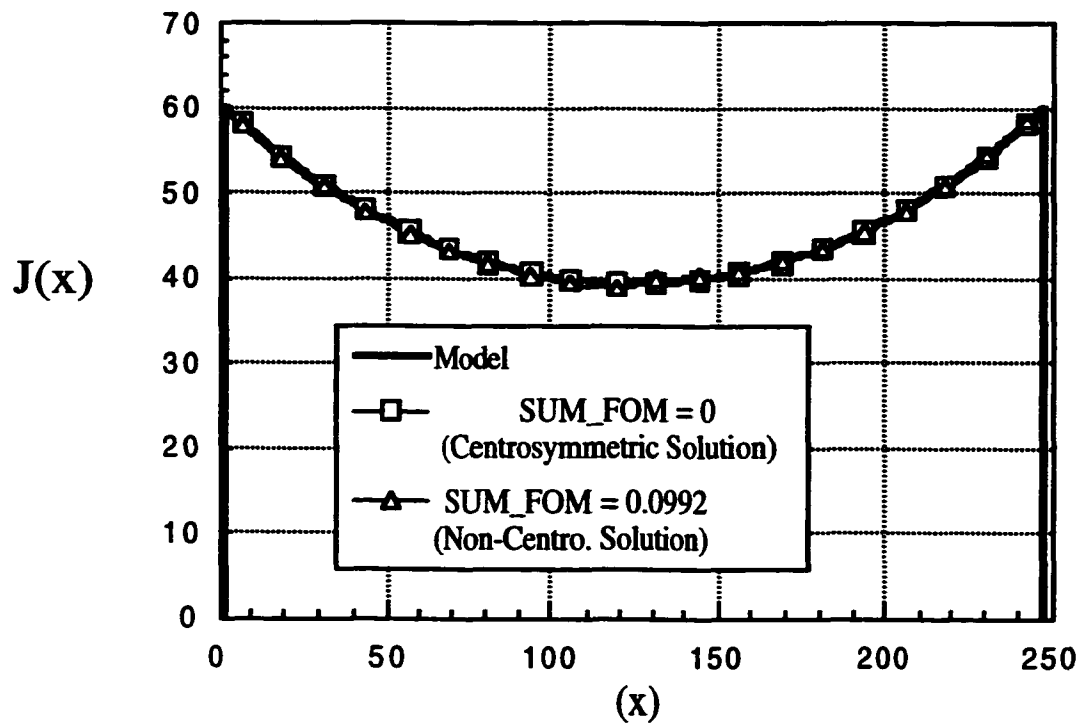
Figure 5.4 Sinusoidal model where the centrosymmetric solutions corresponds to a zero Figure of Merit.
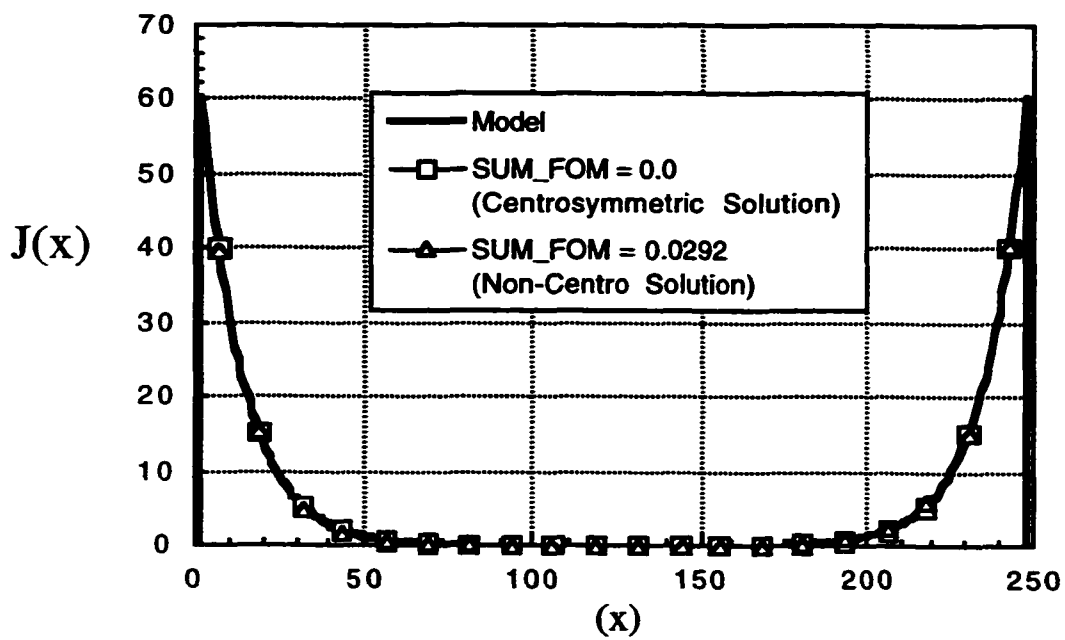
Figure 5.5 Sinusoidal model where the centrosymmetric solutions
corresponds to a zero Figure of Merit.
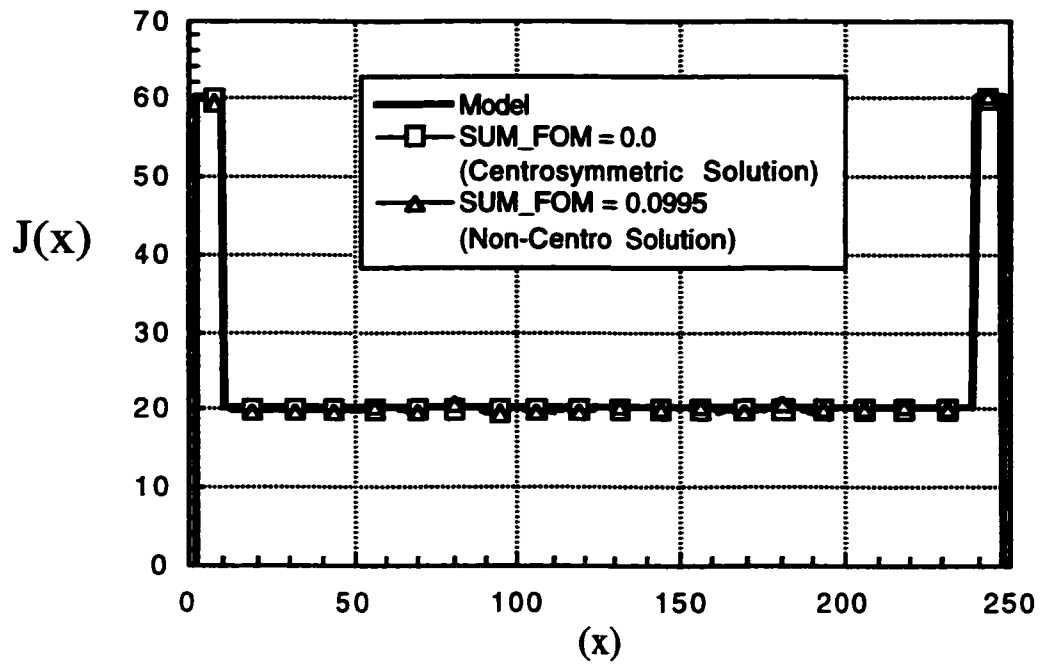
Figure 5.6 Square model where the centrosymmetric solutions corresponds to a zero Figure of Merit.
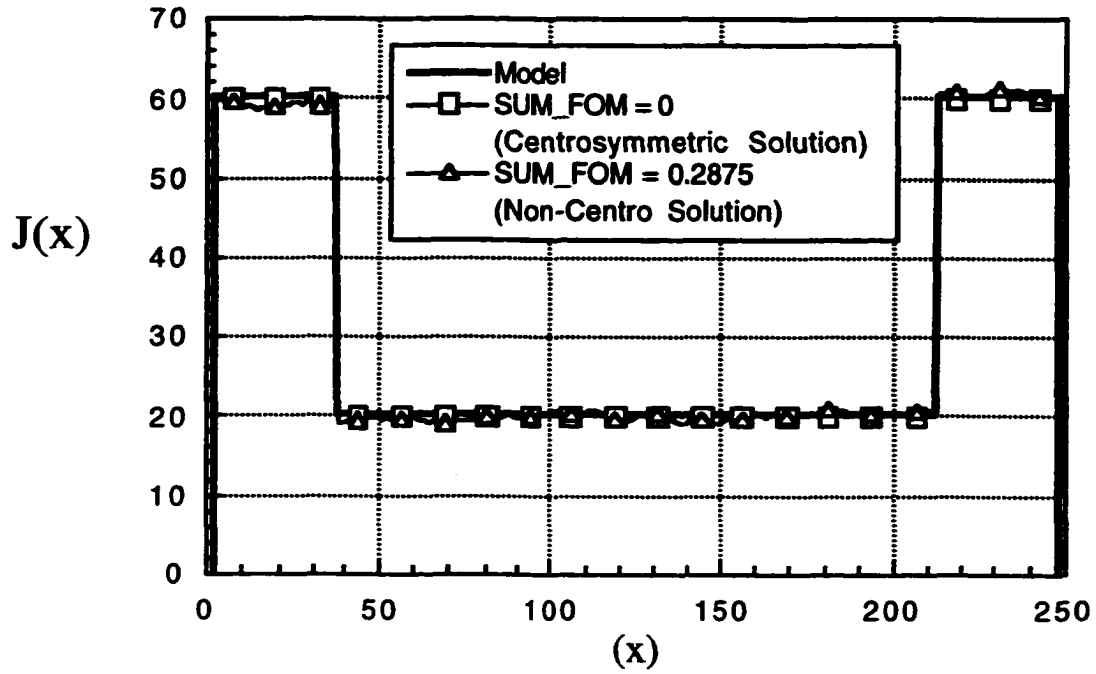
Figure 5.7 Square model where the centrosymmetric solutions
corresponds to a zero Figure of Merit.
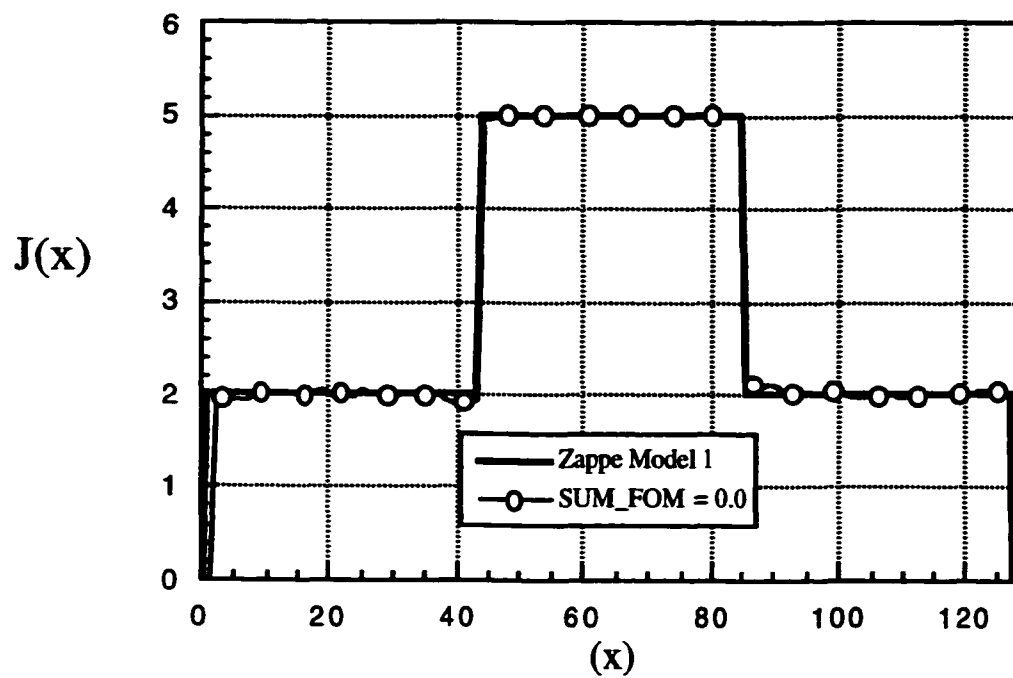
Figure 5.8 Zappe model with same Fourier modulus and the model in 5.9.
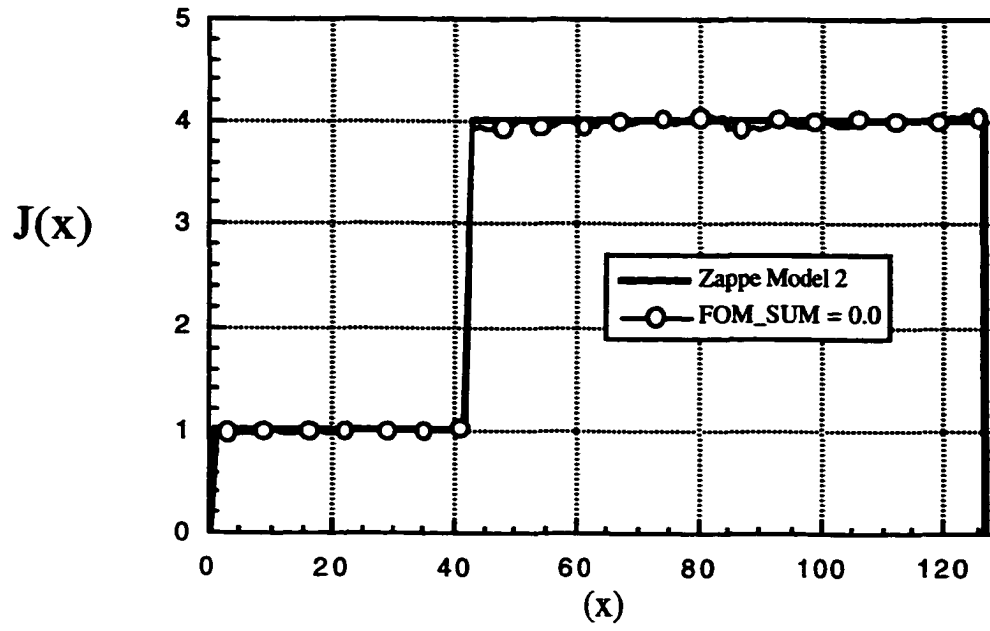
Figure 5.9 Zappe model with same Fourier modulus and the model in 5.8.
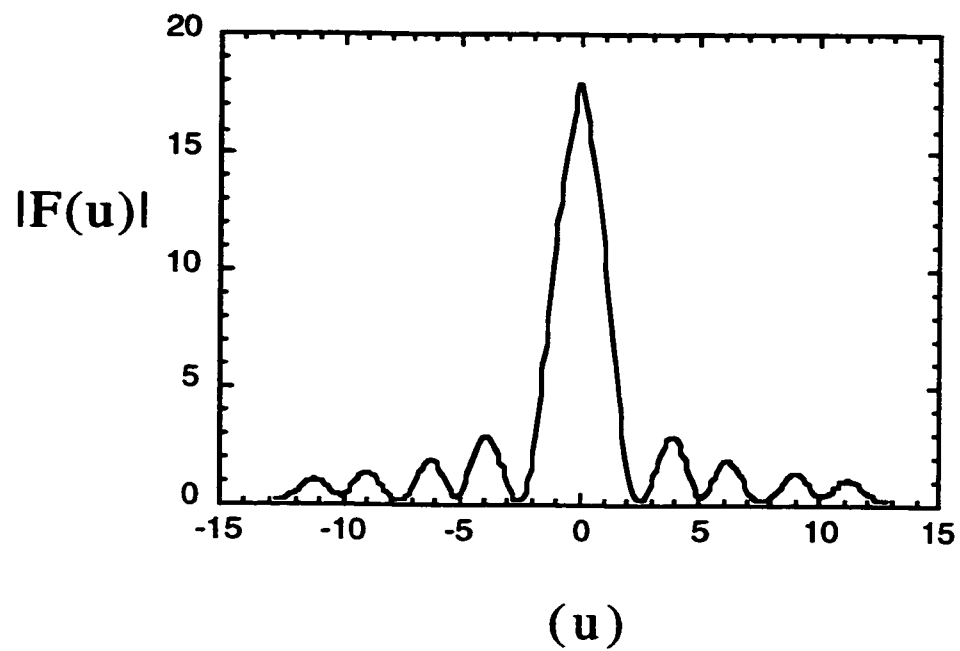
Figure 5.10 Fourier modulus |F(u)| for both Zappe models Figures 5.8 and 5.9.
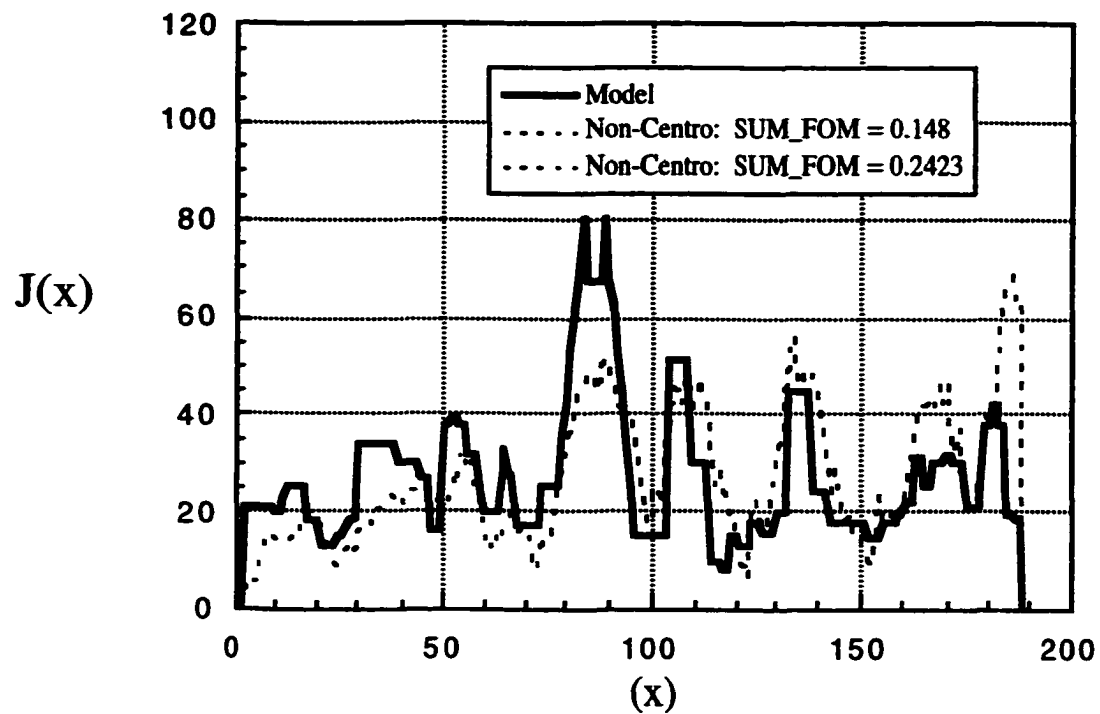
Figure 5.11 Complex boundary model with non-centrosymmetric solutions allowing starting phases to vary from 0 - 2π.
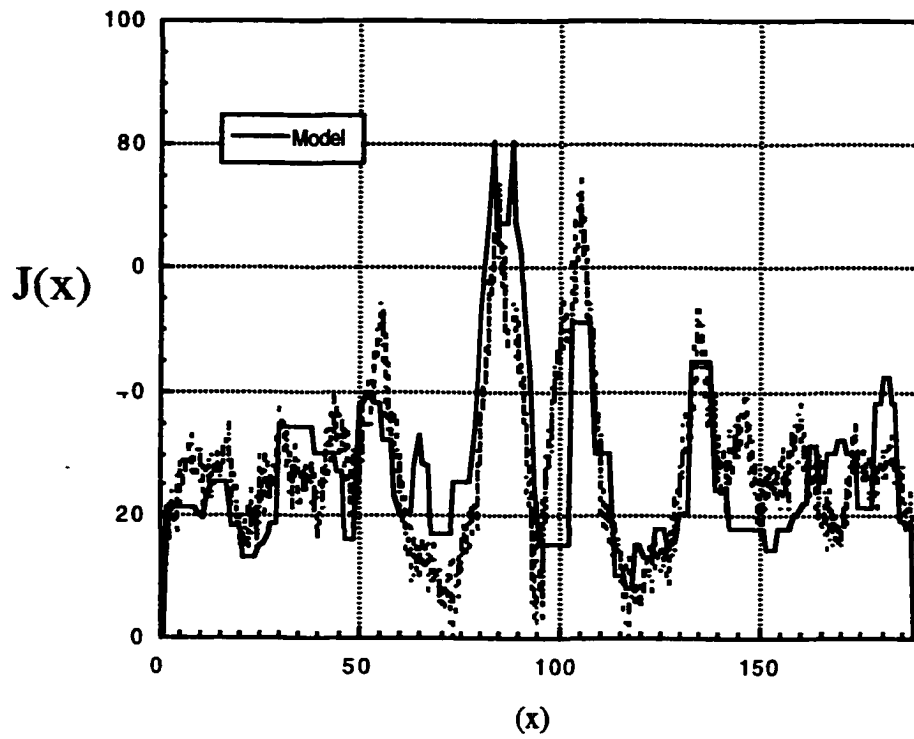
Figure 5.12 Complex boundary model with 100 iteration solutions found using the centrosymmetric constraint.
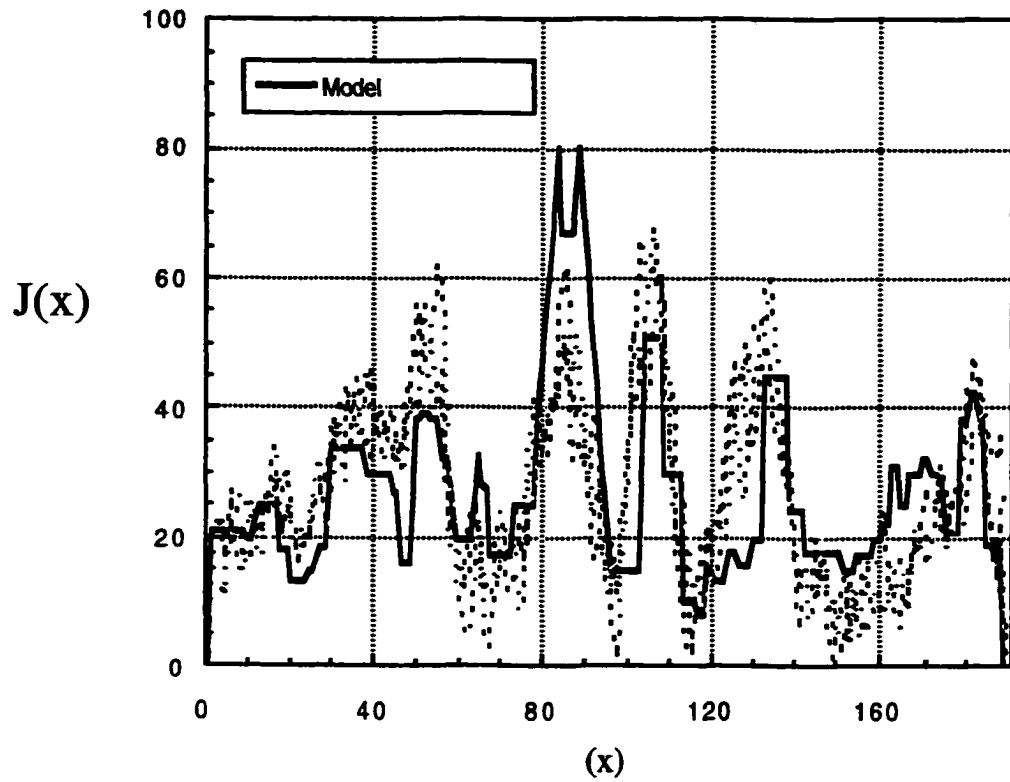
Figure 5.13 Complex boundary model with pseudo-centrosymmetric phase constraints.

The phase problem for 1-D objects is notoriously difficult to solve since the possibility exists for multiple solutions. Any real space object $J(x)$ that is consistent with all of the available constraints is a possible (feasible) solution. It is important to mention that without making assumptions about the object $J(x)$ it would be impossible to distinguish between two different solutions, both with a zero FOM. When evaluating the test models above, three different types of solutions were observed.

A. Type I.

The first type of solution was one in which the real space object was found to have only one solution. Thus, any starting set of phases that were given to the phase-retrieval algorithm resulted in the same unique solution. The test models from Barone are examples of this type (Barone 1982). Type I solutions (Fig. 5.4 - 5.7) are ideal since they are unique and need no further interpretation. The solution is simply the restored current density profile $J(x)$.

B. Type II.

The second type of solution was one in which there existed multiple real space objects that when Fourier transformed produce the same Fourier Moduli $I_c(u)$. The model from Zappe (Fig. 5.8 and 5.9) is an example of this type of solution (Zappe 1975). Type II solutions have previously been considered the stopping point for working with the 1-D phase restoration problems. Variations in the initial phases would result in different solutions and determining the "correct" solution was considered impossible without making further assumptions about the real space object $J(x)$.

We have taken a different approach to the problem. Instead of attempting to make assumptions about J(x), we simply use the real space constraints mentioned earlier to limit the number of possible solutions. By using the known constraints on J(x), we are able to reduce the number of possible solutions which are consistent with the boundary conditions. We have solved numerous models from simple symmetric cases to complex random models, and without exception, the number of solutions that are found within the box has been limited to $\approx$ 2-3 different solutions per model. Finding a small set of solutions that contains the correct solution would be a vast improvement over the existing options. However, it is known that the current density is dependent on the microstructure of the boundary. Thus when multiple solutions to the 1-D phase problem exist (type II solutions), it is possible to compare the small number of possible current density maps calculated by the phase retrieval algorithm to the microstructure of the boundary and determine the one correct solution.

C. Type III.

The third type of solution that was found was the least desirable of the three types. For type III solutions (Fig. 5.11 - 5.13), the phase retrieval algorithm was not able to correctly restore the phases such that a perfect match between the model and the restored solution was found. However, the algorithm was able to produce a profile J(x) that exhibited the correct "feel" to the solution. Peaks and valleys in the solution corresponded to peaks and valleys in the model and in most cases the relative height of the peaks was correct, but the absolute values of the solution was incorrect. Consequently, the restored model was only good for qualitative comparison. Fortunately type III solutions are usually

distinguishable from type I and type II solutions. For a type III solution, the top ten or twenty solutions all had the same "feel" (were qualitatively the same) but they were all slightly different . For a type II solution the top twenty FOMs all corresponded to a small set (2-3) of solutions while there was only one solution for a type I. Therefore, it is quite easy to distinguish type I and II solutions from type III solutions.

Unfortunately, the number of possible solutions is dependent on the shape of the real space object $J(x)$. Therefore, it is not possible to know *a priori* what type of solution one may be dealing with. Since there may always exist multiple solutions to the problem, it is not necessarily important to be able to find a unique solution using the phase retrieval algorithm, but rather it is more important to be able to find all possible solutions. The phase retrieval algorithm used for the test cases above has been extremely successful in finding all of the solutions for a given problem.

Since the shape of the object is unknown, it is important to know as accurately as possible the constraints that will be used to limit the number of solutions. Definition of the width of the junction (dimension (a) from Fig. 5.1) is important since the set of all possible solutions must fall within the width of the junction. If the width for the junction used in the phase restoration algorithm is too wide, solutions may exist in the final set that do not represent a possible current density profile. If the width used for the restoration is less than the actual width it may result in the elimination of possible solutions from the final solution set. Therefore, it is important to use the width corresponding to the actual measured width of the junction.

The critical current density J_c is used to place an upper limit on the possible solution profiles. J_c is a bulk property defined as the critical current I_c carried by the junction divided by the cross-sectional area of the junction. The width of the junction used to calculate the area and the actual width of the junction that is carrying supercurrent is not always the same. Variations of the microstructure along the length of the boundary may result in non-superconducting regions along the boundary. Thus, the actual width of the junction carrying supercurrent can be less than the measured width of the boundary. This may result in over estimation of the cross-sectional area of the boundary and consequently an underestimation of J_c. Unfortunately, different values of J_c used in the phase restoration algorithm can result in adding or subtracting solutions from the final solution set. We have taken care to overestimate the value of J_c so as not to eliminate possible correct solutions.

The specific parameters used to optimize the genetic algorithm search routine are strongly problem dependent. Although the parameters are problem dependent, the genetic algorithm has one major advantage over other minimization techniques. It searches solution space without any *a priori* information on the function that is being minimized. The experimentally measured moduli, the real space constraints on the junction and the initial parameters for the genetic algorithm are all that is needed to begin the search algorithm. It has also been shown to be more efficient than standard random number generators or grid searches.

V.7 Summary

By using a phase retrieval algorithm similar to the Gerchberg-Saxton error-reduction algorithm with a generalized projection onto sets form, it is possible to restore the phase information that is not measured when experimentally recording $I_c(u)$ data for Josephson junctions without making any assumptions about the current density distribution $J(x)$. In general it is not possible to find a unique solution for the 1-D phase problem, however it is possible with the assistance of a search algorithm (such as a genetic algorithm) to efficiently find all possible solutions. If multiple solutions exist for a junction, the set of all possible solutions can be compared against the boundary microstructure and the correct solution can be determined. When searching for multiple solutions, problems with convergence can arise because of the non-convex nature of the two constraint sets and will be discussed in detail in a later chapter.

VI. Uniqueness of the 1-D phase retrieval problem

This chapter will explore the uniqueness of the 1-D phase retrieval problem and develop the conditions for possible uniqueness. The phase retrieval algorithm developed in chapter V is capable of finding solutions to the phase problem that are consistent with the known boundary constraints. For thin film Josephson junctions, the phase retrieval problem is one-dimensional (1-D). The 1-D phase retrieval problem is generally considered non-unique, however, enforcing certain boundary constraints can often ensure uniqueness of the 1-D phase problem. These boundary constraints and their applicability to Josephson junctions will be considered.

VI.1 Introduction

The lack of uniqueness of the 1-D phase retrieval problem has long been a source of ambiguity for physical applications of restoration from magnitude algorithms. The basic problem can be stated as follows: Given the Fourier transform relation between $F(u)$ and $f(x)$ which for the continuous case can be written as;

$$F(u) = \int_{-\infty}^{\infty} f(x)\exp(iux)dx \qquad (6.1)$$

or for the discrete case can be written as;

104

$$F(u) = \sum_{x=0}^{N-1} f(x)\exp(iux),$$ (6.2)

is it possible to calculate a real space object f(x) from the experimentally measured Fourier modulus IF(u)I. It is well known that the 1-D phase restoration problem can have multiple solutions and thus ambiguities in interpreting the physical significance of particular solutions. Walther demonstrated that when the modulus IF(u)I is given, it is possible to multiply IF(u)I by a phase function term,

$$IF(u)Iexp(i\theta),$$ (6.3)

then by reverse Fourier transforming to generate a real space object f(x)(Walther 1962). However, Walther pointed out that any phase function exp(iθ) of modulus 1 arrived at randomly can be multiplied by IF(u)I and transformed to generate a real space object f(x). Thus when the only information available is the Fourier modulus IF(u)I, there can potentially exist an infinite number of solutions to the 1-D phase retrieval problem. Thus when there exists infinite ambiguity in the solutions f(x), no relevant physical information is obtainable without additional constraints on the problem.

Walther considered the case of finite (compact) support where the function f(x) is known to be band limited to an interval [a,b] on the real x-line. Figure 6.1 shows a
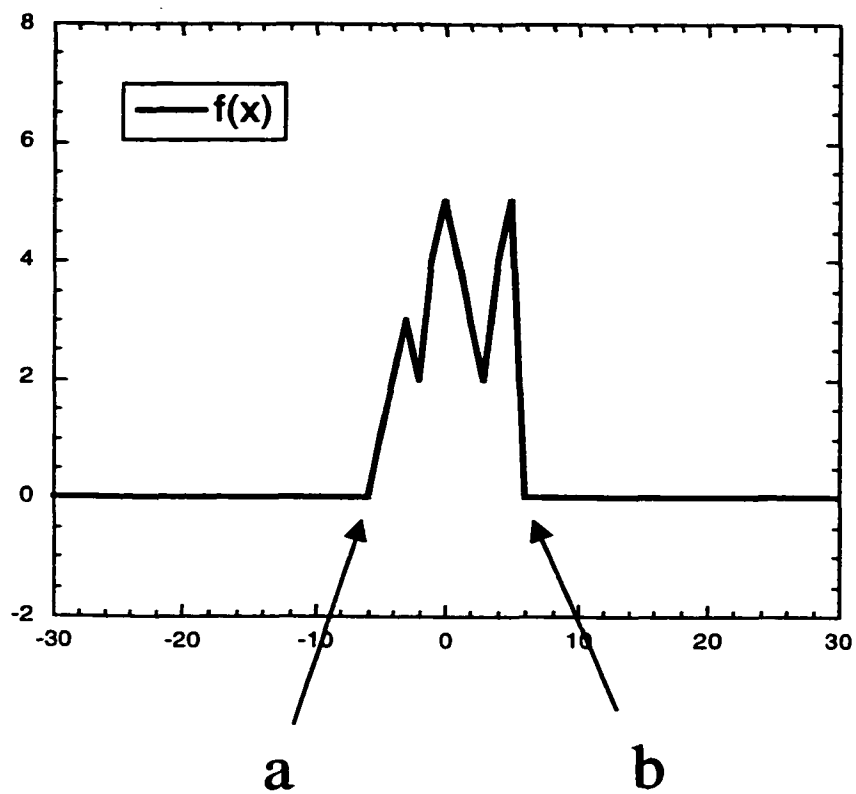
Figure 6.1 real space object f(x) is of finite (compact) support
(f(x) = 0 outside of the interval [a,b]).

function that is band limited to the interval [a,b] where f(x) = 0 everywhere outside the region [a,b]. Walther showed that when |F(u)| is multiplied by a random phase function as in equation 6.3, the resulting real space object f(x) almost never conforms to the requirement that f(x) = 0 outside the interval [a,b]. Therefore, by requiring f(x) to be zero outside a fixed interval [a,b], it places a severe restriction on the possible phases that can be used to generate a function f(x) that conforms to the band limit [a,b]. Although the possible phases have been severely restricted by the band-limit constraint, there can still exist many different solutions f(x) that when Fourier transformed have the same modulus |F(u)|. Consequently, the compact support constraint does not in general guarantee a unique solution.

Several key papers by Greenaway, Crimmins, Fienup and Sault attempted to understand the requirements for uniqueness in the 1-D phase retrieval problem and to define conditions and constraints on the real space object f(x) that would guarantee uniqueness (Greenaway 1977; Crimmins et al. 1981; Crimmins et al. 1982; Sault 1984). Starting with the Fourier transform relationship,

$$F(u) = \int_{-\infty}^{\infty} f(x)\exp(iux)dx \qquad (6.4)$$

where f(x) is the real space object of interest. F(u) can be extended into the complex z-plane as;

$$F(z) = \int_{-\infty}^{\infty} f(x)\exp(izx)dx \qquad (6.5)$$

where $z = u + iv$ in the complex plane. $F(z)$ is defined as an entire function which means it is analytic over the entire z-plane. Entire functions exhibit a unique property that they may only take the value of zero ($F(z) = 0$) at a set of isolated points that are unique to that function and are distributed throughout the z-plane in such a way that they tend to lie close to the real u-axis. The locations of the zero points (zeros) determine the modulus $|F(u)|$ on the real line.

It can be shown that if there exist two functions $F(z)$ and $F_1(z)$ where $|F(u)| = |F_1(u)|$, then $F_1(z)$ can be thought of as being obtained from $F(z)$ by the following relation;

$$F_1(z) = F(z)\left(\frac{z - \bar{z}_o}{z - z_o}\right) \qquad (6.6)$$

where z_o is a zero of $F(z)$ and $\bar{z}_o$ is the complex conjugate of z_o. Therefore, $F_1(z)$ can be thought of as being obtained by removing a zero at location z_o and then adding a zero at location $\bar{z}_o$. The zero at z_o was "flipped" or conjugated about the real line to produce a new function $F_1(z)$ that has the same Fourier modulus $|F(u)|$ along the real line. Flipping any number of complex zeros about the real line will result in a new function $F(z)$ that

has the same Fourier modulus lF(u)l. Then it can be shown that a function F(z) with M

complex zeros can have 2^M different unique combinations of zero flips and thus 2^M

different solutions to the phase problem (Greenaway 1977). Consequently, functions with

no complex zeros (M = 0) must generate only a single unique real space function f(x)

since there are no complex zeros that can be flipped about the real line to produce new

functions with the same modulus. Therefore, functions F(z) with only real zeros must

produce unique solutions to the phase problem.

VI.2 Possible 1-D Uniqueness Conditions

Greenaway attempted to show constraints that could be placed on the real space

function f(x) that would guarantee only real zeros and thus produce unique solution to the

phase problem (Greenaway 1977). Greenaway argued that if a real space object f(x) had

a region within the function that was equal to zero (disconnected support) then the

solutions generated by phase retrieval should be unique. Figure 6.2 shows a function

with disconnected support where the function is defined to be non-zero over the intervals

[a,b] and [c,d] and defined to be zero everywhere else. Crimmins and Fienup showed

that the disconnected support constraint used by Greenaway was not always unique

(Crimmins et al. 1981). They argued that the disconnected regions must be sufficiently

separated to guarantee uniqueness (Crimmins et al. 1982). To ensure uniqueness, the

region within the function constrained to be zero must be greater in extent than the non-
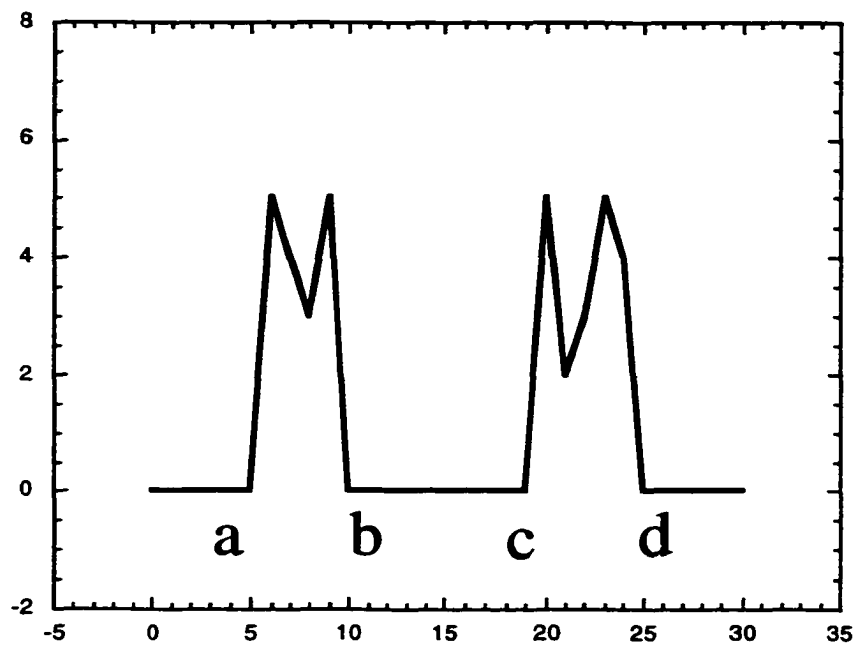
Figure 6.2 Object with disconnected support f(x) ≠ 0 [a,b] and [c,d].

zero regions. Figure 6.2 shows a real space function with sufficiently disconnected support where region [b,c] is greater in length than region [a,b] and [c,d]. Figure 6.3 shows a real space function with two zero regions within the function f(x). The separation condition requires that region [b,c] and [d,e] to be longer than regions [a,b] or [c,d] to ensure uniqueness.

The uniqueness criterion postulated by Greenaway, Crimmins and Fienup made no assumptions about the function f(x) being real or positive. Crimmins later showed that to guarantee uniqueness in all cases the function f(x) must be real and positive, however functions conforming to the separation condition that were not real or positive were "usually" unique (Crimmins et al. 1981).

VI.3 Application to Josephson Junctions

The current crossing a single Josephson junction can only traverse the region of the boundary that is defined by the length of the microbridge. Therefore the current must be zero outside of the junction length (finite support). The finite support of the boundary guarantees that there is not an infinite number of solutions to the phase retrieval problem. The current crossing the boundary is also known to be real which acts an additional constraint to reduce the total number of possible solutions. For grain boundary junctions with tilt angles less than 45°, it is assumed that the current must be positive at all locations along the boundary which also acts to reduce the total number of possible
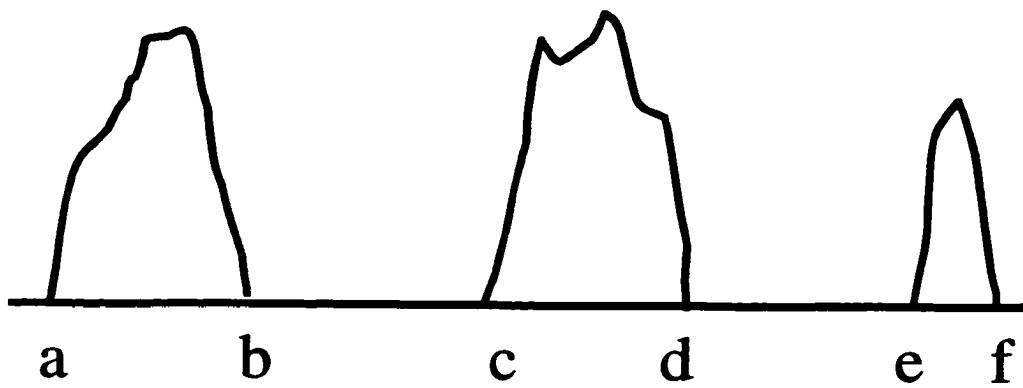
Figure 6.3 Interval [b,c] and [d,e] must be greater than [a,b], [c,d] and [e,f].

solutions. These three powerful constraints can often be used to find a unique, or physically unique solution. However, it is also possible to use micro-patterning techniques (photolithography or Focused Ion Beam) to damage areas along the boundary length to ensure that these regions carry zero current. These zero current regions can be used to enforce a disconnected support criterion within the current distribution and thus guarantee the uniqueness of the phase retrieval solution. This technique will be used to enforce uniqueness in chapter X.

VII. Demagnetization

To calculate the local current density distribution J(x) with the phase retrieval

algorithm developed in chapter V, the Fourier modulus as a function of an applied

magnetic field $I_c(H)$ must be measured experimentally. The specific experimental

techniques used will be described in detail in the next chapter, however, a numerical

technique must be used to correct the magnetic field measurements due to

demagnetization effects. The ability of a superconductor to expel a magnetic field is one

of the hallmark traits of superconductivity and is discussed in chapter II. The expulsion

of the magnetic field acts to focus the field at the boundary of the superconductor thus

increasing the total field strength near the boundary of a superconductor. Thus when a

magnetic field is applied to a Josephson junction (superconductor-barrier-

superconductor) the two adjacent superconductors act to enhance the field strength at the

barrier layer between them. This enhancement of the magnetic field at the barrier must

be corrected for when attempting to calculate J(x) from $I_c(H)$ measurements.

VII.1 Flux Focusing

The critical current crossing the boundary in a Josephson junction was shown to

oscillate as a function of an applied magnetic flux (B) in chapter III. The periodicity of

114

this oscillation (shown in Figure 7.1) can be theoretically calculated form the Fourier

Josephson equation. The width of this period (ΔB) can be written as;

$$\Delta B \approx \frac{\Phi_o}{w(2\lambda + d)}.$$

(7.1)

The periodicity's of the experimentally measured diffraction patterns for

Josephson junctions show large variations from the $\Delta B = \dfrac{\Phi_o}{w(2\lambda + d)}$ period expected

from equation (7.1). Rosenthal *et al.* pointed out that the period spacings for grain

boundary Josephson junctions were reasonable if they were corrected for

demagnetization effects (Rosenthal *et al.* 1991).

When a superconducting sample of permeability μ and susceptibility χ is placed

in a magnetic field, the internal magnetic field H_{in} of the sample is oriented parallel to the

applied magnetic field but is of different magnitude than the applied field H_{app} due to a

demagnetization field. The internal magnetic field is related to the applied field H_{app}

according to the relation:

$$H_{in} = H_{app} + H_d = H_{app} - DM$$

(7.2)

Φ_0 – flux quantum
W = junction width
λ – London depth

$$\Delta B = \Phi_0/W(2\lambda) \qquad \cong \qquad 1/W$$
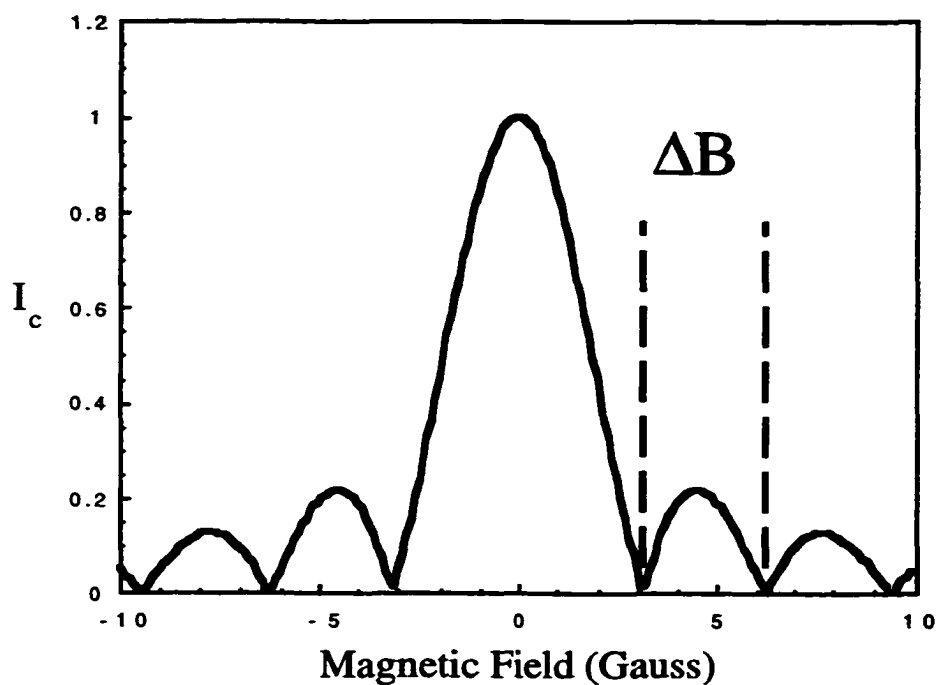
Figure 7.1 Schematic of period width (ΔB) determined from the Josephson equation.

where H_d is the demagnetization field, M is the magnetization and D is the

demagnetization factor (Osborn 1945; Cronemeyer 1991). From Maxwell's equations the

internal magnetic field can be written as;

$$\mu_0(H_{in} + M) = (1 + \chi)\mu_0 H_{in} \tag{7.3}$$

where μ_0 is the permeability of a vacuum $(4\pi \times 10^{-7} \text{ N/A}^2)$ and χ is the susceptibility of

the superconducting sample. Equation (7.3) can be simplified and written as;

$$H_{in} + M = (1 + \chi)H_{in} \tag{7.4}$$

$$M = \chi H_{in} \tag{7.5}$$

Substituting equation (7.5) into equation (7.2) gives

$$H_{in} = \frac{H_{app}}{1 + \chi D} \tag{7.6}$$

For an ideal Type I. superconductor or a Type II. superconductor below the first critical

field $H_{c,1}$, $\chi = -1$ and thus equation (7.6) can be written as;

$$H_{in} = \frac{H_{app}}{1 - D} \tag{7.7}$$

A new demagnetization factor D' can be defined such that;

$$D' = \frac{1}{(1-D)}$$

(7.8)

then it is possible to write

$$H_{in} = D' H_{app}$$

(7.9)

where the internal magnetic field differs from the applied magnetic field by a multiplication factor D' (Kunchur et al. 1991; Zeldov et al. 1994; Zheng et al. 1996; Brandt 1994). The demagnetization factor D' is a geometry dependent factor and thus must be calculated for each different sample geometry of interest. For an ellipsoidal sample the magnetization is uniform within the sample and thus the demagnetization factor D is a constant and can be obtained by a simple calculation or from calculated tables for various spheroid objects. Rosenthal assumed an ellipsoidal geometry to simplify the calculation by using the assumption that spheroid objects are uniformly magnetized and thus the demagnetization factor is a constant. Rosenthal assumed that a grain boundary junction could be approximated by two thin flat ellipsoidal disks (see figure 7.2) with aspect ratio of W/t where W is the diameter of the disk and t is the thickness of the disk (see figure 7.3). Rosenthal assumed a flat disk geometry with the

Flat spheroid geometry
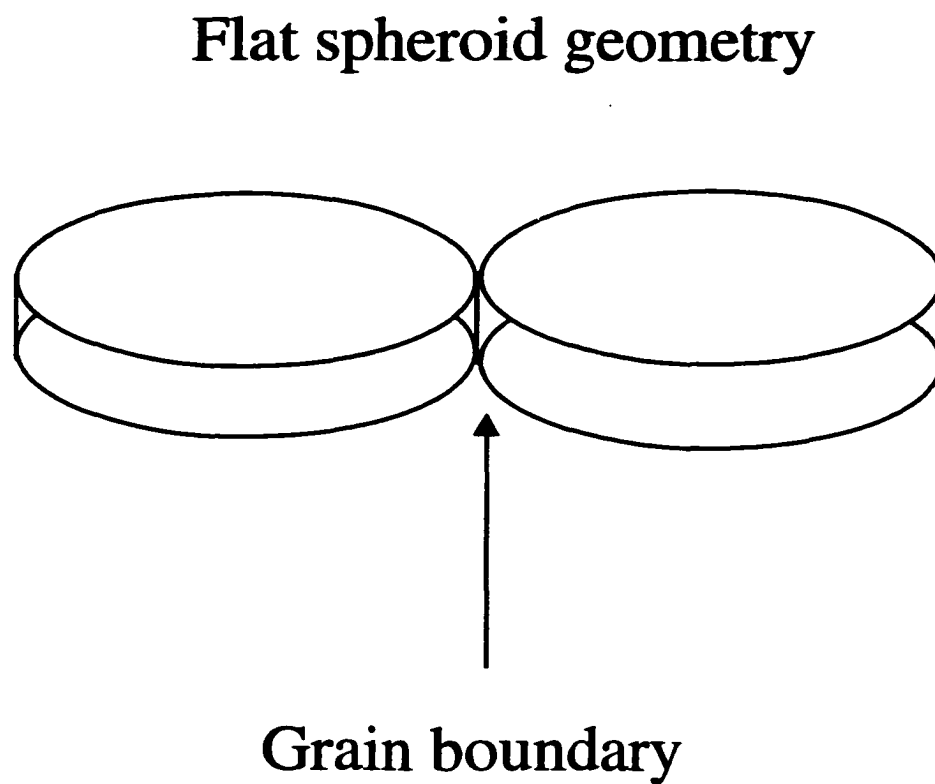
Grain boundary

Figure 7.2 Schematic of flat ellipsoidal grain boundary model used by Rosenthal to calculate a uniform demagnetization factor.

For thin film W>> t
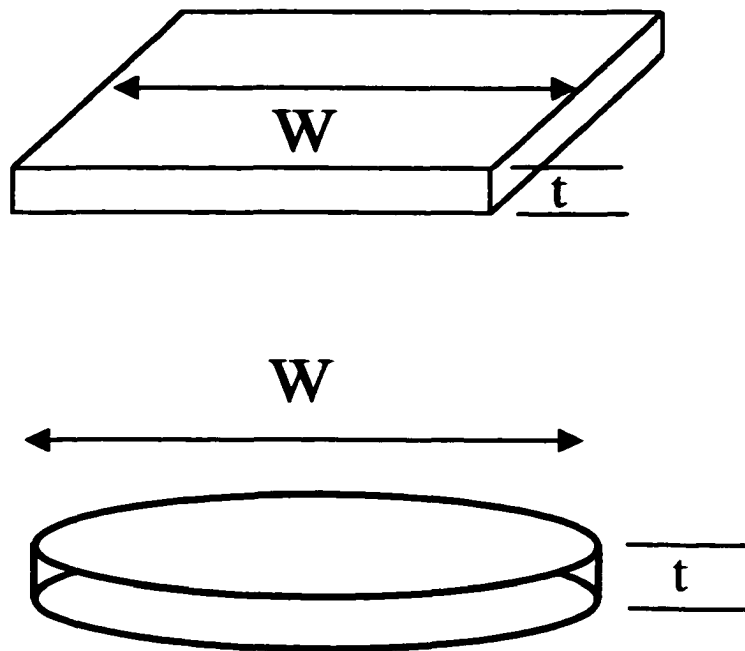
Figure 7.3 The flat disk geometry used by Rosenthal assumed that each disk had the same aspect ratio (W/t) as the rectangular prism above.

same aspect ratios as the microbridge (Osborn 1945; Cronemeyer 1991). The

demagnetization factor D' for this geometry can be written as;

$$D = 1.2(W/t) \qquad (7.10)$$

where W is the junction width and t the film thickness. The flat disk approximation used

by Rosenthal improved the data fit for many junctions but tended to overestimate the flux

focusing effect for much of the data published in the literature.

A typical grain boundary junction microbridge geometry is rectangular (see figure

7.4). The demagnetization factor for a non-ellipsoidal geometry is nonuniform.

Consequently, a numerical approximation of the demagnetization factor must be used to

approximate the sample magnetization. The approach used to improve the

demagnetization factor calculation was similar to the one used by Joseph and Schlomann

(Joseph *et al.* 1964). Joseph and Schlomann assumed a rectangular prism with principal

axes of length 2a, 2b, and 2c (see figure 7.5). Using a first order approximation, the

demagnetization factor D(x,y,z) as a function of position within the sample can be written

as;

$$D(x,y,z) = (\frac{1}{4\pi})\{\cot^{-1}(f(x,y,z)) + \cot^{-1}(f(-x,-y,z))$$
$$+ \cot^{-1}(f(x,-y,z)) + \cot^{-1}(f(x,y,-z)) + \cot^{-1}(f(-x,-y,z)) \qquad (7.11)$$
$$+ \cot^{-1}(f(x,-y,-z)) + \cot^{-1}(f(-x,y,-z)) + \cot^{-1}(f(-x,-y,-z))\}$$

barrier layer (grain boundary)

superconductor-barrier-superconductor
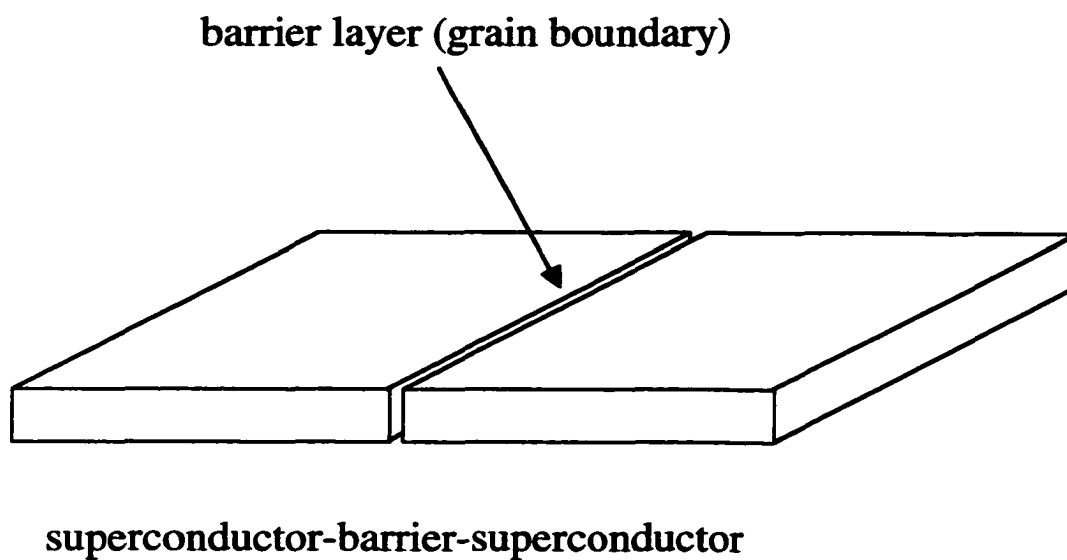
Figure 7.4 Schematic of typical rectangular microbridge across a Josephson junction
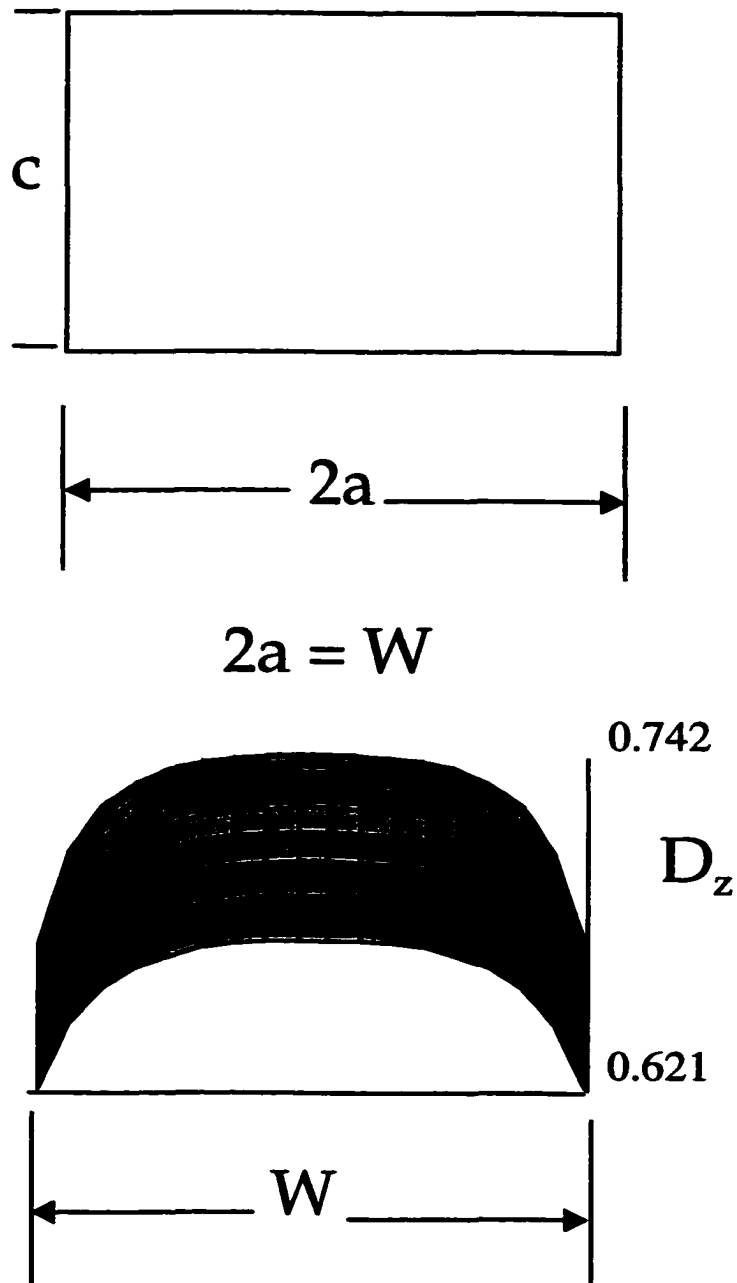
Figure 7.5 Rectangular geometry and the corresponding positional variation of the demagnetization factor D.

where f(x,y,z) can be written as;

$$f(x,y,z) = \frac{[(a-x)^2 + (b-y)^2 + (c-z)^2]^{1/2}(c-z)}{(a-x)(b-y)}$$

(7.12)

. By solving equation 7.11 and 7.12 it is possible to calculate the local variation of the demagnetization factor along the length of a Josephson junction and thus correct the magnetic field measurements for demagnetization errors.

Figure 7.5 shows a plot of equation 7.11 for a 5 μm wide Josephson junction. Note the variation of D' with position. This is a strong deviation from the ellipsoidal approximation used by Rosenthal. Figure 7.6 shows that the demagnetization factor varies in the direction along the boundary width W of the junction as well as into the superconductor. Figure 7.7 shows that the variation of D' with position varies less than 10% and thus can be averaged to obtain a single demagnetization factor D'. Table 7.8 shows a comparison for two Josephson junction widths between the ellipsoidal D' used by Rosenthal and the rectangular D' calculated using the numerical approach for rectangular bodies. Table 7.8 highlights the over estimation of D' made when using the approach by Rosenthal. Therefore, when attempting to obtain quantitative information about the magnetic field along the boundary in a Josephson junction it is important to consider the proper demagnetization factor for the geometry of interest.
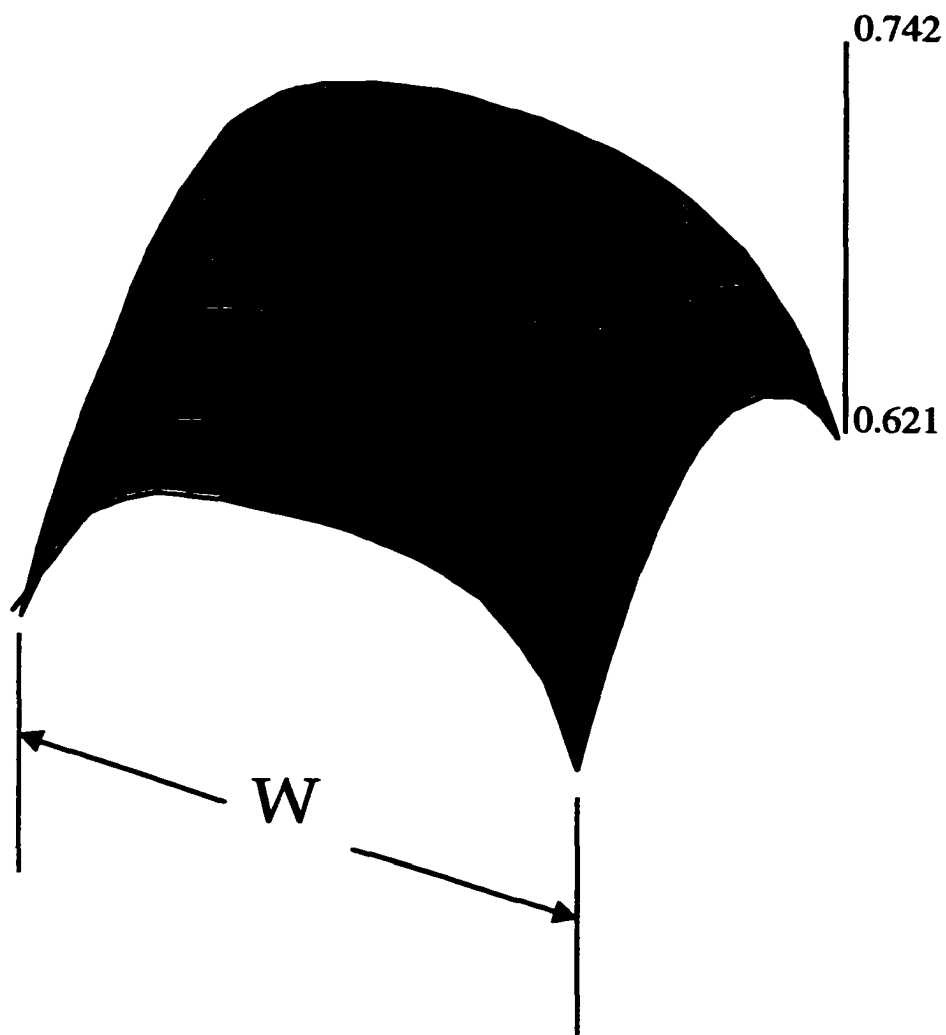
Figure 7.6 Shows variation of D both along the boundary and away from the boundary plane into the page.
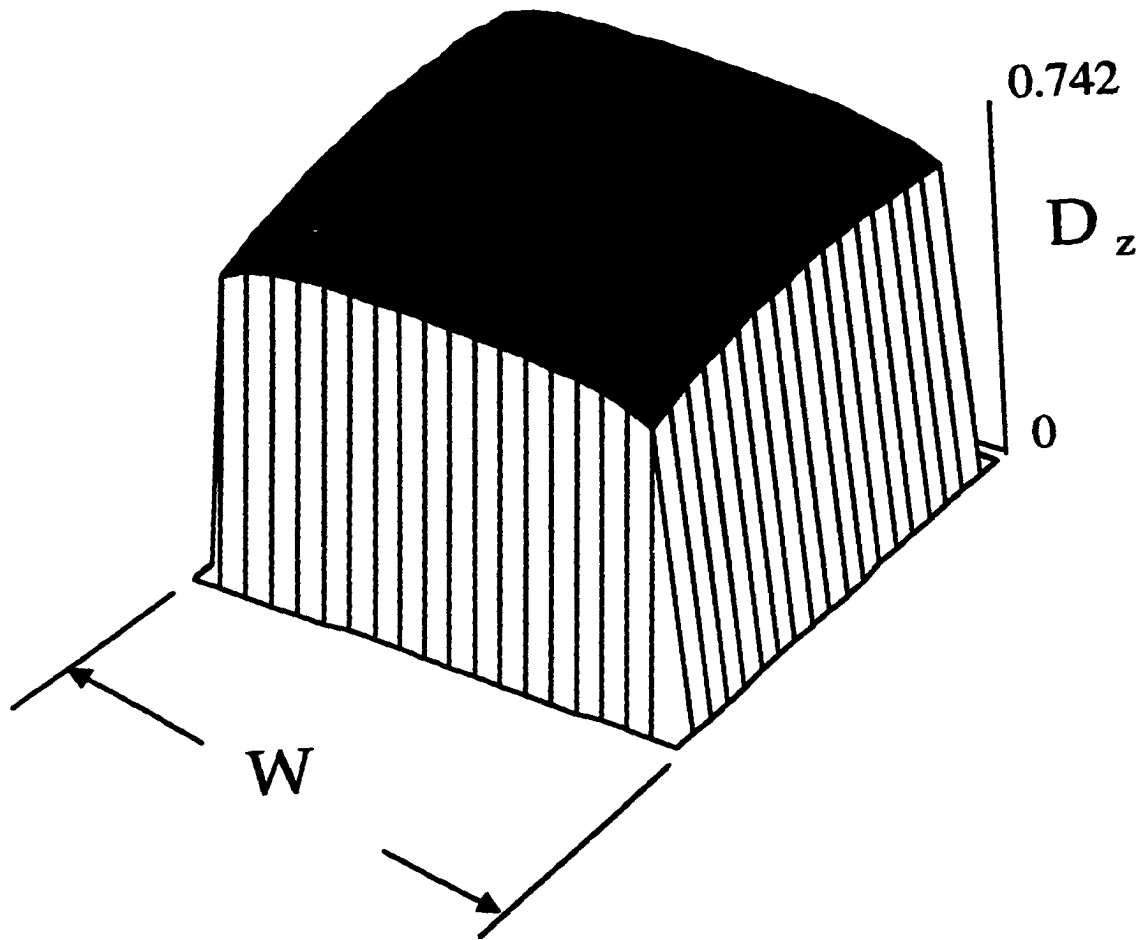
Figure 7.7 D_z can vary between 0 and 1. Therefore the small variation of D with position can be averaged.

Boundary Width	D ' Ellipsoidal	Average D ' Rectangular
2 μm	~ 10.5	~ 4.9
5 μm	~ 25.53	~ 14.47

Table 7.8 Table comparing the ellipsoidal approximation used by Rosenthal and the rectangular approximation used during this thesis.

VIII. Experimental Techniques

The goal of this study is to gain a fundamental understanding of the local current transport along the length of a Josephson junction in order to understand the underlying mechanism controlling the transport process. Thus the experimental approach was to form grain boundary Josephson junctions, isolate a section of the boundary for study, characterize the transport properties along this section and attempt to understand the local variations in the current from a material perspective. This chapter describes the experimental equipment and procedures used during the realization of this thesis. The techniques, methodologies and equipment are discussed in detail. Several pieces of equipment were designed or modified specifically for this research and will be highlighted in this chapter.

VIII.1 Grain Boundary Formation

Two basic types of YBCO grain boundaries were studied, thin film [001] 24° symmetric tilt grain boundaries and thin film [001] 45° asymmetric tilt grain boundaries. Two techniques were used to create artificial grain boundaries for isolation and study; bicrystal substrates and sputter induced epitaxy (SIE). This bicrystal technology was pioneered by IBM for the isolation and study of tilt grain boundary configurations in high-T_c systems (Chaudhari *et al.* 1988; Dimos *et al.* 1988; Mannhart *et al.* 1988; Dimos *et al.* 1990; Chaudhari *et al.* 1989). The technique involves clamping, high temperature

128

sintering and polishing of two single crystals with a relative misorientation angle (θ) between them. The resulting polished bicrystal, with an artificial grain boundary between the two single crystals, is used as a template for epitaxial thin film growth. Figure 8.1 shows a schematic of the bicrystal geometry used for thin film growth. The resulting thin film grows with a single grain boundary with the same orientation as the bicrystal boundary. This bicrystal technique is now widely used to study grain boundaries in both superconducting and non-superconducting systems.

VIII.1 24° Grain Boundary Formation

Commercial symmetric [001] tilt $SrTiO_3$ bicrystals were used as templates for epitaxial film growth and YBCO grain boundary formation. $SrTiO_3$ has a cubic structure with a good lattice match (a = b = c = 3.905 Å) with the a-b plane of YBCO (a = 3.82 Å, b = 3.89 Å) and acts as a good template for epitaxial film growth. The orientation of YBCO grown epitaxially on $SrTiO_3$ is the cube-on-cube orientation (YBCO [001] $\parallel$ $SrTiO_3$ [001] and YBCO [110] $\parallel$ $SrTiO_3$ [110]). Thin film YBCO was grown epitaxially on the $SrTiO_3$ bicrystal substrates using two different techniques; Pulse Laser Deposition (PLD) and Pulsed Organometallic Beam Epitaxy (POMBE).
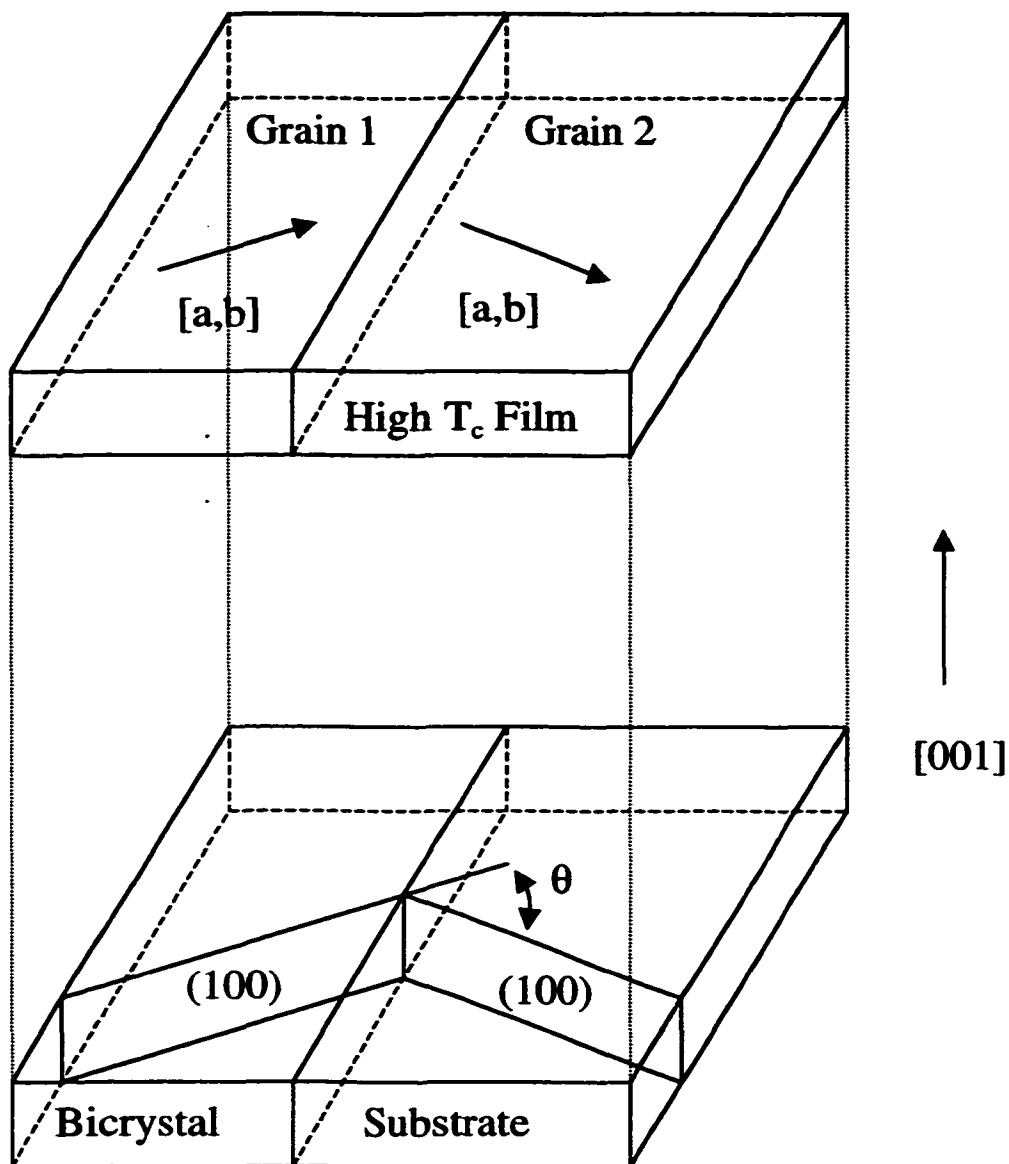
Figure 8.1 Schematic of the bicrystal geometry where a substrate with a tilt grain boundary with a misorientation of θ is used as a template for thin film growth.

VIII.1.2 Pulsed Laser Depostion

The PLD deposition was performed at Argonne National Laboratory by Dr. Mike Chudzik. The Argonne system is show in figure 8.2. For thin film growth the system is evacuated to a nominal base pressure of 10^{-6} Torr. A bicrystal substrate is placed in close proximity to the target material in a background oxygen environment of 100 mTorr (see figure 8.3). A 248 nm Kr-F eximer laser, pulsed at 10 Hz with an energy density of 1.5 J/cm^2, is focused onto the target YBCO material. During deposition, the substrate stage is heated to between 750-780°C to obtain epitaxial film growth. After growth, the sample is slow cooled to room temperature in a 760 Torr O_2 atmosphere to eliminate reduction of the YBCO. Typical epitaxial films of YBCO were grown with current densities (J_c) in the 1-5 x 10^6 A/cm^2 range with T_c near 90 Kelvin.

VIII.1.3 Pulsed Organometallic Molecular Beam Epitaxy

A second technique that was used for thin film growth was Pulsed Organometallic Molecular Beam Epitaxy (POMBE) developed by Professor. R.P.H. Chang's research group at Northwestern University (Buchholz *et al.* 1994; Duray *et al.* 1991). POMBE is a thin film growth technique whereby oxide films can be grown in a microwave assisted oxygen plasma. Solid or liquid organometallic precursors with metallic cations are sequentially pulsed by a computer controlled feedback loop and carried to the substrate via a helium carrier gas. The specific sources used during deposition were

**Deposition Chamber
and Pumping Stack**

KrF Pulsed-Excimer Laser

**Beam Guard
and Optics Bench**
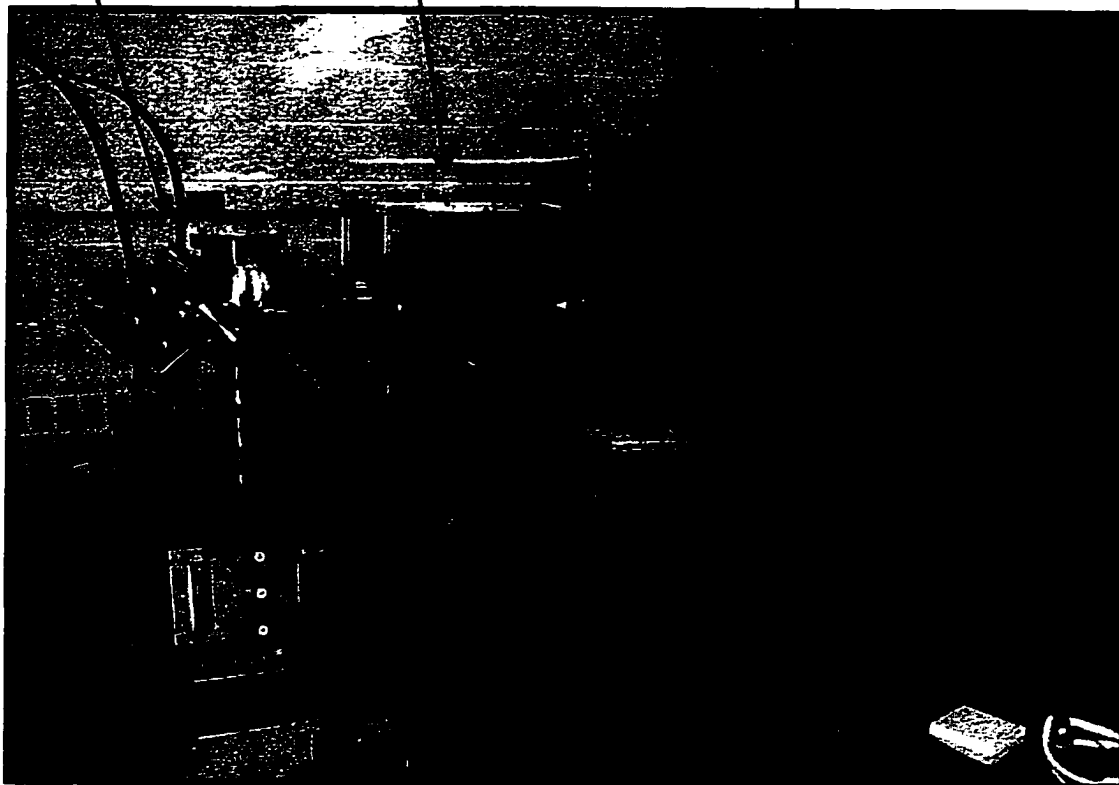
Figure 8.2 Photo of Argonne Pulsed Laser Deposition Chamber.(courtesy of Dr. Mike Chudzik)
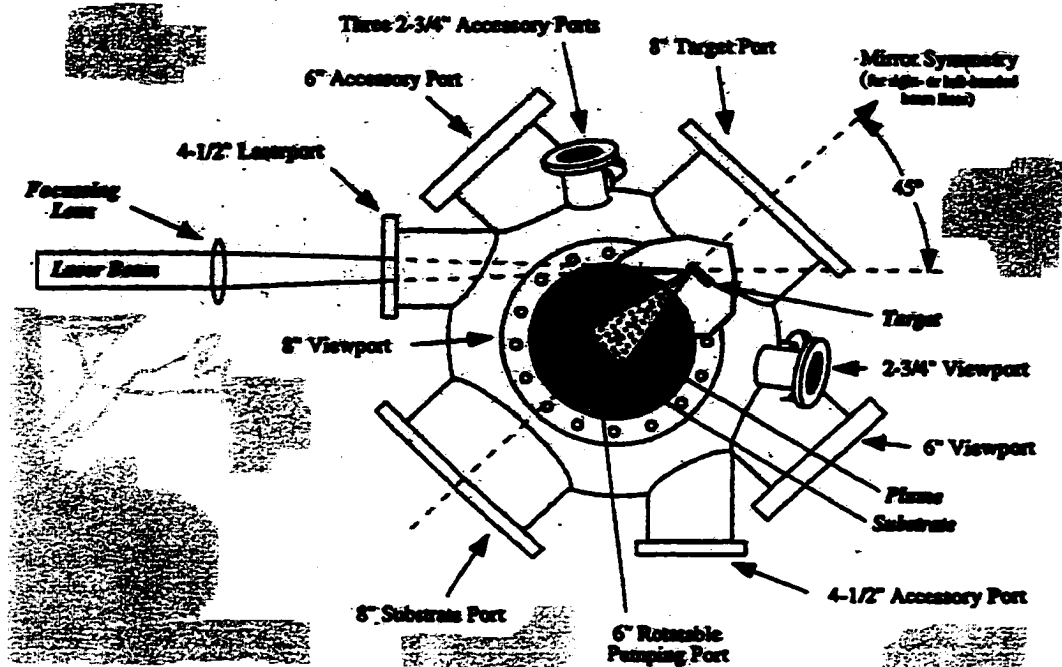
Figure 8.3 Schematic of pulsed laser deposition chamber.(T. Venkatesan, Neocera and Picture by M.A. Savell, MRS bulletin Feb 1992.)

Y(dipivaloylmethanate)$_3$, Cu(dipivaloylmethanate)$_2$ and

Ba(hexafluoroacetylacetonate)$_2$tetraglyme. The substrate is heated to the growth

temperature (650-750°C) and held at that temperature in a microwave assisted oxygen

plasma for approximately 30 minutes cleaning the surface of any contaminants. The

background oxygen pressure in the chamber during deposition is between 10^{-2} and 10^{-3}

torr. For YBa$_2$Cu$_3$O$_{7-x}$ film growth, the pulse sequence is (-Cu-Ba-Cu-Y-Cu-Ba) and is

pulsed such that the film grows at atomic scale increments. After each pulse the sample

is soaked in the oxygen plasma to ensure complete oxygenation of the oxide film.

VIII.2 45° Grain Boundary Formation Sputter-Induced Epitaxy (SIE)

MgO has been used as a growth template for epitaxials films because of its

reasonable lattice match (a = b = c = 4.21 Å) with the a-b plane of YBCO (a =3.82 Å, b =

3.89 Å). YBCO can be grown with several different epitaxial relations relative to the

MgO substrate. The most common epitaxial relationship observed is YBCO [001] ‖

MgO [001] and YBCO [110] ‖ MgO [110] commonly referred to as the cube-on-cube

orientation. A second common orientation observed is the YBCO [001] ‖ MgO [001] and

YBCO [100] ‖ MgO [110] where the YBCO unit cell is rotated 45° about the [001] axis

relative to the cube on cube orientation and is often referred to as modified epitaxy (Shin

et al. 1989; Giess et al. 1990; Hollmann et al. 1994; Schlom 1992a).

Work published by Chew et al. suggested that an ion beam modification of the

MgO substrate could induce a modified epitaxy, however the result was not reproducible

due to variations in the experimental conditions (Chew *et al.* 1988). Vuchic *et al.* was

able to reproduce the results and developed the technique into a viable grain boundary

formation technique (Vuchic *et al.* 1995a; Vuchic *et al.* 1995b).

The technique devised by Vuchic *et al.* was used extensively for the fabrication of

[001] 45° asymmetric tilt boundaries. The remainder of this section details the specifics

of the SIE technique developed by Vuchic *et al.* and used for the formation of 45° tilt

grain boundaries.

A commercially acquired (100) MgO substrate was partially covered with a

physical mask (hard baked photoresist mask) then irradiated with low-voltage argon ions

(50-500 eV) at room temperature for $\approx$ 2 minutes with a beam current density of 1

mA/cm^2 (see figure 8.4). After irradiating half of the sample, a thin film of YBCO

usually 2000 - 3000 Å thick is grown eptiaxially on the surface with the Pulsed

Organometallic Beam Epitaxy Technique (POMBE). The resultant epitaxial relationship

of the film to the substrate can be either cube-on-cube on the unsputtered region of the

substrate, and rotated by 45° about the [001] on the sputtered region or vice versa

depending on the growth conditions (Buchholz *et al.* 1994; Huang *et al.* 1999) (see figure

8.5).

Physical Mask
(Hard baked photoresist)

Ar Ions
(50-500 eV)

(100) MgO
Substrate
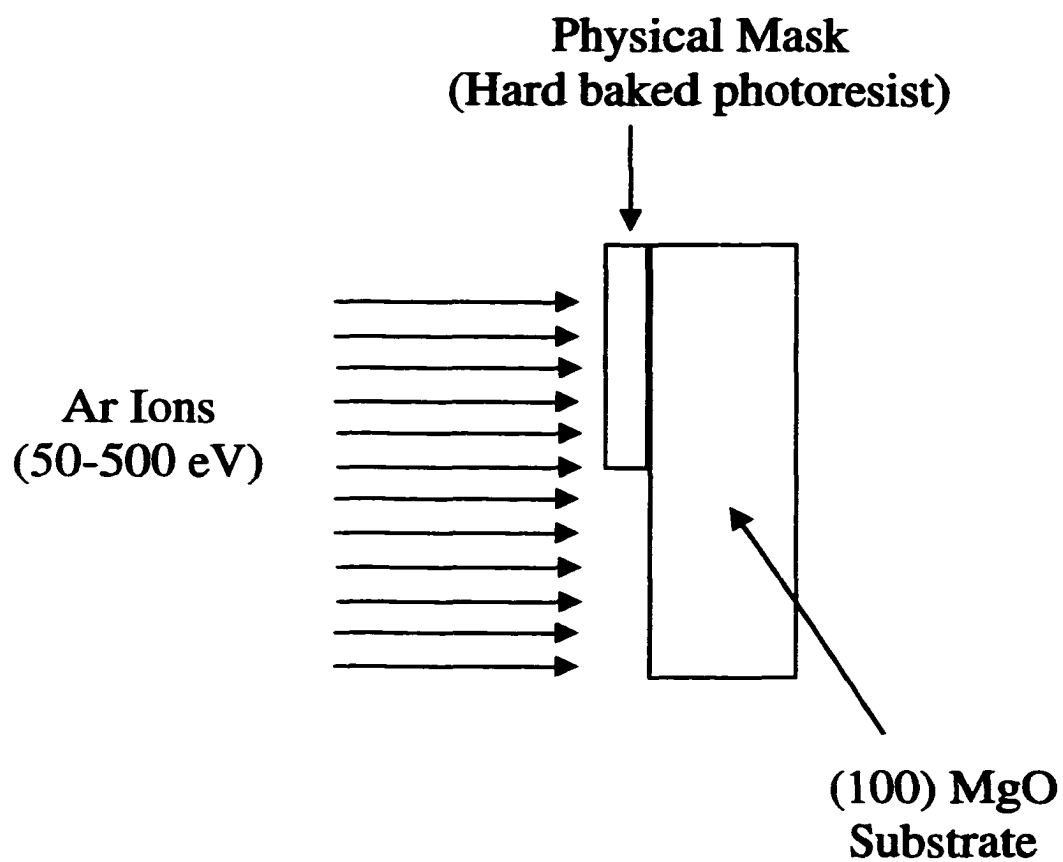
Figure 8.4 Schematic of ion milling procedure for sputter induced epitaxy (SIE).

45° [001] asymmetric
tilt grain boundary

[001]

[100]

[001]

[110]

YBCO
film

Unsputtered
Region of
substrate

MgO
Substrate

Sputtered
Region of
substrate
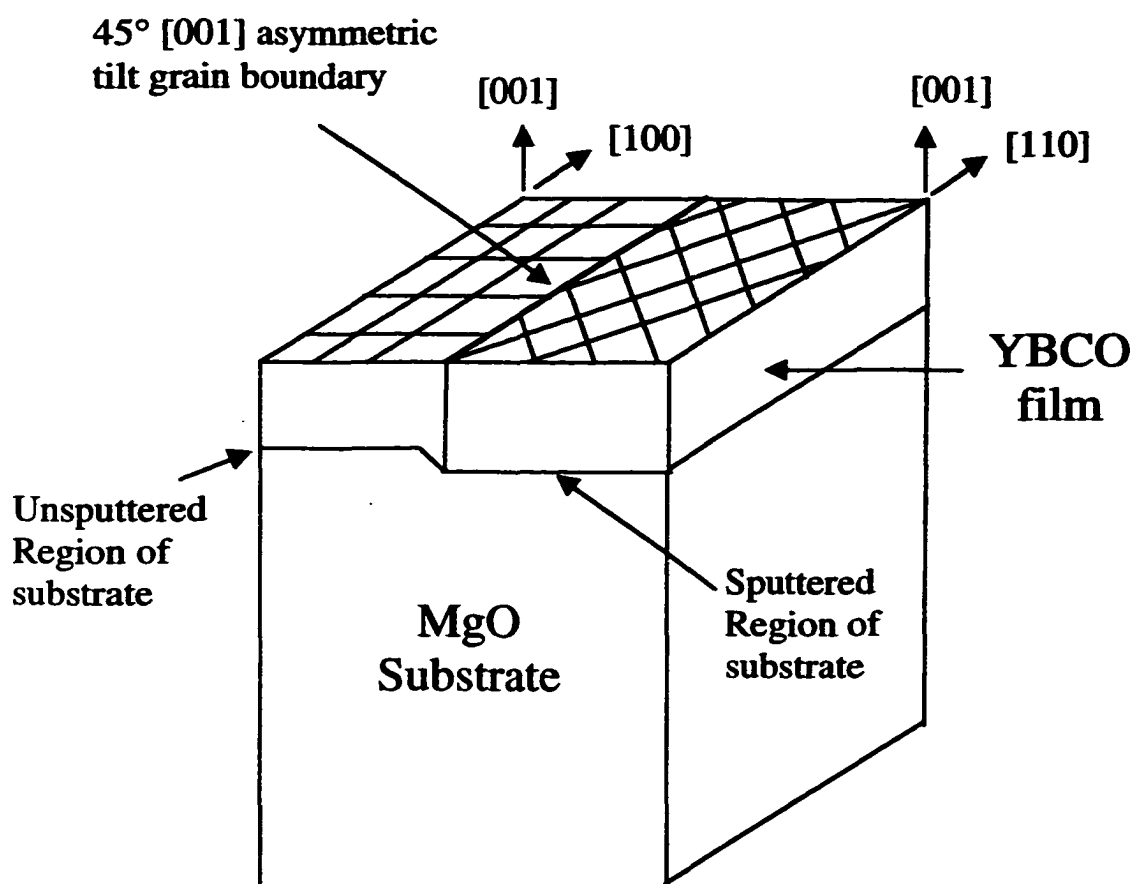
Figure 8.5 Schematic of final orientation relationship for sputter induced epitaxy (SIE).

VIII.2.1 Ion Mill

A low voltage ion mill is used to irradiate the MgO substrates prior to film growth for 45° sputter-induced epitaxy junctions and for film removal after patterning with photolithography techniques. Figure 8.6 and Figure 8.7 are schematic drawings of the ion milling apparatus and vacuum pumping system. The ion source is a Kaufman type Ion Tech Model 3.0-1500-100 Ion Source with a heated tungsten filament that acts as its cathode to emit electrons. The emitted electrons ionize the source gas (Argon). The argon ions are accelerated by negatively biased graphite grids to a final energy between 50 eV and 500 eV. The accelerator grid holes are 3 cm in diameter that also act as an aperture. A tungsten filament located beyond the accelerator grids act as a neutralizer by thermally emitting electrons.

The sample is thermally anchored to a copper stub with silver paint. The sample holder can be rotated by an external electric motor through 360°. The sample holder can also be tilted to any desired angle relative to the beam direction. When the sample holder is perpendicular to the beam direction the surface of the sample is 4 inches from the graphite girds. The sample stage can also be connected to a liquid nitrogen cold finger for sample cooling during ion bombardment. The primary vacuum pump on the chamber is a He cryopump with a pumping speed of 660 liters/second (for argon) with a throughput of 300 standard cubic centimeters of argon. This chamber maintains a nominal background pressure of 6×10^{-7} Torr with no argon flow. During sputtering the

chamber pressure is maintained at 2 x 10-4 Torr. A hinged door on top of the chamber
allows quick sample access.

VIII.3 Photolithography

The transport samples are patterned using standard photolithographic techniques
using micro-bridges that we developed specifically for this research. A thin layer of
Shipley Type S-1813 positive photoresist was spun on the samples to be patterned at
3000 rpm leaving an approximate 1.25-1.5 mm thick layer of photoresist on the entire
sample. The coated sample is baked at 80-100°C for 20 minutes. A Cr metal mask
manufactured by Advanced Reproductions containing specific pattern designs is
positioned over the sample with the pattern side down aligning the bridge area with the
location of the grain boundary. Figure 8.8 is a photomicrograph of the Cr mask used to
pattern the microbridges on the YBCO samples. A mercury lamp is used to expose the
photoresist patterned samples for the optimal exposure time that is dependent on the
required resolution of the microbridge. The sample is then developed for 20-30 seconds
in Microposit MF-319 developer and rinsed in deionized water. The exposed and
developed sample is then hard baked at 120-130°C for 1 hour. The patterned sample was
then ion milled using the low voltage ion milled described above to remove the unwanted
material. Figure 8.9 shows a SEM micrograph of a patterned and sputtered YBCO grain

boundary microbridge. Using non-clean room facilities, a line resolution of 5 μm was routinely achieved.

VIII.4 Metallization

Forming low resistance contacts between the gold lead wires and the YBCO was necessary to minimize low level noise in the transport signal. Low resistance contacts were formed by metallization of the YBCO with a thin silver coating. Silver was evaporated using resistive heating in a vacuum deposition chamber onto the clean YBCO surface. The YBCO surface to be coated was ion milled briefly to ensure a clean surface for coating. The grain boundary region was physically shielded to avoid contamination of the region. The as-deposited silver on the thin YBCO film was annealed in a flowing oxygen atmosphere at 400°C for 4 hours. At temperatures above 450°C calcium is known to migrate to the (100) surface of MgO, therefore an anneal temperature below 450°C was selected for metallization. Gold wires with a 50 μm diameter were placed in direct contact with each silver pad. Silver paint was used to affix the gold wires to the contacts. A very small amount of silver paint was used to affix the gold wires and allowed to dire. Once the silver paint had dried a larger amount of silver paint was used to cover the end of each wire attached to the sample. The sample leads were tested at room temperature for electrical shorts.

VIII.5 Transport Measurement System

The transport measurements were performed in a Janis Research SuperTran - VP Continuous Flow Cryostat (see figure 8.10). Inside the cryostat there is a copper cold finger with 12 electrical lead pins (see figure 8.11). The cold finger (along with the sample) sits in flowing helium gas. The samples are connected to the lead pins in the cryostat with low temperature Indium solder. The helium gas is heated by an externally controlled resistance heater. The temperature of the copper cold finger is measured by a silicon diode thermometer that is thermally anchored to the copper near the sample. The heater coil temperature is controlled by a separate silicon diode thermometer that is located near the heater coil (see figure 8.10). The entire cold finger is surrounded by a radiation shield to prevent radiant heating. An outer shell encapsulates the radiation shield and the cold finger. A mechanical roughing pump is used to maintain a vacuum between the outer shell and the radiation shield for thermal insulation from the surrounding room. The lowest temperature that can be measured is 4.2 K.

The system is controlled by a Macintosh Plus computer using a QuickBasic program that has been developed and refined by the interface group at Argonne National Lab. The temperature is measured and controlled by a LakeShore 330 Temperature Controller and the current is controlled by a Keithley 224 Programmable Current Source. The current passes through a 100 Ohm standard resistor with a Keithley 197A Digital

Voltmeter attached in parallel to measure the voltage drop across the resistor. The voltage across the resistor divided by the 100 Ohm resistor is the value recorded as the applied current. The applied current is driven across the sample with the voltage drop across the sample measured by a Keithley 182 Sensitive Voltmeter. Each lead pole can be measured separately with the use of a Hewlett-Packard 3459A Scanner which scans the various channels of interest. A Mac 488B Bus Controller is used to interface the various pieces of equipment and the computer that controls the operation. The data measured by this apparatus is stored as an ASCII file in the computer. The entire system is grounded to a common ground to eliminate any stray current loops. Figure 8.12 shows a schematic of the computer controlled current source and voltmeters.

The transport measurements are performed using a standard current biased four-point probe technique. A current is driven across the sample using a current source and the voltage drop across an area of interest is measured. The sample is anchored to the copper cold finger with Type N Apiezon grease. The four-probe technique is used to remove contact resistance from the measurements by driving a current across two leads and measuring the voltage drop across two different leads. The voltage drop is a passive measurement with very small amounts of current being drawn because of the high impedance such that the contact resistance is not measured. The standard measurements performed on this system include current vs. voltage (I-V), resistance vs. temperature (RT) and current vs. applied magnetic flux ($I_c(B)$). Figure 8.11 shows the configuration

of the measurement scheme on the copper cold finger. The measurement is a current

biased technique where a d.c. current is driven across a small section of the sample and

the voltage drop across that section in measured.

VIII.6 Low Temperature Transport Measurements

The cryogenic transport measurements were performed with the standard four-

point probe technique where the current is driven across a section of sample and the

voltage drop across the section is measured. Figure 8.13 shows a SEM micrograph of a

YBCO grain boundary microbridge with the two current leads and the two voltage leads

marked for four-point probe measurements. For current vs. voltage (I-V) measurements,

the current bias starts at zero and is incrementally ramped up to a maximum current (I_m),

ramped back down through zero to negative I_m and then back to zero again to ensure no

hysteresis in the measurements. The maximum current I_m and the incremental current

steps (ΔI) are controlled by the computer and are input by the user. The voltage response

to an applied current has a time dependent component. The steady state condition is the

experimental state of interest, therefore a short dwell time after each current increment is

required to allow the transient voltages to dissipate. The dwell time at each new current

increment before the voltage measurement is recorded is controlled by the computer and

is input by the operator before each measurement run. The voltage readings at each

current increment are an average of typically ten measurements. The average is calculated via;

$$\overline{V_i} = \frac{\sum_{n=1}^{10} V_n}{n}$$

(8.1)

where $\overline{V_i}$ is the average voltage at the ith current increment and V_n is the nth Voltage measurement at the ith current increment. The standard deviation σ is calculated from;

$$\sigma^2 = \frac{\sum_{n=1}^{10} (\overline{V_i} - V_n)}{n}$$

(8.2)

to ensure that no major voltage fluctuations have occurred during the measurement due to current or temperature variations.

For Resistance vs. Temperature (RT) measurements, a bias current is chosen by the user and driven across the sample. The standard current bias that defines the onset of the normal state is 0.001 mA. The temperature interval (starting and ending temperature) and the incremental steps between measurements (ΔT) are also input by the user and controlled by the computer. The temperature variation around a fixed temperature (acceptable error) for each temperature can also be controlled. Typically the temperature

increment is 0.2 K with ± 0.05 K allowable error. For RT measurements the thermal voltage offset is subtracted out to verify superconductivity. This is accomplished by measuring the voltage drop with a positive current bias, then measuring the voltage drop with a negative current bias, subtracting the two values and dividing by two. (equation 8.3)

$$V = \frac{V_+ - V_-}{2}$$

(8.3)

The thermal offset voltage of equation 8.3 is typically not subtracted out of current vs. voltage measurements for historical reasons. The resistance R of the boundary is defined as;

$$R = \frac{\rho L}{A}$$

(8.4)

where L is the length of the area usually defined by the microbridge length, ρ is the resistivity and A is the cross-sectional area. For a thin film superconductor the area A is dependent on the thickness of the thin film and the width of the boundary. For a grain boundary Josephson junction the cross-sectional area is difficult to define due to the meandering of the grain boundary and thus the uncertainty of the actual boundary width.

This system can also be used to measure the critical current as a function of an applied magnetic flux $I_c(B)$ at low temperatures. The magnetic field variation of the critical current is central to this thesis since the $I_c(B)$ data will be used in concert with the phase retrieval algorithm outlined in chapter V to determine the local current variation along the boundary of a Josephson junction. The magnetic field near the sample is measured with a Magnos 1600 Gaussmeter. The magnetic field strength is controlled by a current source and can be varied from 0 to 5000 Gauss with a control of ± 0.01 Gauss. The field direction can be reversed independent of the current direction in the sample. The sample can be rotated through 360° to allow the magnetic field to be applied with any orientation relative to the sample. Mu metal was used for zero field measurements to ensure a zero field condition within 0.01 Gauss. Typically an offset current is applied to the sample and the voltage variation as a function of an applied magnetic field is measured, however IV curves as a function of an applied magnetic flux can be measured and the $I_c(B)$ behavior determined from them.

Finally, Josephson junctions are extremely sensitive to radio-frequency (R-F) radiation. R-F radiation can be observed as small steps in the current-voltage measurements (Shapiro steps)(Shapiro *et al.* 1964). Thus all transport measurements were performed in a (quiet room) copper mesh shield room with a mesh size about 1 mm² to eliminate noise in the measurements due to R-F radiation. Electrical control equipment

such as voltmeters, control computers and scanner were isolated from the cryostat and located in a separate room from the shield room where the measurements were being taken. The electrical lines are all shielded to prevent noise and 100 Ohm resistors were placed in series on every line to increase the damping of the lines and prevent R-F interference.

VIII.7 Electron Microscopy

Various electron microscopy techniques were used to gain a better understanding of the boundary structure and geometry. A Hitachi 4500 Field Emission Gun (FEG) scanning electron microscope at Northwestern and a similar scope at Argonne National Laboratory were used to image the boundary plane and map the boundary meandering and large scale irregularities along the length of the junction.

Local variations of the microstructure were observed using a High Resolution Electron Microscopy (HREM). The primary instrument used for this research was the JEOL 4000 EXII at Argonne National Laboratory. YBCO is sensitive to electron beam damage. The oxygen content can be reduced as a function of time because of beam damage, therefore, much of the HREM work on YBCO was performed at 300 kV or less to minimize this effect (Richards *et al.* 1989).

Hinged door for sample entry

Ion Gauge

Valve

Ion Gun

Turbo
Pump

CryoPump

Gate Valve

RoughingPump
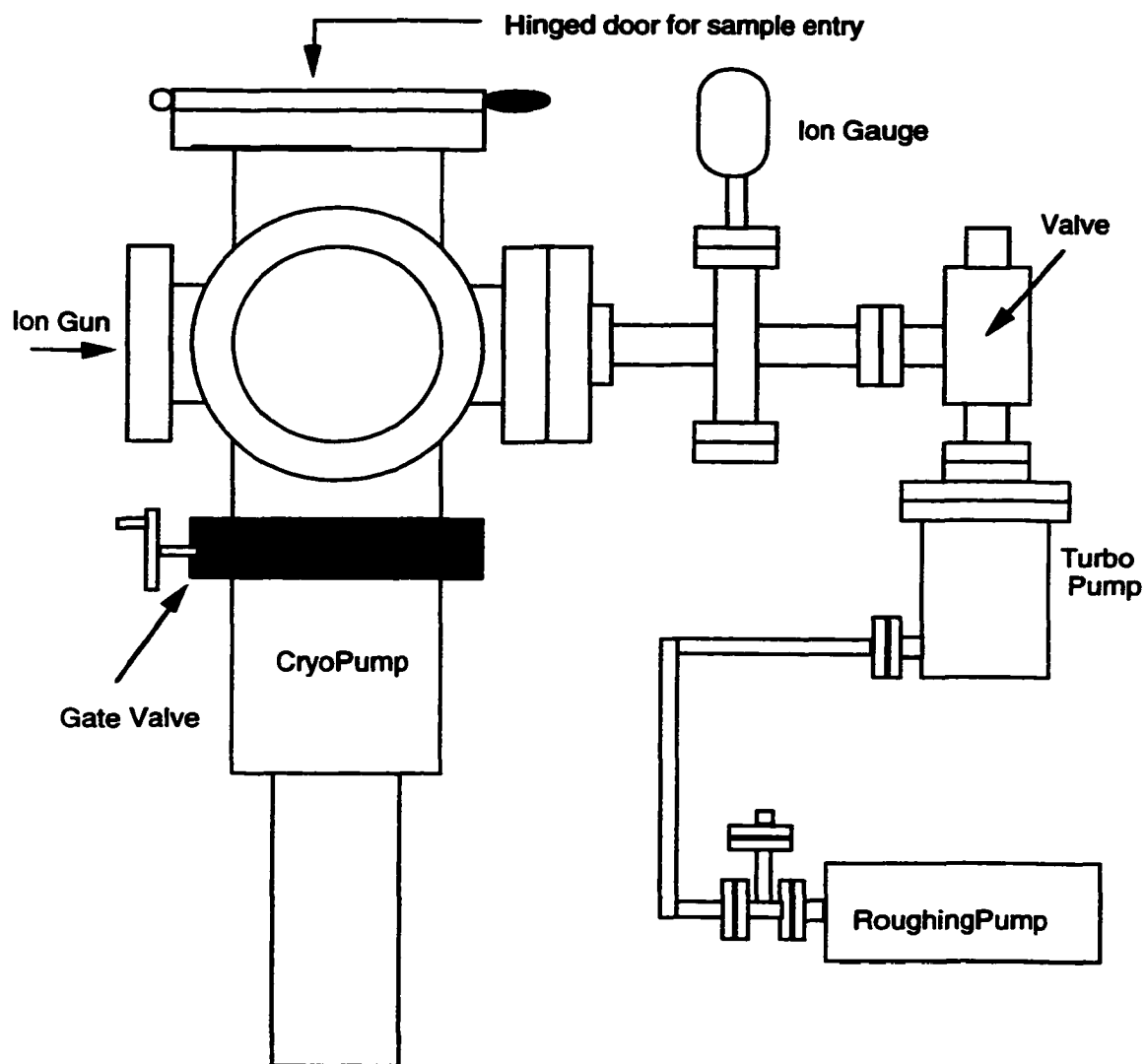
Figure 8.6 Schematic of the Ion Milling Chamber and pumping system.
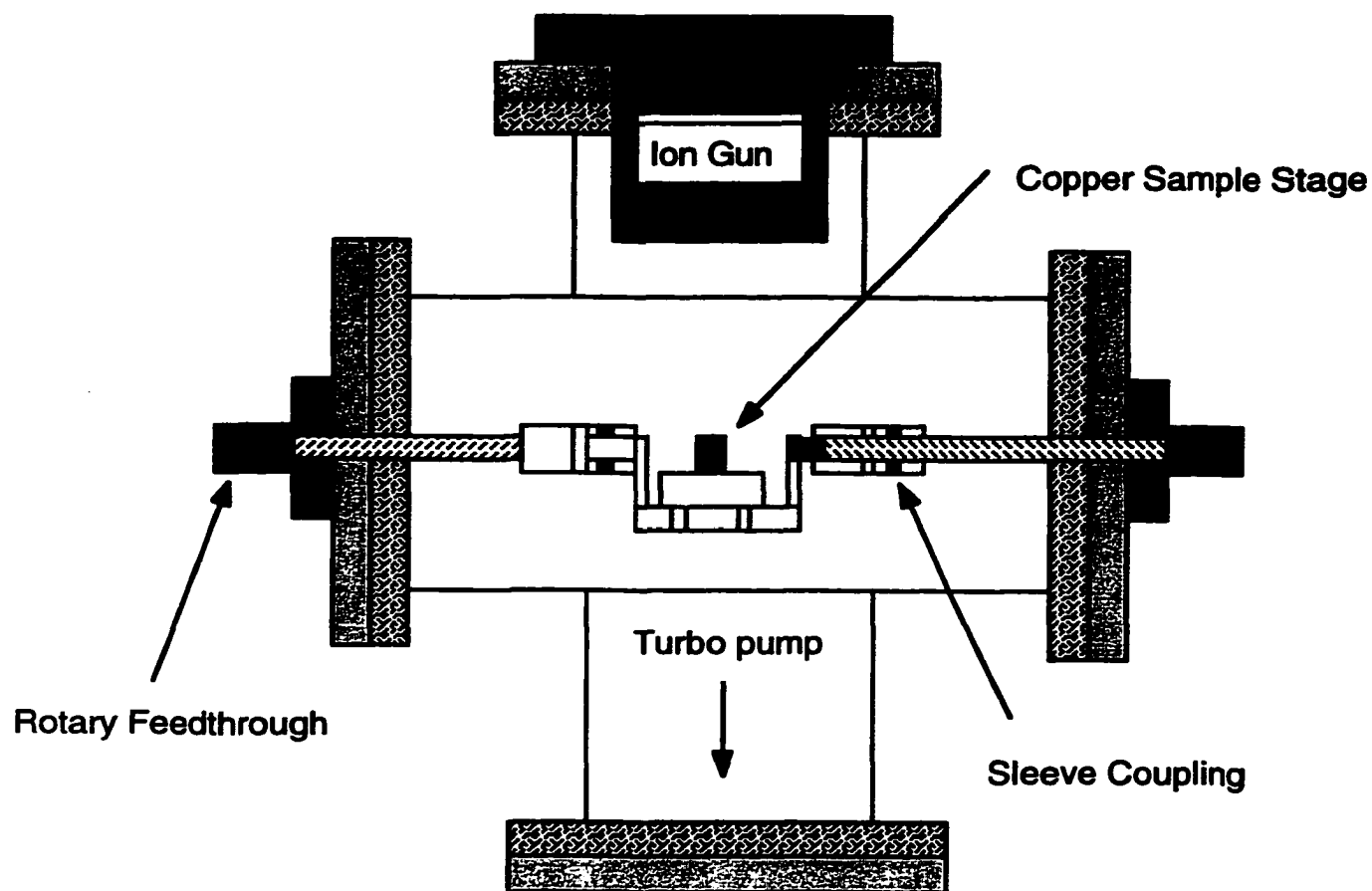
Figure 8.7 Schematic Ion Milling chamber and Kaufman type Ion source, sample mounting location and rotary feedthrough.
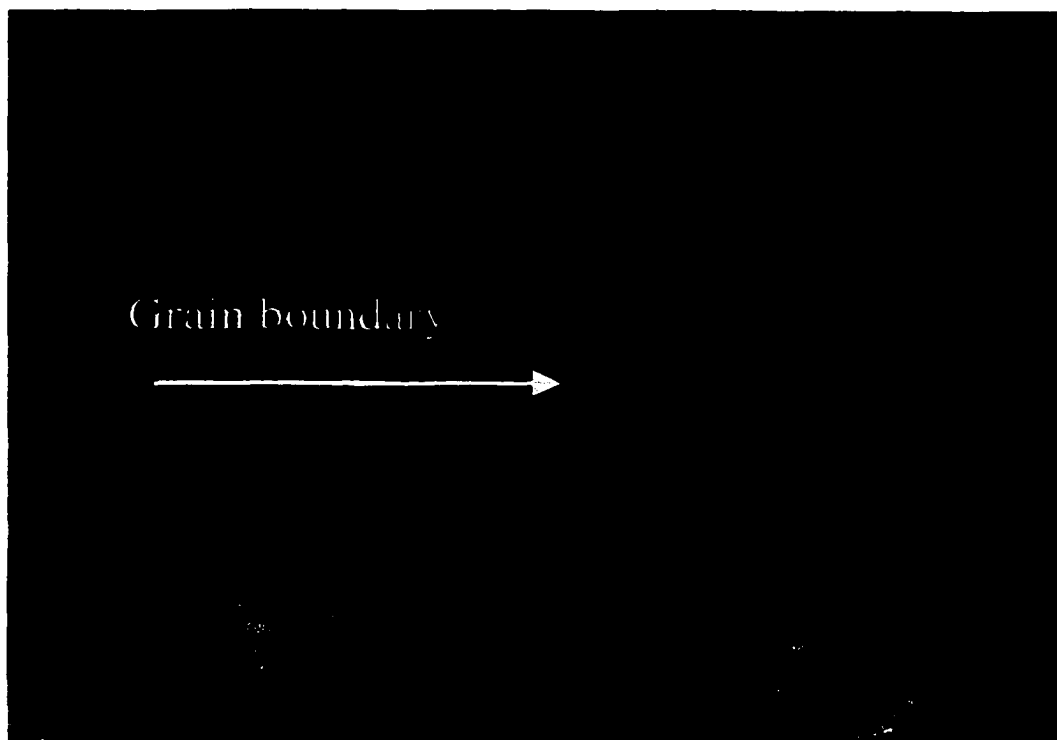
Figure 8.8 Photomicrograph of photolithography mask manufactured by Advance Reproductions. The light region in the micrograph are Cr metal and block the photoresist from being exposed to light. The region marked grain boundary is aligned with the grain boundary of the bicrystal thus producing a microbridge across the grain boundary region.

10 μm

Location of grain boundary
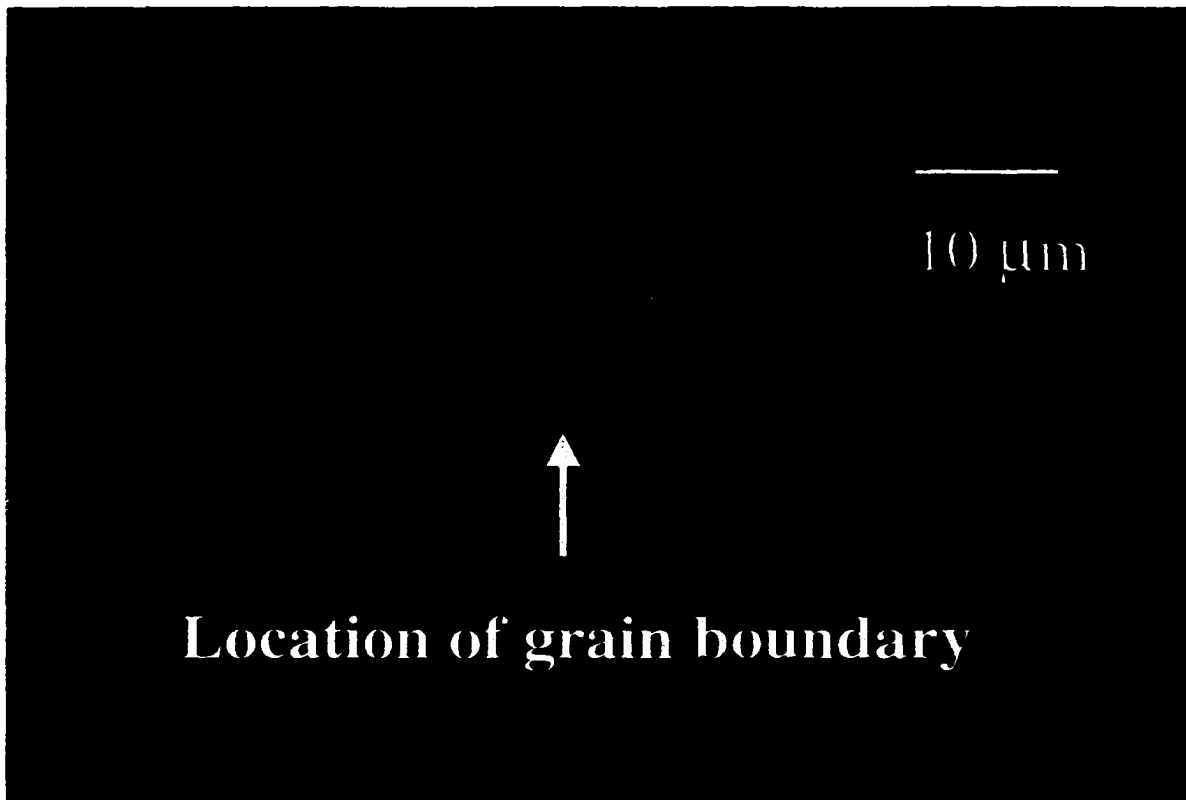
Figure 8.9 SEM micrograph of microbridge across a grain boundary. The location of the grain boundary is marked.
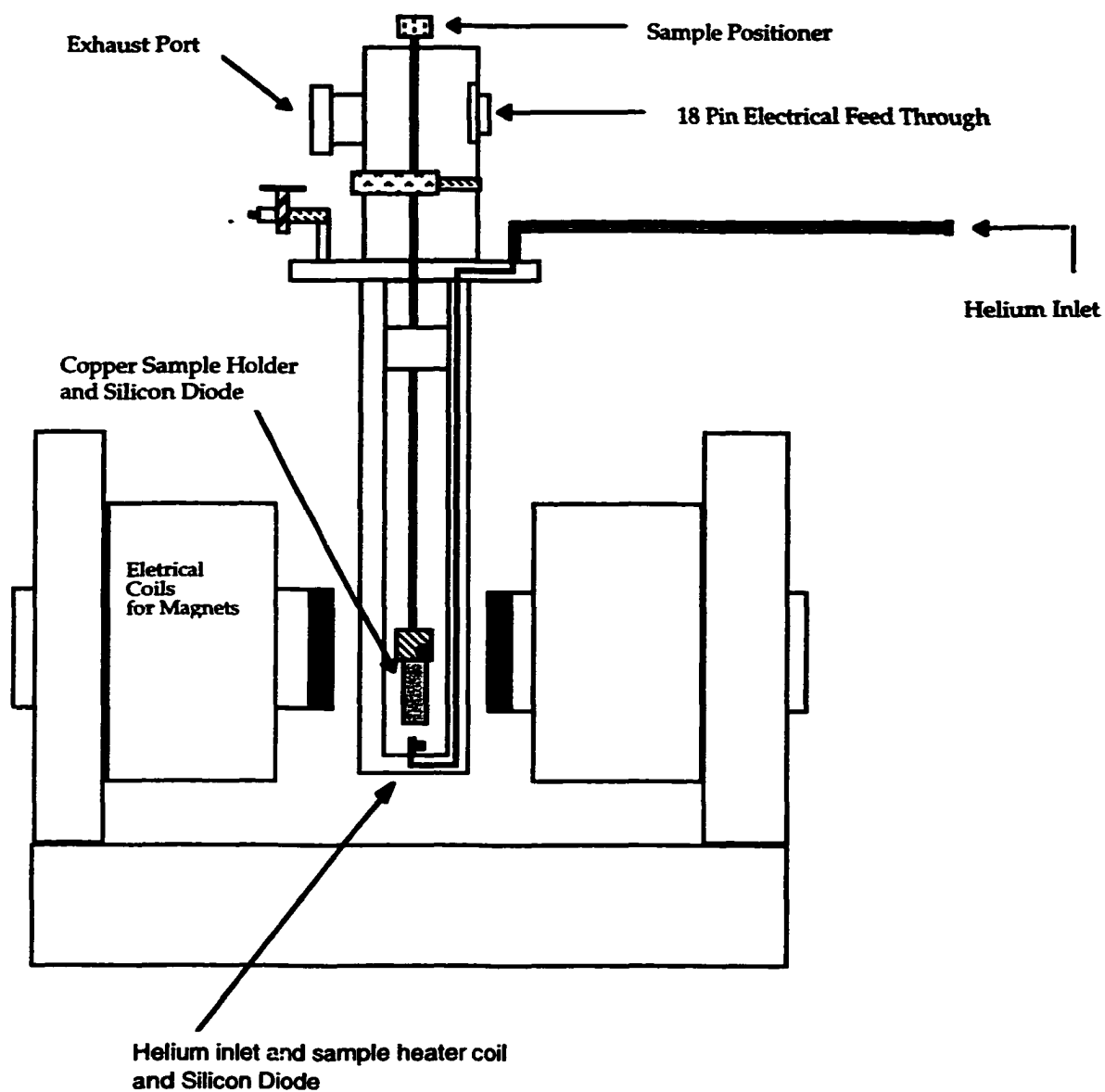
Figure 8.10 Schematic of Janus Supertran continuous flow low temperature cryostat with electrical coils for magnetic field measurements.

Silicon diode
thermometer

12 Contact Electrodes Pins

sample

Copper Sample Holder
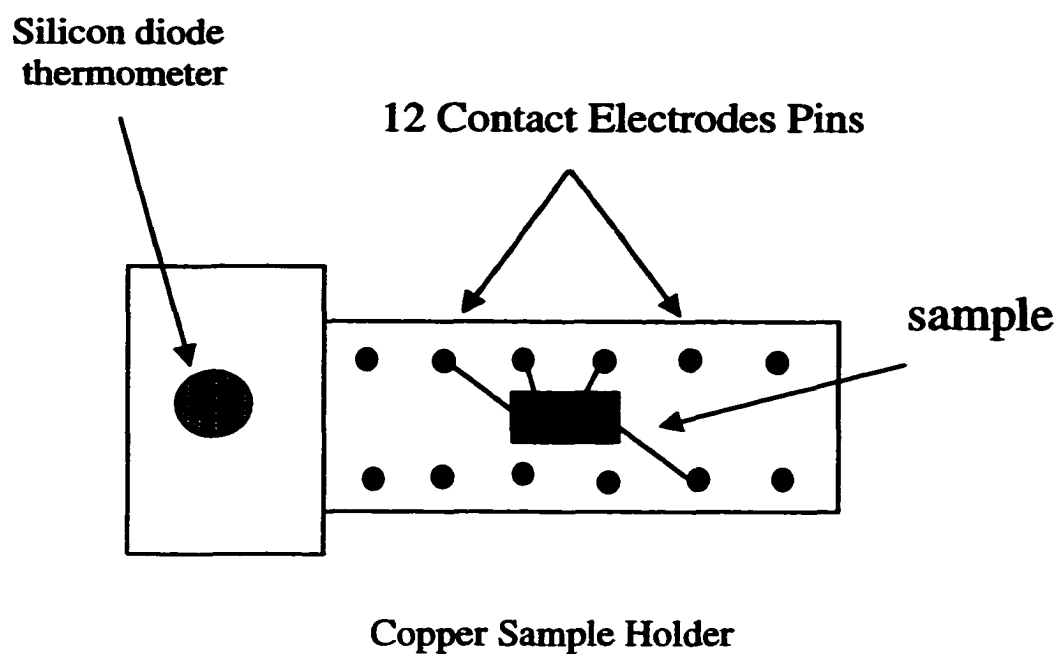
Figure 8.11 Copper cold finger within cryostat with 12 lead pins. The gold wires from the sample are indium soldered to the lead pins. The wires to the lead pins are run into a scanner that determines which pins receive current and which pins the voltage drop is measured across.
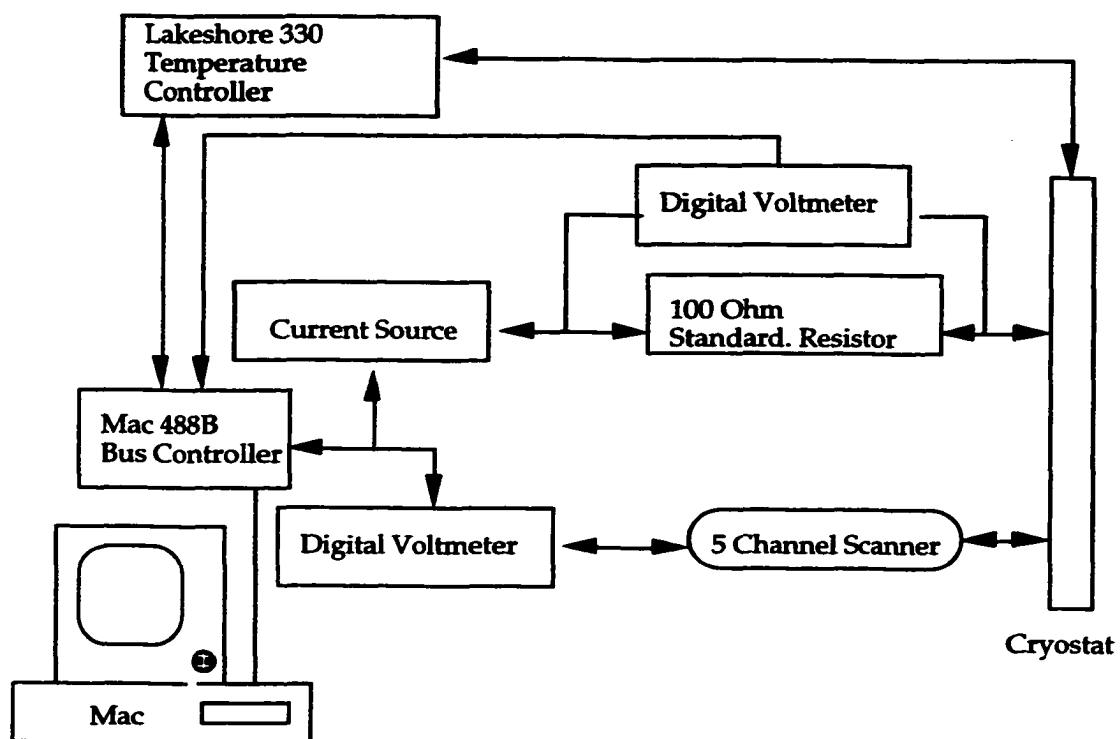
Figure 8.12 Schematic of computer controlled low temperature cryostat system.
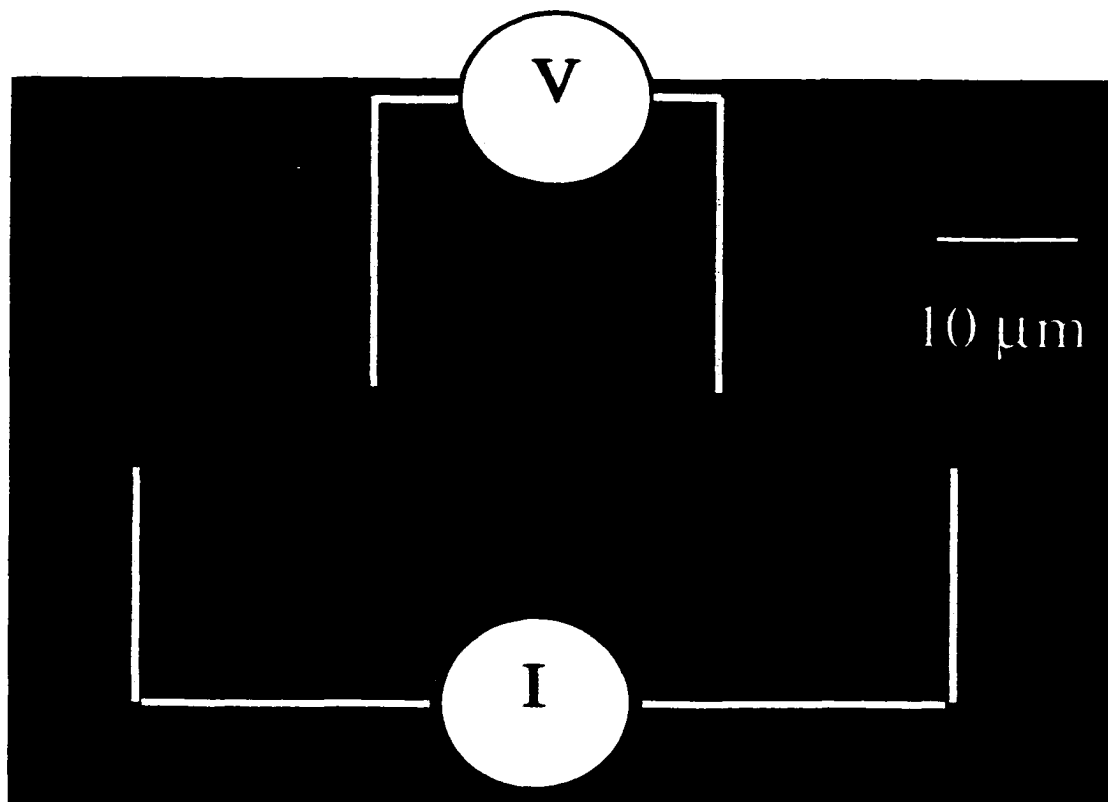
Figure 8.13 SEM micrograph of boundary showing where the current and voltage leads are connected for standard four-point current vs. voltage measurements

IX.   Current Transport Across Symmetric 24° Tilt Grain Boundaries

Transport measurements were performed on thin film symmetric 24° tilt grain boundaries fabricated using the POMBE and PLD techniques described in Chapter VIII. The resistance vs. temperature (RT), current vs. voltage (I-V) and current vs. applied magnetic field ($I_c(B)$)) measurements were performed to analyze the current transport along the boundary plane. The $I_c(B)$ measurements were used in concert with the phase retrieval technique developed and detailed in Chapter V and used to calculated local current variations along the length of the grain boundary.

IX.1 Resistance vs. Temperature

The RT characteristics of a superconducting sample can be used to understand basic structural-transport relationships within a superconducting sample. Figure 9.1 shows the RT curve of a single crystal [001] oriented YBCO film grown epitaxially on a [001] single crystal $SrTiO_3$ substrate using pulsed laser deposition. For a single crystal superconductor, the transition between the superconducting and non-superconducting state should be abrupt because of the uniformity of T_c from region to region within the superconductor. The transition temperature of the sample in figure 9.1 is approximately 90 K. The slope of the normal region (temperature region from T_c to room temperature) is linearly increasing with temperature and continues to room temperature similar to a metallic conductor.

156
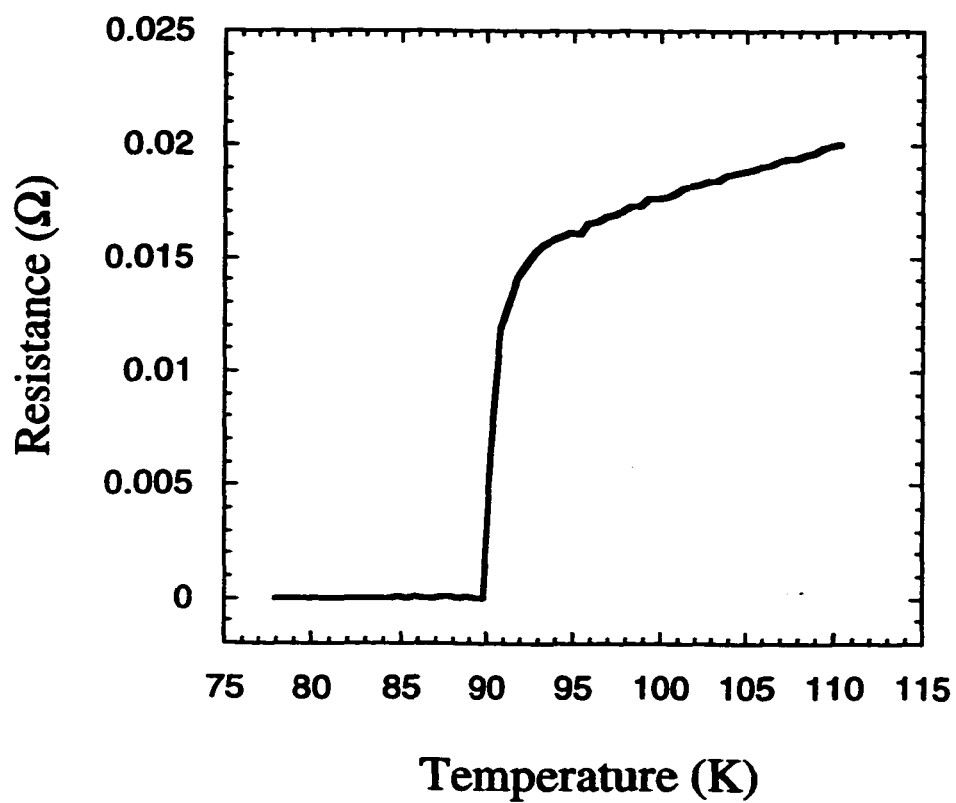
Figure 9.1 Resistance vs. Temperature (RT) curve for a single crystal YBCO Thin film sample on a $SrTiO_3$ substrate. Note the abrupt transition from the superconducting state to the normal state for a single crystal.

Structural imperfections within a superconductor such as grain boundaries can act to disrupt the flow of supercurrent across the sample and result in suppressed critical current flow. Figure 9.2 shows the RT curve measured across a single symmetric 24° tilt YBCO grain boundary grown by PLD. The abrupt transition at T_c evident in the single crystal sample of figure 9.1 disappears and is replaced by a broadened transition region. The onset of the resistive transition at a temperature below T_c indicates weakened superconductivity across the grain boundary plane. The broadened transition region across a single grain boundary is commonly referred to as a foot structure. The foot structure of the grain boundary can be attributed to thermally activated transport channels that form near T_c as the temperature is increased. These thermally activated transport channels are a result of phase slippage across the boundary due to slight thermal fluctuations near T_c. Thermally Activated Phase Slippage (TAPS) across the boundary plane results in a small finite resistance across the grain boundary while both of the adjacent grains are still superconducting (Gross 1992). The size of the foot structure is dependent on the bias current driven across the boundary for RT measurements. Using a large bias current results in large voltage drops across thermally activated conduction channels and therefore result in large foot structures. Figure 9.3 shows a RT curve for another 24° grain boundary. The foot structure due to the grain boundary and the linear normal region are both evident. Figure 9.4 shows an enlargement of the foot structure region of the sample from figure 9.3. The basic shape of the foot-structure is evident where a finite resistance is present down to approximately 75 K.
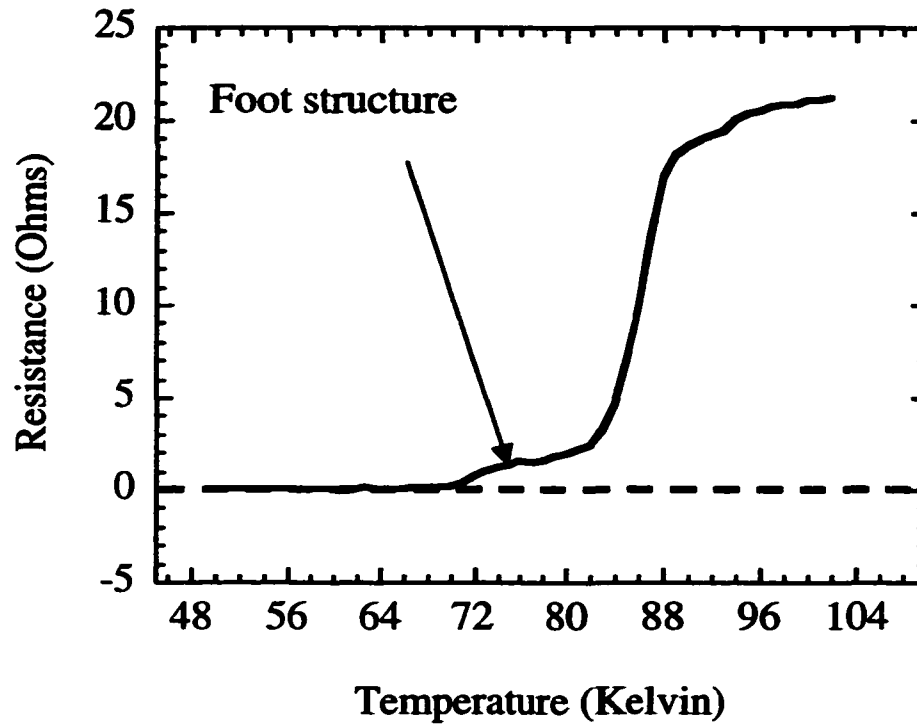
Figure 9.2 Resistance vs. Temperature (RT) curve for a single YBCO grain boundary. Note the broad transition "foot structure" from the superconducting state to the normal state for a single crystal.
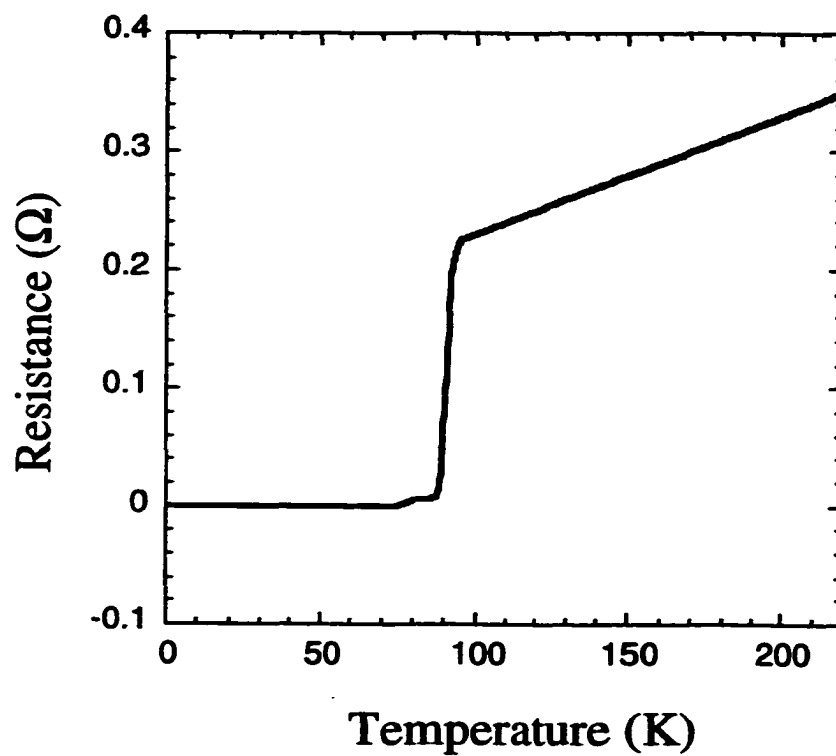
Figure 9.3 Resistance vs. Temperature (RT) curve for a single 24° YBCO grain boundary. Note the "foot structure" and the linear normal region.
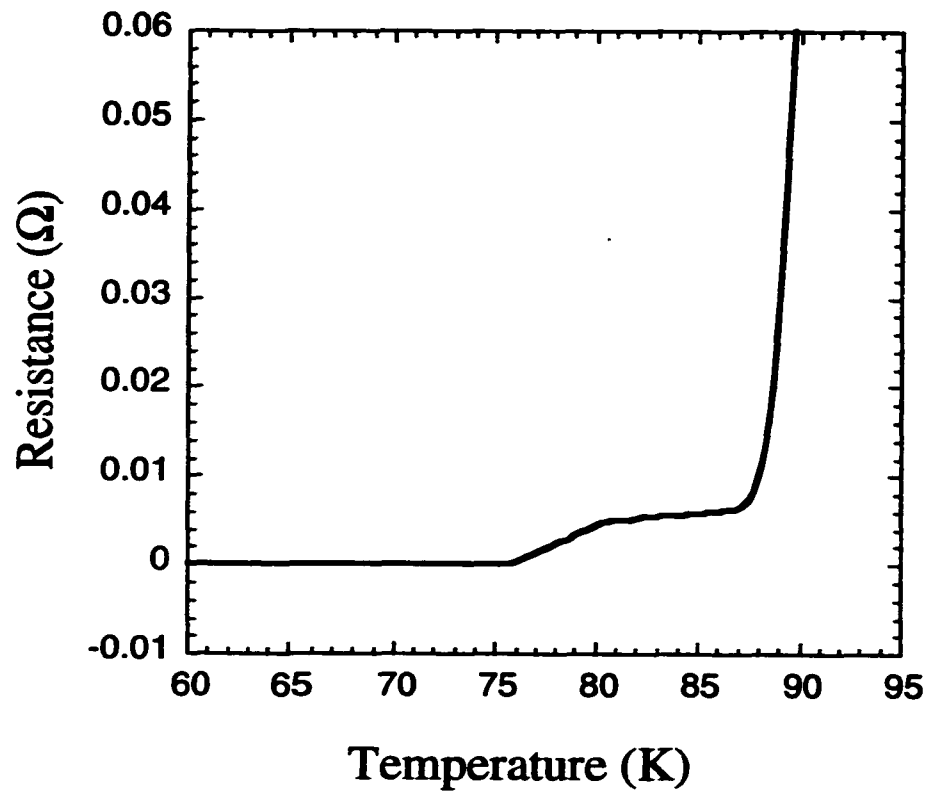
Figure 9.4 Enlargement of foot structure region from figure 9.3.

Figure 9.5 shows a RT curve of a single grain boundary curve that shows a foot-structure and two different transition temperatures corresponding to different T_c values for the YBCO crystals on each side of the grain boundary. Figure 9.5 shows a foot structure starting at approximately 75 K. At approximately 82 K one of the grains starts to transform to the normal state and has a distinct transition temperature. At $\approx$ 89 K the second grain transforms to the normal state with a second distinct transition temperature apparent.

IX.2 Current - Voltage Measurements

Current voltage measurements across the microbridge are used to obtain two crucial pieces of information about the superconducting sample; The critical current I_c and the shape of the normal state resistance R_n region of the curve. The shape of the normal region of the curve determines whether the grain boundary is a flux-flow type or a zero capacitance RSJ junction. The curvature of the I-V graph indicates the type of coupling across the boundary. The critical current is a hallmark property of a superconductor and is used for design purposes. The critical current is the sum of all the current channels across the boundary plane. The concept of locally varying current along the length of the boundary is important for understanding the magnetic field behavior of Josephson junctions.
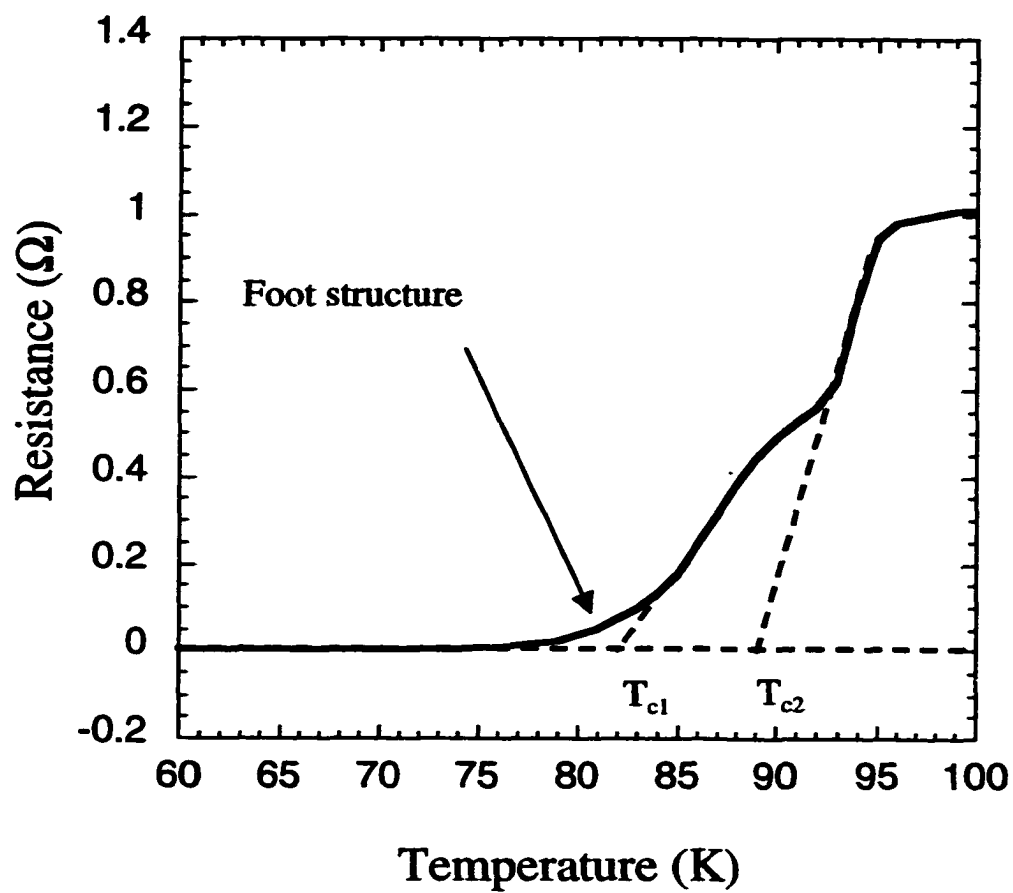
Figure 9.5 Resistance vs. Temperature (RT) curve for a single 24° YBCO
grain boundary. Note the double transition at T_{c1} and T_{c2} indicating a slightly
different transition temperature for the single crystal on one side of
gain boundary from the other.

The total current crossing the boundary I_{total} can be thought of as the integrated current along the length of the boundary,

$$I_{Total} = \int_0^W I_c(x)dx \tag{9.1}$$

or in terms of the total current density J_{total}

$$J_{total} = \int_0^W J(x)dx. \tag{9.2}$$

The spatial varying nature of the current along the length of the grain boundary is not observable in I-V measurements, however the spatially varying current determines the total current crossing the boundary.

Most 24° grain boundary junctions have RSJ-like I-V behavior. Figure 9.6 shows a typical I-V curves of 24° grain boundary junctions with zero capacitance RSJ behavior. The zero capacitance RSJ model (from chapter III) can be simplified to

$$V = I_c R_n \sqrt{\left(\frac{I}{I}\right)^2 - 1} \quad \text{for I} > I_c \tag{9.3}$$

and

$$V = 0 \text{ for } I < I_c \qquad (9.4)$$

where the junction is modeled by a Josephson element in parallel with a resistor. At temperatures near T_c the RSJ behavior of 24° grain boundaries is replaced by flux flow type behavior that is characterized by a positive curvature in the normal region of the curve. The lower critical currents at temperatures near T_c are not sufficient to prevent Josephson flux motion along the grain boundary. Also a small resistance is present at temperatures near T_c because of TAPS.

The variation of the critical current with temperature $I_c(T)$ for 24° grain boundary junctions follows;

$$I_c(T) = I_{c,o}(1 - \frac{T}{T_c})^2 \qquad (9.5)$$

which is predicted for superconductor-normal-superconductor type junctions. This would suggest a disrupted region along the boundary similar to a normal metal.
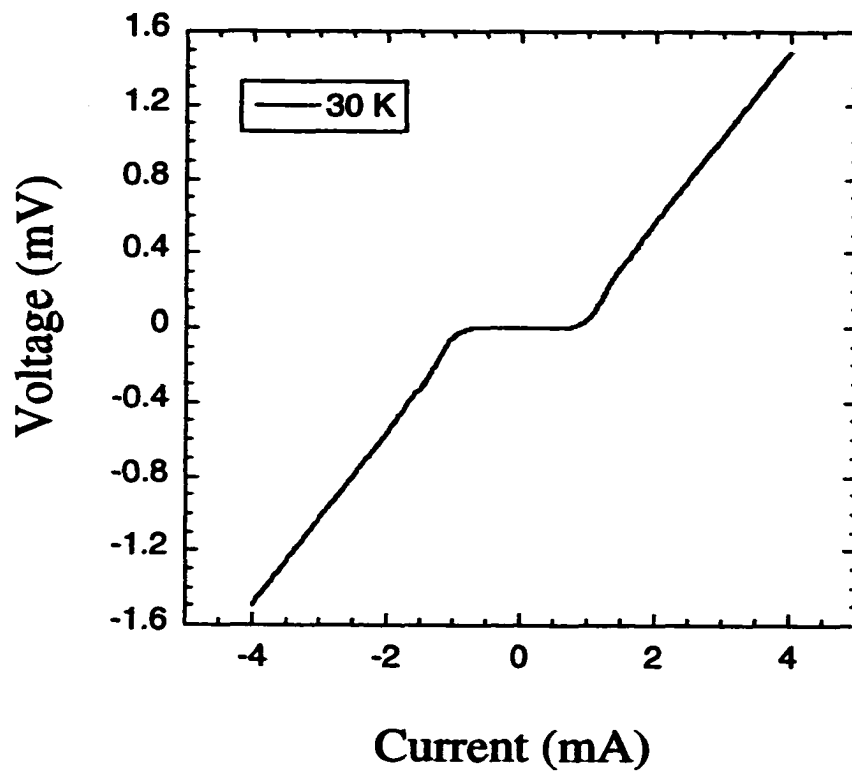
Figure 9.6 Current vs. Voltage curve for a typical 24° grain boundary
junction exhibiting zero capacitance RSJ behavior.

IX.3 Magnetic Field Behavior

The magnetic field behavior of grain boundary junctions is complex and not well understood. An ideal junction with a uniform current distribution should have a near Fraunhofer pattern when the critical current is measured as a function of an applied magnetic field. Most low temperature superconductor Josephson junctions exhibit near Fraunhofer critical current vs. applied magnetic field patterns, however it was recognized early on that grain boundary Josephson junctions in high temperature superconductors deviated significantly from the ideal Fraunhofer case. As discussed earlier in chapter III, the magnetic variation of the critical current varies as the modulus of the Fourier transform of the local current variation and can be written as;

$$I_c(u) = \left| \int_0^W J(x)\exp(iux)dx \right| \tag{9.6}$$

where u is the normalized applied magnetic field defined in chapter III. From equation 9.6 it is evident that variations in the local current J(x) would result in deviations from the ideal Fraunhofer pattern. Deviations from the ideal Fraunhofer pattern can result from self-induced magnetic fields along the length of the boundary. When the width of a grain boundary junction is larger than four times the Josephson depth ($W > 4\lambda_j$) self-field effects can dominate. Self induced magnetic fields can result in asymmetric $I_c(B)$ distributions depending on the magnetic field history of the sample. Figure 9.7 shows the
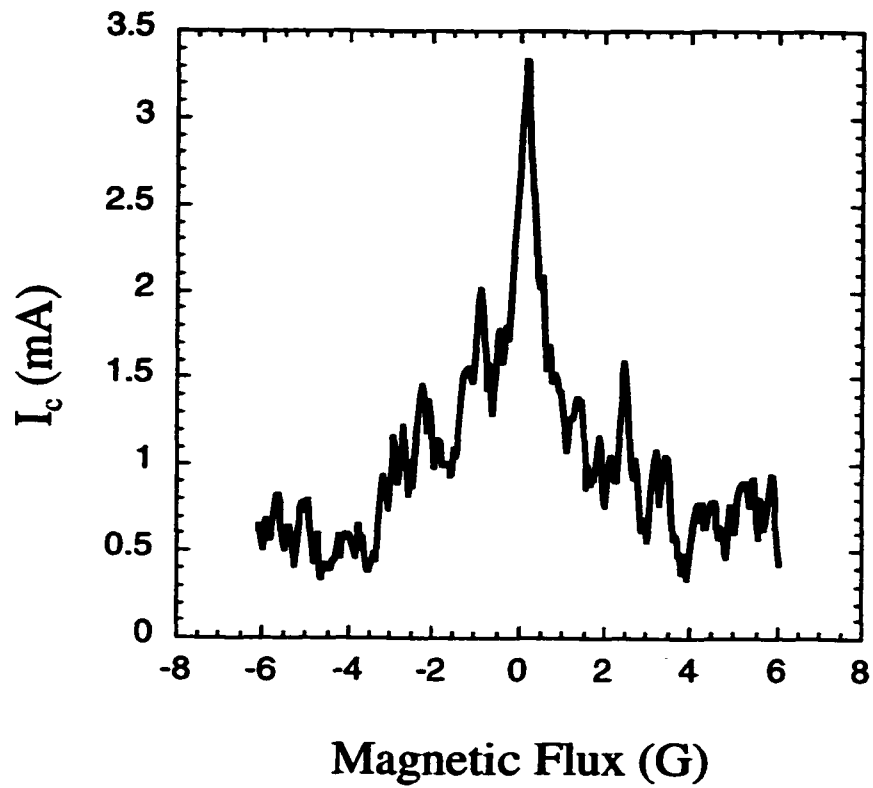
Figure 9.7 Critical current vs. applied magnetic flux for a long Josephson junction where self field effects result in nonsymmetric $I_c(B)$ behavior.

$I_c(B)$ data for a large single symmetric 24° grain boundary junction. The distribution

is typical of large junctions where the deviations from Fraunhofer behavior are increased

by the self-induced magnetic fields along the boundary. The $I_c(B)$ distribution for large

junctions such as the one in **Figure 9.7** show a large non-symmetric component and the

measurements are often non-reversible depending on the magnetic history of the sample.

Large junctions often show a measurement hysteresis that will be highlighted in chapter

X.

When short junctions $(W < 4\lambda_j)$ are measured, the self field effects are considered

negligible and the $I_c(B)$ data is usually reversible and repeatable. Consequently, the

deviations from the ideal Fraunhofer pattern may be attributed to variations in the local

current $J(x)$ as related in equation 9.6. The remainder of the chapter will focus on short

junctions where self-induced magnetic fields do not alter the $I_c(B)$ measurements.

Figure 9.8 shows a $I_c(B)$ curve for a single [001] symmetric 24° grain boundary

junctions measured at 4.2 K. The maximum current is located at B = 0 and the current

oscillates in a regular repeating pattern. Notice that the oscillating current never goes to

zero as the magnetic field is increased. For an ideal uniform junction, there is perfect

cancellation of the current at integral flux values. When the current along the junction is

non-uniform the flux cancellation of the current is expected to be non-uniform and thus

result in "excess current" in the $I_c(B)$ measurements. The excess current that is the result

of non-uniform currents along the boundary is indicated in figure 9.8.
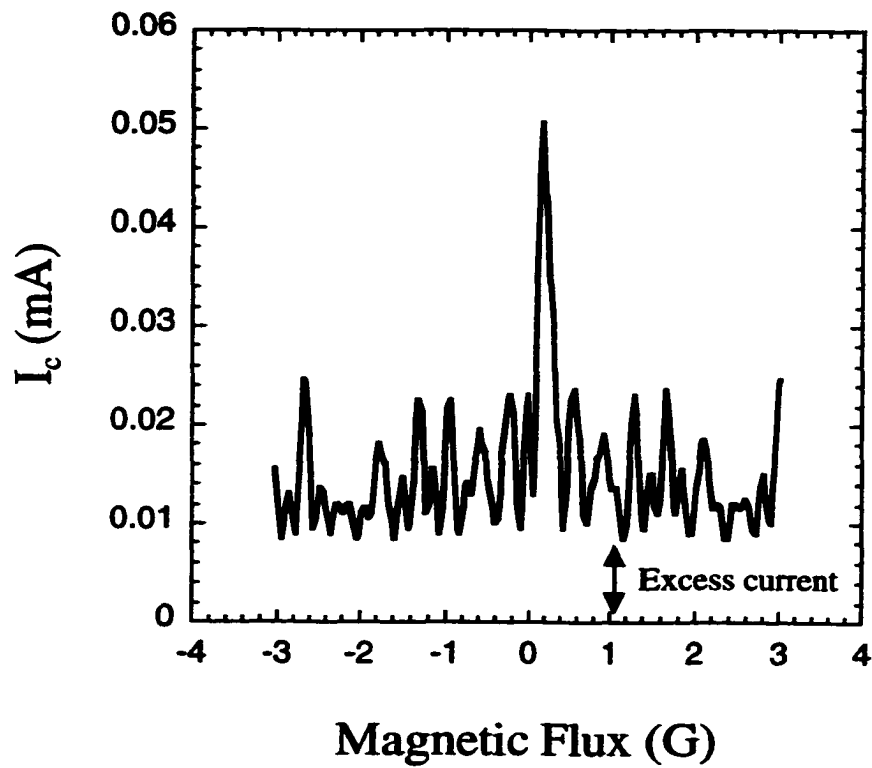
Figure 9.8 Critical current vs. applied magnetic flux for a short Josephson junction where self field effects are negligible and therefore the I_c(B) behavior is symmetric about B = 0.

Figures 9.9 and 9.10 shows the $I_c(B)$ curve of two different single 24° grain boundary junctions measured at 4.2 K. The maximum current is located at B = 0 and the current oscillates in a regular repeating pattern. The large deviations from Fraunhofer and the excess current both indicate large deviations from a uniform current distribution along the length of the boundary.

A significant amount of evidence suggests that the current distribution along the length of a grain boundary in high-T_c superconductors is non-uniform. High field measurements that show current oscillation up to 12 Tesla indicate current variations at the sub-nanometer length scale (Froehlich *et al.* 1995; Sarnelli *et al.* 1993c; Daumling *et al.* 1992). Chapter III discussed the parallel conduction channel models and highlighted the importance of local chemistry on the variation of the local current along the boundary. All of these studies suggest a non-uniform current distribution, but it has never been directly observed or calculated.
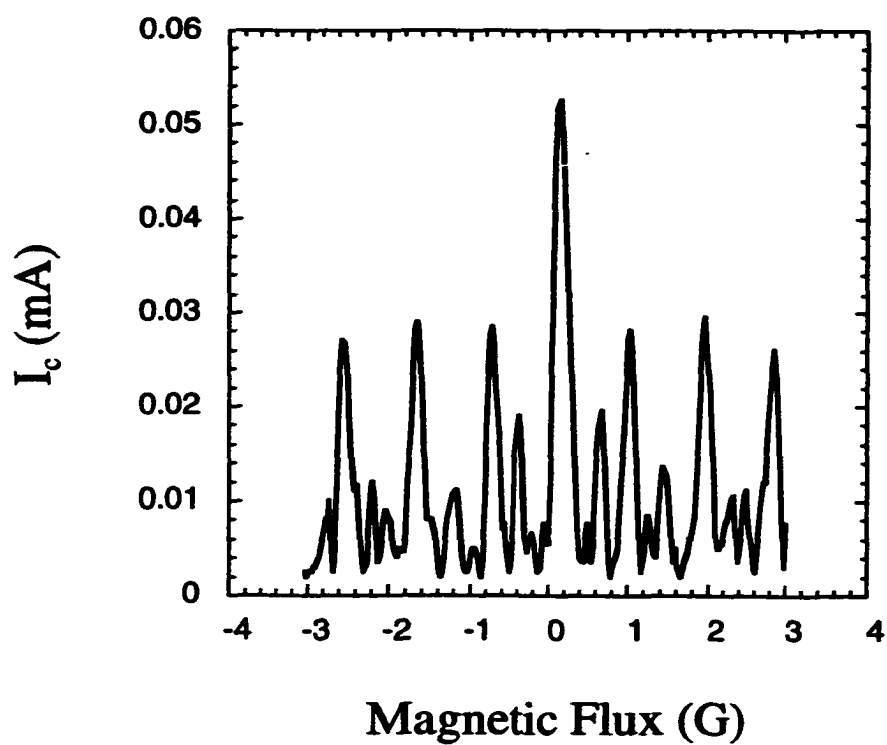
Figure 9.9 Critical current vs. applied magnetic flux for a short Josephson junction where self field effects are negligible and therefore the $I_c(B)$ behavior is symmetric about B = 0.
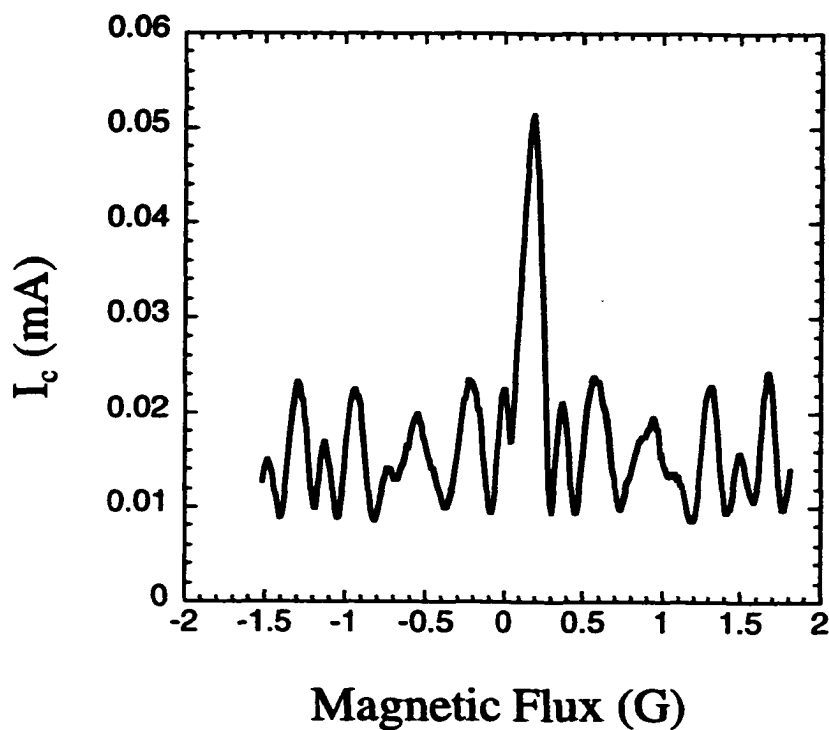
Figure 9.10 Critical current vs. applied magnetic flux for a short Josephson junction where self field effects are negligible and therefore the $I_c(B)$ behavior is symmetric about B = 0.

IX.4 Local Current Variation

The phase retrieval algorithm detailed in chapter V was used to determine the local variation of the current crossing the boundary from $I_c(B)$ measurements. The $I_c(B)$ measurements were performed in the transport system detailed in chapter VIII and the data was corrected for demagnetization according to the method detailed in chapter VII. When multiple solutions were found the solutions are presented in terms of their figure of merit (FOM).

Figure 9.11 shows the $I_c(B)$ measurements from a single 5 μm wide, symmetric [001] 24° tilt boundary measured at 4.2 K. The $I_C(B)$ data sets were measured in both the positive and negative field directions. The $I_c(B)$ measurements were completely reversible with respect to field direction which is a requirement for this type of Fourier analysis. The current density J(x) from equation (9.6) is assumed to be real. Therefore $I_c(B)$ must be symmetric about zero. Consequently, for calculation purposes, slight non-symmetries in the $I_c(B)$ data were averaged out. There also existed in much of the data a residual current independent of the applied field that was subtracted out of the data before the algorithm was applied. The resolution of J(x) in real space is determined by the magnetic field sweep. The spacing in real space between any two consecutive data points Δx is proportional to the inverse of the magnetic field sweep.

$$\Delta x = \frac{\Phi_o}{2\pi D \Delta B N} \tag{9.7}$$

where ΔB is the magnetic field spacing, $D = 2\lambda_L$ and N is the total number of data points in the magnetic field sweep from $-B_{max}$ to B_{max}. The applied magnetic field values must be corrected for demagnetizing effects as pointed out by Rosenthal *et al.* and detailed in chapter VII (Rosenthal *et al.* 1991)

The phase retrieval algorithm produces solutions for J(x) that are consistent with the known physical constraints on the boundary. Since the possibility exists for multiple solutions, we have used a search algorithm (genetic algorithm) to rigorously search solution space for all possible solutions. When multiple solutions are identified we present all possible current distributions across the boundary.

Typically the algorithm found between one and three possible correct solutions. However, all of the solutions were similar, i.e. mathematically different but represented the same physical current distribution. Figure 9.12 shows two different solutions (both have zero FOM) that the phase retrieval algorithm found for the data set from figure 9.11. The spatial resolution of the data points calculated from equation (9.7) (correcting for the demagnetization field) is ≈ 0.13 μm. There is a strong peak to peak correspondence between the solutions and the relative peak heights are similar. The two solutions determined by the phase retrieval algorithm for the data set in figure 9.11 represent within the accuracy of the measurement the same current distribution. Whenever multiple distinctly different solutions are mathematically possible, all solutions
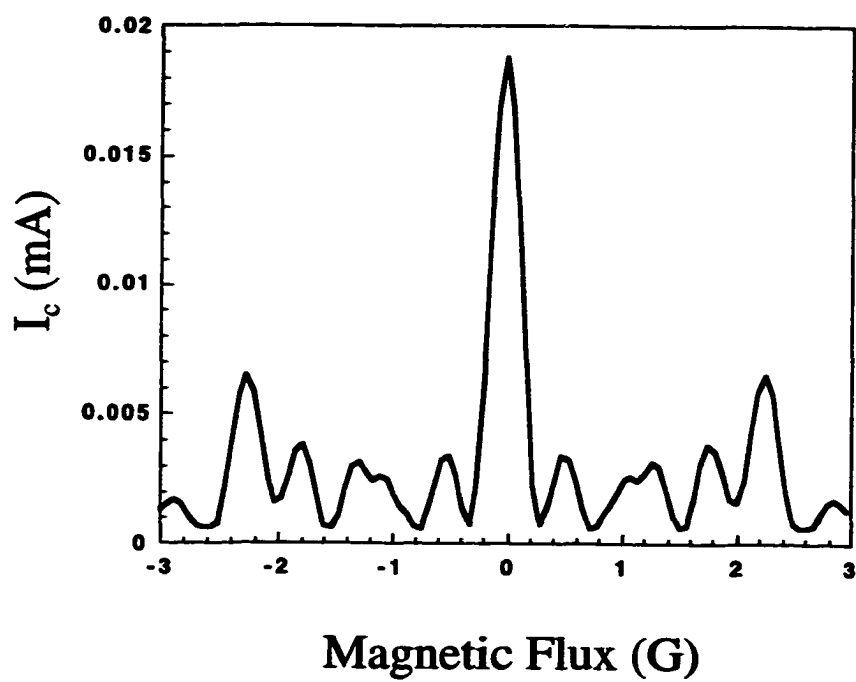
Figure 9.11 Critical current vs. applied magnetic flux for a single 24° symmetric tilt boundary measured at 4.2 K.
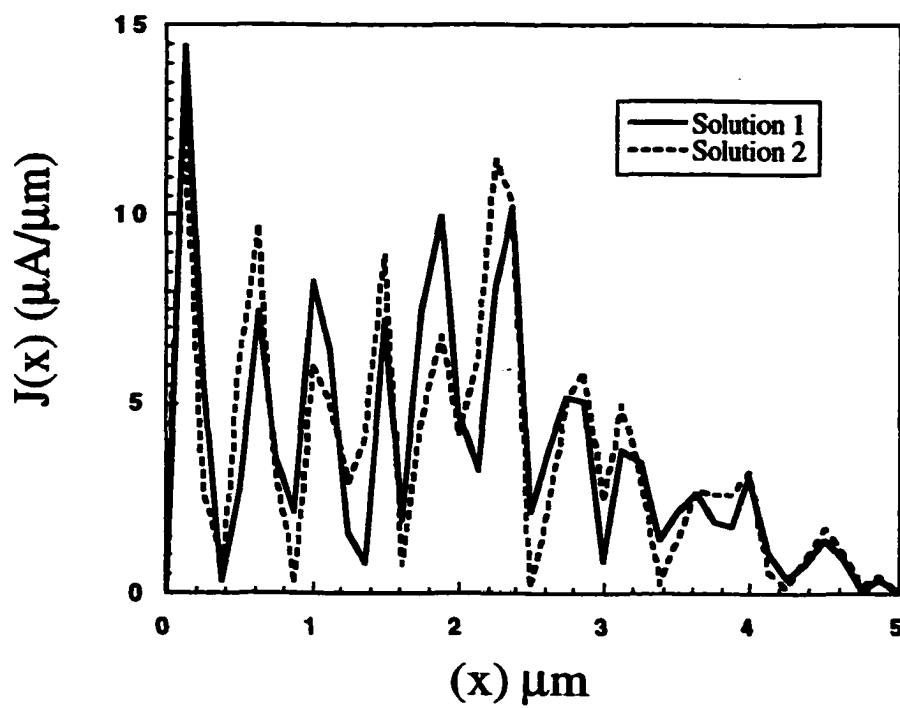
Figure 9.12 Local current distributions calculated from the data in figure 9.11. Although the two current distributions are mathematically different, they represent the same physical current distribution.

that conform to a zero FOM must be considered a possible correct solution. Thus it is extremely important to quantitatively rank the various solutions to determine which are actually correct solutions distinct from trap or tunnel solutions where the algorithm has stagnated. The fact that the algorithm used has always found just one type of solution within the accuracy of the experimental measurements and the validity of equation (9.6) indicates that our procedure is quite robust.

Figure 9.13 Shows $I_c(B)$ data from a 5 μm wide boundary measured at two different temperatures. The positional current $J(x)$ across the boundary was calculated for each data set with a spatial resolution of approximately 0.13 μm. Figure 9.14 shows the only solution found by the algorithm for both the 4.2 K and 60 K measurements. There is strong physical agreement between both solutions, with good correspondence of peak positions and peak shape similarity between the 4.2 K and the 60 K measurements. The 4.2 K sample shows a significantly larger total current crossing the boundary which is consistent with the variation of the critical current with temperature. The results of figure 9.14 indicate that by calculating the positional critical current $J(x)$ as a function of temperature $J(x,T)$, it may be possible to map specific areas along the boundary that have a different superconducting to normal transition temperature than that of the averaged total grain boundary transition temperature. Also, the current distribution at two different temperatures should be similar as in figure 9.14. Thus any solutions found at an intermediate temperature must also conform to the same physical current distribution. Therefore, if there were actually physically different solutions, it would be possible by
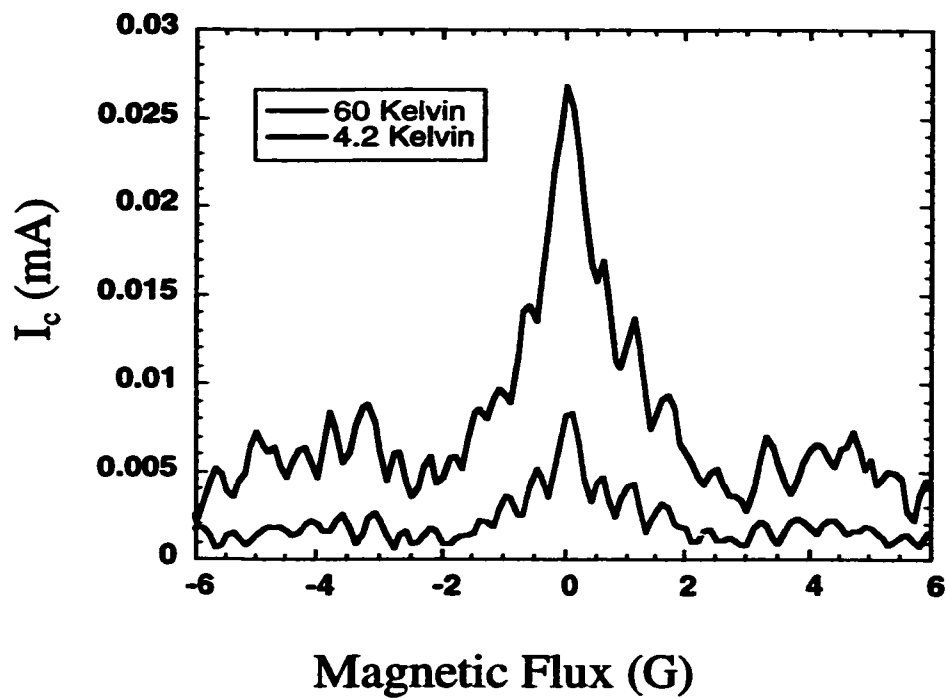
Figure 9.13 Critical current vs. applied magnetic field for a 5 μm wide 24° tit grain boundary measured at 4.2 K and 60 K. The lower temperature measurement has the larger I_c value.
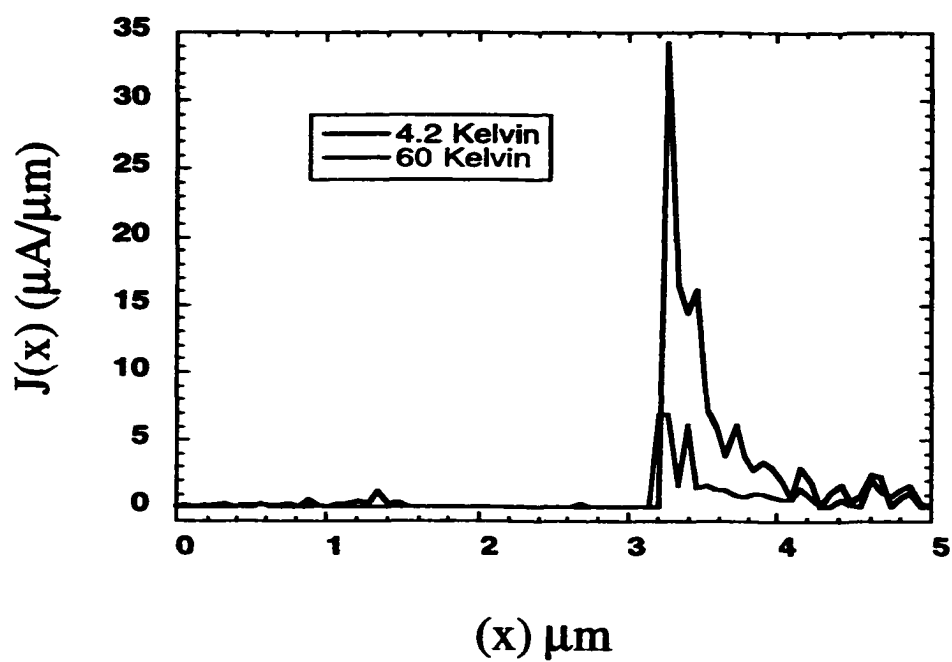
Figure 9.14 Local current distributions calculated from the data in figure 9.13. Note the strong correlation between the solutions determined at two different temperatures.

performing these measurements at various temperatures to eliminate "non-physical" current distributions and determine a unique solution to the problem.

The ultimate goal is to correlate these current inhomogeneities to structural and compositional variations along the length of the grain boundary. Small deviations of the current from point to point may be very difficult to distinguish microstructurally. Studies of the oxygen stoichiometry along the length of the boundary have revealed that the oxygen content can vary from point to point along the boundary which may account for some variations in the local transport properties, but would be very difficult to quantify experimentally. However, as shown above, large areas along the boundary that carry no current (such as the sample in figure 9.14) may have some microstructural irregularities that are distinguishable and can be directly compared with the positional current $J(x)$ solutions.

Figure 9.15 shows a $I_c(B)$ measurement for a 10 μm wide 24° grain boundary junction measured at 70 K. The junction is wider than most of the junctions that were studied, but because of the relatively high measurement temperatures it is close to the short limit and useful information about the local current should be obtainable. The $I_c(B)$ measurement shows at least two distinct frequency of oscillation that should correspond to two distinct conduction paths across the boundary plane. Figure 9.16 shows the local current distribution determined from the data in figure 9.15 and the phase retrieval
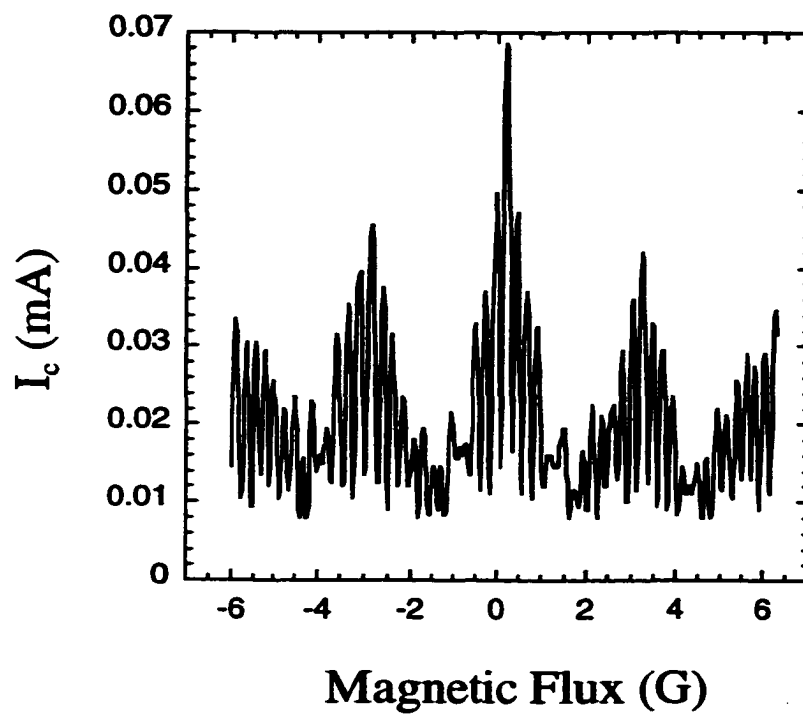
Figure 9.15 $I_c(B)$ measurement at 70 K for a 10 mm wide junction. Note the two distinct oscillation frequencies.
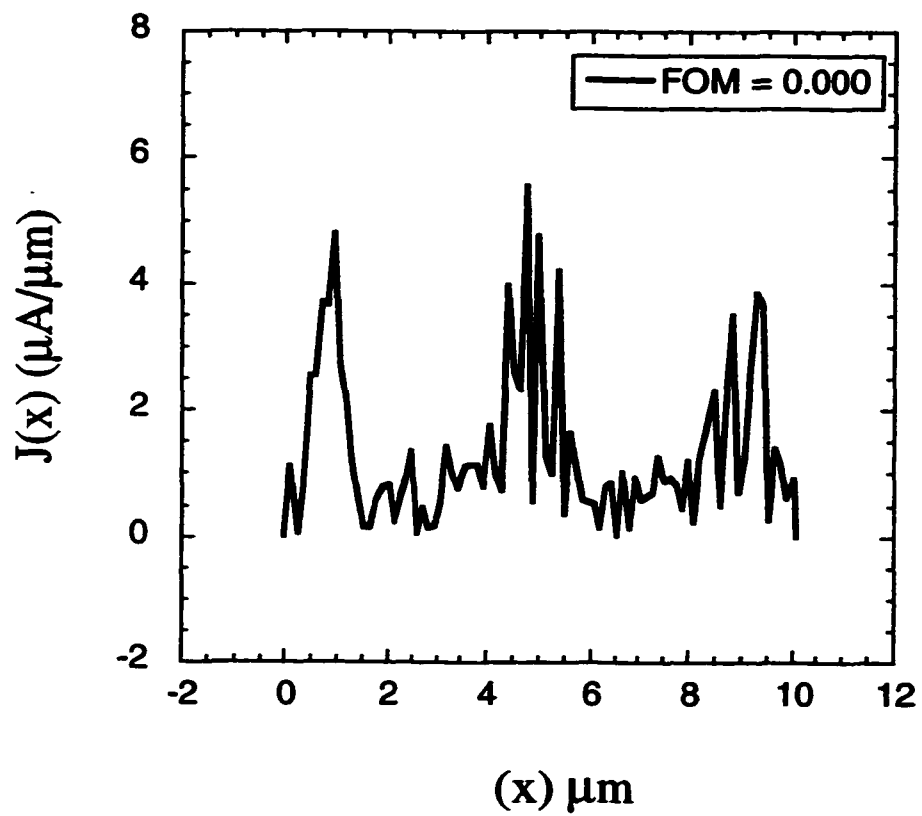
Figure 9.16 Local current distributions calculated from the data in figure 9.15. Note the three distinct regions along the boundary that carry most of the current.

algorithm. The current distribution shows three distinct conduction regions along the boundary that carry the majority of the current.

Note that all of these solutions indicate that the majority of the current is carried by a small number of superconducting segments along the boundary separated by regions that carry little or no current. There have been several grain boundary models (see chapter III) that suggest the current across the boundary is carried by a series of small (nanometer length scale - μm length scale) superconducting filaments along the length of the boundary. Our results in no way contradict these models, however due to the limited magnetic field sweep of our data and the resulting lower resolution of the current distributions, we would expect our boundaries to appear more uniform than the microfilamentary models would suggest.

The general current behavior along the length of our boundaries is quite similar to the current variations reported by Nesher and Ribak (Nesher *et al.* 1997). Notice that the current varies quite extensively from region to region along the length of the boundary in figure 9.12. Laser scanning microscopy (LSM) imaging and Low Temperature Scanning Microscopy (LTSEM)of the spatial variation of the critical current in high-T_C grain boundaries has shown similar oscillations in the current along the length of the boundary (Gerdemann *et al.* 1994; Fisher *et al.* 1994; Mannhart *et al.* 1990; Divin *et al.* 1996; Shadrin *et al.* 1998). However, because of the increased resolution and sensitivity of the phase retrieval technique over LTSEM and LSM measurements, many of the

inhomogeneities of the current distributions can not be resolved by these scanning techniques. Therefore, boundaries studied by these scanning techniques would appear more uniform on a larger scale than the boundaries studied here.

X. Current Transport Across Asymmetric 45° Tilt Grain Boundaries

Transport measurements were performed on thin film asymmetric 45° tilt grain boundaries fabricated using the Sputter Induced Epitaxy (SIE) technique developed by Vuchic *et al.* and described in Chapter VIII (Vuchic *et al.* 1995). The resistance vs. temperature (RT), current vs. voltage (I-V) and current vs. applied magnetic field ($I_c(B)$)) measurements were performed to analyze the current transport along the boundary plane. The $I_c(B)$ measurements were used in concert with the phase retrieval technique developed and detailed in Chapter V and used to calculate local current variations along the length of the grain boundary. The results are discussed in terms of boundary microstructure, local chemistry and the d-wave symmetry of the order parameter.

X.1 Resistance vs. Temperature

Figure 10.1 shows a RT curve of a typical single [001] oriented asymmetric 45° grain boundary junction. The linear normal region and the foot - structure are evident. Figure 10.2 shows an enlargement of the foot-structure of the sample in figure 10.1. Note the resistance of the grain boundary continues down to approximately 58 K. Figure 10.3 shows the RT curve across a single grain boundary and across an adjacent grain. Note the abrupt transition of the grain vs. the foot-structure of the grain boundary. The size of the foot-structure is dependent on the bias current used during the measurement. The standard bias current is 0.001 mA.

186
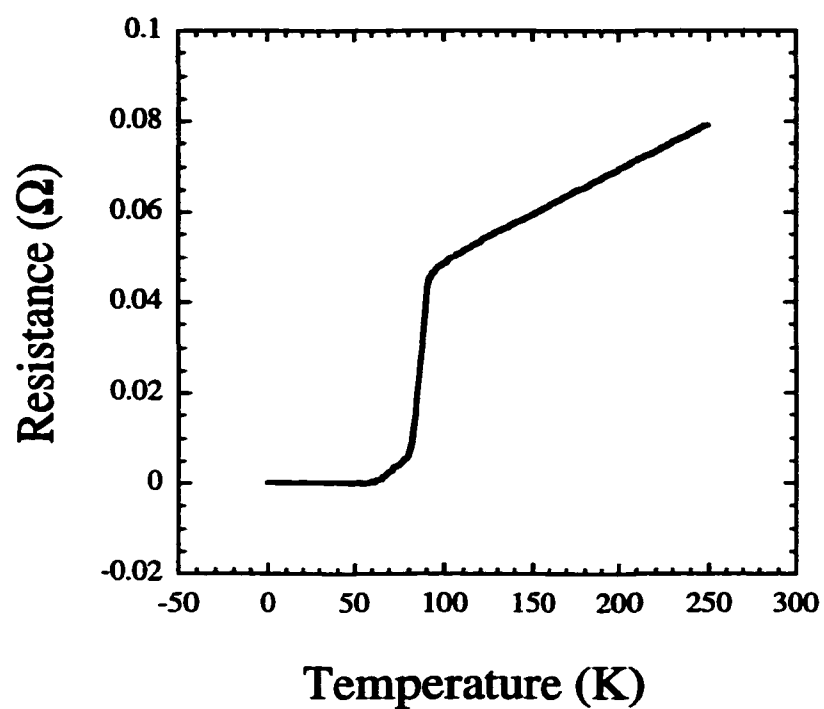
Figure 10.1 Resistance vs. Temperature measurement across a single 45°
asymmetric tilt grain boundary. The linear normal region above T_c and
the foot structure just below T_c are evident.
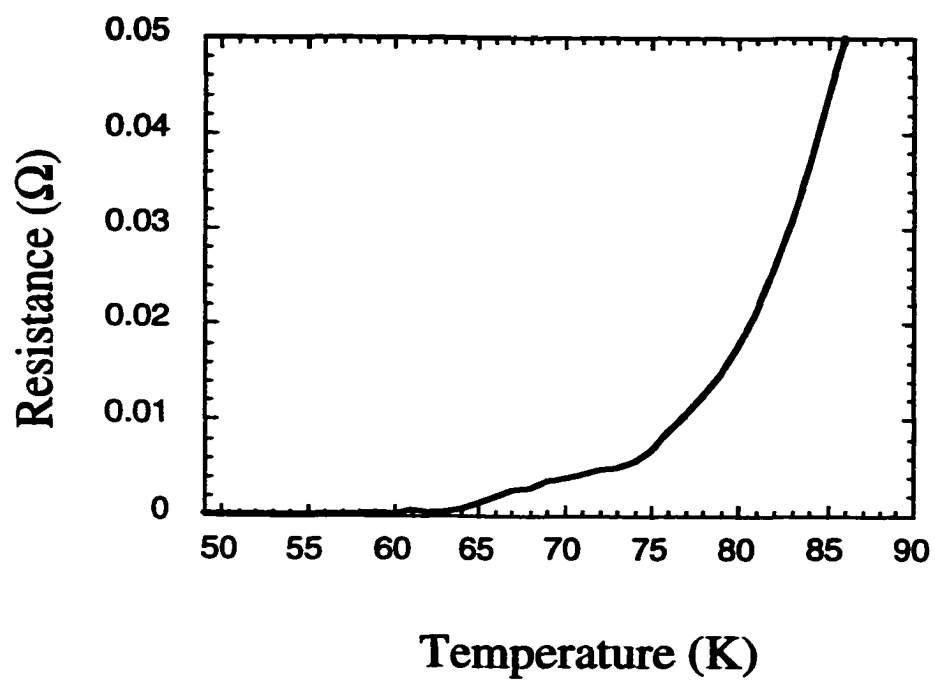
Figure 10.2 Enlargement of foot structure region of figure 10.1.
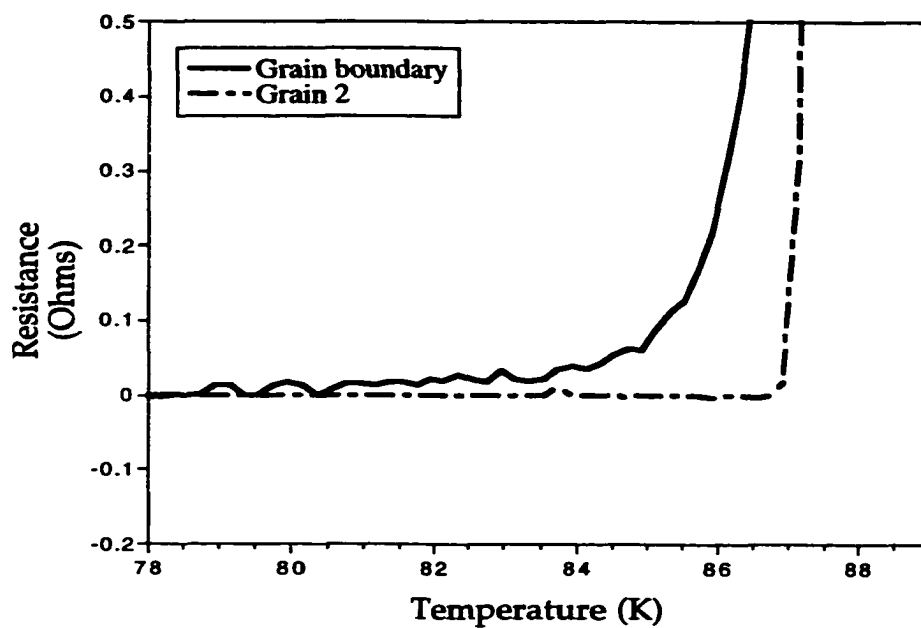
Figure 10.3 RT measurement across a single grain and across a single 45° grain boundary. The resistance of the grain boundary continues down to a lower temperature than the adjacent grain.

The current driven across any boundary will seek the path of least resistance. Consequently, when performing bulk transport measurements (RT or I-V measurements) it is important to understand that the current will find the least resistive path across a single grain boundary or across multiple grain boundaries in a polycrystalline sample. For a single grain boundary, regions along the boundary may have different T_c values because of local microstructure or chemistry variations, therefore, as the temperature is increased a greater portion of the boundary will become resistive and thus will change the transport measurements. Unfortunately, bulk measurements such as RT or I-V measurements are not sensitive to local variations along the boundary and only the total current is measured.

X.2 Current vs. Voltage Measurements

Figure 10.4 - 10.6 show the current vs. voltage (I-V) behavior for a single 45° grain boundary junction. The I-V characteristics of most 45° grain boundary junctions can be described as a zero capacitance RSJ model junction similar to the 24° grain boundaries. Care must be taken when performing the measurements to ensure that the sample was cooled in a zero field environment and that the sample is in the short junction limit where the width $W < 4\lambda_J$. Trapped flux in short junctions or self-generated flux in long junctions can result in flux-flow type I-V characteristics which are shown in figure
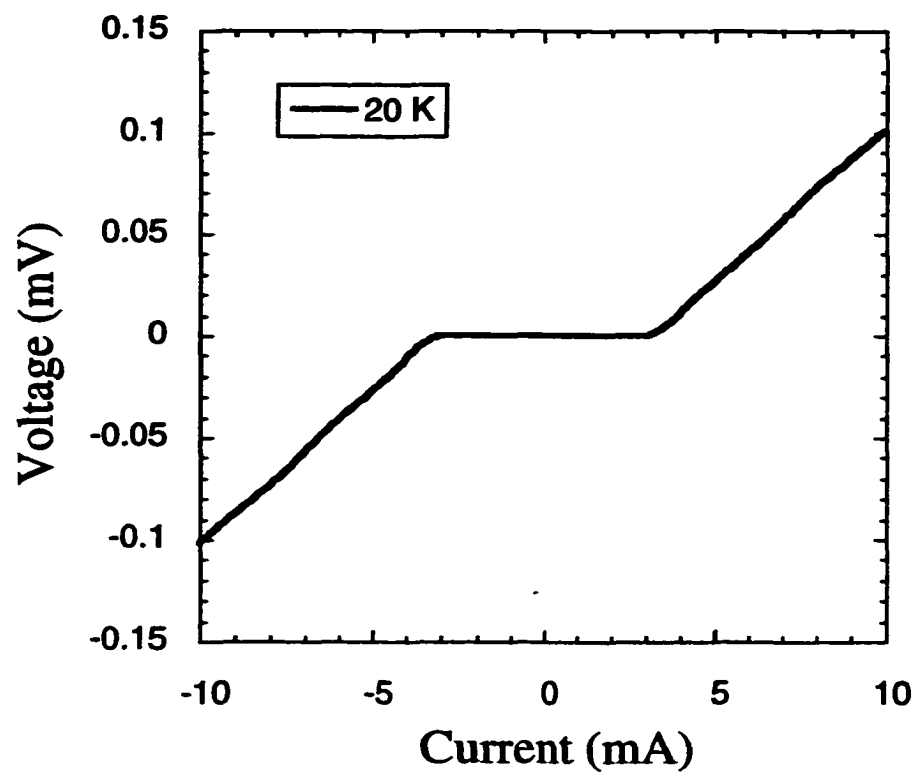
Figure 10.4 I-V curve of a single 45° grain boundary junction that follows the zero capacitance RSJ form.
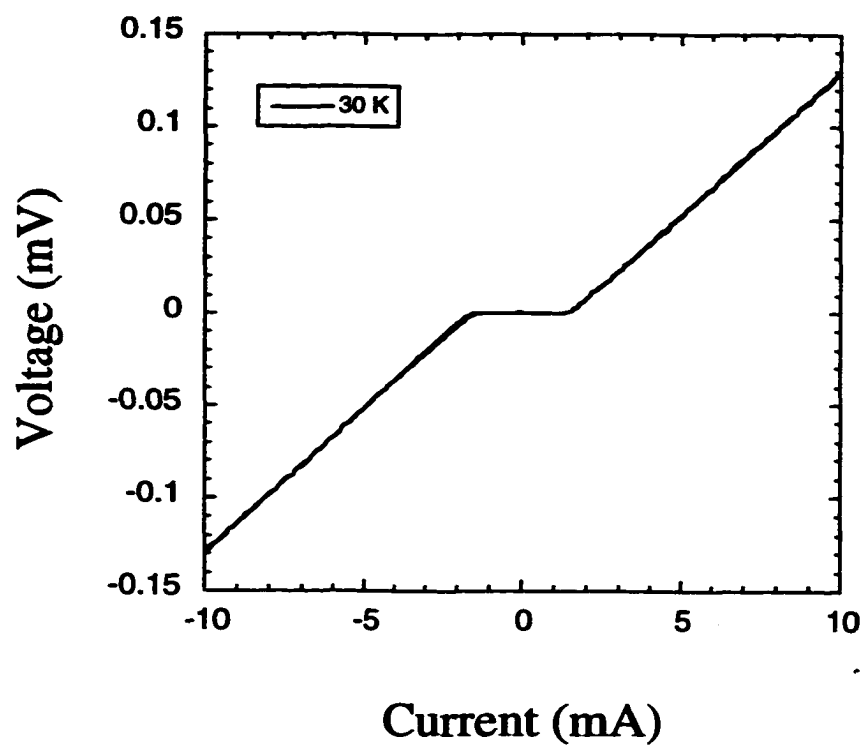
Figure 10.5 I-V curve of a single 45° grain boundary junction that follows the zero capacitance RSJ form.
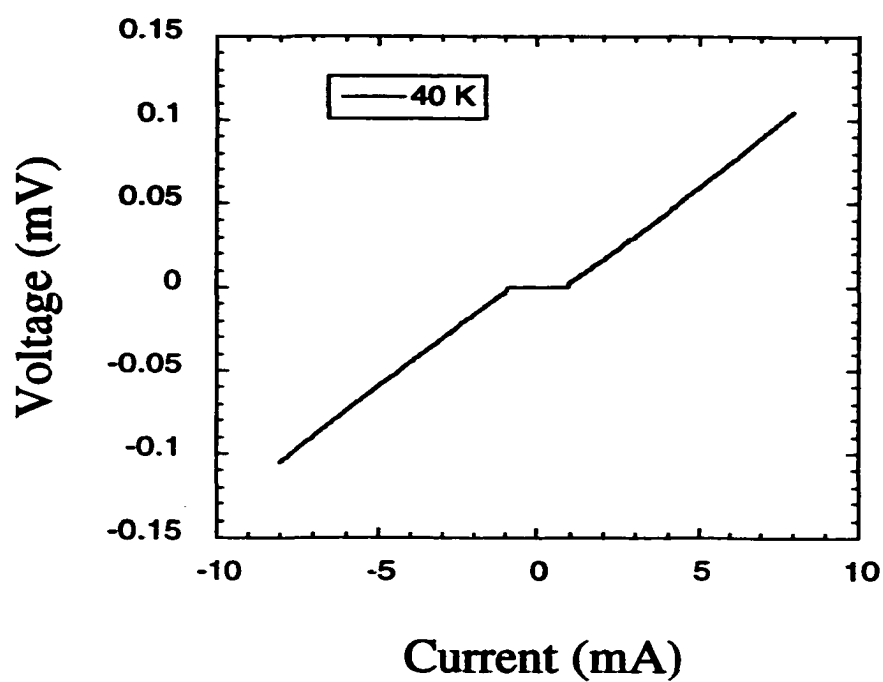
Figure 10.6 I-V curve of a single 45° grain boundary junction that follows the zero capacitance RSJ form.
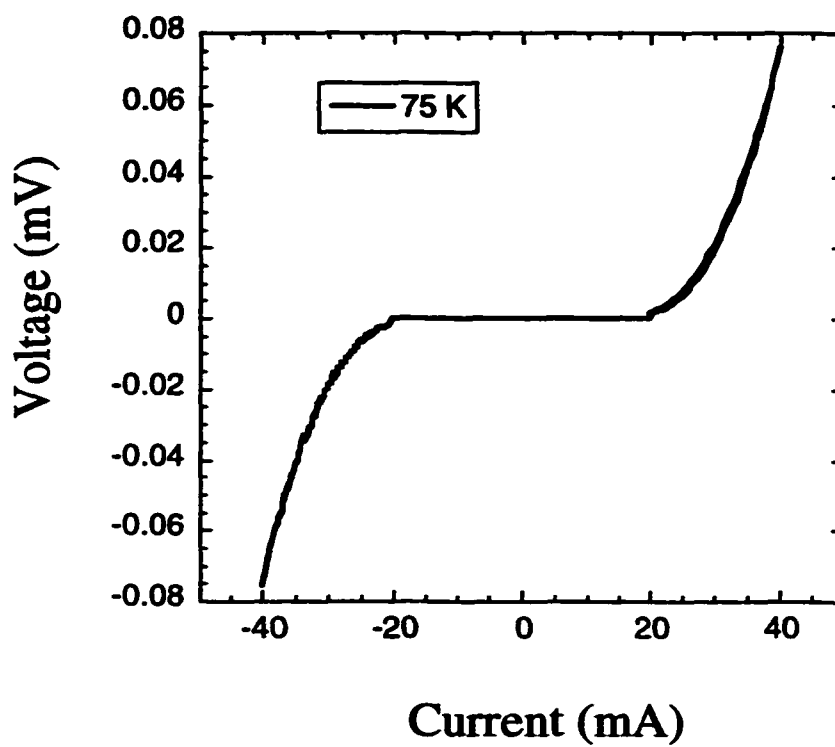
Figure 10.7 I-V curve of a single 45° grain boundary junction that shows flux-flow type rounding of the I-V curve.
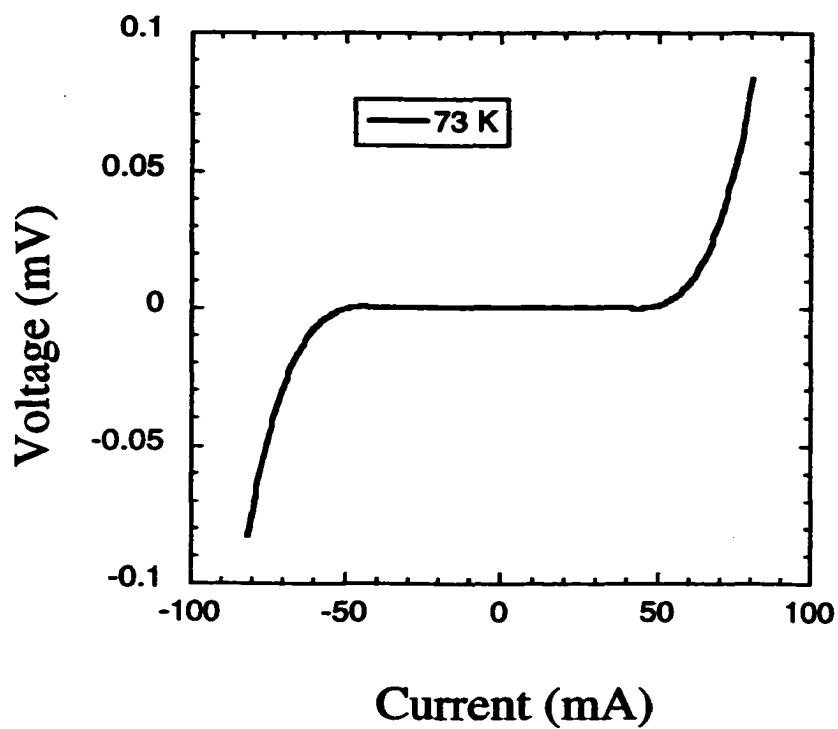
Figure 10.8 I-V curve of a single 45° grain boundary junction that shows flux-flow type rounding of the I-V curve.

10.7-10.8. Moeckly *et al.* also attributed the rounding of the I-V curve to oxygen disorder (Moeckly *et al.* 1993).

X.3 Magnetic Field Behavior

The magnetic field behavior of [001] oriented 45° tilt grain boundaries in YBCO is complex and poorly understood. Early on it was recognized that many 45° tilt grain boundaries did not follow the standard Fraunhofer type magnetic field patterns of most Josephson junctions (Mannhart *et al.* 1996; Hilgenkamp *et al.* 1996; Copetti *et al.* 1995; Vuchic *et al.* 1995). However there were also groups that reported magnetic field patterns for 45° tilt boundaries that showed large central peaks and regular oscillations of the critical current similar to the ideal Fraunhofer pattern (Copetti *et al.* 1995; Nicoleti *et al.* 1997; Lathrop *et al.* 1991).

Recent work has shown that the d-wave symmetry of the order parameter can be used to explain many of the anomalous magnetic field patterns that are observed for 45° tilt grain boundaries (Sigrist *et al.* 1995; Mannhart *et al.* 1996; Copetti *et al.* 1995; Hilgenkamp *et al.* 1996). The details involved with d-wave symmetry are explained in chapter IV. The major difference with 45° tilt boundaries from lower angle tilt boundaries is the possibility of locally negative currents. For 24° tilt boundaries it was assumed that the current crossing the boundary at zero applied magnetic field was always in the direction of the current bias (always locally positive). For 45° tilt boundaries,

because of the d-wave symmetry of the order parameter, it is possible for locally

negative currents to exist that flow opposite to the current bias direction. This possibility

must be accounted for when applying the phase retrieval algorithm when attempting to

determine the local current distribution J(x).

Critical current vs. applied magnetic field measurements for 45° tilt boundaries

suffer from the same problems as the 24° boundaries. Figure 10.9 shows a typical $I_c(B)$

measurement for a single 45° grain boundary. The current oscillates with an applied field

similar to 24° boundaries, however there is no large central current peak at $B = 0$. For

many junctions, at $B = 0$ the current shows a minimum as in figure. 10.9. Figure 10.10

shows a $I_c(B)$ measurement for a long $(W > 4\lambda_J)$ 45° boundary where self-field effects

dominate the $I_c(B)$ behavior. The critical current for the sample in figure 10.10 was first

measured in an increasing field and then a decreasing field environment. The hysteresis

in the $I_c(B)$ measurement is evident in figure 10.10. The data used for the phase retrieval

algorithm must be reversible with no evident hysteresis in the measurements.

Consequently, as with 24° junctions, only short junctions $(W < 4\lambda_J)$ with symmetric $I_c(B)$

distributions that are reversible may be used for phase retrieval.
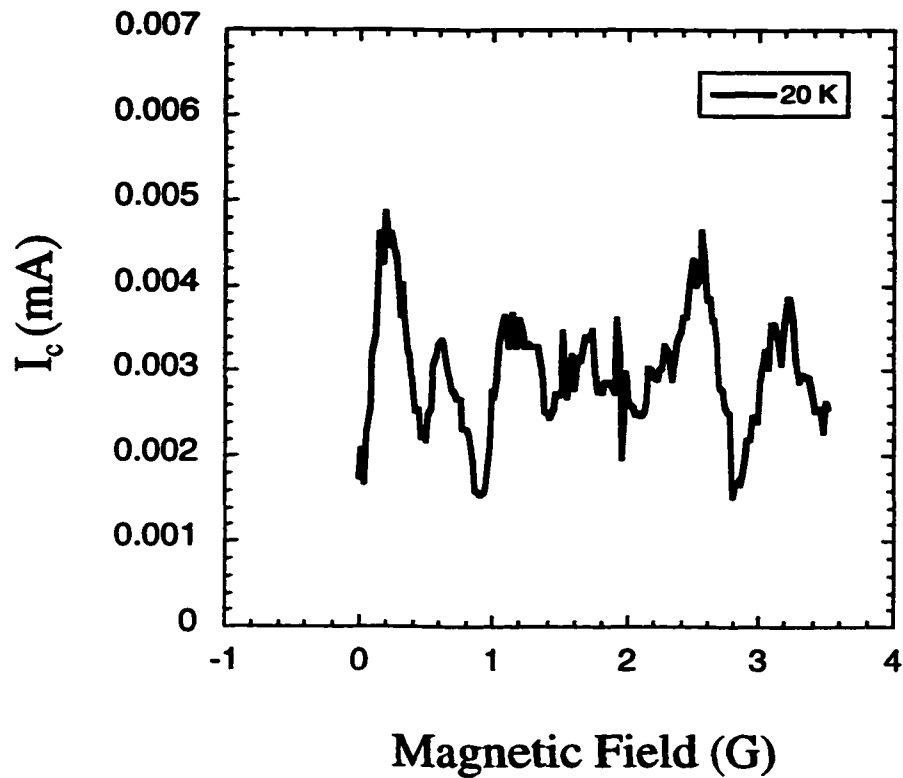
Figure 10.9 $I_c(B)$ curve of a single 45° grain boundary junction that shows Josephson oscillations of the critical current with significant excess current and no large central peak located at B = 0.
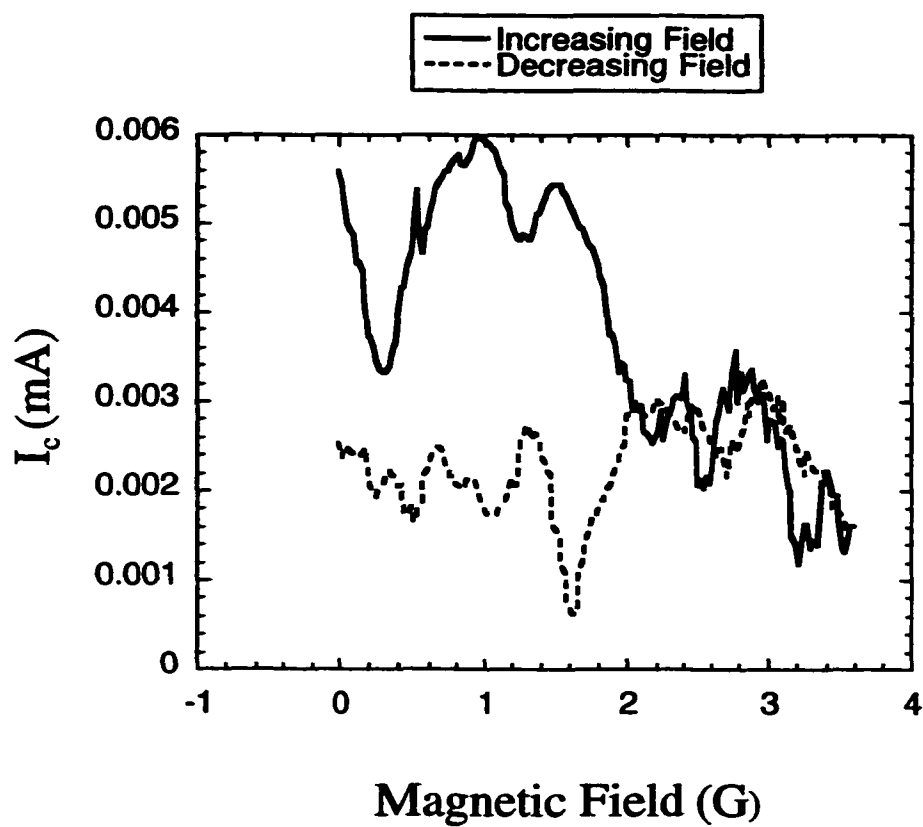
Figure 10.10 $I_c(B)$ curve of a single long 45° grain boundary junction measured in both an increasing and decreasing magnetic field environment. Note the hysteresis in the measurement.

X.4 Local Current Variation

The phase retrieval algorithm detailed in chapter V was modified to allow locally negative currents along the length of the boundary and was used to determine the local variation of the current crossing the boundary from $I_c(B)$ measurements. The $I_c(B)$ measurements were performed in the transport system detailed in chapter VIII and the data was corrected for demagnetization according to the method detailed in chapter VII. By allowing for locally negative currents an extra degree of freedom was added at each location along the boundary and thus the number of possible solutions was greatly increased. The lack of uniqueness for the 1-D phase retrieval problem was discussed in great detail in chapters V and VI. The increased probability of multiple solutions must be dealt with before useful information can be obtained from the phase retrieval algorithm for 45° grain boundary junctions.

In chapter VI the disconnected support constraint proposed by Greenaway, Crimmins, Fienup and Sault was discussed (Greenaway 1977; Crimmins *et al.* 1981; Crimmins *et al.* 1982; Sault 1984). The basic idea was to fix a certain size region within the real space object to be zero. This additional support can be used to guarantee a unique solution to the 1-D phase problem even when locally negative currents are permitted.

A Hitachi Focused Ion Beam (FIB) was used to etch channels along the boundary plane. The FIB etched away the YBCO leaving channels along the boundary plane that carry zero current. These zero current channels were patterned to ensure a sufficiently disconnected support constraint and thus guarantee the uniqueness of the 1-D phase retrieval algorithm.

Figure 10.11 shows a SEM micrograph of a photolithographically patterned and FIB etched microbridge across a 45° boundary. The FIB etched channel is $\approx 6~\mu m$ in width and conforms to the sufficiently disconnected support criterion that is required for uniqueness of the phase retrieval solution. Cryogenic measurements were made of the critical current as a function of an applied magnetic field. Figure 10.12 shows the experimentally measured $I_c(B)$ behavior of the junction shown in figure 10.11. The diffraction pattern is typical of many 45° grain boundary junctions where the maximum critical current is located at $B \neq 0$. The absence of a large central peak is indicative of locally negative currents along the boundary. The regions etched by the FIB that are evident in the photomicrograph can be assumed to carry zero current and thus can be used as a constraint in the phase retrieval algorithm. Figure 10.13 shows the local current distribution $J(x)$ determined from the $I_c(B)$ of figure 10.12. The FIB etched regions within the junction satisfies the sufficiently disconnected support constraint and thus the current distribution in figure 10.13 should be unique. Note the large variation in the local current along the length of the boundary as well as the current reversals (negative local currents) along the boundary. The Fourier Josephson relation requires locally negative
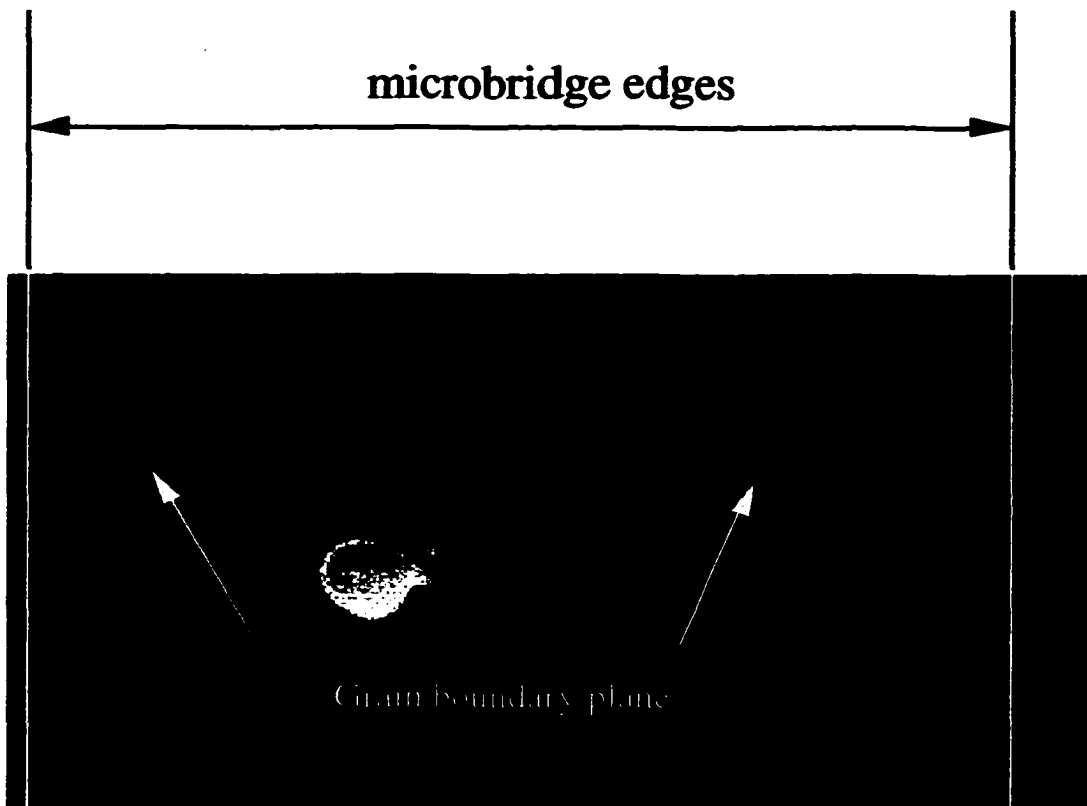
Figure 10.11 SEM micrograph of a FIB etched 45° grain boundary junction.
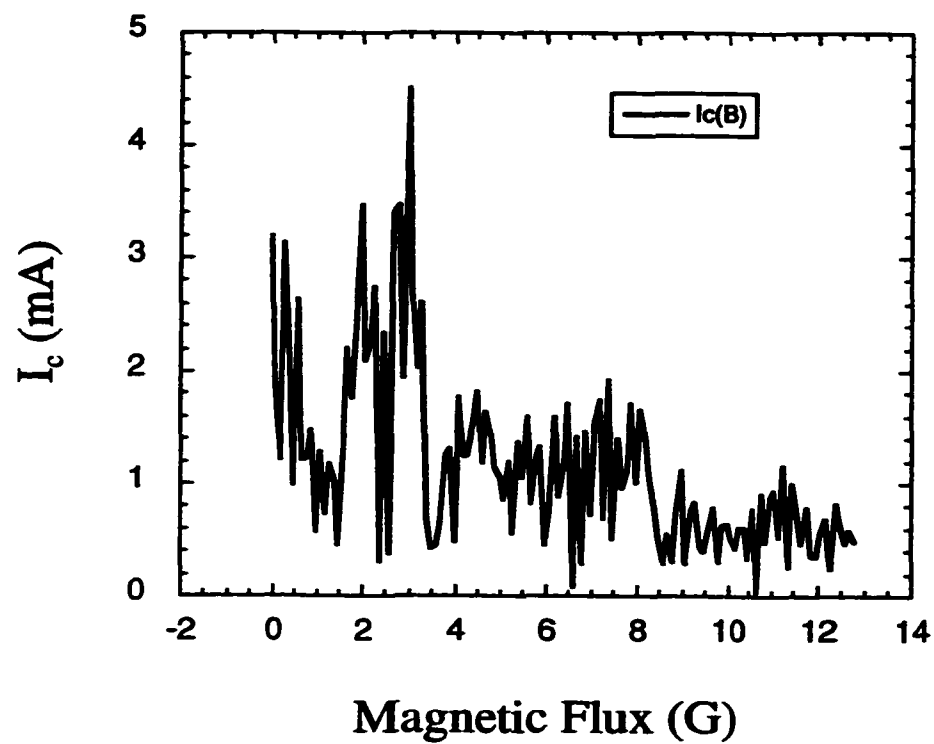
Figure 10.12 $I_c(B)$ data for FIB patterned grain boundary shown in Figure 10.11.
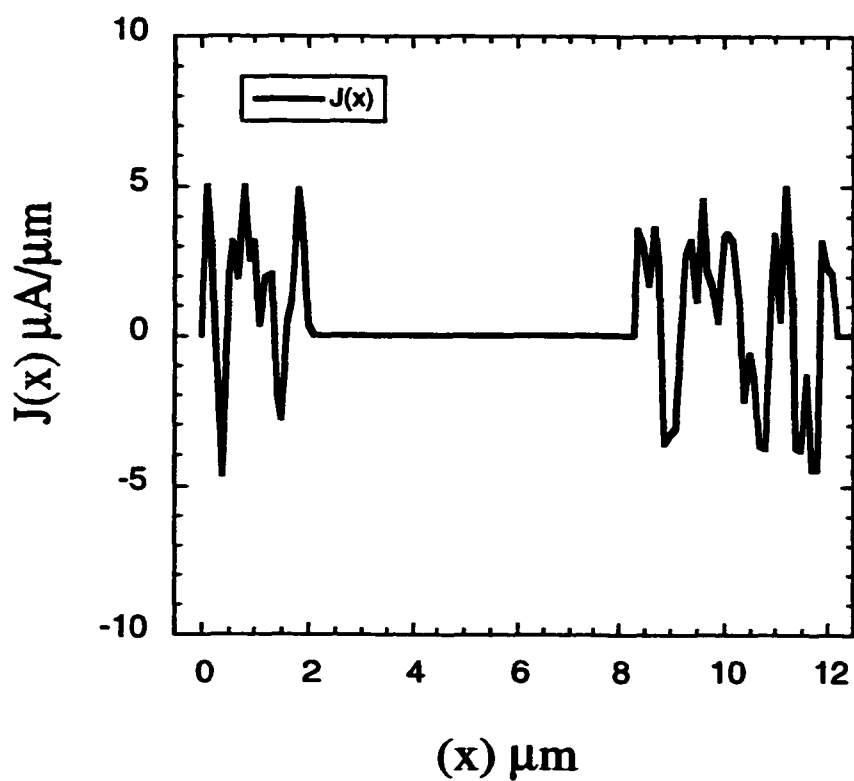
Figure 10.13 Local current distribution J(x) determined from the data in figure 10.12. The large region in the middle of the junction was known to be zero from the FIB damage and used as a constraint to guarantee unique solution.

currents along the boundary when the maximum current across a Josephson junction is not located at B = 0.

Figure 10.14 is a SEM micrograph of a 45° grain boundary junction where two channels across the boundary plane have been etched with a FIB. The etched channels cannot carry current and thus act as the disconnected support for the phase retrieval algorithm, however, this particular sample does not conform to the stringent requirement of sufficiently disconnected support as put forth by Crimmins and Fienup (Crimmins *et al.* 1982). Figure 10.15 shows the $I_c(B)$ pattern measured from the sample in figure10.14. Note again the large oscillations of the current and that the maximum critical current is not located at B = 0. Figure 10.16 shows the current distribution solution J(x) determined from the phase retrieval technique. Only one solution was obtained to the phase retrieval problem, even though the possibility for more than one solution existed because of the lack of sufficient constraints to guarantee uniqueness.
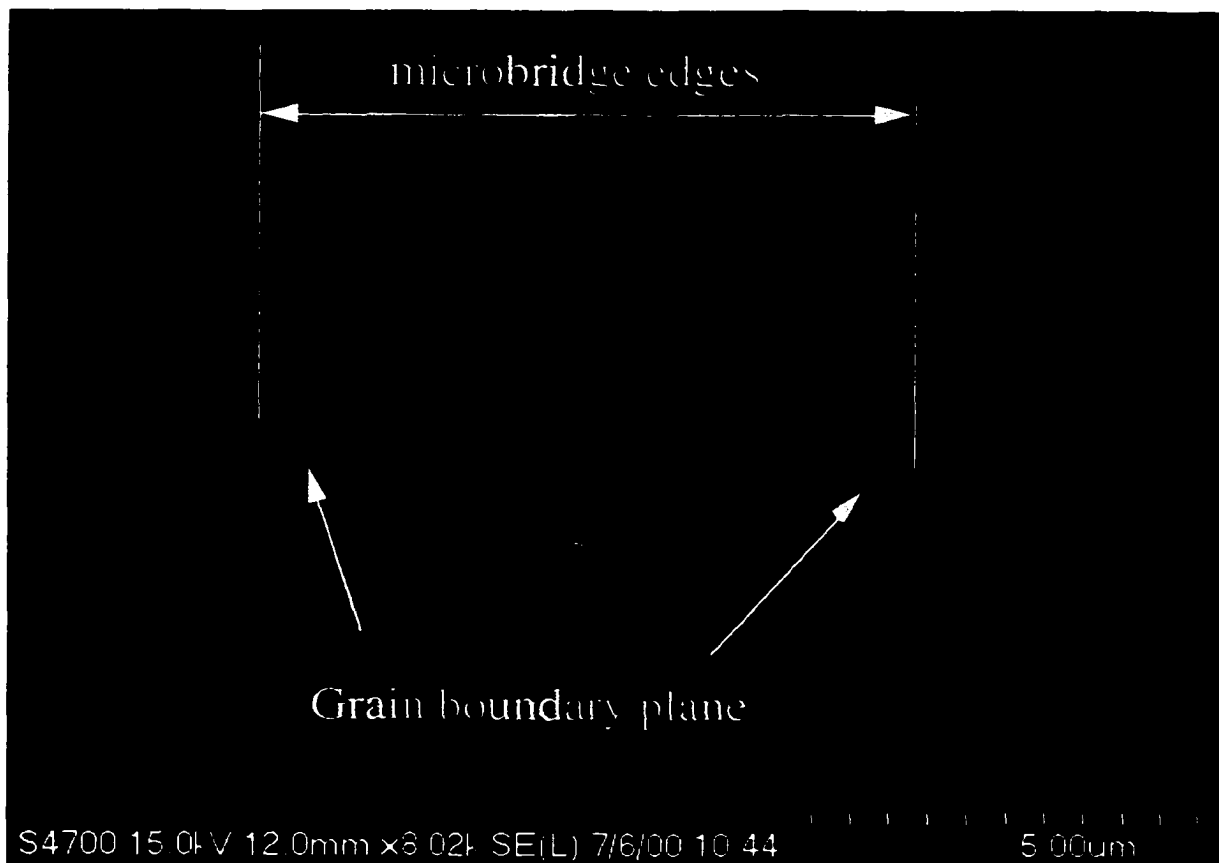
Figure 10.14 SEM micrograph of FIB etched 45° grain boundary junction.
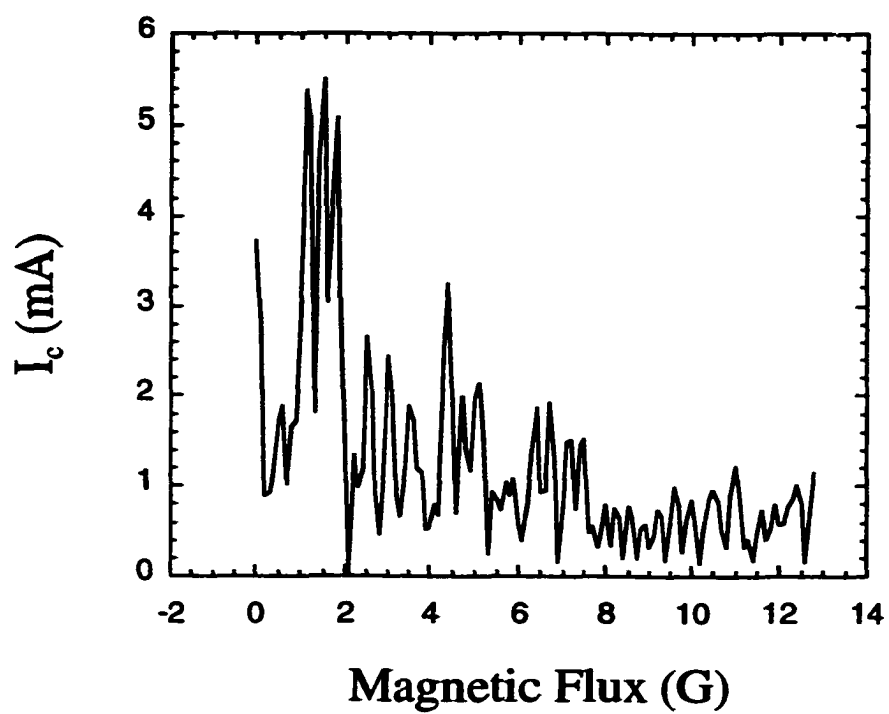
Figure 10.15 I$_c$(B) data for FIB patterned grain boundary shown in Figure 10.14.
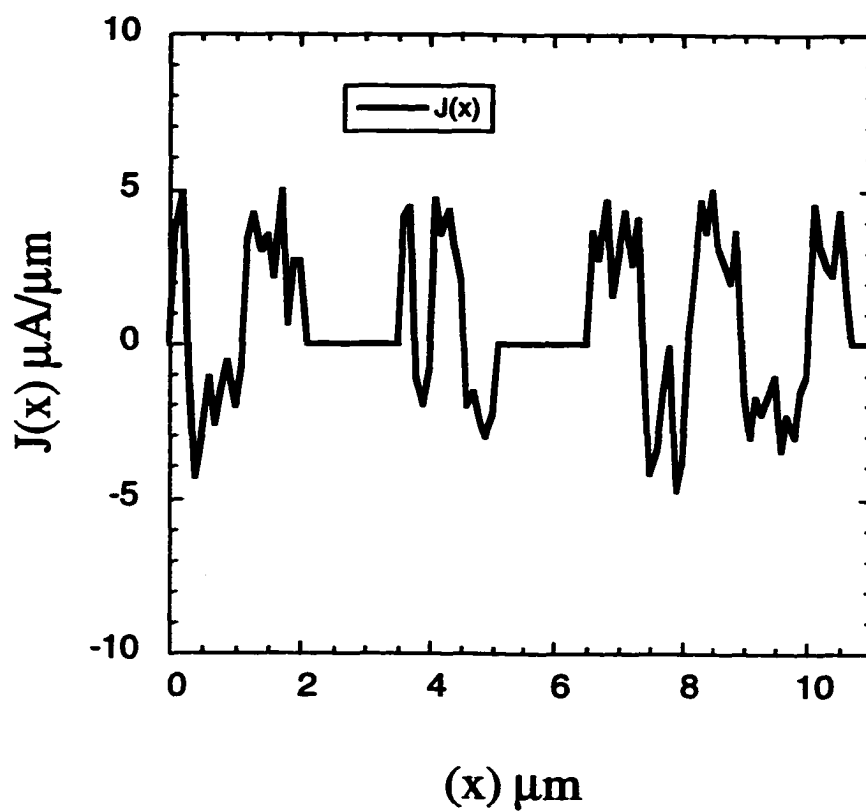
Figure 10.16 Local current distribution J(x) determined from the data in figure 10.15. The two large zero regions in the middle of the junction were used as a constraint to guarantee unique solution.

Figure 10.17. shows the $I_c(B)$ behavior of a single 45° grain boundary junction

where no channels were etched with the FIB. The single junction shows the typical 45°

diffraction pattern with no large central current peak located at B = 0. The $I_c(B)$ data

from figure 10.17 was used to determine local current distributions J(x) for the junction.

The junction does not have channels etched with the FIB that can be set to zero and used

as a constraint to guarantee uniqueness of the solution. The constraints that can be used

are the finite support of the junction (junction width is fixed and the current must be zero

outside of the junction), the local current must always be less than a maximum, $J_{c,max}$ and

the total current must be positive even though locally it can be negative. Using these

constraints the phase retrieval was used to calculate possible current distributions for the

junction. Figure 10.18 shows the different current distributions determined using the

known boundary constraints and the phase retrieval algorithm. The phase retrieval

algorithm was able to find several different solutions from the data in figure 10.17. The

solutions are non-unique in a strict mathematical sense, but share many similar physical

traits. All of the solutions share common large peaks toward the left-hand side of the

solutions. Peaks largely correspond to peaks and troughs correspond to trough thus

representing similar current distributions. Some of the smaller peaks toward the right

side of the distribution in figure 10.18 are out of phase and thus represent ambiguities in

the physical interpretation of the current distributions. It may be useful to average the

various current distributions since the large peaks have a strong correlation between

solutions. Figure 10.19 shows the average of the three different solutions found in figure

10.18. The large-scale features common to all three solutions remain intact because of

the strong correlation between solutions, however much of the fine scale detail is lost

due to variations in the individual solutions.
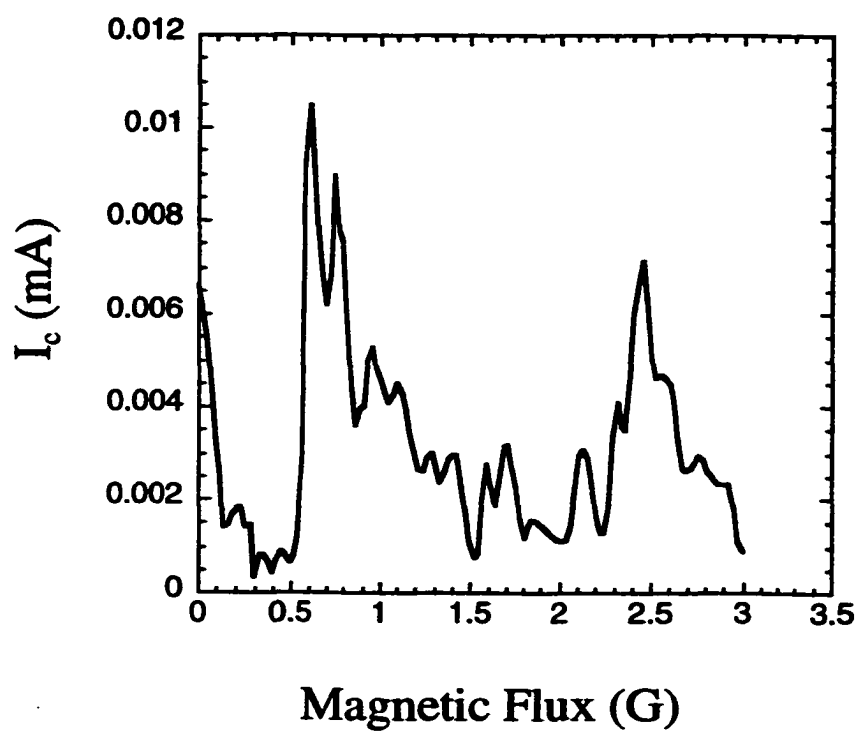
Figure 10.17 Critical current vs. applied magnetic field data for a single 45°
grain boundary junction.
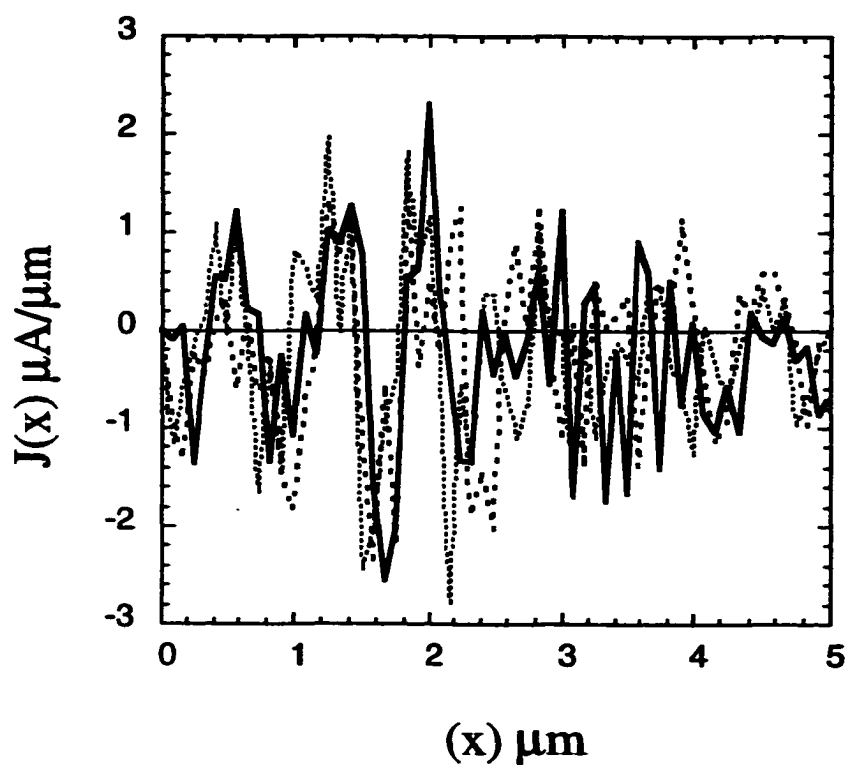
Figure 10.18 Multiple local current distributions J(x) calculated from the data in figure 10.17. Multiple solutions to the phase problem exist for a single junction without disconnected support. Note the similarity between the large scale features in the different solutions. The extra degree of freedom at each data point results in many different possible solutions to the 1-D phase problem.
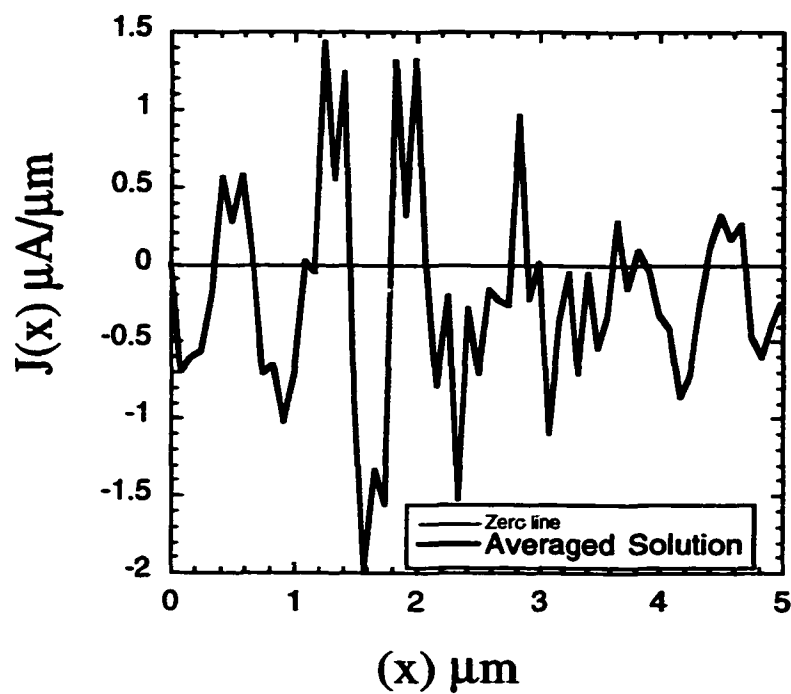
Figure 10.19 Averaged solution calculated from the solutions in figure 10.18.
The large scale features have been retained in the averaged solution because of the
similarities between solutions. Some of the small scale features have been lost or
averaged out due to the various solutions being slightly out of phase.

XI. Ramp-Edge Josephson Junctions

XI.1 Introduction

High-T_c Josephson junctions have shown large scatter in their transport properties. The vast scatter in the transport properties found in the various types of Josephson junctions can be largely attributed to the variation of the interface barrier structure from one junction to another. High angle grain boundaries have shown large scatter in both their transport properties and microstructure and thus are not reliable yet for reproducible devices.

One promising type of Josephson junction for device applications are the superconductor/barrier/superconductor ramp-edge Josephson junctions. The microstructure of the interface between the superconducting electrodes in these junctions can play an important role in determining the uniformity of the junction transport properties and thus the junction's potential usefulness for device applications (Hunt *et al.* 1988; Huang *et al.* 1999; Jia et *al.* 1995; Char *et al.* 1993; Char 1994; Rozeveld *et al.* 1995; Ono *et al.* 1991; Olsson *et al.* 1994; Merkle *et al.* 1999; Olsson *et al.* 1993; Rozeveld *et al.* 1996; Wen *et al.* 1995; Blank *et al.* 1997; Char *et al.* 1993; Char 1997).

213

XI.2 Superconductor-Barrier-Superconductor Ramp-Edge Junctions

The basic ramp-edge junction of interest is an epitaxial multilayer device with the superconducting/barrier /superconducting structure where the barrier layer can be either a normal (SNS) or insulating (SIS) material. High-T_c junctions are potentially useful for many electronic applications, however significant performance barriers have prohibited applications thus far. Specifically, any useful high-T_c junction must posses large I_cR_n products (> 1 mV), good ac and dc Josephson magnetic field response, high critical current density and reproducibility. These epitaxial multilayer junctions have great potential to satisfy all of the necessary requirements for commercial device implementation.

Low-T_c superconductor SNS and SIS Josephson junctions have been extensively studied and show ideal properties for device applications. The junctions studied by Dynes and Fulton were SIS (Sn-oxide-Sn) multilayer devices and showed near ideal Fraunhofer magnetic field responses to an applied magnetic field (see figure 11.1)(Dynes *et al.* 1971). It was hoped that high-T_c ramp-edge junctions would demonstrate similar ideal and repeatable transport properties as their low-T_c counterparts. Unfortunately, complications arising from the complex crystal structures involved and the resulting local microstructure has resulted thus far in poor performance and reproducibility of high-T_c ramp-edge junctions.
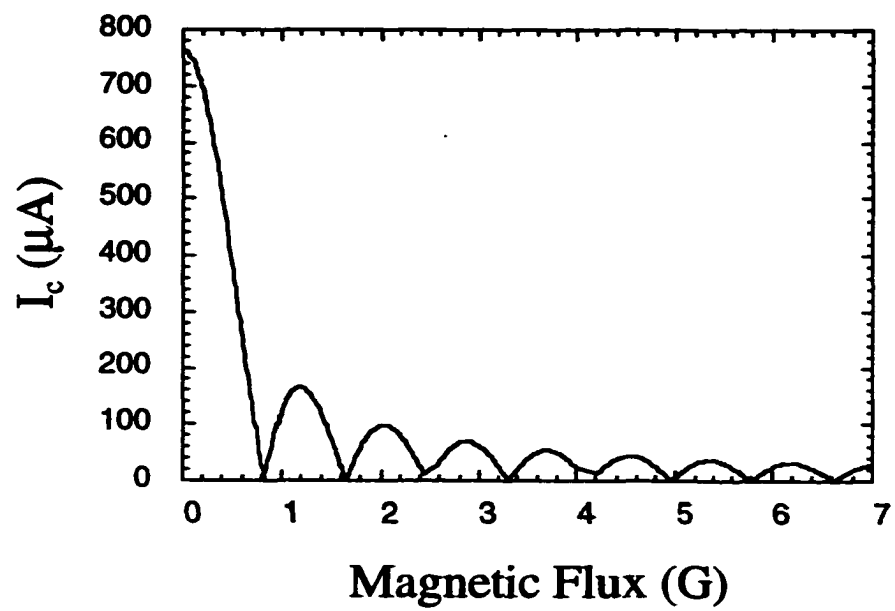
Figure 11.1. Critical current vs. applied magnetic flux $I_c(B)$ for a SNS low-T_c Josephson junction. (From Dynes *et al.* 1971)

Many different barrier layer materials, both normal and insulating, have been used to form YBCO superconductor-barrier-superconductor Josephson junctions. Table 11.2 is a partial list of materials (normal and insulating) that have been used to form Josephson junctions with YBCO. The basic structure is a sandwich type structure shown in Figure 11.3 with the barrier layer separating the two YBCO electrodes. The basic superconductor-barrier-superconductor device structure is usually fabricated in the ramp geometry shown in Figure 11.3. Typically a YBCO base layer is grown epitaxially on a suitable cubic or near cubic substrate material (MgO, $LaAlO_3$, $SrTiO_3$, CeO_3 etc.). A ramp edge is then sputtered at a predetermined angle (typically 30 °). A thin barrier layer material (typically 10-50 nm) is then deposited on the ramp surface. A second YBCO layer is deposited on top of the barrier layer to act as the second electrode in the multilayer structure. Figure 11.4 shows a schematic of the current transport geometry across the multilayer device. The current is driven across the barrier layer in the [100] or [010] direction of the YBCO electrodes. For magnetic field detection, the magnetic field is applied perpendicular to the current direction and parallel to the [001] of both the substrate and the two YBCO layers.

The current-voltage characteristics of most ramp-edge YBCO junctions can be described by a zero capacitance RSJ junction model similar to grain boundary Josephson junctions. The normal state resistance R_n determined from the current-voltage curves is constant and does not vary with temperature.

Normal Materials
Au
Ag
Pb
$CaRuO_3$
$SrRuO_3$
$PrBa_2Cu_3O_{2-d}$
$Y_{0.6}Pr_{0.4}Ba_2Cu_3O_{7-d}$
Nb-doped $SrTiO_3$
$(CaSr)RuO_3$
$(LaSr)CoO_3$
Ca-doped YBCO
Co-doped YBCO
$(LaSr)_2CuO_4$
$SrTiO_3$*
MgO*
$NdGaO_3$*

* indicates insulating material (SIS) junction

Figure 11.2. Materials that have been used to form
Superconductor/barrier/Superconductor Josephson junctions with YBCO.

Barrier layer
normal or insulating
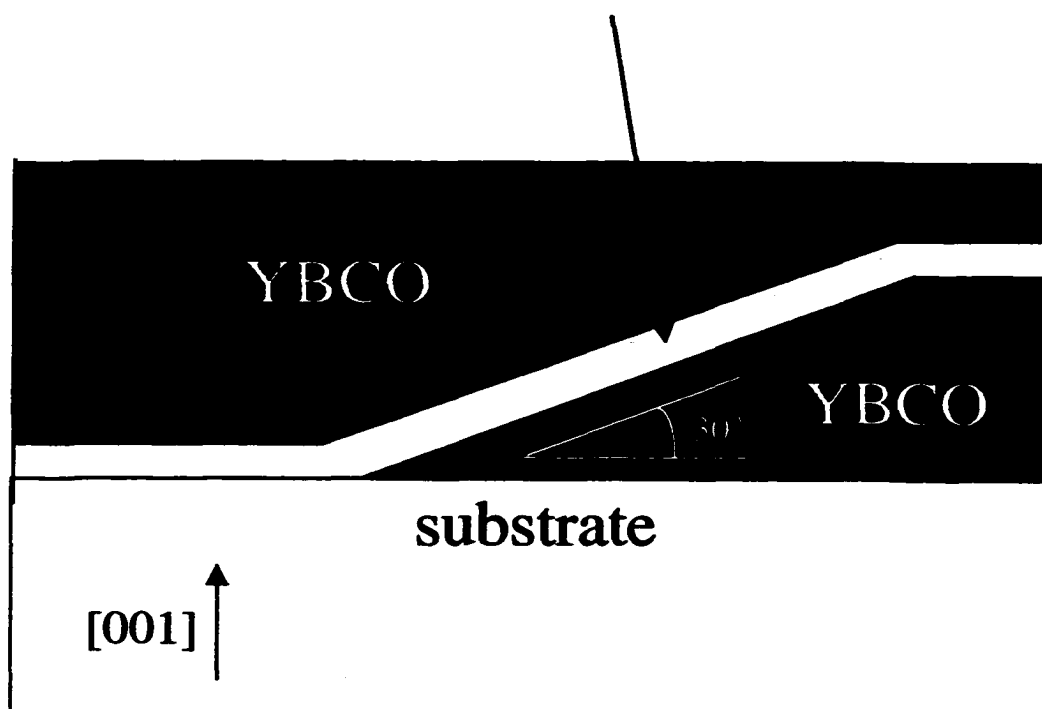
Figure 11.3. Standard ramp geometry of SNS Josephson junction.
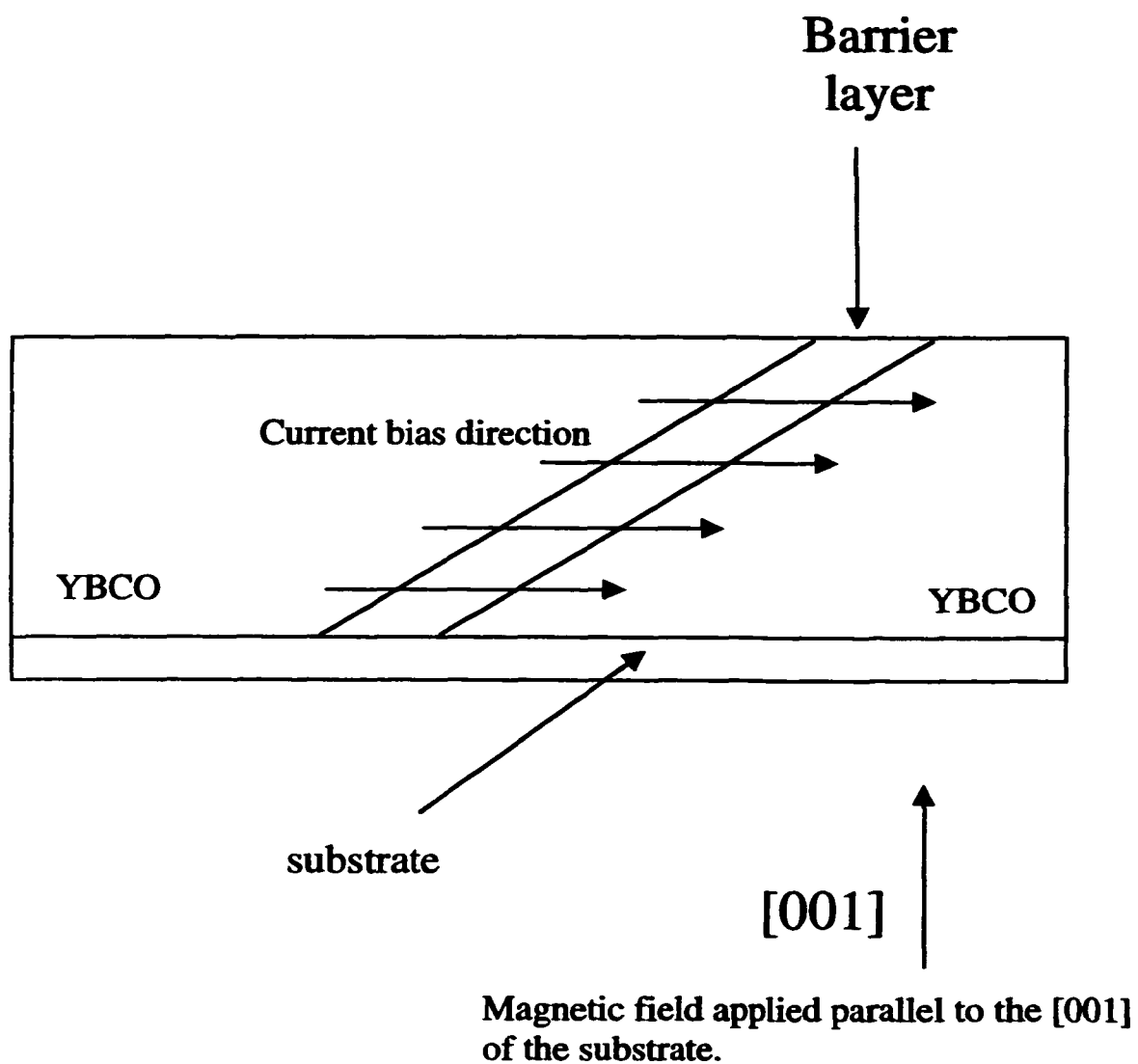
Figure 11.4. Current driven across the barrier perpendicular to the direction of the applied magnetic field. The magnetic field is applied parallel to the [001] of the substrate and the two YBCO electrodes.

It is believed that the structural uniformity of the barrier layer is directly related to the current crossing the boundary and therefore determines the reproducibility of these junctions (Olsson *et al.* 1994; Wen *et al.* 1995; Huang *et al.* 1998; Huang *et al.* 1997; Rozeveld *et al.* 1995; Blank *et al.* 1997; Hunt *et al.* 1998; Zhou *et al.* 1998; Antognazza *et al.* 1995; Rozeveld *et al.* 1996; Char *et al.* 1993; Merkle *et al.* 1999; Harada *et al.* 1991; Jia *et al.* 1995). There are many factors that can influence the uniformity of the barrier layer and thus the current distribution across the boundary. Local oxygen content variation, boundary precipitates, interfacial strain fields and boundary microstructure can all play an important role.

XI.3 Interface Engineered Ramp-Edge Junctions

Previous work on plasma treated and ion milled YBCO surfaces have shown that these surface treatments result in structural changes to the YBCO. These treated YBCO surfaces can act as a Josephson barrier for ramp-edge type junctions. Understanding that the interface layer can play a dominant role in controlling the reproducibility in manufacturing Josephson junctions, Moeckly and Char developed a method for fabricating ramp-edge Josephson junctions without the growth of a heterophase interlayer (Moeckly *et al.* 1997; Moeckly *et al.* 1998). Instead, they applied an Ar/O plasma treatment to the surface of the first $YBa_2Cu_3O_{7-x}$ (YBCO) layer in the ramp edge junction forming an intermediate layer which acts as a Josephson junction barrier. These interface engineered junctions have been shown to be highly reproducible with resistively-shunted

junction like I-V characteristics, Fraunhofer-like magnetic field response and I_cR_n values
between 0.1 – 0.5 mV (Moeckly *et al.* 1997; Moeckly *et al.* 1998).

To gain a better understanding of the properties as they relate to the
reproducibility of the interface engineered junctions, we have studied the current
distribution across ramp-edge YBCO Josephson junctions. Understanding how the
current distribution across the boundary varies from one junction to another and how that
variation correlates to the boundary microstructure will provide insight to the mechanism
controlling the transport process across the boundary. Calculations of the critical current
variations along the length of the boundary were performed, based on critical current vs.
applied magnetic field measurements. Critical current vs. applied magnetic field
measurements on YBCO interface engineered ramp-edge junctions with the magnetic
field applied perpendicular to the substrate surface. The current distribution along the
length of the boundary (as defined in figure 11.4.) for each sample was calculated using
the phase retrieval algorithm.

Critical current vs. applied magnetic field measurements were performed on 4 μm
wide interface engineered junctions for analysis of the current distribution. Figure 11.5
shows the $I_c(B)$ data from a typical ramp-edge interface engineered junction measured at
4.2 K. Compared with grain boundary junctions, the $I_c(B)$ patterns are highly uniform
and close to the ideal Fraunhofer diffraction pattern. The current oscillates to near zero
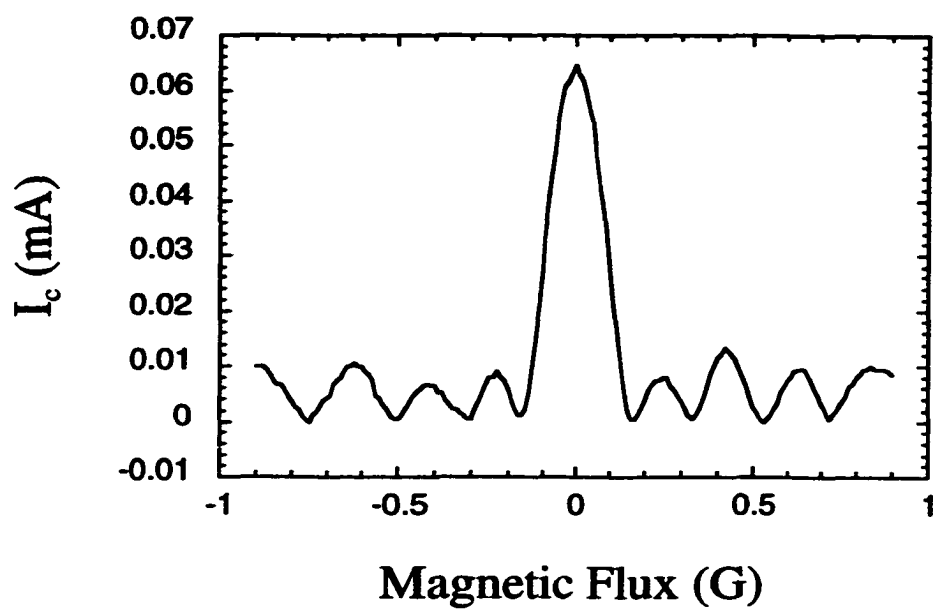
Figure 11.5 $I_c(B)$ data from a typical ramp-edge interface engineered Josephson junction measured at 4.2 K. Note the near Fraunhofer shape and oscillations.

and therefore has little or no excess current compared to grain boundary junctions.

Figure 11.6 depicts the critical current vs. applied magnetic field of another typical interface engineered junction. Measurements were performed on the junction at 40 K and 60 K. The $I_c(B)$ data was corrected for demagnetization effects using the same procedure as for grain boundary junctions and used to determine the local current distributions $J(x)$ at each temperature. Figure 11.7 shows the critical current distributions $J(x)$ along the length of the boundary for each measured temperature from the sample in figure 11.6. The current distributions are highly uniform and demonstrate good agreement between the two measured temperatures. It is important to note that the magnetic field dependence of the sample in figure 11.6 shows only minor deviations from the ideal Fraunhofer pattern and therefore should (and does) results in a fairly uniform current distribution along the length of the boundary shown in 11.7.
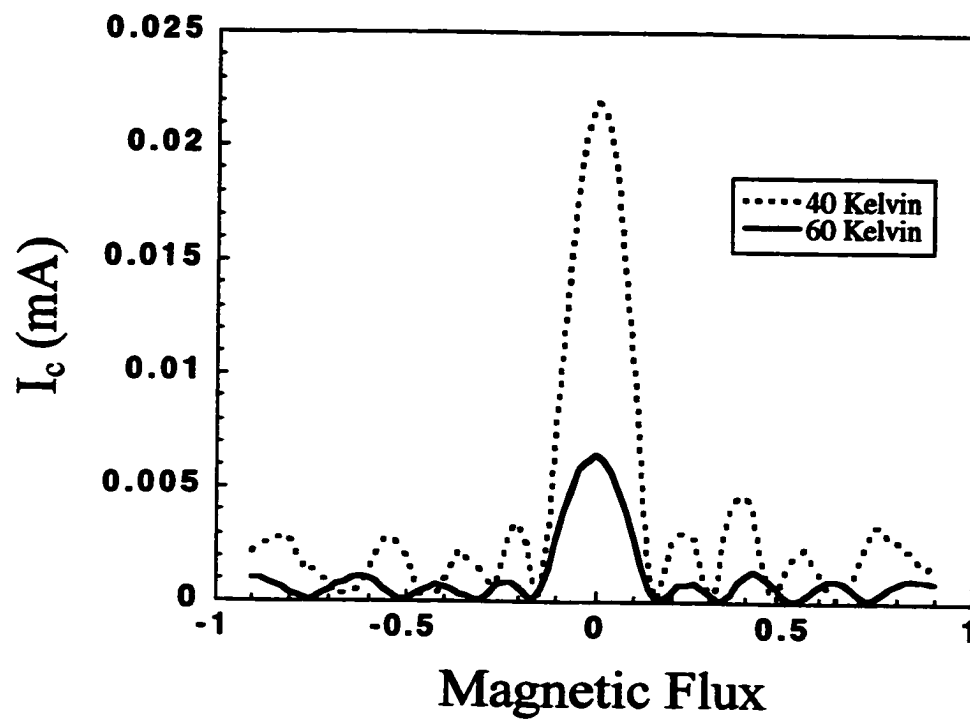
Figure 11.6 I_c(B) data from a 4mm wide junction measured at 40 and 60 K.
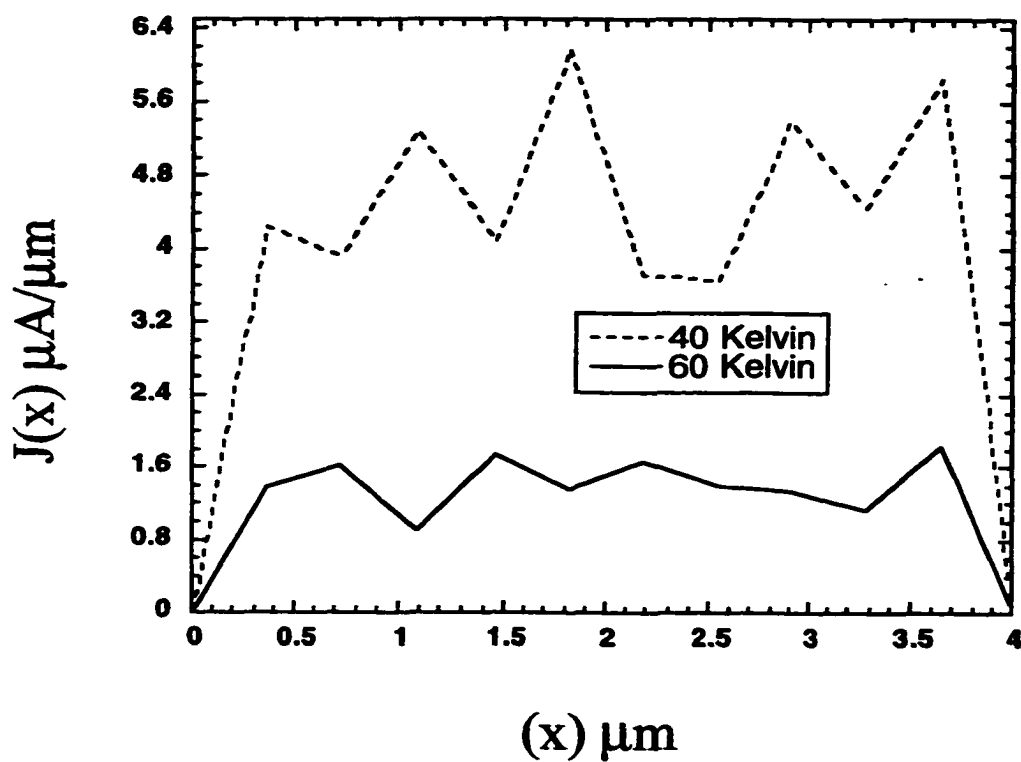
Figure 11.7 Local current distribution determined from the Ic(B) data shown in figure 11.6. The highly uniform local current distributions are in stark contrast to the highly varying patterns found for grain boundary junctions.

XII. Understanding 24°, 45° and Ramp-Edge Josephson Junctions

XII.1 Introduction

The theoretical understanding of high-T_c Josephson junctions originates from the theories developed for low-T_c superconductors. Most of the relevant theoretical background for low-T_c Josephson junctions was presented in chapters II and III. The most important relationship is the Josephson equation,

$$I_c(u) = \left| \int_a^b J_c(x) \exp(iux) dx \right|,$$ (12.1)

that has been explored and exploited extensively in this thesis. Figure 11.1 from chapter XI (shown again in this chapter as figure 12.1) is the $I_c(B)$ data from a low-T_c Josephson junction measured by Dynes and Fulton (Dynes *et al.* 1971). The $I_c(B)$ data in figure 12.1 follows in close agreement with the ideal Fraunhofer equation. Equation 12.1 was developed for low temperature superconductors that have a relatively large coherence length compared to high-T_c materials and a non-directional (s-wave) symmetry of the superconducting order parameter. Any disruption of the material on the same length scale of the order parameter is capable of destroying the supercurrent flow. For low-T_c superconductors, the coherence length can be as large as 0.5 µm, therefore, it requires very large scale disruptions of the microstructure to alter the supercurrent flow

226
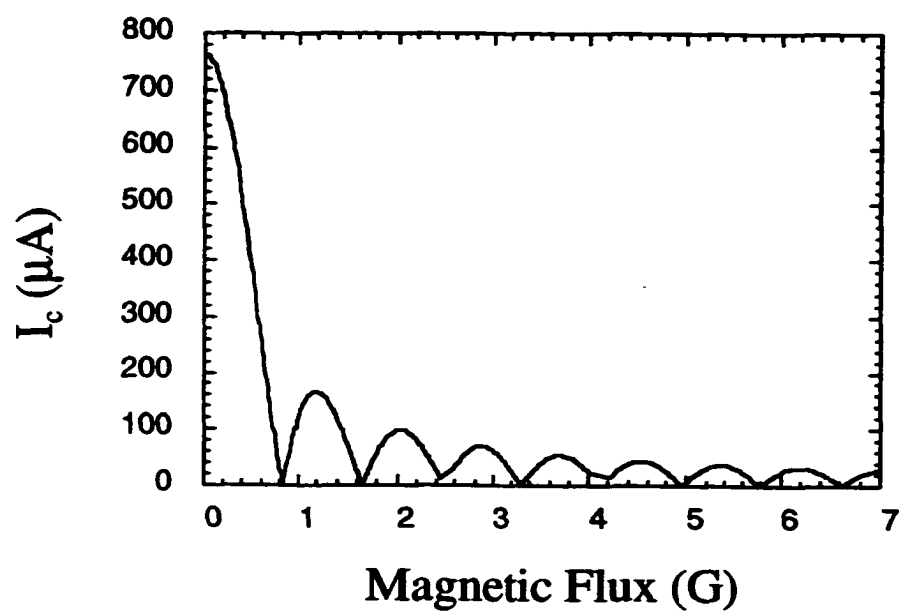
Figure 12.1 Critical current vs. applied magnetic flux $I_c(B)$ for a
SIS low-T_c Josephson junction.(From Dynes and Fulton)(Dynes *et al.* 1971)

along the boundary of a low-T_c Josephson junction. Consequently, most low-T_c Josephson junctions follow closely to the ideal Fraunhofer pattern as in figure 12.1.

Compared to low-T_c superconductors, high-T_c superconductors such as YBCO have a coherence length on the nanometer length scale and a highly directional symmetry (d-wave) of the order parameter. Consequently, any disruption of the material on the nanometer length scale is capable of altering or destroying the superconductivity of a high-T_c superconductor.

XII.2 24° Symmetric Tilt Grain Boundary Junctions

The weak link nature of grain boundaries in high-T_c superconductors has been discussed in previous chapters. The structure of grain boundaries can have disruptions on the same length scale as the coherence length and therefore result in regions of suppressed or destroyed superconductivity. The basic structure of grain boundaries was discussed in chapter III. Symmetric 24° tilt boundaries were used in this thesis to study grain boundary transport. Transmission electron microscope studies of grain boundary junctions have shown large variations in the boundary microstructure along the length of the boundary. Boundary precipitates, meandering of the boundary on the order of hundreds of nanometers and faceting on the 10-100 nanometer length scale (the length and orientation of the facets are dependent on the grain boundary orientation) are dominant features of most grain boundary junctions. Meandering is believed to be

caused by rapid growth in the a-b plane of the YBCO over the template bicrystal resulting in a YBCO grain boundary junction that does not follow the bicrystal template closely. Studies of symmetric 24° YBCO grain boundaries have indicated that, although the underlying SrTiO$_3$ substrate is prepared as a symmetric bicrystal, large areas along the boundary are not symmetric due to the boundary meandering. Figure 12.2 shows and high resolution electron microscope (HREM) micrograph of a YBCO 24° symmetric tilt grain boundary looking down the [001] direction from Huang (Huang et al. 1997). The length of the boundary shown in figure 12.2 is relatively straight and the grain boundary plane is near a symmetric orientation. The grain boundary core appears disordered in a region less than a nanometer in width. Figure 12.3 shows an HREM image of a different region along the same YBCO grain boundary. Here the grain boundary is inclined relative to the film normal but largely parallel to (010) of the top crystal. The appearance of asymmetric facets is typical of large regions of the grain boundary. The Morié pattern in figure 12.3 evident at the boundary is indicative of an incline and overlapping of the two crystals in the direction of the electron beam. The HREM image of figure 12.4 depicts another asymmetric region of the same grain boundary. Again, the large width of the Morié pattern at the grain boundary indicates considerable crystal overlap due to the inclined grain boundary plane. Adjacent grains that are well connected, in contrast to cores that are strongly disordered, are expected to carry higher critical currents. Figures 12.2 - 12.4 demonstrate the great variation in the local microstructure of grain boundaries, which is to a large extent due to the grain boundary meandering, as discussed below.
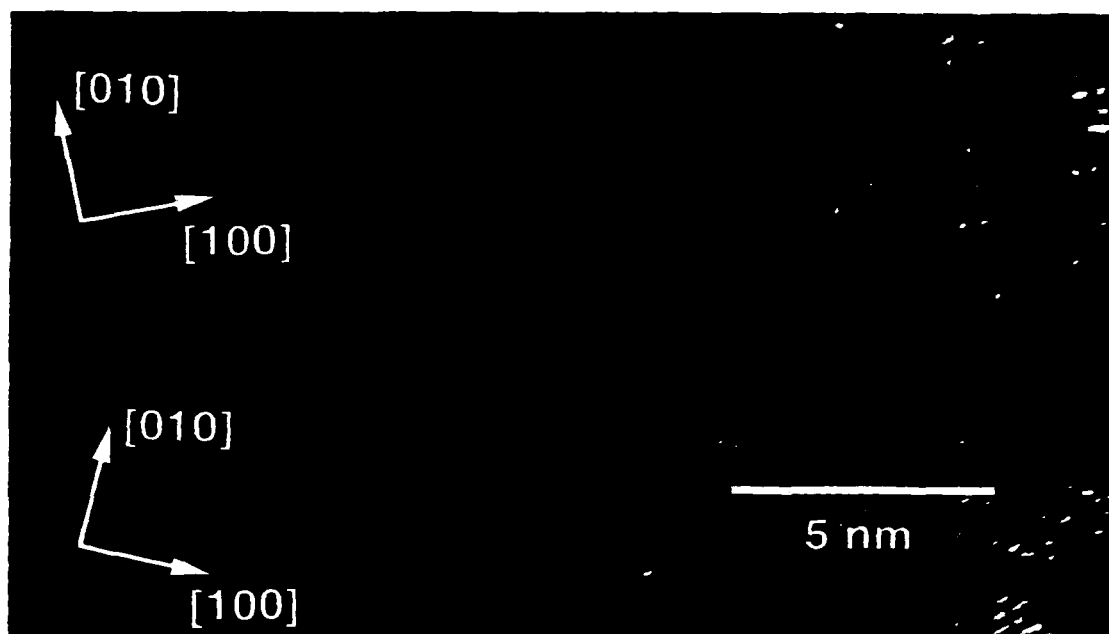
Figure 12.2 HREM of [001], 24° YBCO grain boundary grown on a [001] symmetric SrTiO₃ bicrystal template. Note that this area of the grain boundary is straight and has a disordered region at the grain boundary. (Image courtesy of Y. Huang)(Huang *et al.* 1999)

[010]

5 nm

[100]

[010]

[100]
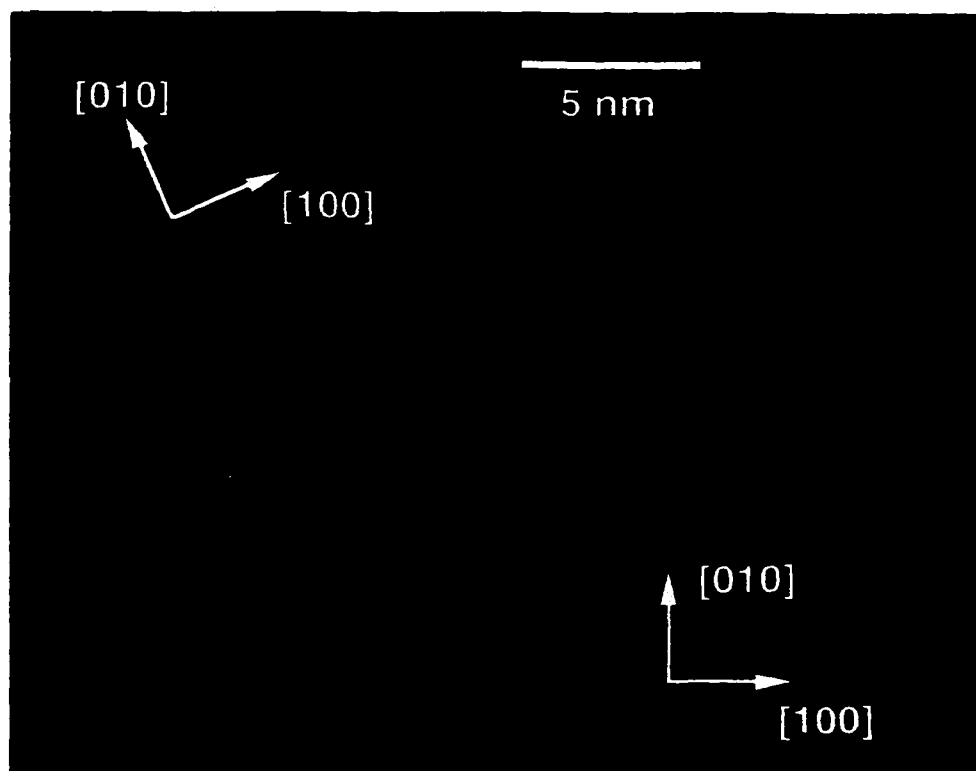
Figure 12.3 HREM image of a 24° YBCO grain boundary grown on a [001] symmetric SrTiO₃ bicrystal template. Note that this area of the grain boundary is asymmetric which is caused by macroscopic boundary meandering. The Morié pattern at the boundary indicates an overlap of the two grains. Therefore, the grain is of mixed character (tilt and twists). (Image courtesy of Y. Huang)(Huang *et al.* 1999)
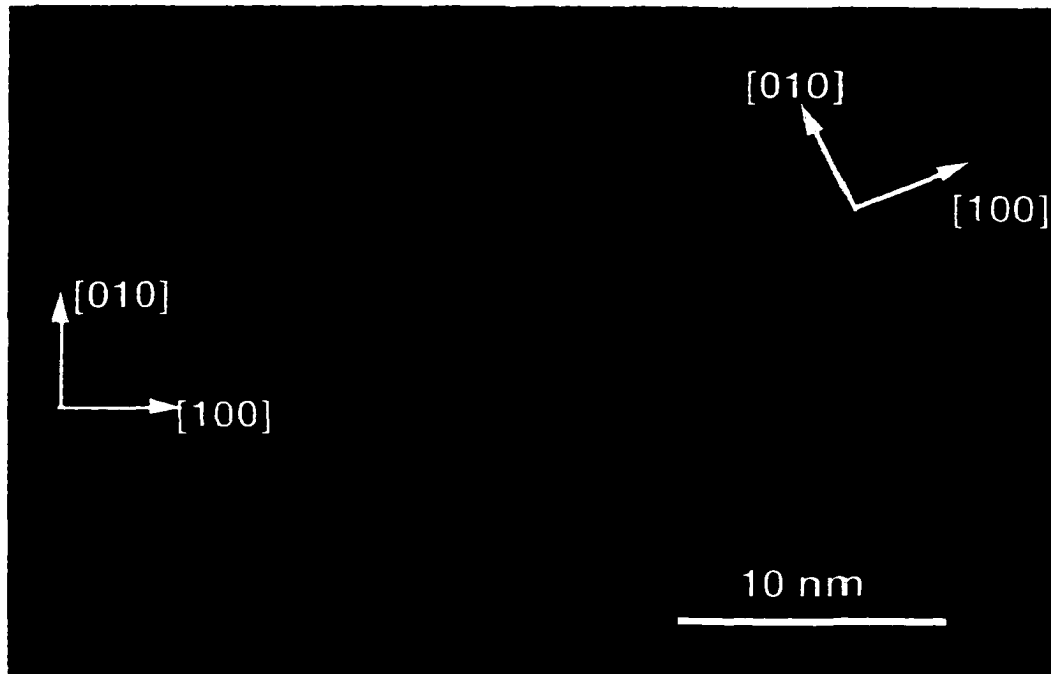
Figure 12.4 HREM image of a 24° YBCO grain boundary junction. The large Morie' pattern indicates considerable overlapping of the grains. (Image courtesy of Y. Huang)(Huang *et al.* 1999)

It is evident that the local symmetry at the grain boundary is controlled by the meandering of YBCO across the template bicrystal boundary. Thus the notion of distinguishing between symmetric and asymmetric boundaries when discussing the transport properties of grain boundary Josephson junctions is questionable. The nominally symmetric 24° grain boundary junctions used for our analysis show large areas with asymmetric facets. Thus it is important to understand that regardless of the macroscopic symmetry across the grain boundary, no purely symmetric YBCO grain boundary junctions are obtained by the conventional YBCO thin film synthesis techniques. The boundary meanders and twists from different tilt and twist orientations along the length of the boundary.

As we have shown in chapter IX, the current distributions for 24° grain boundary junctions show large-scale variations along the length of the boundary. In many incidents there are sizable regions of the grain boundary that carry no current. The large variation of the local microstructure is partly responsible for these variations, however variations in the oxygen content can have a dominant role in controlling the variation in the local current distribution. The variation of the local oxygen content and the role it can have in controlling the local transport properties was highlighted in chapter III.

Clearly, the vast variation in microstructures observed along the length of single grain boundaries, as illustrated in figures 12.2-12.4, suggest corresponding variations in the local current carrying capacity of the grain boundary. Structural and chemical

disorder, such as amorphous grain boundary phases and oxygen depletion severely limit current transport. Whether or not and to what extent grain boundaries that deviate from the tilt configuration (inclined grain boundaries) limit supercurrent transport properties is not clear. However, when accompanied with structural disorder, it is expected that the current flow will also be impeded.

Considering the vast variations of the boundary microstructure along the length of a single boundary we conclude that the local structural and chemical variations control the local transport properties across the boundary and result in the current variations along the boundary. Since the total critical current for a junction (in zero field for example) is dependent on the sum of the local $J(x)$ contributions, it is clear that to maximize the current density of the junction $J_{c,max}$, the local critical currents must be uniform and at there highest possible values. Obviously, this is not the case for a typical grain boundary junction. Thus, the great range of critical currents that have been reported in the literature for junctions of the same macroscopic grain boundary geometry can be explained on the basis of differences in the current variations along the grain boundary.

XII.3 45° Asymmetric Tilt Grain Boundary Junctions

In contrast to 24° tilt boundaries, 45° tilt boundaries have been shown to have

highly unusual $I_c(B)$ patterns where the maximum current is not necessarily at $B = 0$.

These $I_c(B)$ patterns can be explained in terms of current reversals that occur along the

length of the boundary and where shown in chapter X.

The non-uniform current distributions are believed to be caused by similar

structural and stoichiometric considerations as in 24° tilt boundaries, however, the current

reversals (circular currents) and self generated flux are unique to 45° boundaries. As

with 24° boundaries, the length of the grain boundary is dominated by meandering (see

figure 12.5). The boundary meandering is accommodated by a staircase structure of

(100)(110) facets that form along the length of the junction (see figure 12.6). The local

current along 45° (and 24°) grain boundary junctions can theoretically vary at the same

length scale of the facets (hundreds of nanometers) due to variations in the carrier

concentration along sections of the boundary. The current reversals are believed to be

caused by a phase shift that is generated by a reversal in symmetry of the d-wave order

parameter interaction across the boundary plane (see chapter IV). It has been proposed

for 45° grain boundary junction dominated by the d-wave symmetry of the order

parameter that the (100)(110) facets act as a series of "0" and "π" junctions where each

facet of the boundary can experience a phase shift of π relative to the adjacent facet. A

consequence of this configuration is that adjacent facets can have critical currents flowing

in the opposite direction of the applied current bias even at zero applied field (H = 0). These locally negative currents are responsible for the suppressed critical currents and the spontaneously generated flux at zero applied magnetic field.

It is believed that changes in the facet geometry that result in a reversal of symmetry of the order parameter manifest as a "π" phase shift and thus are responsible for the areas along the boundary with locally negative currents. The boundary schematic in figure 12.6 starting from the left side shows a series of long (110)(100) type facets separated by small 45° steps along (100)(110) type planes. At location (A) in figure 12.6, the orientation of the long straight facets change from (110)(100) to (100)(110). This reversal at location (A) is the type of reversal believed to be responsible for a "π" phase shift that can results in the reversal of the current direction at point (A). Consequently, not all adjacent (100)(110) type facets have a "π" phase shift associated with the interaction of the order parameter across the grain boundary plane, rather only those changes in boundary orientation that result in the reversal of symmetry of the long facets such as at location (A) in figure 12.6.

The local current distributions of the 45° grain boundaries from chapter X demonstrate the variability from one junction to another fabricated under identical processing parameters. The phase retrieval method is capable of determining on the submicron length scale variations of J(x) along the boundary as well as the location of self generated flux cores at current reversal centers. Scanning SQUID microscopy
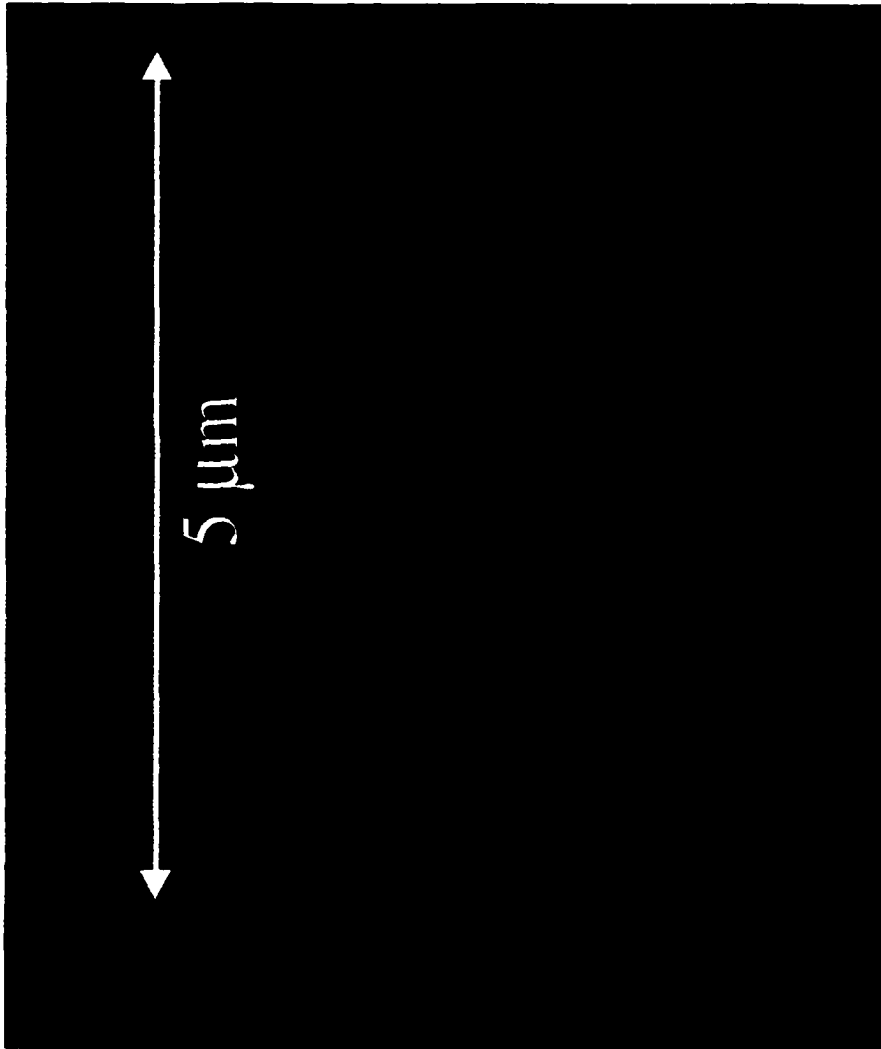
Figure 12.5 SEM micrograph of a 45 tilt grain boundary showing the boundary meandering along the length of the boundary.
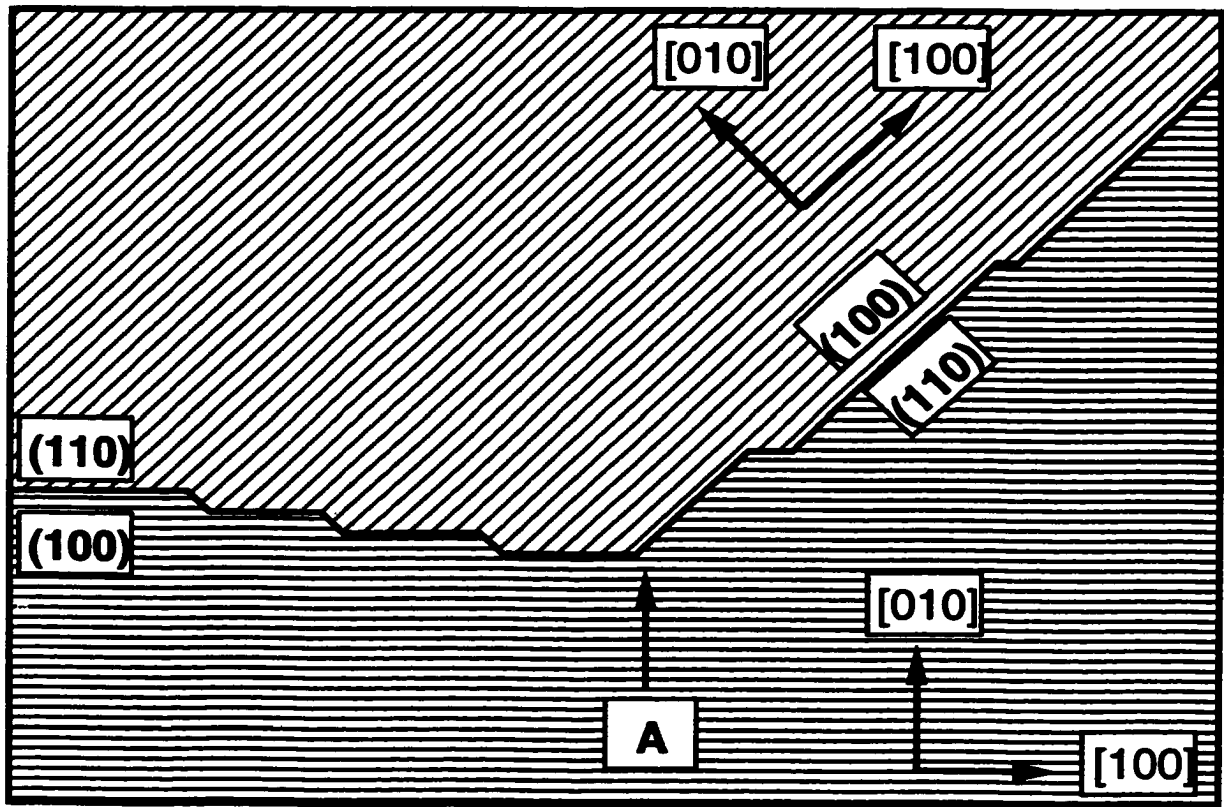
Figure 12.6 Schematic of the (100)(110) staircase facet geometry of 45 grain boundary junctions. The reversal of symmetry center is located at A and is believed to be the current reversal center as well.

studies have been able to locate and confirm the presence of these self generated flux fields for long 45° grain boundary Josephson junctions.

Theoretical predictions based on geometric arguments for 45° grain boundaries suggest that the locally alternating current between positive and negative should vary at the same length scale as the facets. Therefore, for a typical 2 μm wide junction, there should exist approximately 2-10 vortices of self- generated flux due to current reversals. The nature, size and distribution of these vortices for large junctions have been considered, but it is not clear as to the nature or distribution for the narrow junction limit. The phase retrieval method thus far has the greatest potential for mapping the small-scale (submicron) distribution of these currents and self generated flux.

XII.4 Interface Engineered Ramp-Edge Junctions

Compared to both 24° and 45° grain boundary junctions, the current distributions for the interface engineered junctions appear to be highly uniform along the length of the boundary. High resolution electron microscope investigations of the barrier layer by Huang has shown that a very uniform layer along the boundary is formed during junction fabrication (Huang *et al.* 1999). Figure is a HREM cross-section of the barrier region of an interface engineered junction. The boundary region is free of pinholes, second phases and significant strain fields. This is consistent with the uniform current distributions found across the boundaries. Although YBCO is known to be a d-wave superconductor,

the YBCO electrodes from each side of the junction share the same epitaxial orientation relative to the substrate and thus have no misorientation between the a-b planes from each side of the barrier. The alignment of the a-b planes across the boundary layer is evident in figure 12.7 and minimizes any d-wave contributions, therefore the current distributions are expected to be highly uniform and free of current reversals which is what was found in chapter XI.

The direct correlation between a uniform barrier layer and a uniform current distribution highlights the important relationship between the two and thus underscores the notion that future improvements in the transport behavior of all high-T_c Josephson junctions must be sought by controlling the quality of the interface region.
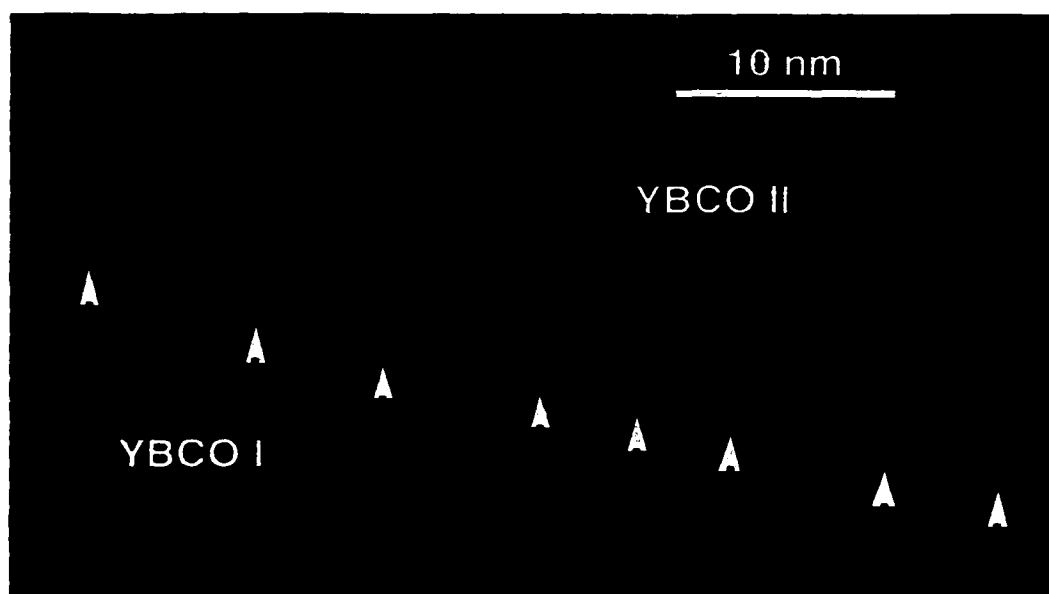
Figure 12.7 HREM cross-section image of the barrier layer of an interface engineered ramp-edge junction. The barrier layer is (2-3 nm), continuous and free of pinholes. (Image courtesy of Y. Huang)(Huang *et al.* 1999)

XII. Conclusions and Future Work

The major result of this work is the development of a novel technique for determining the local current distribution along the length of the boundary in a Josephson junction. The technique was used to map and understand the local current variations along both grain boundary and ramp-edge YBCO Josephson junctions at the sub-micron length scale. The technique developed for determining the local current $J(x)$ along the length of the boundary is a phase retrieval technique that exploits the Fourier relationship between the experimentally measurable critical current as a function of an applied field $I_c(B)$ and the local current distribution $J(x)$. The critical current was measured as a function of an applied magnetic field at cryogenic temperatures and the data was used in concert with the phase retrieval algorithm to determine the local current distributions. The current distribution is a 1-D distribution and therefore the phase problem is also a 1-D problem. The 1-D phase problem is usually non-unique and often has many different mathematically correct solutions. Boundary constraints are used to greatly reduce the number of possible solutions and a search algorithm is used to search solutions space for all possible solutions that fit the known boundary constraints. A focused ion beam (FIB) was used to damage an area along the boundary to add an additional constraint and force the algorithm to converge to a unique solution. A numerical technique was used to calculate the enhanced magnetic field at the boundary that results from demagnetization and flux focusing of the field at the boundary plane.

242

The current distribution for symmetric, [001] oriented, 24° tilt grain boundaries were found to be highly non-uniform. Most of the boundaries can be characterized as being composed of a few regions along the boundary that carry most of the current separated by areas along the boundary that carry little or no current. The phase retrieval algorithm was able to find a small number of possible solutions for each boundary and in some cases only one solution was found. When a junction had multiple solutions the individual solutions were often physically similar such that they represented the same current distribution along the boundary. Current distributions determined from measurements at multiple temperatures show good agreement with one another.

The current distributions $J(x)$ for asymmetric, [001] oriented, 45° tilt grain boundaries were found to be highly non-uniform. The uniformity of the 45° junctions were similar to the 24° junctions where most of the current was carried along a few regions separated by areas along the boundary that carry little or no current. For the 45° boundaries, the constraint that the local current be positive was relaxed to allow for locally negative currents that result from the d-wave symmetry of the order parameter. The local current distributions with the best FOM were found to be those that have locally negative currents along the length of the boundary. It is argued that the current reversals take place along the boundary where the (100)(110) facet symmetry of the grain boundary plane reverses. The locally negative currents may also be thought of as circular currents that must generate a magnetic field at the core of the field reversal. The local current distributions determined for 45° boundaries suggest there are approximately 2-10

current reversal (flux centers) for a 2 μm wide junction. These results are consistent with the scanning SQUID measurements of 45° boundaries performed by Mannhart *et al.* where the self generated flux along a boundary was measured (Mannhart *et al.* 1996).

Critical current vs. an applied magnetic field $I_c(B)$ measurements were used to determine the local current distribution $J(x)$ along ramp-edge interface engineered junctions. The current distributions for the ramp-edge junctions were found to be highly uniform along the length of the junction. This is in stark contrast to grain boundary junctions that showed large variations in the local current. The uniformity of the ramp-edge junctions were confirmed by performing measurements at multiple temperatures along a single device.

The variation of the current along the length of the boundary in both grain boundary and ramp-edge Josephson junctions can be explained in terms of microstructural features and stoichiometric variations along the length of each boundary. The variation of the oxygen content along the length of the boundary was shown in chapter III to play a dominant role in controlling the local current variation. These studies of the oxygen variation have shown that the oxygen content can vary in a manner similar to the superconducting segments found in the local current distributions for grain boundary junctions in this study.

The microstructure of grain boundary junctions discussed in chapter III varies significantly along the length of the junction. The length of the boundary is dominated by large scale boundary meandering and faceting. Most boundaries typically meander on the length scale of several hundreds of nanometers. The local microstructure along the boundary is dominated by facets that tend to form along low index planes such as the (110) and the (100) planes. This variation of the microstructure at the nanometer length scale suggest variations in the local current at similar length scales and is consistent with the local current distributions determined during this study.

The current distributions for 45° grain boundary junctions shows the unique property of current reversals along the length of the boundary. These current reversals are believed to be caused by the unique interaction of the order parameter when the local microstructure is dominated by (100)(110) type facets. At locations along the boundary where the facet symmetry reverses it is possible for the current direction to reverse. These reversals were mapped for the first time by this study.

The microstructure across ramp-edge junctions was found to be highly uniform along the length of the boundary. There is no orientation difference between the YBCO on one side of the barrier and the YBCO on the other side of the barrier. Consequently, the d-wave symmetry of the order parameter should have little control on the local current distributions. The ramp-edge junction should behave as if it were an s-wave

superconductor because of the lack of an orientation difference across the barrier layer. The highly uniform current distributions found during this study support this belief.

This project has contributed significantly to the understanding of the local current variation along the length of single Josephson junctions and how that current variation can control the total quality and reproducibility of a junction. Along the way new questions about the fundamental understanding of grain boundary Josephson junctions have surfaced and will be presented as possible future work.

None of the existing grain boundary transport models directly consider the variation of the local current. Many make assumptions about the local current distribution based on microstructural or chemical variations along the boundary plane, or based on high magnetic field measurements, but none directly use information about the local current distribution. Consequently, these models can only describe the basic behavior of grain boundary junctions with a limited degree of success. This thesis has shown that the local current can vary significantly from junction to junction (fabricated under identical processing parameters), therefore, the local current distribution must be used when interpreting chemical or microstructural data from an individual boundary.

This thesis has shown that there is significantly different transport behavior between 24° and 45° grain boundary junctions. The local current is always positive at

24° tilt angles, while the local current can be negative at the tilt angle of 45°. It has been argued that the current reversals are due to the d-wave symmetry of the order parameter and the node-lobe alignment across the boundary plane that exists along the (100)(110) asymmetric facets found in 45° tilt boundaries. It is presently not known if these current reversals occur at tilt angles less than 45°. If the current reversals do exist at lower tilt angles, at what tilt angle between 24° and 45° does the transition occur? It would be interesting to study the local current variation and the corresponding microstructure and oxygen stoichiometry as a function of tilt angle (at tilt angles near 45°) to determine at what tilt angle the transition occurs.

It has been previously argued that variations in the local oxygen content can dominate the transport process along the length of a grain boundary. Several transport models discussed in chapter III use the oxygen variation as a basis for the variability of the local current. Using the phase retrieval approach, it is possible to directly map the local current variation as a function of temperature $J(x,T)$ from near 0 K to T_c. By mapping the current variations as a function of temperature it would be possible to distinguish regions along the boundary that have locally different T_c values than the bulk. These local variations of T_c could then be directly correlated to carrier concentration measurements (such as PEELS measurements) performed on the same samples as used for transport measurements.

The limiting factor prohibiting a direct correlation between local current and local microstructure and chemistry variations is the resolution of the phase retrieval technique. The resolution of the phase retrieval technique is controlled by the strength of the applied magnetic field used in the measurements. The real space spacing is an inverse relation with the applied magnetic field. Theoretically, by increasing the magnetic field to higher and higher fields would result in a finer real space resolution. Unfortunately, two practical considerations prohibit infinitely small resolution of the phase retrieval technique; the lower critical field H_{c1} and flux focusing. The lower critical field ($\sim$ 200 G for YBCO) is the highest field that can be applied to the boundary before the field starts to penetrate non-uniformly throughout the sample in the form of vortices. Fortunately, the H_{c1} value for YBCO still theoretically allows for sub-nanometer length scale resolution of the local current distribution $J(x)$. Therefore, the limiting factor for resolution control is flux focusing. Chapter VII details the method used to numerically correct the applied magnetic field values because of demagnetization and flux focusing issues. This technique requires a geometry factor that is dependent on the shape of the photolithographically patterned microbridge. Using a rectangular geometry as used during this thesis, the numerical technique used to correct for demagnetization and flux focusing limited the resolution to approximately 0.1 μm ultimate resolution. By using a circular disk bridge geometry similar to the one proposed by Rosenthal et al. and discussed in chapter VII would allow for an exact analytic correction for demagnetization and flux focusing and greatly improve the resolution of the local current distribution $J(x)$. With an improved resolution, direct correlation of $J(x)$

with local microstructure and local chemistry may be possible. The direct correlation

would result in a microstructure based transport model that accurately depicted the

behavior of high-T_c Josephson junctions that may result in improved device fabrication

and performance.

References

Abrikosov, A. A. "On the magnetic properties of superconductor of the second group." Soviet Physics JETP 5 (1956): 1174-1182.

Abrikosov, A. A. "Tunneling conductance of the S-N layered model of HTSC." Physica C 201 (1992): 413-420.

Akimitsu, J., M. Uehara, et al. "Superconductivity in the new compound (Y1-xCax)0.95Sr2.05Cu2.4(CO3)0.6Oy." Physica C 201 (1992): 320-324.

Akoh, H., H. Sato, et al. "Scaling behavior of YBACuO/PrBaCuO/YBaCuO trilayer Josephson junctions." Japanese Journal of Applied Physics Part 2 33 (1994): L766-L768.

Akoh, H., H. Sato, et al. "Anomalous temperature dependence of critical current in YBaCuO/PrBaCuO/YBaCuO trilayer Josephson junctions." IEEE Transactions on Applied Superconductivity (1995):

Alarco, J. A., E. Olsson, et al. "Microstructure of an artificial grain boundary weak link in an YBa2Cu3O7-d thin film grown on a (100)(110), [001]-tilt Y-ZrO2 bicrystal." Ultramicroscopy 51 (1993): 239-246.

Alff, L., G. M. Fischer, et al. "Dry-etching processes for high-temperature superconductors." Physica C 200 (1992): 277-286.

Alff, L., B. Mayer, et al. "Magnetic field effect three terminal device based on YBCO grain boundary junctions." Journal of Applied Physics 75 (1994): 1843-1845.

Ambegaokar, V. and A. Baratoff "Tunneling between superconductors." Physical Review Letters 10 (1963): 486-489.

Ambegaokar, V. and B. I. Halperin "Voltage due to thermal noise in the dc Josephson effect." Physical Review Letters 22 (1969): 1364-1366.

Anderson, P. W. "Theory of flux creep in hard superconductors." Physical Review Letters 9 (1962): 309-311.

Anderson, P. W. "Theories on High-Temperature Superconductivity." International Journal of Modern Physica B 4 (1990): 181-200.

Anderson, P. W. and Y. B. Kim "Theory of motion of Abrikosov flux lines." Reviews of Modern Physics (1964): 40-43.

250

Anderson, P. W. and R. Schrieffer "A dialogue on the theory of high Tc." Physics Today 44 (1991): 55-61.

Antognazza, L., S. J. Berkowitz, et al. "Proximity effect in YBCO/YBCCoO/YBCO junctions: From the clean limit to the dirty limit with pair breaking" Physical Review B 51 (1995): 8560-8563.

Antognazza, L., K. Char, et al. "Conductance-voltage characteristics of interfaces between YBCO and metallic oxides." Applied Physics Letters 68 (1996): 1009-1011.

Antognazza, L. K. Char, et al. "Josephson coupling of YBCO through a ferromagnetic barrier SrRuO3." Applied Physics Letters 63 (1993): 1005-1007.

Antognazza, L., B. H. Moeckly, et al. "Properties of high-Tc Josephson junctions with YCaBCO barrier layers." Physical Review B 52 (1995): 4559-4567.

Antonik, M. D. and R. J. Lad "Faceting, reconstruction and defect microstructure at ceramic surfaces revealed by atomic foce microscopy." Journal of Vacuum Science Technology A 10 (1992): 669-673.

Babcock, S.E., X.Y. Cai, et al. "A TEM-EELS study of hole concentration near strongly and weakly coupled grain boundaries in electromagnetically characterized YBCO bicrystals." Physica C 227 (1994): 183-196.

Babcock, S.E. and D.C. Larbalestier "Evidence for local composition variation within YBCO grain boundaries." Applied Physics Letters 55 (1989): 393-395.

Babcock, S.E., Na Zhang, et al. "Microstructure and composition of electromagnetically characterized YBCO grain boundaries." Journal of Advanced Science (1991).

Balogg, B. "Physical properties of high-Tc superconductors." Physics Today (1991): 44-50.

Bardeen, J., L. N. Cooper, et al. "Theory of Superconductivity." Physical Review 108 (1957): 1175.

Barner, J.B., C.T. Rogers, et al. "All a-axis oriented YBCO-PRBCO-YBCO Josephson devices operating at 80 K." Applied Physics Letters 59 (1991): 742-744.

Barnett, S. A., C.-H. Choi, et al. "Ion-assisted deposition of thin films."

Barone, A. Physics and Applications of the Josephson Effect, Wiley, (1982).

Barron, E.M. and P.T. Gough "One-dimensional image reconstruction from noisy differential Fourier phase." Inverse Problems 2 (1986): 363-374.

Batson, P. E. "Simultaneous STEM imaging and electron energy-loss spectroscopy with atomic-column sensitivity." Nature 366 (1993): 727-728.

Batson, P. E. and M. F. Chisholm "Preliminary study of electron-energy-loss spectra of YBa2Cu3O7-∂." J. Elec. Micr. Tech. 8 (1988): 311-315.

Bean, C. P. "Magnetization of hard superconductors." Physical Review Letters 8 (1962): 250-253.

Bean, C. P. "Magnetization of high-field superconductors." Reviews of Modern Physics (1964): 31-39.

Beck, A., A. Stenzel, et al. "Fabrication and superconducting transport properties of bicrystal grain boundary Josephson junctions on different substrates." IEEE Transactions on Applied Superconductivity 5 (1995): 2191-2195.

Bednorz, J. G. and K. A. Müller "Possible high Tc superconductivity in the Ba-La-Cu-O system." Z. Phys. B 64 (1986): 189-193.

Bell, A. M. T. "Calculated x-ray powder diffraction patterns and theoretcial densities for phases encountered in investigations of Y-Ba-Cu-O superconductors." (1990): 55-61.

Benz, S. P., C. D. Reintsema, et al. "Step-edge and stacked-heterostructure high-Tc Josephson junctions for voltage-standard arrays." IEEE Transactions on Applied Superconductivity (1995):

Bhattacharya, S., X. X. Xi, et al. "Optical response of an ultrathin film and a large-angle grain boundary in superconducting YBa2Cu3O7-d." Applied Physics Letters 62 (1993): 3510-3512.

Blank, H.A. and Horst Rogalla "The effect of ion milling on the morphology of ramp-type Josephson junctions." Journal of Materials Research 12 (1997): 2952-2957.

Blank, D. H. A., F. J. G. Roesthuis, et al. (1994). "High quality YBaCuO on NGO, using a CeO2 template layer." Workshop on HTS Josephson Junctions and 3-Terminal Devices, University of Twente, The Netherlands,

Blonder, G. E., M. Tinkham, et al. "Transition from metallic to tunneling regimes in superconducting microconstrictions: Excess current, charge imbalance, and supercurrent conversion." Physical Review B 25 (1982): 4515-4532.

Blue, C. T., C. A. Blue, et al. "Comparison of transport and magnetization critical currents in c-axis-oriented YBa2Cu3O7-d thin films." Journal of Applied Physics 72 (1992): 1021-1029.

Bollmann, W. (1970). *Crystal Defects and Crystalline Interfaces, chapter 12*. Berlin: Springer-Verlag.

Bonnell, D. A. and I. Solomon "Measurement of space charge adjacent to oxide grain boundaries by tunneling spectroscopy." Ultramicroscopy 42-44 (1992): 788-792.

Bosch, J., R. Gross, et al. "Measurement of the spatial distribution of the maximum Josephson current in superconducting tunnel junctions." Journal of Low Temperature Physics 68 (1987): 245-268.

Bourgault, D., P. de Rango, et al. "Magnetically melt textured YBa2Cu3O7-d disagreement between Jc determined by magnetic and direct transport measurements." Physica C 194 (1992): 171-176.

Brames, B.J. "Unique phase retrieval with explicit support information." Optics Letters 11 (1986): 61-63.

Brames, B.J. "Testing for support irreducibility." Journal Optical Society of America A 4 (1987): 135-147.

Brandt, E.H. "Thin superconductors in a perpendicular magnetic ac field: General formulation and strip geometry." Physical Review B 49 (1994): 9024-9039.

Brown, L. M. "The ultimate analysis." Nature 366 (1993): 721.

Browning, N. D., M. F. Chisholm, et al. "Cell-by-cell mapping of carrier concentrations in high-temperature superconductors." Interface Science 1 (1993): 309-320.

Browning, N. D., J. Yuan, et al. "Determination of the local oxygen stoichiometry in YBa2Cu3O7-d by electron energy loss spectroscopy in the scanning transmission electron microscope." Physica C 202 (1992): 12-18.

Bruder, C. A. van Otterlo, et al. "Tunnel junctions of unconventional superconductors." Physical Review B 51 (1995): 12904-12907.

Bryntse, I. and S. N. Putilin "Electron microscopy studies of the mercury-based superconductor." Physica C 212 (1993): 223-227.

Buchholz, D. B., S. J. Duray, et al. "Surface morphology studies of Y-Ba-Cu-oxide thin films prepared by pulsed organometallic beam epitaxy." Materials Chemistry and Physics 36 (1994): 377-382.

Buckett, M. I. and K. L. Merkle "Determination of grain boundary volume expansion by HREM." Ultramicroscopy 56 (1994): 71-78.

Cai, X. Y., K. Usami, et al. "Fabrication and properties of YBCO tunnel junction by ion beam sputtering." IEEE Transactions on Applied Superconductivity (1995):

Cao, W. and L. E. Cross "Theory of tetragonal twin structures in ferroelectric perovskites with a first-order phase transition." Physical Review B 44 (1991): 5-12.

Cardona, A. H., H. Suzuki, et al. "Transport characteristics of Tl2Ba2CaCu2O8 bicrystal grain boundary junctions at 77 K." Applied Physics Letters 62 (1993): 411-413.

Carmody, M., E. Landree, et al. "Determination of the current density distribution in Josephson junctions." Physica C 315 (1999): 145-153.

Carmody, M., K.L. Merkle, et al. "The relation between barrier structure and current uniformity in YBCO Josephson junctions." Interface Science 8 (2000): 231-242.

Carmody, M., B.H. Moeckly, et al. "Spatial variation of the current in grain boundary Josephson junctions." Journal of Applied Physics 87 (2000): 2454-2459.

Carter, C. B. and S. L. Sass "Electron diffraction and microscopy techniques for studying grain-boundary structure." Journal of American Ceramics Society 64 (1991): 335-345.

Carter, C. B. and L. A. Tietz (1989). "Interfaces in high-Tc superconducting oxides." Meeting of the Electron Microscopy Society of America, San Francisco Press, Inc.

Catana, A., J. G. Bednorz, et al. "Surface outgrowths on sputtered YBa2Cu3O7-x films: A combined atomic force microscopy and transmission electron microscopy study." Applied Physics Letters 63 (1993): 553-555.

Cava, R. J., B. Batlogg, et al. "Superconductivity near 30K without copper: the Ba0.6K0.4BiO3 perovskite." Nature 332 (1988): 814-817.

Cava, R. J., B. Batlogg, et al. "Bulk superconductivity at 91 K in single-phase oxygen-deficient perovskite Ba2YCu3O9-d." Physical Review Letters 58 (1987): 1676-1679.

Cava, R. J., A. W. Hewat, et al. "Structural anomalies, oxygen ordering and superconductivity in oxygen deficient Ba2YCu3Ox." Physica C 165 (1990): 419-433.

Chan, S.-W. "Nature of grain boundaries as related to critical currents in superconducting YBa2Cu3O7-x." (1994):

Chan, S.-W., E.W. Chase, et al. "Superconducting YBCO thin films on alkaline earth fluorides." Applied Physics Letters 54 (1989):2032-2034.

Chan, S.-W., D. M. Hwang, et al. (1990). "Study of Y-Ba-Cu-O Thin Films Grown on Single Crystal SrTiO3: Not all High Angle Grain Boundaries Destroy Jc." AIP Conference Proceedings 200, High Tc Superconducting Thin Films, American Institute of Physics.

Chan, S. W., D. M. Hwang, et al. "Microstructure of YBa2Cu3O7-x thin films grown on single crystal SrTiO3." Journal of Applied Physics (1989):

Chang, C. C., X. D. Wu, et al. "Origin of surface roughness for c-axis oriented Y-Ba-Cu-O superconducting films." Applied Physics Letters 57 (1990): 1814-1816.

Chapman, B. Glow Discharge Processes, New York: John Wiley & Sons (1980).

Char, K., "Crystal interface Engineering in high Tc Oxides." MRS Bulletin Sept. (1994): 51-55.

Char, K., "HTS SNS Josephson junctions: interface and mechanisms." Physica C 282-287 (1997): 419-422.

Char, K., L. Antognazza, et al. "Study of interface resistances in epitaxial YBa2Cu3O7-x/barrier/YBa2Cu3O7-x junctions." Applied Physics Letters 63 (1993):2420-2422.

Char, K., L. Antognazza, et al. "Properties of YBCO/YBC2.79O/YBCO edge junctions." Applied Physics Letters 65 (1994): 904-906.

Char, K., M. S. Colclough, et al. "Bi-epitaxial grain boundary junctions in YBa2Cu3O7." Appl. Phys. Lett. 59 (1991): 733-735.

Char, K., M. S. Colclough, et al. "Extension of the bi-epitaxial Josephson junction process to various substrates." Applied Physics Letters 59 (1991): 2177-2179.

Char, K., M. S. Colclough, et al. "High Tc superconductor-normal-superconductor Josephson junctions using CaRuO3 as the metallic barrier." Applied Physics Letters 62 (1993): 196-198.

Char, K., N. Newman, et al. "Microwave surface resistance of epitaxial YBa2Cu3O7 thin films on sapphire." Applied Physics Letters 57 (1990): 409-411.

Chaudhari, P. "Critical Currents, Grain Boundaries and Squids in the High Temperature Cuprate Superconductors." Physica C 185-189 (1991): 292-296.

Chaudhari, P. (1991). "Some implications of a short coherence length in high-temperature superconductors." The Toshiba International School of Superconductivity, Kyoto, Japan, Springer-Verlag.

Chaudhari, P., D. Dimos, et al. "Critical current measurements in single crystals and single grain boundaries in YBCO films." IBM Journal of Research and Development 33 (1989): 299-306.

Chaudhari, P., R. H. Koch, et al. "Critical-current measurements in epitaxial films of YBa2Cu3O7-x compound." Physical Review Letters 58 (1987): 2684-2686.

Chaudhari, P., J. Mannhart, et al. "Direct Measurement of the Superconducting Properties of Single Grain Boundaries in YBa2,CuO." Physical Review Letters 60 (1988): 1653-1656.

Chen, P.T., M.A. Fiddy et al. "Blind deconvolution and phase retrieval from point zeros." Journal Optical Society of America A 13 (1996): 1524-1531.

Chen, P.T. and M.A. Fiddy "Image reconstruction from power spectral data with use of point-zero locations." Journal Optical Society of America A 11 (1994): 2210-2214.

Chen, C. T., F. Sette, et al. "Electronic states in La2-xSrxCuO4+d probed by soft x-ray absorption." Physical Review Letters 66 (1991): 104-107.

Chen, C. T., L. H. Tjeng, et al. "Out-of plane orbital characters of intrinsic and doped holes in La2-xSrxCuO4." Physical Review Letters 68 (1992): 2543-2546.

Chen, F. R. and A. H. King "Large-angle grain-boundary structures in hexagonal close-packed metals." Philosophical Magazine A 57 (1988): 431-455.

Chen, J., T. Yamashita, et al. "YBCO artificial grain boundary junctions on Si." IEEE Transactions on Applied Superconductivity 3 (1993): 2333-2336.

Chen, J., T. Yamashita, et al. "YBCO angle grain boundary junction on Si." preprint (1992):

Chern, C. S., J. Zhao, et al. "In situ growth of YBa2Cu3O7-x high Tc superconducting thin films directly on sapphire by plasma-enhanced metalorganic chemical vapor deposition." Applied Physics Letters 57 (1990): 721-723.

Chew, N. G., J. A. Edwards, et al. "Effect of composition and oxygen content on the microwave properties of evaporated Y-Ba-Cu-O thin films." IEEE Transactions on Applied Superconductivity (1995):

Chew, N. G., S. W. Goodyear, et al. "Orientation control of YBa2Cu3O7 thin films on MgO for epitaxial junctions." Applied Physics Letters 60 (1992): 1516-1518.

Chiang, Y., J. A. S. Ikeda, et al. "Grain boundary segregation and critical current density in YBa2Cu3O7-x superconductors." In Ceramic Superconductors edited by M. F. Yan. Westerville, OH: The American Ceramic Society, (1988).

Chin, D.K. and T. Van Duzer "Novel all-high Tc epitaxial Josephson junctions." Applied Physics Letters 58 (1991): 753-755.

Chisholm, M. F. and S. J. Pennycook "Structural origin of reduced critical currents of YBa2Cu3O7-d grain boundaries." Nature 351 (1991): 47-49.

Chisholm, M. F., S. J. Pennycook, et al. "Atomic structure of grain boundaries in YBa2Cu3O7-x as observed by Z-contrast imaging." Interface Science 1 (1993): 339-346.

Chisholm, M. F. and D. A. Smith "Low-angle tilt grain boundaries in YBa2Cu3O7 superconductors." Phil. Mag. A 59 (1989): 181-197.

Cho, C., J. Shin, et al. "Microwave response of YBa2Cu3O7-x grain boundary junction." Journal of Applied Physics 77 (1995): 2193-2195.

Chu, C. W., P. H. Hor, et al. "Evidence for superconductivity above 40 K in the La-Ba-Cu-O compound system." Physical Review Letters 58 (1987): 405-407.

Clarke, D. R., T. M. Shaw, et al. "Issues in the processing of cuprate ceramic superconductors." Journal of the American Ceramics Society 72 (1989): 1103-1113.

Clarke, J., S. M. Freake, et al. "A new experimental technique for determining the BCS interaction parameter in normal metals." Solid State Communications 11 (1972): 689-693.

Clemens, B. M., C. W. Nieh, et al. "Nucleation and growth of YBaCuO on SrTiO3." Applied Physics Letters 53 (1988): 1871-1873.

Combettes, P.L. Advanced Imaging Electron Physics 95 (1996): 155.

Copetti, C.A., F. Ruders, et al. "Electrical properties of 45 degree grain boundaries of epitaxial YBACuO, dominated by crystalline microstructure and d-wave-symmetry" , Physica C 253, (1995): 63-75.

Cooper, L. N. "Bound electron pairs in a degenerate Fermi gas." Physical Review 104 (1956): 1189-1190.

Crimmins, T.R. "Phase retrieval for discrete functions with support constraints." Journal Optical Society of America A 4 (1987): 124-134.

Crimmins, T.R. and J.R. Fienup "Ambiguity of phase retrieval for functions with disconnected support." Journal Optical Society of America Letters 72 (1981): 1026-1028.

Crimmins, T.R. and J.R. Fienup "Uniqueness of phase retrieval for functions with sufficiently disconnected support." Journal Optical Society of America 73 (1983): 218-221.

Cronemeyer, D.C. "Demagnetization factors for general ellipsoids." Journal of Applied Physics 70 (1991): 2911-2914.

Dainty, J.C. and M.A. Fiddy "The essential role of prior knowledge in phase retrieval." Optica Acta 31 (1984): 325-330.

Daly, K. P., W. D. Dozier, et al. "Substrate step-edge YBa2Cu3O7 rf SQUIDs." Applied Physics Letters 58 (1991): 543-545.

Daly, K. P., W. D. Dozier, et al. "Substrate step-edge YBaCuO rf SQUIDs." Applied Physics Letters 58 (1991): 543-545.

Daumling, M., E. Sarnelli, et al. "Critical current of a high-Tc Josephson grain boundary junction in high magnetic field." Applied Physics Letters 61 (1992): 1355-1357.

Davidson, A. and N. F. Pederson "Discrete models of Abrikosov vortex flow transistors." IEEE Transactions on Applied Superconductivity (1995):

Dayem, A. H. and J. J. Wiegand "Behavior of thin-film superconducting bridges in a microwave field." Physical Review 155 (1967): 419-428.

de Bruyn Outboter, R. "Superconductivity: Discoveries During the Early Years of Low Temperature Research at Leiden, 1908-1914." IEEE Transactions on Magnetism MAG-23 (1987): 355-370.

de Lozanne, A. L., E. E. Ehrichs, et al. "Four-point resistance measurements of wires written with a scanning tunneling microscope." In Atomic and Nanoscale Modification of Materials edited by P. Avouris. Kluwer Academic Publisher, (1993).

Dean, K. A., D. B. Buchholz, et al. "YBaCuO on Mgo films grown by pulsed organometallic beam epitaxy for fabrication of grain boundary junctions." Journal of Materials Research (submitted):

DeGroot, D. C., Rudman, D. A., et al. "Planar microwave devices fabricated by ion-implantation patterning of high-temperature superconductors." Applied Physics letters 69 (1996): 2119-2121.

Den, T., T. Kobayashi, et al. "Superconductor with Tc up to 80 K in the compound (Ln, Ca)(Sr, Ba)2(C,Cu)Cu2O7-x." Physica C 208 (1993): 351-355.

Deutscher, G. and P. Chaudhari "Scaling behavior of the critical current of grain-boundary junctions." Physical Review B 44 (1991): 4664-4665.

Deutscher, G. and K. A. Müller "Origin of superconductive glassy state and extrinsic critical currents in high-Tc oxides." Physical Review Letters 59 (1987): 1745-1747.

Deutscher, G. and R. W. Simon "On the proximity effect between normal metals and cuprate superconductors." Journal of Applied Physics 69 (1991): 4137-4139.

DiIorio, M. S., S. Yoshizumi, et al. "Practical high Tc Josephson junctions and dc SQUIDs operating above 85K." Applied Physics Letters 58 (1991): 2552-2554.

Dimos, D., P. Chaudhari, et al. "Orientation dependence of grain boundary critical currents in YBCO bicrystals." Physical Review Letters 61 (1988): 219-221.

Dimos, D., P. Chaudhari, et al. "Superconducting transport properties of grain boundaries in YBa2Cu3O7 bicrystals." Phys. Rev. B 41 (1990): 4038-4049.

Dimos, D., P. Chaudhari, et al. "Orientation Dependence of Grain-Boundary Critical Currents in YBa2Cu3O7 Bicrystals." Phys. Rev. Lett. 61 (1988): 219-222.

Dinger, T. R., T. K. Worthington, et al. "Direct observation of electronic anisotropy in single-crystal YBa2Cu3O7-x." Physical Review Letters 58 (1987): 2687-2690.

Divin, Y. Y., J. Mygind, et al. "Josephson oscillations and noise temperatures in YBa2Cu3O7-x grain-boundary junctions." Applied Physics Letters 61 (1992): 3053-3055.

Divin, Y. Y., J. Mygind, et al. "Linewidth of Josephson oscillations in YBa2Cu3O7-x grain-boundary junctions." IEEE Transactions on Applied Superconductivity 3 (1993): 2337-2340.

Divin, Y.Y., F.Ya. Nad, et al. "Laser probing of high-Tc superconducting thin films." IEEE Transactions on Magnetics 27 (1991): 1101-1104.

Divin, Y.Y., H. Schulz, et al. "YBCO thin film Josephson junctions on 2x12 bicrystal (110) NdGaO3 substrates." Physica C 256 (1996): 149-155.

Divin, Y.Y., and P.M. Shadrin "Imaging of electrical inhomogeneities in YBCO thin-film structures by room temperature laser scanning microscopy." Physica C 232 (1994): 257-262.

Dolan, G. J., G. V. Chandrashekhar, et al. "Vortex structure in YBa2Cu3O7 and evidence for intrinsic pinning." Physical Review Letters 62 (1989): 827-830.

Dömel, Regina, C. Horstmann, et al. "Resonant tunneling transport across YBCO-SrRuO3 interfaces." Applied Physics Letters 67 (1995): 1775-1777.

Domenges, B., M. Herviewu, et al. "Ordered substitution of "CO3" groups for CuO4 square groups in the "123" structure." Physica C 207 (1993): 65-78.

Dong, S. Y. and H. S. Kwok "Observation of Jc oscillations in bitextured YBa2Cu3O7-d films." Physical Review B 48 (1993): 6488-6491.

Dravid, V. P., H. Zhang, et al. "Inhomogeneity of charge carrier concentration along the grain boundary plane in oxide superconductors." Physica C 213 (1993): 353-358.

Duray, S. J., D. B. Buchholz, et al. "Pulsed organometallic beam epitaxy of complex oxide films. Applied Physics Letters 59 (1991): 1503-1505.

Dutta, P. and P. M. Horn "Low-frequency fluctuations in solids: 1/f noise." Reviews of Modern Physics 53 (1981): 497-516.

Dynes, R.C. and T.A. Fulton "Supercurrent density distribution in Josephson junctions." Physical Review B 3 (1971): 3015-3023.

Early, E. A., A. F. Clark, et al. "Half-integral constant voltage steps in high-Tc grain boundary junctions." Applied Physics Letters 62 (1993): 3357-3359.

Early, E. A., R. L. Steiner, et al. "Evidence for parallel junctions within high-Tc grain-boundary junctions." Physical Review B 50 (1994): 9409-9418.

Edwards, H. L., J. T. Markert, et al. "Energy gap and surface structure of YBa2Cu3O7-x probed by scanning tunneling microscopy." Physical Review Letters 69 (1992): 2967-2970.

Edwards, J. A., J. S. Satchell, et al. "YBa2Cu3O7 thin-film step junctions on MgO substrates." Applied Physics Letters 60 (1992): 2433-2435.

Eibl, O., H. E. Hoenig, et al. "Extended defects in YBa2Cu3O7/PrBa2Cu3O7 superlattices deposited on (100) MgO single crystals." Physica C 172 (1990): 373-382.

Eibl, O. and B. Roas "Microstructure of YBa2Cu3O7-x thin films deposited by laser evaporation." Journal of Materials Research 5 (1990): 2620-2632.

Eibl, O., P. van Aken, et al. "EELS of YBa2Cu3O7-x in the TEM." Physica Status Solidi 128 (1991): 129-137.

Ekin, J. W. "Offset criterion for determining superconductor critical current." Applied Physics Letters 55 (1989): 905-907.

Ekin, J. W., A. I. Braginski, et al. "Evidence for weak link and anisotropy limitations on the transport critical current in bulk polycrystalline Y1Ba2Cu3Ox." Journal of Applied Physics 62 (1987): 4821-4828.

Ekin, J. W., H. R. J. Hart, et al. "Transport critical current of aligned polycrystalline Y1Ba2Cu3O7-∂ and evidence for a nonweak-linked component of intergranular current conduction." Journal of Applied Physics 68 (1990): 2285-2295.

Ekin, J. W., T. M. Larson, et al. "High Tc superconductor/noble-metal contacts with surface resistivities in the 10-10 ohm cm2 range." Applied Physics Letters 52 (1988): 1819-1821.

Ekin, J. W., A. J. Panson, et al. "Method for making low-resistivity contacts to high-Tc superconductors." Applied Physics Letters 52 (1988): 331-333.

Ekin, J. W., S. E. Russek, et al. "In situ noble metal YBa2Cu3O7 thin-film contacts." Applied Physics Letters 62 (1993): 369-371.

Eom, C. B., A. F. Marshall, et al. "Epitaxial and Smooth Films of a-axis YBaCuO." Science 249 (1990): 1549-1552.

Eom, C. B., A. F. Marshall, et al. "Absence of weak-link behaviour in YBa2Cu3O7 grains connected by 90 [010] twist boundaries." Nature 353 (1991): 544-547.

Eom, C. B., J. M. Phillips, et al. "Microstructure and transport properties of various 90° grain boundaries in YBa2Cu3O7 thin films." Interface Science 1 (1993): 267-286.

Faley, M. I., U. Poppe, et al. "Application of Josephson edge type junctions with a PrBa2Cu3O7 barrier prepared with Br-Ethanol etching or cleaning." IEEE Transactions on Applied Superconductivity (1995):

Faley, M. I., U. Poppe, et al. "Proximity effect in edge type junctions with PrBa2Cu3O7 barriers prepared by Br-ethanol etching." IEEE Transactions on Applied Superconductivity (1995):

Feng, Y., Y. E. High, et al. "Evidence for preferential formation of the (Bi,Pb)2Sr2Ca2Cu3Ox phase at the Ag interface in Ag-sheathed (Bi,Pb)2Sr2Ca2Cu3Ox tapes." Applied Physics Letters 62 (1993): 1553-1555.

Feng, Y. and D. C. Larbalestier "Texture relationships and interface structure in Ag-sheatherd Bi(Pb)-Sr-Ca-Cu-O superconducting tapes." Interface Science 1 (1993): 401-410.

Fernandes, A. A. R., I. N. Chan, et al. "Scaling of critical currents in high-temperature superconducting superlattices and thin films." Applied Physics Letters 61 (1992): 3181-3183.

Field, M. B., X. Y. Cai, et al. "Transport Properties Across Individual Grain Boundaries in Melt-Textured YBa2Cu3O6+x Bi-Crystals." preprint (1992):

Field, M. B., A. Pashitski, et al. "Experimental evidence for electromagnetic coupling inhomogeneity along the grain boundary plane in high angle melt-textured YBa2Cu3O6+x bicrystals." IEEE Transactions on Applied Superconductivity (1995):

Fienup, J.R. "Reconstruction of an object from the modulus of its Fourier transform." Optics Letters 3 (1978): 27-29.

Fienp, J.R. "Reconstruction of a complex-valued object from the modulus of its Fourier transform using a support constraint." Journal of the Optical Society of America A 4 (1987): 118-123.

Fienp, J.R. "Reconstruction of object having latent reference points." Journal of the Optical Society of America 73 (1983): 1421-1426.

Fienup, J.R. "Phase retrieval using boundary conditions." Journal Optical Society of America A 3 (1986): 284-288.

Fienup, J.R. and C.C. Wackerman "Phase-retrieveal stagnation problems and solutions." Journal Optical Society of America A 3 (1986): 1897-1907.

Fischer, G. M., B. Mayer, et al. "Spatially resolved observation of static magnetic flux states in YBa2Cu3O7-d grain boundary Josephson junctions." Science 263 (1994): 1112-1114.

Fjellvag, H., P. Karen, et al. "Carbonatization of YBa2Cu3O6+x." Acta Chemica Scandinavica A A42 (1988): 178-184.

Fleshler, S., W. K. Kwok, et al. "Anisotropy and Lorentz-force dependence of twin-boundary pinning and its effect on flux-lattice melting in single-crystal YBa2Cu3O7-d." Physical Review B 47 (1993): 14448-14461.

Fleshler, S., M. P. Maley, et al. "Transport properties of Tl2Ba2CaCu2O8 meander lines." IEEE Transactions on Applied Superconductivity (1995):

Flett, A., Y. He, et al. "An investigation of flux noise processes in biepitaxial YBCO junctions." LT20 (1994):

Foley, C. P., G. J. Sloggett, et al. "Josephson behaviour and flux penetration effects in YBCO double tilt-angle step-edge junctions." IEEE Transactions on Applied Superconductivity (1995):

Frenkel, A., C. C. Chang, et al. "SEM and electrical studies of current induced superconducting-resistive transitions in YBa2Cu3O7-x thin films." Journal of Materials Research 5 (1990): 691-703.

Frenkel, A., E. Clausen, et al. "Imaging of current-induced superconducting-resistive transitions by scanning electron microscopy in laser-deposited superconducting thin films of YBa2Cu3O7-x." Applied Physics Letters 55 (1989): 911-913.

Friedl, G., B. Roas, et al. "Transport properties of epitaxial YBa2Cu3Ox films at step edges." Applied Physics Letters 59 (1991): 2751-2753.

Froehlich, O. M., H. Schulze, et al. "Analysis of the critical current density in grain boundary Josephson junctions on a nanometer scale." Applied Physics Letters **66** (1995): 2289-2291.

Froehlich, O.M., H. Schulze, et al. "Sueprcurrent density correlation function of YBCO grain boundary Josephson junctions." IEEE Transactions on Applied Superconductivity **5** (1995): 2188-2191.

Fuke, H., H. Yoshino, et al. "Microstructure effects on Jc-B properties in YBCO thin films." M2S-HTSC-III (1991):

Fulton, T. A., L. N. Dunkleberger, et al. "Quantum interference properties of double Josephson junctions." Physical Review B **6** (1972): 855-875.

Gallagher, P. K., G. S. Grader, et al. "Some effects of CO2, CO and H2O upon the properties of Ba2YCu3O7." MRS Bulletin **23** (1988): 1491-1499.

Gao, J., Y. Buguslavskij, et al. "Characteristics of advanced YBa2Cu3Ox/PrBa2Cu3Ox/YBa2Cu3Ox edge type junctions." Applied Physics Letters **59** (1991): 2754-2756.

Gao, Y., G. Bai, et al. "Microstructure and defects in a-axis oriented YBa2Cu3O7-x thin films." Physica C **173** (1991): 487-500.

Gao, J., Yu. M. Boguslavskij, et al. "YBCO/PrBCO/YBCO Josephson ramp junctions" Journal of Applied Physics **72** (1992): 575583.

Gao, Y., K. L. Merkle, et al. "Structure and composition of grain boundary dislocation cores and stacking faults in MOCVD-grown YBa2Cu3O7-x thin films." Physica C **174** (1991): 1-10.

Gao, Y., K. L. Merkle, et al. "[001] tilt grain boundaries in YBa2Cu3O7-x thin films." Ultramicroscopy **37** (1991): 326-340.

Gao, J. and W. H. Wong "Formation of outgrowths at the initial growing stage of YBCO ultrathin films on ZrO2 substrates" Applied Physics Letters **67** (1995): 2232-2234.

Gao, Y., C.-T. Wu, et al. "TEM study of grain boundaries in Ag-clad Bi2Sr2CaCu2Ox tapes." Applied Superconductivity **1** (1993): 131-140.

Garrison, S. M., N. Newman, et al. "Observation of two in-plane epitaxial states in YBa2Cu3O7-x films on yttria-stabilized ZrO2." Applied Physics Letters **58** (1991): 2168-2170.

Gausepohl, S. C. and Mark Lee "Magnetoresistance probe of spatial current variations in high-Tc YBCO-SrRuO3-YBCO Josephson junctions." Applied Physical Letters 67 (1995): 1313-1315.

Gausepohl S. C., and Mark Lee "Supercurrent distributions and flux penetration in YBCO-YBCoCO-YBCO edge junctions." Journal of Applied Physics 82 (1997): 2427-2434.

Gavaler, J. R., J. Talvacchio, et al. "Effect of oxygen over-doping on Tc and Rs of YBCO films." IEEE Transactions on Applied Superconductivity (1995):

Gawalek, W., W. Michalke, et al. "Preparation of high-Tc Y-Ba-Cu-O and Bi-Sr-Ca-Cu-O thin films by RF magnetron sputtering." Phys. Stat. Sol. A 109 (1988): 503-509.

Gayle, F. W. and D. L. Kaiser "The nature of [001] tilt grain boundaries in YBa2Cu3O7-x." Journal of Materials Research 6 (1991): 908-915.

Gerchberg, R.W. Opt. Acta 21 (1974): 709.

Gerchberg, R.W. and W.O. Saxton Optik 35 (1975): 237.

Gerdemann, R., K.D. Husemann, et al. "Spatially resolved analysis of high-Tc grain boundary Josephson junctions and arrays." Journal of Applied Physics 76 (1994): 8005-8015.

Giaever, I. "Electron tunneling between two superconductors." Physical Review Letters 5 (1960): 464-466.

Giaever, I. "Energy gap in superconductors measured by electron tunneling." Physical Review Letters 5 (1960): 147-148.

Giess, E. A., R. L. Sandstrom, et al. "Lanthanide gallate perovskite-type substrates for epitaxial, high-Tc superconducting Ba2YCu3O7-x films." IBM Journal of Research Development 34 (1990): 916-925.

Gijs, M. A. M. and R. J. E. Jansen "Microwave response of YBaCuO thin-film Dayem bridges." Applied Physics Letters 56 (1990): 1484-1486.

Girard, J. C., Y. Samson, et al. "STM study of the nucleation and annealing of ion bombardment induced defects on Cu (100)." Surface Science 302 (1994): 73-80.

Gleiter, H. "On the structure of grain boundaries in metals." Materials Science and Engineering **52** (1982): 91-131.

Goldberg, D.E. *Genetics Algorithms in Search Optimization and Machine Learning*, Addison-Wesley, New York (1989).

Gonnelli, R. S., D. Puttero, et al. "The intrinsic determinants of the critical current in SIS' and SIS high-tc Josephson junctions." Applied Physics Letters **68** (1996): 2433-2435.

Goodenough, J. B. "Chemical and structural relationships in high-Tc materials." Supercond. Sci. Technol. **3** (1990): 26-37.

Goodrich, L. F. and S. L. Bray "High-Tc superconductors and critical current measurement." Cryogenics **30** (1990): 667-677.

Goodrich, L. F. and F. R. Fickett "Critical current measurements: a compendium of experimental results." Cryogenics (1982): 225-241.

Goodyear, S. W., N. G. Chew, et al. "Vertical c-axis microbridge junctions in YBa2Cu3O7/PrBa2Cu3O7 thin films." IEEE Transactions on Applied Superconductivity (1995):

Gough, C. E. (1991). "Flux Quantixation and Its Application to rf and dc SQUIDs." The Toshiba International School of Superconductivity, Kyoto, Japan, Springer-Verlag.

Granato, E., and D. Dominguez "Current-voltage characteristics of diluted Josephson junction arrays: Scaling behavior at current and percolation threshold." Physical Review B **56** (1997): 14671-14676.

Gray, K. E., D. H. Kim, et al. "High anisotropy and a dimensionality crossover in the irreversibility behavior of oxygen-deficient YBa2Cu3O7-y." Physical Review B **45** (1992): 10071-10074.

Greedan, J. E., A. H. O'Reilly, et al. "Oxygen ordering in the crystal structure of the 93-K superconductor YBa2Cu3O7 using powder neutron diffraction at 298 and 79.5 K." Phys. Rev. B **35** (1987): 8770-8773.

Greenaway, A.H. "Proposal for phase recovery from a single intensity distribution." Optics Letters **1** (1977): 10-12.

Greene, L.H., B.G. Bagley, et al. "Off-axis sputter deposition of YBCO thin films for microwave applications." Applied Physics Letters **59** (1991): 1629-1631.

Grimme, H. "Disorientations and coincidence rotations for cubic lattices." Acta Crystallographica A30 (1974): 685-688.

Gross, R. "Grain boundary Josephson junctions in the high temperature superconductors." In Interfaces in superconducting systems edited by S. L. Shinde and D. Rudman. New York: Springer Verlag, (1992).

Gross, R., P. Chaudhari, et al. "Thermally Activated Phase Slippage in High-Tc Grain Boundary Josephson Junctions." Phys. Rev. Lett. 64 (1990): 228-231.

Gross, R., P. Chaudhari, et al. "Scaling beharior in electrical transport across grain boundaries in YBa2Cu3O7-∂ superconductors." Phys. Rev. B 42 (1990): 10735-10737.

Gross, R., P. Chaudhari, et al. "Superconducting transport charateristics of YBa2Cu3O7-d grain boundary junctions." IEEE Trans. Mag. 27 (1991): 3227-3230.

Gross, R., P. Chaudhari, et al. "Low noise YBa2Cu3O7-d grain boundary junction dc SQUIDs." Applied Physics Letters 57 (1990): 727-729.

Gross, R., P. Chaudhari, et al. "Characteristics of YBa2Cu3O7-d grain boundary junction dc-SQUIDs." IEEE Trans. Mag. 27 (1991): 2565-2568.

Gross, R., K. Hipler, et al. "Spatial Imaging of the critical current density in epitaxial YBCO films." Applied Physics Letters 55 (1989): 2132-2134.

Gross, R. and B. Mayer "Transport processes and noise in YBa2Cu3O7-d grain boundary junctions." Physica C 180 (1991): 235-242.

Grundler, D., J. P. Krumme, et al. "YBCO ramp-type junctions and superconducting quantum interference devices with an ultrathin barrier of NdGaO3" Applied Physics Letters 65 (1994): 1841-1843.

Gupta R., and Quing Hu "Near-millimeter-wave response of high Tc ramp-type Josephson junctions" Applied Physics letters 62 (1993): 3351-3535.

Gupta, A., J. Z. Sun, et al. "Mercury-based cuprate high-transition temperature grain-boundary junctions and SQUIDs operating above 110 Kelvin." Science 265 (1994): 1075-1077.

Gyorgy, E. M., R. B. van Dover, et al. "Anisotropic critical currents in Ba2YCu3O7 analyzed using an extended Bean model." Applied Physics Letters 55 (1989): 283-285.

Gyorgy, E. M., R. B. van Dover, et al. "Sharp angular sensitivity of pinning due to twin boundaries in Ba2YCu3O7." Applied Physics Letters 56 (1990): 2465-2467.

Haefke, H., H. P. Lang, et al. "Mg2TiO4 as a novel substrate for high-temperature superconducting thin films." Applied Physics Letters 61 (1992): 2359-2361.

Haage, T., J.Q. Li, et al. "Substrate mediated anisotropy of transport properties in YBCO thin films." Solid State Communications 99 (1996): 553-557.

Halbritter, J. "Pair weakening and tunnel channels at cuprate interfaces." Physical Review B 46 (1992): 14861-14871.

Haung, C. J., Y. C. Chen, et al. "Flux motion dependence of resistive properties in superconducting YBa2Cu3O7-x thin films." Journal of Applied Physics 72 (1992): 1007-1012.

Häuser, B., B. B. G. Klopman, et al. "Response of YBaCuO thin-film microbridges to microwave irradiation." Applied Physics Letters 54 (1989): 1368-1370.

Hawley, M., I. D. Raistrick, et al. "Growth mechanism of sputtered films of YBa2Cu3O7 studied by scanning tunneling microscopy." Science 251 (1991): 1587-1589.

Heinz, A. and P. Neumann "Representation of orientation and disorientation data for cubic, hexagonal, tetragonal and orthorhombic crystals." Acta Crystallographica A47 (1991): 780-789.

Herrmann, K., Y. Zhang, et al. "Step edge in YBCO." Superconducting Science and Technology 4 (1991): 582.

Hervieu, M., B. Domenges, et al. "Twins and oriented domains in the orthorhombic superconductor YBa2Cu3O7-d." Physical Review B 36 (1987): 3920-3922.

Hettinger, J. D., D. H. Kim, et al. "Effective electric field in dc magnetization measurements: Comparing magnetization to transport critical currents." Applied Physics Letters 60 (1992): 2153-2155.

Hinaus, B.M., R.D. Redwing, et al. "Flux penetration in bicrystal-substrate thin film YBCO Josephson junctions." Applied Physics Letters 70 (1997): 517-519.

Hilgenkamp, H. and J. Mannhart "Superconducting and normal-state properties of YBaCu3O7-x bicrystal grain boundary junctions in thin films." Applied Physics Letters 73 (1998): 265-267.

Hilgenkamp, H., J. Mannhart, et al. "Implications of dz2y2 symmetry and faceting for the transport properties of grain boundaries in high-Tc superconductors." Physical Review B 53 (1996): 14586-14593.

Hinks, D. G., L. Soderholm, et al. "Phase diagram and superconductivity in the Y-Ba-Cu-o system." Applied Physics Letters 50 (1987): 1688-1690.

Hirth, J. P. and J. Lothe (1982). Theory of Dislocations, chapter 19 (2nd ed.). New York: John Wiley & Sons.

Holland, J.H. Adaptation in Naural and Artifical Systems U.ofM. Press, Ann Arbor (1975).

Hollmann, E. K., O. G. Vendik, et al. "Substrates for high-Tc superconductor microwave integrated circuits." Superconductor Science and Technology 7 (1994): 609-622.

Hor, P. H., L. Gao, et al. "High-Pressure Study of the New Y-Ba-Cu-O Superconducting Compound System." Physical Review Letters 58 (1987): 911-912.

Horiuchi, S. "Distribution of oxygen atoms in YBa2Cu3O6.4 superconductor visualized by ultra-high resolution electron microscopy." Japanese Journal of Applied Physics Part 2 31 (1992): L1335-L1338.

Huang, Y. and K.L. Merkle "A new procedure for making TEM specimens of superconductor devices." Materials Research Society Symposium Proceedings 480 (1997): 235-243.

Huang, Y., K.L. Merkle, et al. "Microstructural origin of 1/f noise in high Tc bicrystal SQUID magnetometers." Applied Physics Letters 71 (1997): 3703-3705.

Huang, Y., K.L. Merkle, et al. "The effect of microstructure on the electrical properties of YBCO interface-engineered Josephson junctions." Physica C 314 (1999): 36-42.

Huang, Y. B.V. Vuchic, et al. "The mechanism of sputter induced epitaxy modification in YBCO (001) films grown on MgO (001) substrates." Journal of Materials Research 13 (1998): 3378-3388.

Hubler, N. "Fundamentals of Ion-beam-assisted Deposition: Technique and Film Properties." Materials Science and Engineering A A115 (1989): 181-192.

Huebener, R. P. and J. R. Clem "Magnetic flux structures in superconductors."

Huebener, R.P., J.R. Clem et al. "Meissner shielding currents and magnetic flux penetration in thin-film superconductors." Journal of Low Temperature Physics 6 (1972): 275-285.

Hull, D. (1965). *Introduction to dislocations, chapter 9.* Oxford: Pergamon Press.

Humphreys, R.G. and J.A. Edwards "YBCO thin film grain boundary junctions in a perpendicular magnetic field." Physica C 210 (1993): 42-54.

Humphreys, R.G., J.S. Satchell, et al. "YBCO thin film Josephson junctions." IEEE Transactions on Applied Superconductivity 3 (1993): 2026-2029.

Hunt, B.D., M.C. Foote, et al. "All high Tc edge-geometry weak links utlilizing YBCO barrier layers." Applied Physics Letters 59 (1991): 982-984.

Hunt, B.D., M.G. Forrester, et al. "High-resistance HTS SNS edge junctions." Applied Superconductivity 5 (1998): 365-371.

Hurd, Magnus "Current-voltage relation for superconducting d-wave junctions." Physical Review B 55 (1997): R11993-R11996.

Hwang, D. M., T. S. Ravi, et al. "Application of a near coincidence site lattice theory to the orientations of YBa2Cu3O7-x grains on (001) MgO substrates." Applied Physics Letters 57 (1990): 1690-1692.

Hylton, T. L. and M. R. Beasley "Flux-pinning mechanisms in thin films of YBa2Cu3Ox." Physical Review B 41 (1990): 11669-11672.

Hylton, T. L., A. Kapitulnik, et al. "Weakly coupled grain model of high-frequency losses in high Tc superconducting thin films." Applied Physics Letters 53 (1988): 1343-1345.

Iguchi, I. and Z. Wen "Experimental evidence for d-wave pairing state in YBCO from a study of YBCO/insulator/Pb Josephson tunnel junctions." Physical Review B 49 (1994): 12388-12391.

IJsselsteijn, R. P. J., J. W. M. Hilgenkamp, et al. "Bi-epitaxial template grain boundaries with different in-plane angles on (100) MgO substrates." Journal of Alloys and Compounds 195 (1993): 231-234.

Il'ichev, E., V. Zakosarenko, et al. "Nonsinusoidal current-phase relationship of grain boundary Josephson junctions in high-Tc superconductors." Physical Review Letters 81 (1998): 894-897.

Isernia, T., G. Leone, et al. "Role of support information and zero location in phase retrieval by a quadratic approach." Journal Optical Society of America A. 16 (1999): 1845-1856.

Ivanov, Z. G., P. Å. Nilsson, et al. "Weak links and dc SQUIDs on artificial nonsymmetric grain boundaries in YBa2Cu3O7-d." Applied Physics Letters 59 (1991): 3030-3032.

Ivanov, Z. G., P. A. Nilsson, et al. (1991). "YBa2Cu3Ox DC-SQUIDs on Y-ZrO2 Bicrystals." IV. International Conference on Superconducting and Quantum Effect Devices and their Applications, Berlin, Germany,

Jagannadham, K. and J. Narayan "Grain boundary modeling in high critical temperature superconductors." Material Science and Engineering B8 (1991): 5-21.

Jia, C.L., M.I. Faley, et al. "Effect of chemical and ion-beam etching on the atomic structure of interfaces in YBCO/PrBCO Josephson junctions." Applied Physics Letters 67 (1995): 3635-3637.

Jia, C. L., B. Kabius, et al. "Interfacial defects in YBa2Cu3O7/PrBa2Cu3O7-heterostructures on SrTiO3 substrates." Physica C 172 (1990): 81-89.

Jia, C. L., B. Kabius, et al. "Step edges in YBCO thin films." Physica C 175 (1991): 543.

Jia, C. L., B. Kabius, et al. "The microstructure of epitaxial YBa2Cu3O7 films on steep steps in LaAlO3 substrates." Physica C 196 (1992): 211-226.

Jia, C. L. and K. Urban "Structure of grain boundaries in YBa2Cu3O7 thin-film step-edge junctions." Interface Science 1 (1993): 291-308.

Jin, S., T. H. Tiefel, et al. "Thousandfold change in resistivity in magnetoresistive La-Ca-Mn-O films." Science 264 (1994): 413-415.

Jirmanus, M. N. "Introduction to laboratory cryogenics" Janis Research Company. (1990):

Johnson, B. R., K. M. Beauchamp, et al. "In situ growth of DyBa2Cu3O7-x thin films by molecular beam epitaxy." Applied Physics Letters 56 (1990): 1911-1913.

Jones, H., L. Cowey, et al. "Contact problems in Jc measurements on high Tc superconductors." Cryogenics 29 (1989): 795-799.

Jorgensen, J. D. "Defects and superconductivity in the copper oxides." Physics Today (1991): 34-40.

Jorgensen, J. D., M. A. Beno, et al. "Oxygen ordering and the orthorhombic-to-tetragonal phase transition in YBa2Cu3O7-x." Physical Review B 36 (1987): 3608-3616.

Jorgensen, J. D., B. W. Veal, et al. "Structural properties of oxygen-deficient YBa2Cu3O7-d." Physical Review B 41 (1990): 1863-1877.

Joseph, R.I. and E. Schlömann "Demagnetizing field in nonellipsoidal bodies." Journal of Applied Physics 36 (1965): 1579-1592.

Josephson, B. D. "Possible new effects in superconductive tunneling." Physical Letters 1 (1962): 251-253.

Josephson, B. D. "Coupled Superconductors." Reviews of Modern Physics (1964): 216-220.

Kale, G. M. and K. T. Jacob "Gibbs energies of formation of CuYO2 and Cu2Y2O5 and phase relations in the system Cu-Y-O." Chemistry of Materials 1 (1989): 515-519.

Kamei, M., Y. Aoki, et al. "In situ observation of Ba oxide layer at the interface between YBa2Cu3O7-x film and MgO substrate." Journal of Applied Physics 74 (1993): 436-439.

Kautz, R. L., R. H. Ono, et al. "Effect of thermal noise on Shapiro steps in high-Tc Josephson weak links." Applied Physics Letters 61 (1992): 342-344.

Kawasaki, M., P. Chaudhari, et al. "1/f noise in YBa2Cu3O7-d superconducting bicrystal grain-boundary junctions." Physical Review Letters 68 (1992): 1065-1068.

Kawasaki, M., P. Chaudhari, et al. "Submicron YBa2Cu3O7-x grain boundary junction dc SQUIDs." Applied Physics Letters 58 (1991): 2555-2557.

Kawasaki, M., E. Sarnelli, et al. "Weak link behavior of grain boundaries in Nd-, Bi-, and Tl-based cuprate superconductors." Applied Physics Letters 62 (1993): 417-419.

Keene, M. N., J. S. Satchell, et al. "Low noise HTS gradiometers and magnetometers constructed from YBa2Cu3O7-x/PrBa2Cu3O7-x thin films." IEEE Transactions on Applied Superconductivity (1995):

Kelly, R. and N. Q. Lam "The Sputtering of Oxides Part 1: A Survey of the Experimental Results." Radiation Effects 19 (1973): 39-47.

Kim, D. H., K. E. Gray, et al. "Possible origins of resistive tails and critical currents in high-temperature superconductors in a magnetic field." Physical Review B 42 (1990): 6249-6258.

Kim, D. H., K. E. Gray, et al. "Lorentz-force independence of resistance tails in magnetic fields near Tc for the low-temperature superconductor granular NbN: A Josephson junction model." Physical Review B 41 (1990): 11642-11645.

King, A. H., A. Singh, et al. "Principles of grain boundary geometry in noncubic materials, with applications to YBa2Cu3O7-x." Interface Science 1 (1993): 347-360.

Kirtley, J. R. "Tunneling measurements of the energy gap in high-Tc superconductors." Int. J. Mod. Phys. B 4 (1990): 201-237.

Kirtley, J. R., S. Washburn, et al. "Direct measurement of potential steps at grain boundaries in the presence of current flow." Physical Review Letters 60 (1988): 1546-1549.

Kleinsasser, A. W. "Excess currents and voltages in superconducting junctions." Applied Physics Letters 62 (1993): 193-195.

Kleinsasser, A. W., F. M. Rammo, et al. "Degradation of superconducting tunnel junction characteristics with increasing barrier transparency." Applied Physics Letters 62 (1993): 1017-1019.

Klemm, R.A., C.T. Rieck, et al. "Order parameter symmetries in high termperature superconductors.", submitted Physical Review B, (1999)

Koch, R. H., W. Eidelloth, et al. "Identifying the source of 1/f noise in SQUIDs made from high-temperature superconductors." Applied Physics Letters 60 (1992): 507-509.

Kogure, T., Y. Zhang, et al. "Grain boundary structure of YbBa2Cu3O7-x formed by oxidation of metallic precursors." Physica C 156 (1988): 707-716.

Krebs, H.U., Ch. Krauns, et al. "Island growth and surface topography of epitaxial YBCO thin films on MgO." Applied Physics Letters 59 (1991): 2180-2182.

Kroeger, D. M., A. Choudhury, et al. "Grain-boundary compositions inYBa2Cu3O7-x from Auger electron spectroscopy of fracture surfaces." Journal of Applied Physics 64 (1988): 331-335.

Krumme, J.-P., V. Doormann, et al. "Ion-beam sputter deposition process for YBa2Cu3O7-x thin-film structures." Journal of Materials Research 9 (1994): 2747-2760.

Krusin-Elbaum, L., A.P. Malozemoff, et al. "Temperature dependence of lower critical fields in YBCO crystals." Physical Review B 39 (1989): 2936-2939.

Krusin-Elbaum, L., R.L. Greene, et al. "Direct measurement of the temperature dependent magnetic penetration depth in YBCO crystals." Physical Review Letters 62 (1989): 217-220.

Kunchur, M.N., and S.J. Poon "Critical fields and critical currents of superconducting disks in transverse magnetic fields." Physical Review B 43 (1991): 2916-2920.

Kupriyanov, M. Y. and K. K. Likharev "Towards the quantitative theory of the high-Tc Josephson junctions." IEEE Transactions on Magnetics 27 (1991): 2460-2463.

Kussmaul, A., E. S. Hellman, et al. "Superconductor-insulator-superconductor tunneling in Ba1-xKxBiO3 grain boundaries." Applied Physics Letters 63 (1993): 2824-2826.

Kwok, W. K., G. W. Crabtree, et al. "Electronic behavior of oxygen-deficient YBa2Cu3O7-d." Physical Review B 37 (1988): 106-110.

Kwok, W. K., S. Fleshler, et al. "Vortex lattice melting in untwinned and twinned single crystals of YBa2Cu3O7-d." Physical Review Letters 69 (1992): 3370-3373.

Kwok, W. K., U. Welp, et al. "Direct observation of dissipative flux motion and pinning by twin boundaries in YBCO single crystals." Physical Review Letters 64 (1990): 966-969.

Lacquaniti, V., S. Maggi, et al. "Effects of idle region geometry on the magnetic field curves of Nb/Al-AlOx/Nb Josephson junctions." Institute of Physics Conference Series 158 (1997): 543-546.

LaGraff, J.R., H. Chan, et al. "Novel method for fabrication of integrated resistors on bilayer Ag/YBCO films using Ni implantation." Applied Physics Letters 71 (1997): 2199-2201.

Laibowitz, R. B., R. P. Robertazzi, et al. "Tunneling in all-high-Tc edge junctions with deposited barriers." Physical Review B 46 (1992): 14830-14833.

Laibowitz, R. B., J. Z. Sun, et al. "High-Tc, multilevel edge junction superconducting quantum interference devices with SrTiO3 barriers operating at 77 K." Applied Physics Letters 64 (1994): 247-249.

Larbalestier, D. "Critical currents and magnet applications of high-Tc superconductors." Physics Today (1991): 74-82.

Larbalestier, D. C., S. E. Babcock, et al. (1989). "Recent results on the weak link problem in bulk polycrystalline REBa2Cu3O7." Tokai University International Workshop the Science of Sueprconductivity and New Materials, Tokyo, Japan, World Scientific.

Larbelestier, D. C., S. E. Babcock, et al. "Electrical transport across grain boundaries in bicrystals of YBa2Cu3O7-ð." Physica C 185-189 (1991): 315-320.

Lathrop, D. K., B. H. Moeckly, et al. "Transport properties of high-angle grain boundary weak links in Y-Ba-Cu-O thin films." Applied Physics Letters 58 (1991): 1095-1097.

Lawrence, W. E. and S. Doniach "Theory of Layer Structure Superconductors."

Lean, H. W., E. J. Tarte, et al. "Supercurrents in YBCO-silver-indium junctions." Journal of Physics: Condensed Matter 2 (1990): 9077-9084.

Lee, D. F., M. Mironova, et al. "Structure and defects at Y2BaCuO5 interface in melt-textured YBa2Cu3Ox superconductors." Interface Science 1 (1993): 385-400.

Lee, P. A. "Effect of noise on current-voltage characteristics of a Josephson junction." Journal of Applied Physics 42 (1971): 325-334.

Lee, S.-T., S. Chen, et al. "Microstructure of epitaxially oriented superconducting YBa2Cu3O7-x films grown on (100) MgO by metalorganic decomposition." Applied Physics Letters 55 (1989): 286-288.

Lee, S. H., S. C. Bae, et al. "Oxygen diffusion in epitaxial YBa2Cu3O7-x thin films." Physical Review B 46 (1992): 9142-9146.

Le Page, Y., T. Siegrist, et al. "Structural properties of Ba2RCu3O7 high-Tc superconductors." Physical Review B 36 (1987): 3617-3621.

Lesueur, J., L. H. Greene, et al. "Zero bias anomalies in YBa2Cu3O7 tunnel junctions." Physica C 191 (1992): 325-332.

Li, D. J., J. P. Zhang, et al. "Trigonal Phases in YBa2Cu3O6.5." Journal of Solid State Chemistry 81 (1989): 165-172.

Li, D. X., X. K. Wang, et al. "Microstructure studies of epitaxial YBa2Cu3O7-d films." Journal of Applied Physics 66 (1989): 5505-5509.

Li, Q., O. Meyer, et al. "Growth charcterization of YBa2Cu3O7-x thin films on (100) MgO." Applied Physics Letters 55 (1989): 310-312.

Li, Y. Q., J. Zhao, et al. "Effects of Y2O3 precipitates on critical current anisotropy in YBa2Cu3O7-x thin films prepared by plasma-enhanced metalorganic vapor deposition." Applied Physics Letters 60 (1992): 2430-2432.

Liang, Y. H., J. Chen, et al. "Identification of oxygen vacancies in YBaCuO superconductors by high-resolution electron microscopy." Applied Physics Letters 54 (1989): 368-370.

Likharev, K. K. "Superconducting weak links." Reviews of Modern Physics 51 (1979): 101-159.

Lindemer, T. B., J. F. Hunley, et al. "Experimental and thermodynamic study of nonstoichiometry in YBa2Cu3O7-x." Journal of the American Ceramics Society 72 (1989): 1775-1788.

Linzen, S, F. Schmidl, et al. "High Tc step-edge Josephson junctions on silicon substrates." Applied Physics Letters 67 (1995): 2235-2237.

Little, W. A. "Experimental constraints on theories of high-transition temperature superconductors." Science 242 (1988): 1390-1395.

Liu, L., E. R. Nowak, et al. "High-angle grain boundary junctions in YBCO: Normal-state resistance and 1/f noise." Physical Review B 51 (1995): 16164-16167.

Liu, L., K. Zhang, et al. "Normal-state resistance fluctuations in high-Tc cuprate films." Physical Review B 49 (1994): 3679-3682.

Lu, H. B., T. W. Huang, et al. "Artificial grain boundaries of YBa2Cu3O7-x on MgO bicrystals." IEEE Transactions on Applied Superconductivity 3 (1993): 2325-2328.

Lubkin, G. B. "Applications of high-temperature superconductors approach the marketplace." Physics Today (1995): 20-23.

Luo, J. S., N. Merchant, et al. "Growth of c-axis-oriented films of YbBa2Cu3O7-d on single and polycrystalline MgO substrates by oxidation of a liquid alloy precursor." Physica C 192 (1992): 356-361.

Luo, J. S., N. Merchant, et al. (1992). "Synthesis of c-oriented YbBa2Cu3O7-d films on single and polycrystalline substrates by oxidation of liquid alloys." Materials Research Society, Boston, MA,

Maeda, H., Y. Tanaka, et al. "A New high-Tc Oxide Superconductor Without a Rare Earth Element." Japanese Journal of Applied Physics 27 (1988): L209-L210.

Maggi, S., and V. Lacquaniti "Analysis of magnetic field patterns of single Josephson tunnel junctions with large idle regions." Journal of Low Temperature Physics 106 (1997): 393-398.

Mahajan, S., W. Ito, et al. "Fabrication and characteristics of all YBCO sandwich-type junctions using highly crystalline DC sputtered superconducting a-axis oriented YBa2Cu3O7-x films." Physica C 220 (1994): 227-232.

Mahajan, S., W. Ito, et al. "Effects of target and template layer on the properties of highly crystalline superconducting a-axis films of YBa2Cu3O7-x by DC-sputtering." Physica C 213 (1993): 445-454.

Mahajan, S., J. G. Wen, et al. "Comparison of crystalline and superconducting properties of sputtered a-axis oriented YBCO films on MgO and SrTiO3 substrates." Physica C 225 (1994): 353-357.

Mannhart, J., J. G. Bednorz, et al. (1993). "High-Tc thin films. Growth modes - structure - applications." Materials and Crystllographic Aspects of HTc-Superconductivity, NATO ASI, Erice, Sicily, Italy, Kluwer Academic Publishers.

Mannhart, J., R. Gross, et al. "Spatially resoved observation of charge transfer across single grain boundaries in YBaCuO films." Cryogenics 30 (1990): 397-400.

Mannhart, J. and H. Hilgenkamp, "Interfaces involving complex superconductors." Physica C 317-318 (1999): 383-391.

Mannhart. J. and J. Hilgenkamp" Possible influence of band bending on the normal state properties of grain boundaries in high-Tc superconductors." Submitted Physical Review B. (1998).

Mannhart, J., H. Hilgenkamp et al. "Generation of magnetic flux by single grain boundaries of YBa2Cu3O7-x." Physical Review Letters 77 (1996): 2782-2785.

Mannhart, J. and P. Martinoli "IcR products of tunnel junctions with depressed order parameter." Applied Physics Letters 58 (1991): 643-644.

Mannhart, J., B. Mayer et al., "Anomalous dependence of the critical current of 45 degree grain boundaries in YBa2Cu3O7-x on an applied magnetic field."Zeitschrift Für Physik B 101 (1996):175-179.

Mannhart, J., M. Scheuermann, et al. "Micropatterning of high-Tc films with an excimer laser." Applied Physics Letters 52 (1988): 1271-1273.

Mannhart, J., J. Ströbel, et al. "Large electric field effects in YBa2Cu3O7-d films containing weak links." Applied Physics Letters 62 (1993): 630-632.

Marezio, M. "Oxygen Stoichiometry in High-Tc Superconductors." Acta Cryst. A47 (1991): 640-654.

Marks, L.D. and E. Landree "A minimum-entropy algorithm for surface phasing problems." Acta Cryst. A54 (1998): 296-305.

Marks, L. D., D. J. Li, et al. "High-Resolution Electron Microscopy of High-Temperature Superconductors." J. Elec. Micr. Tech. 8 (1988): 297-306.

Marshall, A. F. and C. B. Eom "Microfaceting of 90° [001] tilt boundaries in YBa2Cu3O7-x thin films." Physica C 207 (1993): 239-246.

Martin, V., M. Lam Chok Sing, et al. "Magnetometry based sharpened high Tc GBJ Fraunhofer patters." Transactions on Applied Superconductivity 7 (1997): 3079-3082.

Marx, A., K.D. Husemann, et al. "Distribution of the critical current density and flux trapping in YBCO ramp-edge Josephson junctions." Applied Physics Letters 64 (1994): 241-243.

Matsui, T., T. Suzuki, et al. "Properties of tunnel junctions with (103)YBa2Cu3Oy/SrTiO3/(013)YBa2Cu3Oy layered structure." IEEE Transactions on Applied Superconductivity (1995):

Matsui, T., T. Suzuki, et al. "Fabrication of tunnel junctions with YBCO/Insulator/YBCO layered structure using (013)-oriented films as base layer." Japanese Journal of Applied Physics Part 2 32 (1993): L1218-L1221.

Matsui, T., T. Suzuki, et al. (1993). "Fabrication and properties of YBCO/STO/YBCO junctions." 6th International Symposium on Superconductivity, Hiroshima, Springer-Verlag.

Mayer, B., L. Alff, et al. "Superconducting transport properties of Bi2Sr2CaCu2O8+x bicrystal grain boundary junctions." Applied Physics Letters

Mayer, B., S. Schuster, et al. "Magnetic field dependence of the critical current in YBa2Cu3O7-d bicrystal grain boundary junctions." Applied Physics Letters **62** (1993): 783-785.

McCumber, D. E. "Effect of ac Impedance on dc Voltage-current Characteristics of Superconductor Weak-Link Junctions." Journal of Applied Physics **39** (1968): 3113-3118.

McIntyre, P. C. and M. J. Cima "Heteroepitaxial growth of chemically derived ex situ Ba2YCu3O7-x thin films." Journal of Materials Research **9** (1994): 2219-2230.

McKernan, S., M. G. Norton, et al. "The 45° grain boundaries in YBa2Cu3O7-d." Journal of Materials Research **7** (1992): 1052-1059.

Meilikhov, E. Z. "Intergrain boundary asymmetry and the critical current of HTSC ceramics." Physica C **226** (1994): 69-75.

Meng, X., O. Takahashi, et al. "YBCO/metallic oxide/YBCO trilayers for high-Tc superconducting SNS junctions." IEEE Transactions on Applied Superconductivity (1995):

Merchant, N., J. S. Luo, et al. "Epitaxial growth of YbBa2Cu3O7-d films on (100)-oriented MgO and SrTiO3 substrates by oxidation of a liquid alloy precursor." Journal of Materials Research (1992):

Merkle, K. L. (1991), Ultramicroscopy **37**, 130.

Merkle, K. L. "Quantification of atomic-scale grain boundary parameters by high-resolution electron microscopy." Ultramicroscopy **40** (1992): 281-290.

Merkle, K. L. "Atomic structure of grain boundaries." Journal of Phys. Chem. Solids **55** (1994): 991-1005.

Merkle, K.L., Y. Huang, et al. "Electron microscopy of high-Tc Josephson junctions formed in the epitaxial layer ramp-edge geometry: YBCO/barrier/YBCO." Micron **30** (1999): 539-559.

Merkle, K. L. and D. Wolf "Structure and energy of grain boundaries in metals." MRS Bulletin **15** (1990): 42-50.

Merkle, K. L. and D. Wolf "Low-energy configurations of symmetric and asymmetric tilt grain boundaries." Phil. Mag. A **65** (1992): 513-530.

Miao, J., D. Sayre, et al. "Phase retrieval from the magnitude of the Fourier transforms of nonperiodic objects." Journal Optical Society of America A 15 (1998): 1662-1669.

Miller, D. J., T. A. Roberts, et al. ""Meandering" grain boundaris in YBaCuO bi-crystal thin films." Applied Physics Letters 66 (1995): 2561-2563.

Miller, D. L., J. X. Przybysz, et al. "A superconductive sigma-delta modulator demonstration." IEEE Transactions on Applied Superconductivity (1995):

Miller, J. H., G. H. Gunaratne, et al. "Enhanced quantum interference effects in parallel Josephson junction arrays." Applied Physics Letters 59 (1991): 3330-3332.

Miller, J.H., Q.Y. Ying, et al. "Use of tricrystal junctions to probel the pairing state symmetry of YBCO." Physical Review Letters 74 (1995): 2347-2350.

Mints, R.G., "Self-generated flux in Josephson junctions with alternating critical current density." Physical Review B 57 (1998): R3221-R3224.

Mints, R.G. and V.G. Kogan, "Josephson junctions with alternating critical current density." Physical Review B 55 (1997): R8682-R8684.

Missert, N., T. E. Harvey, et al. "High-Tc multilayer step-edge Josephson junctions and SQUIDs." Applied Physics Letters 63 (1993): 1690-1692.

Moeckly, B. and K. Char "Properties of cobalt doped YBCO thin films." Physica C 265 (1996): 283-294.

Moeckly, B.H., K. Char "Properties of interface-engineered high Tc Josephson junctions." Applied Physics Letters 71 (1997): 2526-2528.

Moeckly, B.H., K. Char, et al. "Interface engineered high-Tc Josephson junctions." Applied Superconductivity 6 (1998): 317-323.

Moeckly, B. H., D. K. Lathrop, et al. "Electromigration study of oxygen disorder and grain-boundary effects in YBCO thin films." Physical Review B 47 (1993): 400-417.

Moeckly, B. H., S. E. Russek, et al. "Growth of YBa2Cu3O7 thin films on MgO: The effect of substrate preparation." Applied Physics Letters 57 (1990): 1687-1689.

Mogilevsky, R., R. Levi-Setti, et al. "Direct measurements of room-temperature oxygen diffusion in YBa2Cu3Ox." Physical Review B 49 (1994): 6420-6423.

Moodie, A. F. and H. J. Whitfield "Structure and microstructure in Ba2YCu3O7-x." Ultramicroscopy 24 (1988): 329-338.

Moon, B. M., C. E. Platt, et al. "In situ pulsed laser deposition of superconducting Ba1-xKxBiO3 thin films." Applied Physics Letters 59 (1991): 1905-1907.

Moshchalkov, V. V., L. Gielen, et al. "Quantum interference in a mesoscopic superconducting loop." Nature 361 (1993): 617-620.

Mueller, F. M., S. P. Chen, et al. "Coherent twin boundaries in high-Tc superconducting oxides." Physical Review B 37 (1988): 5837-5840.

Müller, J.-H., R. Gruehn, et al. "TEM and HRTEM cross section investigations of the microstructure of YBa2Cu3O7-x thin films on oriented NiO single crystals." Physica C 210 (1993): 173-178.

Müller, K.-H. and D. N. Matthew "Sample size dependence and irreversibility of the critical current density of ceramic high-temperature superconductors." IEEE Transactions on Applied Superconductivity (1993):

Murphy, D. W., S. Sunshine, et al. "New Superconducting Cuprate Perovskites." Physical Review Letters 58 (1987): 1888-1890.

Myers, K.E., K. Char, et al. "Noise characteristics of YBCO/CaRuO3/YBCO Josephson junctions." Applied Physics Letters 64 (1994): 788-790.

Nakagawa, H., I. Kurosawa, et al. "Fabrication process for a Josephson computer ETL-JC1 using Nb tunnel junctions." IEEE Transactions on Magnetics 27 (1991): 3109-3112.

Nakahara, S., G. J. Fisanick, et al. "On the defect structure of grain boundaries in Ba2YCu3O7-x." Journal of Crystal Growth (1987):

Nakajima, K., K. Yokota, et al. "Electric field effect on the artificial grain boundary of bicrystal YBa2Cu3O7-d films." Applied Physics Letters 63 (1993): 684-686.

Nesher, O. and E.N. Ribak "Retrieval of critical current distribution in small Josephson junctions." Applied Physics Letters 71 (1997): 1249-1251.

Neumann, C., K. Suzuki, et al. "Fabrication of YBaCuO-Josehpson-junctions on MgO-substrates damaged by a focused ion beam prior to film deposition." Japanese Journal of Applied Physics Part 2 32 (1993): L727-L729.

Neumann, C., K. Yamaguchi, et al. "Fabrication of high IcxRn YBCO-Josephson-junctions on MgO-substrates using a focused-ion-beam system." Physica C 210 (1993): 138-146.

Newman, N., K. Char, et al. "YBa2Cu3O7-d superconducting films with low microwave surface resistance over large areas." Applied Physics Letters 57 (1990): 520-522.

Nicol, J., S. Shapiro, et al. "Direct measurement of the superconducting energy gap." Physical Review Letters 5 (1960): 461-464.

Nicoletti, S. and J.C. Villegier "Electrical behavior of YBCO grain boundary junctions under low magnetic field." Journal of Applied Physics 82 (1997): 303-308.

Nilsson, P. Å., Z. G. Ivanov, et al. "Properties of YBCO junctions and SQUIDs on YSZ bicrystals." Physica C 185-189 (1991): 2597-2598.

Norton, M. G. and C. B. Carter (1990). "Effect of substrate on the early stages of the growth of YBa2Cu3O7-x thin films." Materials Research Society, Boston, MA,

Norton, M. G. and C. B. Carter "The nucleation and heteroepitactic growth of YBa2Cu3O7-d thin films on MgO." Journal of Crystal Growth 110 (1991): 641-651.

Norton, M. G. and C. B. Carter "Growth of YBa2Cu3O7-d thin-films - nucleation, heteroepitaxy, and interfaces." Scanning Microscopy 6 (1992): 385-397.

Norton, M. G. and C. B. Carter "Observations on the growth of YBCO thin films." In Interfaces in High-Tc Superconducting Systems edited by S. L. Shinde and D. A. Rudman. New York: Springer-Verlag, (1994).

Norton, M. G., L. A. Tietz, et al. "Observation of the early stages of growth of superconducting thin films by transmission electron microscopy." Applied Physics Letters 55 (1989): 2348-2350.

Noushin, A.J., M.A. Fiddy, et al. "Some new finding on the zeros of band-limited functions." Journal Optical Society of America A 16 (1999): 1857-1863.

Nücker, N., J. Fink, et al. "Evidence for holes on oxygen sites in the high-Tc superconductors La2-xSrxCuO4 and YBa2Cu3O7-y." Physical Review B 37 (1988): 5158-5163.

Nücker, N., H. Romberg, et al. "Electronic structure studies of high-Tc cuprate superconductors by electron energy-loss spectroscopy." In Studies of High Temperature Superconductors edited by A. Narlikar. New York: Nova Science Publishers, (1990).

Nücker, N., H. Romberg, et al. "Symmetry of holes in high-Tc superconductors." Physical Review B 39 (1989): 6619-6629.

Obara, H., S. Kosaka, et al. "Magnetization measurements in epitaxial films of the YBCO compound." Physical Review B 44 (1991): 4532-4538.

O'bryan, H. M. and P. K. Gallagher "Kinetics of the oxidation of Ba2YCu3Ox ceramics." Journal of Materials Research 3 (1988): 619-625.

O'Sullivan, E. J. M. and B. P. Chang "Study of oxygen transport in Ba2YCu3O7-d using a solid-state electrochemical cell." Applied Physics Letters 52 (1988): 1441-1443.

Olsson, E. and K. Char "The role of interfacial morphology in multilayers based on high-Tc YBa2Cu3O7-x." Interface Science 1 (1993): 371-384.

Olsson, E. and K. Char "Origin of non-uniform properties of YBCO/CaRuO3/YBCO Josephson edge junctions." Applied Physics Letter 64 (1994): 1292-1294.

O'Neill, E.L. and A. Walther "The question of phase in image formation." Opt. Acta 10 (1962): 33-40.

Ono, R. H. "Thin film processing of complex multilayer structures of high-temperature superconductors." MRS Bulletin (1992): 34-38.

Ono, R.H., J.A. Beall, et al. "High-Tc superconductors-normal metal-superconductor Josephson microbridge with high-resistance normal metal links." Applied Physics Letters 59 (1991): 1126-1128.

Osborn, J.A. "Demagnetization factors of general ellipsoiod," Physical Review 67 (1945): 351-357.

Ottaviani, G., C. Nobili, et al. "Oxygen in-diffusion processes in tetragonal YBa2Cu3O7-d oxide." Physical Review B 39 (1989): 9069-9073.

Park, J. H., P. Kostic, et al. "Electrical conductivity and chemical diffusion in sintered YBa2Cu3Oy." Material Letters 6 (1988): 393-397.

Pedyash, M.V., W.E. Booij, et al. "Properties of high-Tc Josephson junctions fabricated by electron beam irradiation." Institute of Physics Conference Series 158 (1997): 519-522.

Pei, S., N. J. Zaluzec, et al. "Charge-density waves and superconductivity in the Ba1-xKxBiO3-y system." Physical Review B 39 (1989): 811-814.

Pelloquin, D., M. Caldes, et al. "The bismuth oxycarbonate Bi2Sr4Cu2CO3O8." Physica C 208 (1993): 121-129.

Pennycook, S. J., M. F. Chisholm, et al. "Interdiffusion growth mechanisms, and critical currents in YBa2Cu3O7-x/PrBa2Cu3O7-x superlattices." Physical Review Letters 67 (1991): 765-768.

Peterson, D. E., K. A. Kubat-Martin, et al. "Synthesis of YBa2Cu3O7-x by chemical precursors." Journal of Materials Research 6 (1991): 11-17.

Peterson, R. L. and J. W. Ekin "Airy pattern, weak-link modeling of critical currents in high-Tc superconductors." Physica C 157 (1989): 325-333.

Peterson, R. L. and J. W. Ekin "Critical-current diffraction patterns of grain-boundary Josephson weak links." Physical Review B 42 (1990): 8014-8018.

Polturak, E., G. Koren, et al. "Proximity effects in YBCO YPrBCO junctions." Physical Review Letters 67 (1991): 3038-3041.

Przyslupski, P., R. Herzog, et al. "Preparation and characterization of c-axis in-plane YBa2Cu3O7 thin films and YBCO/PrBCO superlattices by high pressure sputtering." IEEE Transactions on Applied Superconductivity (1993):

Quenter, D., S. Stehle, et al. "Spatially resolved studies of the microwave properties of superconducting devices." Applied Physics Letters 63 (1993): 2135-2137.

Ramesh, R., D. Hwang, et al. "Epitaxy of Y-Ba-Cu-O thin films on single-crystal MgO." Applied Physics Letters 56 (1990): 2243-2245.

Ramesh, R., D. M. Hwang, et al. "Defect structure of laser deposited Y-Ba-Cu-O thin films on single crystal MgO substrate." Journal of Materials Research 5 (1990): 704-716.

Ramesh, R., D. M. Hwang, et al. "Direct observation of structural defects in laser deposited superconducting Y-Ba-Cu-O thin films." Science 247 (1990): 57-59.

Ramesh, R., A. Inam, et al. "The atomic structure of growth interfaces in Y-Ba-Cu-O thin films." Journal of Materials Research 6 (1991): 2264-2271.

Ramos, J., Z. G. Ivanov, et al. "YBa2Cu3O7-d Josephson junctions on directionally ion beam etched MgO substrates." Applied Physics Letters 63 (1993): 2141-2143.

Randle, V. and B. Ralph "A practical approach to the determination of the crystallography of grain boundaries." Journal of Materials Science 21 (1986): 3823-3828.

Randle, V. and B. Ralph "Local texture changes associated with grain growth." Proceedings of the Royal Society of London A 415 (1988): 239-256.

Randle, V., B. Ralph, et al. "The relationship between microtexture and grain boundary parameters." Acata Metallographica 36 (1988): 267-273.

Ravi, T. S., D. M. Hwang, et al. "Grain boundaries and interfaces in Y-Ba-Cu-O films laser deposited on single-crystal MgO." Physical Review B 42 (1990): 10141-10151.

Reintsema, C. D., R. H. Ono, et al. "Phase locking in two-junction systems of high-temperature superconductor-normal metal-superconductor junctions." Applied Physics Letters 64 (1994): 637-639.

Reyes-Gasga, J., T. Krekels, et al. "3-D oxygen vacancy ordered superstructures in YBa2Cu3O7-d prepared by the constant stoichiometry cooling method." Solid State Communications 70 (1989): 269-273.

Rickards, J., A. Oliver, et al. "Electron beam damage in high Tc superconductor materials." Ultramicroscopy 30 (1989): 425-428.

Robbes, D. M. Lam Chok Sing, et al. "A sharpening method of the Fraunhofer magnetic pattern of HTc grain boundary junctions and future improvements." Institute of Physics Conference Series 148 (1995): 1279-1282.

Robertazzi, R.P., R.H. Kock, et al. "YBCO/MgO/YBCO edge Josephson junctions." Applied Physics Letters 61 (1992): 711-713.

Romberg, H., N. Nücker, et al. "Dielectric function of YBa2Cu3O7-d between 50 meV and 50 eV." Zeitschrift für Physik B 78 (1990): 367-380.

Rosenthal, P. A., M. R. Beasley, et al. "Flux focusing effects in planar thin-film grain-boundary Josephson junctions." Applied Physics Letters 59 (1991): 3482-3484.

Rosenthal, P. A., E. N. Grossman, et al. "High temperature superconductor-normal metal-superconductor Josephson junctions with high characteristic voltages." Applied Physics Letters 63 (1993): 1984-1986.

Roshchin, I. V., V. N. Stepankin, et al. "Re-entrant critical current behavior as a common feature of single grain boundary Josephson junctions in bicrystals of copperless oxide superconductors." IEEE Transactions on Applied Superconductivity (1995):

Rozeveld, S., K.L. Merkle, et al. "Interface structure of a YBCO/N/YBCO superconductor/normal metal/superconductor Josephson junction using YBC2.79Co0.21O as the normal barrier N." Journal of Materials Research 11 (1996): 281-287.

Rozeveld, S., K.L. Merkle, et al. "Interface microstructure and composition of a YBCO/N/YBCO SNS edge junction with CaRuO3 as the metallic barrier." Physica C 252 (1995): 348-360.

Rosner, S. J., K. Char, et al. "Microstructure of biepitaxial grain boundary junctions in YBa2Cu3O7." Applied Physics Letters 60 (1992): 1010-1012.

Rothman, S. J. and J. L. Routbort "Oxygen diffusion in high-Tc superconductors." preprint (1992):

Rothman, S. J., J. L. Routbort, et al. "Tracer diffusion of oxygen in YBa2Cu3O7-d." Physical Review B 40 (1989): 8852-8860.

Rothman, S. J., J. L. Routbort, et al. "Anisotropy of oxygen tracer diffusion in single-crystal YBa2Cu3O7-d." Physical Review B 44 (1991): 2326-2333.

Rowell, J. M. "Tunneling between superconductors." Reviews of Modern Physics (1964): 199-200.

Roy, T., K. Sickafus, et al. (1989). "Electron radiation damage in YBa2Cu3O7." Electron Microscopy Society of America, San Francisco Press, Inc.

Russek, S. E., D. K. Lathrop, et al. "Scaling behavior of Y-Ba-Cu-O thin film weak links." Applied Physics Letters 57 (1990): 1155-1157.

Sanders, S. C., S. E. Russek, et al. "Insulating boundary layer and magnetic scattering in YBa2Cu3O7-d /Ag interfaces over a contact resistivity range of 10-8-10-3ohm cm2." Applied Physics Letters 65 (1994): 2232-2234.

Sanders, S. C., S. E. Russek, et al. "Evidence for tunneling and magnetic scattering at In Situ YBCO/Noble-metal interfaces." IEEE Transactions on Applied Superconductivity (1995):

Sarikaya, M., B. L. Thiel, et al. "Microstructural characterization of YBa2Cu3O7-x." Journal of Materials Research 2 (1987): 736-742.

Sarma, C., G. Schindler, et al. "Measurement of current voltage characteristics of single grain boundaries in melt textured bulk YBa2Cu3Ox." Applied Physics Letters 64 (1994): 109-111.

Sarnelli, E., P. Chaudhari, et al. "Residual critical current in high Tc bicrystal grain boundary junctions." Applied Physics Letters 62 (1993): 777-779.

Satoh, T., M. Y. Kupriyanov, et al. "Resonant tunneling transport in YBaCuO/PrBaCuO/YBaCuO edge-type Josephson junctions." IEEE Transactions on Applied Superconductivity (1995):

Sault, R.J. "Uniqueness condition for the phase problem in one dimension." Optics Letters 9 (1984): 325-326.

Savvides, N. and A. Katsaros "Growth and evolution of microstructure of epitaxial YBa2Cu3O7-x ultrathin and thin films on MgO." Physica C 226 (1994): 23-36.

Scalapino, D. J. "Singularities in superconducting tunnel junction I-V characteristics." Reviews of Modern Physics (1964): 205-207.

Schieber, M. "Deposition of high temperature superconducting films by physical and chemical methods." Journal of Crystal Growth 109 (1991): 401-417.

Schieber, M., S. C. Han, et al. "Comparison of thin films of YBCO deposited by physical (laser ablation) and chemical (OMCVD) methods for device applications." Journal of Crystal Growth 115 (1991): 31-42.

Schindler, G., C. Sarma, et al. "Techniques for the isolation and the electrical characterization of individual grain boundaries in polycrystalline superconductors." Cryogenics (1994):

Schindler, G., B. Seebacher, et al. "Electrical characterisation of single grain boundaries in DyBa2Cu3O7-x ceramics." Physica C 196 (1992): 1-6.

Schlom, D. G., D. Anselmetti, et al. (1992). "Defect-mediated growth of YBCO films." Materials Research Society, Boston,

Schmahl, W. W., A. Putnis, et al. "Twin formation and structural modulations in orthorhombic and tetragonal YBa2(Cu1-xCox)3O7-x." Philosophical Magazine Letters 60 (1989): 241-248.

Schmidl, F., L. Alff, et al. "Superconducting transport properties of step-edge Josephson junctions." IEEE Transactions on Applied Superconductivity 3 (1993): 2349-2352.

Schrieffer, J. R. "Theory of electron tunneling." Reviews of Modern Physics (1964): 200-204.

Schuller, I. K. and J. D. Jorgensen "Structure of oxide high-temperature superconductors." MRS Bulletin

Schulte, B., M. Maul, et al. "Carrier gas-free chemical vapor deposition techniquye for in situ preparation of high quality YBa2Cu3O7-d thin films." Applied Physics Letters 59 (1991): 869-871.

Schuster, S., R. Gross, et al. "Thermal-noise-induced resistance and supercurrent correlation function in YBCO grain boundary Josephson junctions." Physical Review B 48 (1993): 16172-16177.

Schwartz, D.B., P.M. Mankiewich, et al. "The observation of the ac Josephson effect in a YBCO/Au/YBCO junction." IEEE Transactions on Magnetics 25 (1989): 1298-1300.

Scivier, M.S. and M.A. Fiddy "Phase ambiguities and the zeros of multidimensional band-limited functions." Journal Optics Society of America A 2 (1985): 693-697.

Seidel, P., E. Heinz, et al. "High-Tc Josephson junctions and DC SQUIDs." IEEE Transactions on Applied Superconductivity 3 (1993): 2353-2356.

Sezan, M. I. "An overview of convex projections theory and its applications to image recovery problems." Ultramicroscopy 40 (1992): 55-67.

Shadrin, P.M., and Y.Y. Divin "Submicrometer electrical imaging of grain boundaries in high-Tc thin-film junctions by laser scanning microscopy." Physica C 297 (1998): 69-74.

Shaked, H., P. M. Keane, et al. Crystal structures of the high-Tc superconducting copper-oxides, Amsterdam: Elsevier Science B.V. (1994).

Shapiro, S., A. R. Janus, et al. "Effect of microwaves on Josephson currents in superconducting tunneling." Reviews of Modern Physics (1964): 223-225.

Shaw, D. T. "Controlled growth of high-temperature superconducting thin films on polycrystalline substrates." MRS Bulletin (1992): 39-44.

Shaw, T.M., S.L. Shinde, et al. "The effect of grain size on microstructure and stress relaxation in polycrystalline YBCO." Journal of Materials Research 4 (1989): 2480256.

Shi, D. "Transport critical currents and grain boundary weak links in bulk YBa2Cu3Ox." Applied Superconductivity 1 (1993): 61-70.

Shin, D. H., J. Silcox, et al. (1989). "High-resolution STEM study of grain boundaries in high-Tc superconducting YBa2Cu3O7-x thin films." Electron Microscopy Society of America, San Francisco, CA, San Francisco Press, Inc.

Shin, D. H., J. Silcox, et al. "Clean grain boundaries and weak links in high Tc superconducting Y-Ba-Cu-O thin films." Applied Physics Letters 57 (1990): 508-510.

Siegrist, T., S. Sunshine, et al. "Crystal structure of the high-Tc superconductor Ba2YCu3O9-∂." Physical Review B 35 (1987): 7137-7139.

Sigrist, M., D.B. Bailey, et al. "Fractional vortices as evidence of time-reversal symmetry breaking in high-temperature superconductors." Physical Review Letters 74 (1995): 3249-3252.

Simon, R. "High-Tc thin films and electronic devices." Physics Today (1991): 64-70.

Singh, A., N. Chandrasekhar, et al. "Coincidence orientations of crystals in tetragonal systems, with applications to YBa2Cu3O7-∂." Acta Cryst. B46 (1990): 117-125.

Singh, R. K., J. Narayan, et al. "Twinning characteristics in Y-Ba-Cu-O superconducting thin films." Materials Science and Engineering B2 (1989): 255-263.

Slakey, F., S. L. Cooper, et al. "Anisotropic electronic Raman scattering in untwinned YBa2Cu3O7-d." Physical Review B 39 (1989): 2781-2783.

Sleight, A. W. "Synthesis of oxide superconductors." Physics Today (1991): 24-30.

Smith, D. A., M. F. Chisholm, et al. "Special grain boundaries in YBa2Cu3O7." Applied Physics Letters 53 (1988): 2344-2345.

Smith, D. A. and R. C. Pond "Bollmann's O-lattice theory; a geometrical approach to interface structure." International Metals Reviews (1976): 61-74.

Song, Y., X.-D. Chen, et al. "Oxygen diffusion in YBa2Cu3O7-d grains: An experimental study of ozone and oxygen annealing processes." Journal of Materials Research 5 (1990): 27-32.

Stark, H. and E.T. Olsen "Projection-based image restoration." Journal of Optical Society of America 9 (1992): 1914-1919.

Steel, D. G., J. D. Hettinger, et al. "Transport properties of [001] tilt bicrystal grain boundaries in YBa2Cu3O7."

Stewart, W. C. "Current-Voltage Characteristics of Josephson Junctions." Applied Physics Letters 12 (1968): 277-280.

Stobbs, W. M. "Boundary characterisation methods using TEM." Ultramicroscopy 40 (1992): 300-312.

Streiffer, S. K., B. M. Lairson, et al. "Growth of YBa2Cu3O7-x on vicinally polished MgO substrates." Applied Physics Letters 57 (1990): 2501-2503.

Streiffer, S. K., B. M. Lairson, et al. "Microstructure of ultrathin films of YBaCuO on MgO." Physical Review B 43 (1991): 13007-13018.

Streiffer, S. K., E. M. Zielinski, et al. "Thickness dependence of the twin density in YBa2Cu3O7-d thin films sputtered onto MgO substrates." Applied Physics Letters 58 (1991): 2171-2173.

Strikovski, M., G. Linker, et al. "Grain-misorientation control of the critical current in high-jc epitaxial YBa2Cu3O7/SrTiO3 films." Physical Review B 45 (1992): 12522-12527.

Sun, J. Z., W. J. Gallagher, et al. "Improved process for high-Tc superconducting step-edge junctions." Applied Physics Letters 63 (1993): 1561-1563.

Sutton, P. and V. Vitek (1983), Phil. Trans. R. Soc. Lond. A 309, 1.

Suzuki, H., Y. Fujiwara, et al. "In-plane orientations and grain boundaries of YBa2Cu3O7-x thin films on (001) MgO substrates grown by metalorganic chemical vapor deposition." Japanese Journal of Applied Physics Part 1 32 (1993): 1601-1611.

Tafto, J., M. Suenaga, et al. "Characterization of planar crystal lattice defects in the high temperature superconductor YBa2Cu3O7."

Takeuchi, I., Z. Trajanovic, et al. "Heterostructure applications of in-plane oriented a-axis YBa2Cu3O7-x films on LaSrGaO4." IEEE Transactions on Applied Superconductivity (1995):

Talisa, S. H., M. A. Janocko, et al. "High-temperature superconducting wide band delay lines." IEEE Transactions on Applied Superconductivity (1995):

Talvacchio, J., M. G. Forrester, et al. "Properties of passive structures for multilayer HTS digital circuits." IEEE Transactions on Applied Superconductivity (1995):

Tamura, H., A. Yoshida, et al. "Plasma oxidation of Ba2YCu3O7-y thin films." Applied Physics Letters 53 (1988): 618620.

Tanaka, Y. and S. Kashiwaya "Theory of the Josephson effect in d-wave superconductors." Physical Review B 53 (1996): R11957-R11959.

Theuss, H., T. Becker, et al. "Influence of geometry on angle-dependent critical current density measurements in thin-film superconductors." Physica C 233 (1994): 179-184.

Theuss, H., A. Forkl, et al. "Current density and magnetic field distribution in hard thin film superconductors." Physica C 190 (1992): 345-352.

Thyssen, N., A.V. Ustinov, et al. "Experimental study of fluxon responses in window-type long Josephson junctions." IEEE Transactions of Applied Superconductivity (1995): 2965-2968.

Tietz, L. A., C. B. Carter, et al. (1988). "Grain boundaries in YBa2Cu3O7-x." Materials Research Society, Boston, MA,

Tietz, L. A., C. B. Carter, et al. "Crystallography of YBaCuO thin film-substrate interfaces." Journal of Materials Research 4 (1989): 1072-1081.

Tietz, L. A., B. C. De Cooman, et al. (1988). "The morphology of YBa2Cu3O7-d thin films grown on ceramic substrates." Materials Research Society, Boston, MA,

Tinkham, M. "Effect of fluxoid quantization on transitions of superconducting films." Physical Review 129 (1963): 2413-2422.

Tinkham, M. "Resistive transition of high-temperature superconductors." Physical Review Letters 61 (1988): 1658-1661.

Tolpygo, S. K., S. Shokhor, et al. "High quality YBa2Cu3O7 Josephson junctions made by direct electron beam writing." Applied Physics Letters 63 (1993): 1696-1698.

Tomita, N., Y. Takahashi, et al. "Preparation of bicrystal in a Bi-Sr-Ca-Cu-O superconductor." Japanese Journal of Applied Physics Part 2 (1990): L30-L32.

Toorn, P.V., A.H. Greenway, et al. "Phaseless object reconstruction." Optica Acta 31 (1984): 767-774.

Traeholt, C., J. G. Wen, et al. "HREM study of the YBCO/MgO interface on an atomic scale." Physica C 230 (1994): 297-305.

Traeholt, C., J. G. Wen, et al. "TEM investigation of YBCO thin films on SrTiO3 bicrystals." Physica C 230 (1994): 425-434.

Tranquada, J. M., D. E. Cox, et al. "Neutron-Diffraction Determination of Antiferromagnetic Structure of Cu Ions in YBa2Cu3O6+x with x=0.0 and 0.15." Physical Review Letters 60 (1988): 156-159.

Tranquada, J. M., S. M. Heald, et al. "Mixed valency, hole concentration, and Tc in YBa2Cu3O6+x." Physical Review B 38 (1988): 8893-8899.

Tsuei, C. C., J. R. Kirtley, et al. "Pairing symmetry and fluz quantization in a tricrystal superconducting ring of YBa2Cu3O7-d." Physical Review Letters 73 (1994): 593-596.

Tu, K. N., S. I. Park, et al. "Diffusion of oxygen in superconducting YBa2Cu3O7-d oxide upon annealing in helium and oxygen ambients." Applied Physical Letters 51 (1987): 2158-2160.

Tu, K. N., N. C. Yeh, et al. "Diffusion of oxygen in superconducting YBa2Cu3O7-d ceramic oxides." Physical Review B 39 (1989): 304-314.

Unger, R., T.A. Scherer, et al. "YBCO Josephson junctions on bicrystalline NdGaO3 substrates." Physica C 241 (1995): 316-318.

Ushida, T., H. Higa, et al. "Preparation and growth mechanism of a-axis-oriented YBa2Cu3O7-d films by laser metal-organic chemical vapor deposition." Journal of Materials Research 9 (1994): 1067-1081.

Vaishnava, P. P., C. A. Taylor, et al. "Electron-energy loss spectroscopy of YBa2Cu3-xFexO7-y superconductors." Physical Review B 41 (1990): 4195-4200.

Valles, J., J.M., R. C. Dynes, et al. "Electron tunneling into single crystals of YBa2Cu3O7-d." Physical Review B 44 (1991): 11986-11996.

van der Merwe, J. H. "Recent Developments in the Theory of Epitaxy." In Chemistry and Physics of Solid Surfaces V edited by R. Vanselow and R. Howe. Berlin: Springer-Verlag, (1984).

van der Pauw, L. J. "A method of measuring specific resistivity and Hall effect of discs of arbitrary shape." Philips Research Reports 13 (1958): 1-9.

Van Tendeloo, G. and S. Amelinckx "Defect structure of superconducting YBa2Cu3O7-d." Journal of Electron Microscopy Technique 8 (1988): 285-296.

Van Tendeloo, G., H. W. Zandbergen, et al. "Electron diffraction and electron microscopic study of Ba-Y-Cu-O superconducting materials." Solid State Communications 63 (1987): 389-393.

Van Tendeloo, G., H. W. Zandbergen, et al. "The vacancy order-disorder transition in Ba2YCu3O7-x observed by means of electron diffraction and electron microscopy." Solid State Communications 63 (1987): 603-606.

Verbist, K., O.L. Lebedev, et al. "Microstructure of YBCO Josephson junction in relation to their properties." Superconductor Science and Technology 11 (1998): 13-20.

Verhoeven, M.A.J., G.J. Gerritsma, et al. "Ramp-type junction parameter control of Ga doping of PrBCO barriers." Applied Physics Letters 69 (1996): 848-850.

Vildic, M., G. Friedl, et al. "Transport properties of YBaCuO step edge Josephson junctions." IEEE Transactions on Applied Superconductivity 3 (1993): 2357-2360.

Vu, L. N., M. S. Wistrom, et al. "Imaging of magnetic vortices in superconducting networks and clusters by scanning SQUID microscopy." Applied Physics Letters 63 (1993): 1693-1695.

Vuchic, B. V. "The formation, transport properties and microstructure of 45° [001] tilt grain boundaries in YBa2Cu3O7-x thin films" Northwestern University. (1995):

Vuchic, B. V., L. D. Marks, et al. "Structure-property relationship in YBCO thin film grain boundaries: a grain boundary model." (submitted):

Vuchic, B. V., K. L. Merkle, et al. "The formation, transport properties and microstructure of individual sputter-induced epitaxy grain boundaries in YBCO thin films." (submitted):

Vuchic, B. V., K. L. Merkle, et al. "Bi-epitaxial grain boundaries in YBCO thin films prepared by pulsed laser deposition and pulsed organometallic beam epitaxy: Direct comparison of transport properties and grain boundary structure." (submitted):

Vuchic, B. V., K. L. Merkle, et al. (1994). "Direct correlation of transport properties and microstructure in YBaCuO thin film grain boundaries." MRS, Boston, MRS.

Vuchic, B. V., K. L. Merkle, et al. "Integrated multi-layer sputter-induced 45° YBCO grain boundary junctions." Applied Physics Letters **67** (1995): 1013-1016.

Vuchic, B. V., K. L. Merkle, et al. "Sputter-induced grain boundary junctions in YBa2Cu3O7-x thin films on MgO." Journal of Applied Physics **77** (1995): 2591-2594.

Vuchic, B. V., K. L. Merkle, et al. "YBaCuO 45° [001] tilt grain boundaries induced by controlled low-energy sputtering of MgO substrates: Transport properties and atomic-scale structure." IEEE Transactions on Applied Superconductivity **5** (1995): 1225-1228.

Walther, A. "The question of phase retrieval in optics." Opt. Acta. **10** (1963): 41-49.

Wang, Y. Y., H. Zhang, et al. "Electronic structure and dielectric function of oxide superconductors via transmission EELS with a cold field emission TEM." Ultramicroscopy **52** (1993): 523-532.

Wang, Z. L., R. Kontra, et al. "Interface and grain boundary structures in YBa2Cu3O7-x and YBa2Cu3O8 materials." Interface Scienc **1** (1993): 321-338.

Welp, U., T. Gardiner, et al. "Magneto-optical study of twin boundary pinning in YBa2Cu3O7-d." (1994):

Welp, U., W. K. Kwok, et al. "Magnetic measurements of the upper critical field of YBa2Cu3O7-d single crystals." Physical Review Letters **62** (1989): 1908-1911.

Wen, J.G., N. Koshizuka, et al. "Microstructure of ramp-edge YBCO/PrBCO/YBCO Josephson junctions on different substrates." Physica C **255** (1995): 293-305.

Williams, E. J. and W. M. Stobbs "The development of orientation relations between sputtered YBa2Cu3O7-d and MgO substrates." Physica C **208** (1993): 96-106.

Winkler, D., Zhang, Y.M., "Electromagnetic properties at the grain boundary interface of a YBCO bicrystal Josephson junction." Physical Review Letters **72** (1994): 1260-1263.

Wire, M. S., R. W. Simon, et al. "Proximity-coupled weak links in YBCO films." IEEE Transactions on Magnetics **27** (1991): 3106-3108.

Wolf, D. and J. F. Lutsko "On the geometrical relationship between tilt and twist grain boundaries." Z. Kristall **189** (1989): 239-262.

Wolf, D. and K. L. Merkle "Correlation between the structure and energy of grain boundaries in metals." In Materials Interfaces Atomic-level structure and properties edited by D. Wolf and S. Yip. London: Chapman & Hall, (1992).

Wollman, D.A., D.J. Van Harlingen, et al. "Experimental determination of the superconducting pairing state in YBCO from the phase coherence of YBCO -Pb SQUIDS." Physical Review Letters 71 (1993): 2134-2137.

Worthington, T. K., W. J. Gallagher, et al. "Anisotropic nature of high-temperature superconductivity in single-crystal YBaCuO." Physical Review Letters 59 (1987): 1160-1163.

Wu, M. K., J. R. Ashburn, et al. "Superconductivity at 93 K in a new mixed-phase Y-Ba-Cu-O compound system at ambient pressure." Physical Review Letters 58 (1987): 908-910.

Wu, X. D., R. C. Dye, et al. "Epitaxial CeO_2 films as buffer layers for high-temperature superconducting thin films." Applied Physics Letters 58 (1991): 2165-2167.

Yan, Y. and M. G. Blanchin "Direct imaging of the oxygen sublattice in thin crystals of orthorhombic $YBa_2Cu_3O_7$-x superconductors observed by HREM at 400 kV." Physica C 198 (1992): 147-161.

Xiu Qiang Lu, K., Wang, S., et al. "The supercurrent spatial distribution of grain boundary junctions." Physica C 282-287 (1997): 2409-2410.

Yan, Xin-Zhong and Chia-Ren Hu, "Magnetic field effect in Josephson tunneling between d-wave superconductors.", Physical Review Letters 83 (1999): 1656-1659.

Yeadon, M., M. Aindow, et al. "Microstructures and properties of laser-ablated epitaxial Y-Ba-Cu-O thin films for electronic device applications." IEEE Transactions on Applied Superconductivity (1995):

Yuan, C. W., A. B. Berezin, et al. "Sep edge $YBa_2Cu_3O_7$-d dc SQUIDs on sapphire substrates." Applied Physics Letters 60 (1992): 2552-2554.

Zandbergen, H. W., W. T. Fu, et al. "Electron microscopy study of grain boundaries in 1-2-3 superconductors." Cryogenics 30 (1990): 628-632.

Zandbergen, H. W. and G. Thomas "Grain Boundaries in Sintered $YBa_2Cu_3O_7$-d." Acta Cryst. A44 (1988): 772-775.

Zappe, H.H. "Determination of the current density distribution in Josephson tunnel junctions." Physical Review B **11** (1975): 2535-2538.

Zeldov, E., J.R. Clem, et al. "Magnetization and transport currents in thin superconducting films." Physical Review B **49** (1994): 9802-9808.

Zhang, H. and V. P. Dravid "Transmission high energy electron energy loss spectrometry (EELS) of cuprate superconductors." Applied Superconductivity **1** (1993): 141-149.

Zhang, H. and V. P. Dravid "Transmission high-energy electron energy loss spectrometry (EELS) analysis of hole formation and charge transfer in p-type doped cuprate superconductors." Journal of the American Ceramics Society **76** (1993): 1143-1149.

Zhang, K., B. S. Kwak, et al. "c-axis oriented YBa2Cu3O7-x superconducting films by metalorganic chemical vapor deposition." Applied Physics Letters **54** (1989): 380-382.

Zhang, L., Jie Chen, et al. "Formation of grain boundary carbon containing phase during annealing of YBCO." Journal of the American Ceramic Society **72** (1989): 1997-2000.

Zhang, X.F., D.J. Miller, et al. " Control of meandering grain boundary configurations in YBCO bicrystal thin films based on deposition rate." Journal of Materials Research **11** (1996): 2440-2449.

Zheng, Guobao, M. Pardavi-Horvarth, et al. "Experimental determination of an effective demagnetization factor for nonellipsoidal geometries." Journal of Applied Physics **79** (1996): 5742-5744.

Zhou, J.P., J.T. McDevitt, et al. "Improved N-layer materials for high-Tc superconductor/normal-metal/superconductor junctions and superconducting quantum interference device sensors." Applied Physics Letters **72** (1998): 848-850.

Zhu, S., D.H. Lowndes, et al. "Growth mechanisms and superconductivity of ultrathin YBCO epitaxial films on (001) MgO substrates." Applied Physics Letters **62** (1993): 3363-3365.

Zhu, Y., Y. L. Corcora, et al. "Grain boundary chemistry and grain boundary dislocations in bulk YBa2Cu3O7-x." Interface Science **1** (1993): 361-370.

Zhu, Y., R. L. Sabatini, et al. "Effects of ozone oxygenation of YBa2Cu3O7-x thin crystals." Journal of Applied Physics **73** (1993): 3407-3410.

Zhu, Y. and M. Suenaga "Twinning dislocations in YBa2Cu3O7-d superconductor." Philosophical Magazine A **66** (1992): 457-471.

Zhu, Y., M. Suenaga, et al. "The interface of orthogonally oriented twins in YBa2Cu3O7-d." Philosophical Magazine A **67** (1993): 1057-1069.

Zhu, Y., M. Suenaga, et al. "Observation of twin boundary layers in pure and alloyed YBa2Cu3O7-d." Applied Physics Letters **54** (1989): 374-376.

Zhu, Y., Z. L. Wang, et al. "Grain-boundary studies by the coincident-site lattice model and electron-energy-loss spectroscopy of the oxygen K edge in YBa2Cu3O7-x." Philosophical Magazine A **67** (1993): 11-28.

Zhu, Y., H. Zhang, et al. "Grain boundary in textured YBa2Cu3O7-d superconductor." Journal of Materials Research **6** (1991): 2507-2518.

Zhu, Y., J. M. Zuo, et al. "Grain boundary constraint and oxygen deficiency in YBa2Cu3O7-d: application of the Coincident Site Lattice model to a non-cubic system." Philosophical Magazine A